Pacific Northwest National Laboratory
Operated by Battelle for the
U.S. Department of Energy

Modeling of Carbon Tetrachloride Flow and Transport in the Subsurface of the 200 West Disposal Sites: Large-Scale Model Configuration and Local-Scale Prediction of Future Carbon Tetrachloride Distribution Beneath the 216-Z-9 Disposal Site

M. Oostrom
P. D. Thorne
F. Zhang
G. V. Last
M. J. Truex

December 2007

Modeling of Carbon Tetrachloride Flow and Transport in the Subsurface of the 200 West Disposal Sites: Large-Scale Model Configuration and Local-Scale Prediction of Future Distribution of Carbon Tetrachloride Beneath the 216-Z-9 Disposal Site

M. Oostrom
P. D. Thorne
F. Zhang
G. V. Last
M. J. Truex

December 2007

Abstract

Carbon tetrachloride (CT, tetrachloromethane) has been discharged to the 216-Z-9, 216-Z-1A, and 216-Z-18 waste sites in the 200-PW-1 Operable Unit in the 200 West Area of the U.S. Department of Energy's (DOE's) Hanford Site in Washington State. Fluor Hanford, Inc. is conducting a *Comprehensive Environmental Response, Compensation, and Liability Act* (CERCLA) remedial investigation/feasibility study (RI/FS) for the 200-PW-1 Operable Unit. As part of this overall effort, Pacific Northwest National Laboratory was contracted to configure a large-scale model of CT flow and transport in the Hanford Site 200 West Area subsurface, and to conduct local-scale predictive simulations of future CT behavior below the 216-Z-9 trench. This work supports DOE's efforts to characterize the nature and distribution of CT in the 200 West Area and to subsequently select an appropriate final remedy.

Three-dimensional simulations considered migration of dense, nonaqueous phase liquid (DNAPL) consisting of CT and co-disposed organics in the subsurface beneath the two disposal sites as a function of the properties and distribution of subsurface sediments and of the properties and disposal history of the waste. Simulations of CT migration were conducted using the Water-Oil-Air mode of Subsurface Transport Over Multiple Phases (STOMP) simulator.

A large-scale model was configured to model CT and wastewater discharge from the major CT and waste-water disposal sites. A base-case simulation was conducted using hydraulic property values used in the base simulations reported in Oostrom et al. (2004; 2006a; 2006b) for local-scale simulations of the individual CT waste sites. Wastewater disposal resulted in increased water saturations in the Cold Creek Unit and a water table increase throughout the computational domain. The increased water saturations in the Cold Creek Unit reduced the downward movement of DNAPL CT and gaseous CT. Two sensitivity simulations were also performed using reduced permeability values and increased nonwetting-fluid entry pressure values for the Cold Creek Unit. The simulations conducted with smaller Cold Creek Unit permeability values than for the base case resulted in reduced DNAPL CT movement across the water table. For each case, additional simulations were conducted from 1993 to 2007 considering soil vapor extraction (SVE) from the well system in the vicinity of the three CT disposal sites. Partly due to the assumption of equilibrium partitioning between the various phase, considerably more CT was removed in the simulations compared to field observations.

In addition to the large-scale simulations, a series of seven local-scale multifluid flow and transport simulations have been completed to quantify DNAPL, aqueous, and gas CT transport in the subsurface of the 216-Z-9 disposal site. This site was chosen for these simulations because, of the three major DNAPL disposal sites, it received the most DNAPL and it has the smallest footprint. For those reasons, previous simulations have shown that DNAPL disposed at this site would be able to penetrate deep into the subsurface (Oostrom et al. 2004; 2006a), potentially to below the water table. In addition, CT concentrations of approximately 350,000 µg/kg were reported in a 1-ft thick lens, located at 19.8 m (65 ft) below the ground surface DOE-RL (2006). Six of the seven simulations (imposed cases 1-6) were conducted with imposed CT quantities in the Cold Creek Unit and/or the 1-ft thick silt lens, located in the Hanford 2 unit below the disposal site. The simulation period for these six cases was from 2007 – 2107. The seventh case (modeled case) simulated flow and transport following aqueous phase and DNAPL disposal at the site using inventory data and SVE of 53,000 kg after 1993. The simulation period for this case was from 1955 – 2107.

The computed aqueous CT mass flow rate across the water table for the modeled case is considerably larger than for imposed cases. The maximum mass flow rate for the modeled case is at least an order of magnitude larger than for the imposed cases. The only simulation with DNAPL CT transport across the water table was the modeled case. The aqueous phase and DNAPL CT fluxes for the modeled case are of the same order of magnitude throughout the simulations. Computed aqueous phase CT mass fluxes (in kg m^{-2} yr^{-1}), based on aqueous phase flux and dissolved CT concentration in the first unsaturated node above the water table, demonstrate that for most imposed cases, the maximum flux is approximately directly below the disposal site. This result is expected because the emplaced CT was in areas directly underneath the disposal site. The main differences between the modeled case and most imposed cases are that for the modeled case, the CT mass fluxes are maintained over a larger area and the values are fairly stable between 2030 and 2107. For the imposed cases, the fluxes continue to increase over time, although the actual values are orders of magnitude less than for the modeled case.

The simulations show that the total CT mass present in the computational domain for each simulation decreased gradually over time. Although some CT was transported across boundaries via gas and aqueous phase transport, the vast majority of the CT mass that was originally present in the domain at 2007 is predicted to be still present in the domain by 2107. It was demonstrated that most of the mass eventually is sorbed to the porous media. This result is directly related to the imposed retardation factor (K_d) of 0.2 mL/g. Only the modeled case is predicted to have DNAPL CT present in the Cold Creek Unit through at least 2107.

The large-scale model can be considered as a base tool for subsequent numerical investigations, such as sensitivity analyses, and remediation simulations. The model configuration also allows for detailed smaller-scale flow and transport modeling in the subsurface of disposal sites of special interest, such as the 216-Z1A, 216-Z-9 and 216-Z-18 DNAPL sites.

A crucial subsequent step for the modeling effort is to reconcile the current large-scale numerical model needs with the detailed conceptual model described in DOE-RL (2006a). Model boundary and initial conditions, as well as the geological model, need to be updated with the findings in DOE-RL (2006a). The large-scale model predicts extraction of more CT by SVE than has been observed in the field (FHI, 2006). There are several possible reasons for the discrepancy between observed and simulated results. Some of the differences result from the current model configuration which is based on equilibrium phase partitioning and the assumption that the DNAPL composition remains unaltered over time. A multicomponent version of the simulator, allowing for kinetic volatilization, is likely needed to improve simulation of SVE.

The local-scale modeling results clearly show the dominance of sorbed CT partitioning. The considerable sorption is directly related to the assumption of a constant K_d of 0.2 mL/g, which was imposed on all porous media. Additional simulations with different K_d values and values that are porous media and moisture-content dependent are needed to obtain a better understanding of the role of sorption for CT transport.

Summary

Carbon tetrachloride (CT) was discharged to waste sites that are included in the 200-PW-1 Operable Unit in the Hanford Site 200 West Area. Fluor Hanford, Inc. is conducting a *Comprehensive Environmental Response, Compensation, and Liability Act* (CERCLA) remedial investigation/feasibility study (RI/FS) for the 200-PW-1 Operable Unit. The RI/FS process and remedial investigations for the 200-PW-1, 200-PW-3, and 200-PW-6 Operable Units are described in the *Plutonium/Organic-Rich Process Condensate/Process Waste Groups Operable Unit RI/FS Work Plan*. As part of this overall effort, Pacific Northwest National Laboratory was contracted to configure a large-scale model of CT flow and transport model in the Hanford 200 West Area subsurface and to conduct predictive simulations of future CT behavior below the 216-Z-9 trench.

In addition to the large-scale simulations, a series of seven local-scale multifluid flow and transport simulations has been completed to quantify DNAPL, aqueous, and gas CT transport in the subsurface of the 216-Z-9 disposal site. This site was chosen for these detailed simulations because, of the three major DNAPL disposal sites, it received the most DNAPL and it has the smallest footprint. For those reasons, previous simulations have shown that DNAPL disposed at this site would be able to penetrate deep into the subsurface (Oostrom et al. 2004; 2006a), potentially to below the water table. Recently, CT concentrations of approximately 350,000 µg/kg were reported in a 1-ft thick lens, located at 19.89 m (65 ft) below the disposal site in the Hanford 2 unit (DOE-RL (2006a). Therefore, for this study, six simulations were conducted in which the initial CT distribution was defined by the observed quantity in the 1-ft thick lens and/or the Cold Creek Unit. These simulations are labeled Imposed Cases 1-6 to indicate that the initial CT distribution was imposed. The simulation period for these six cases was from 2007 to 2107. The seventh simulation did not start with a predefined (i.e., imposed) CT distribution. Instead, CT was simulated based on the aqueous phase and DNAPL disposal at the site using inventory data and SVE of 53,000 kg after 1993. This simulation was labeled the Modeled Case.

Simulations targeted migration of dense, nonaqueous phase liquid (DNAPL) consisting of CT and co-disposed organics in the subsurface of the 200 West Area. The geological representation of the computational domain was extracted from a larger EarthVision® geologic model of the 200 West Area subsurface[1]. Simulations of CT migration were conducted using the Water-Oil-Air mode of the Subsurface Transport Over Multiple Phases (STOMP) simulator (White and Oostrom 2006).

Large-Scale Model Configuration

A large-scale model was configured for a domain size of 1,429 m (east-west) by 1,711 m (north-south). The model assessed CT and waste water discharge from the 216-Z-9, 216-Z-1A, and 216-Z-18 sites, as well as waste water disposal from the 216-U-10, 216-U-14, 216-Z-1:2, 216-Z-3, 216-Z-7, 216-Z-12, 216-Z-17, 216-Z-18, 216-Z-20, 216-Z-1A, 216-T-19, 2607-WA, 2607-WB, 2607-Z, and 284-WB sites. Simulations were conducted with and without soil vapor extraction (SVE) from the well system in the vicinity of the three CT disposal sites. A base-case simulation was conducted using hydraulic property values used in the base simulations reported in Oostrom et al. (2004; 2006a; 2006b) for local-scale simulations of the individual CT waste sites. Two sensitivity simulations were also performed using

---

[1] EarthVision is a registered trademark of Dynamic Graphics, Inc., Alameda, California.

reduced permeability values and increased nonwetting-fluid entry pressure values for the Cold Creek Unit. Waste water disposal resulted in increased water saturations in the Cold Creek Unit and a water table increase throughout the computational domain. The increased water saturations in the Cold Creek Unit reduced the downward movement of DNAPL CT and gaseous CT. Compared to the base-case simulation, the simulations conducted with smaller Cold Creek Unit permeability values resulted in reduced DNAPL CT movement across the water table. Compared to previous modeling exercises (Oostrom et al. 2004; 2006a; 2006b), where no additional water discharges were considered, the SVE, with the assumption of equilibrium volatilization, was very effective despite the larger overall water saturations.

Predicted Future Distribution of Carbon Tetrachloride Beneath the 216-Z-9 Disposal Site

A series of seven multifluid flow and transport simulations have been completed with the Water-Air-Oil mode of the STOMP simulator to quantify NAPL, aqueous, and gas CT transport in the subsurface of the 216-Z-9 disposal site. Six of the seven simulations were conducted with imposed CT quantities in the Cold Creek Unit and/or the 65-ft silt lens. This lens, with a thickness of 1 ft, was located in the Hanford 2 unit below the disposal site. The simulation period for these six cases was from 2007 – 2107. The seventh case simulated flow and transport following aqueous phase and DNAPL disposal at the 216-Z-9 disposal site using inventory data and SVE of 53,000 kg after 1993. The simulation period for this simulation is from 1955 – 2107. An overview of the initial simulation conditions for CT distribution is shown in Table ES-1. The imposed concentrations listed in Table ES-1 are either 100%, 10%, or 1% of the observed concentration of 350,000 µg/kg in the 65-ft silt lens below the 216-Z-9 disposal site.

Table ES-1. Simulation Scenario Initial Conditions for the 216-Z-9 Disposal Site

Simulation and ID	Total DNAPL Input to Disposal Site (kg)	CT Imposed in Cold Creek Unit in 2007[a]	CT Imposed in 65-ft Silt Lens in 2007[b]	Total CT Mass in 2007 (kg)
Imposed Case 1 (IC-1)	Zero	350,000 µg/kg	350,000 µg/kg	607.4
Imposed Case 2 (IC-2)	Zero	35,000 µg/kg	35,000 µg/kg	90.0
Imposed Case 3 (IC-3)	Zero	3,500 µg/kg	3,500 µg/kg	9.0
Imposed Case 4 (IC-4)	Zero	350,000 µg/kg	Zero	585.2
Imposed Case 5 (IC-5)	Zero	Zero	350,000 µg/kg	22.2
Imposed Case 6 (IC-6)	Zero	5% DNAPL Saturation	5% DNAPL Saturation	20,122
Modeled Case 1 (MC-1)	450K (base case)	Zero	Zero	388,676
[a]Areal extent of imposed CT in the Cold Creek Unit is equal to the area of the 216-Z-9 disposal site.				
[b]Areal extent of imposed CT in the 65-ft silt lens is equal to one-half the area of the 216-Z-9 disposal site.				

The computed aqueous CT mass flow rates across the water table for imposed case 6 and the modeled case are considerably larger than for imposed cases 1 – 5. The maximum mass flow rate for imposed case 6 is 45 kg/yr (at 2065) while for the modeled case the maximum rate is about 469 kg/yr (at 2107). The maximum mass flow rate amongst the other five cases is 0.56 kg/yr for imposed case 1 (at 2107). The

maximum mass flow rates for the imposed cases 2, 3, and 5, with smaller total emplaced CT masses than for imposed cases 1 and 4, are several orders of magnitude smaller than the value for imposed case 1. The results for imposed case 4 are similar than the maximum mass flow rate of imposed case 1, also indicating the limited effect of the emplaced CT in the 65-ft silt lens. The only simulation with DNAPL CT transport across the water table was the modeled case. For this case, the maximum mass flow rate across the water table is 450 kg/yr (at 2007). It is of interest that the aqueous phase and DNAPL CT fluxes for the modeled case are of the same order of magnitude for the duration of the simulations.

Computed aqueous phase CT mass fluxes (kg m^{-2} yr^{-1}), based on aqueous phase flux and dissolved CT concentrations in the first unsaturated node above the water table, demonstrate that for imposed cases 1 through 5, the maximum flux is approximately directly below the disposal site. This result is expected because the emplaced CT was in areas directly underneath the disposal site. The fluxes for imposed cases 1 and 4 are considerably larger than for imposed cases 2, 3, and 5. Although the fluxes for these three cases are smaller, they continue to increase over time. For imposed cases 1 and 4, maximum values are obtained between 2050 and 2070, before the values decrease. For imposed case 6, the computed fluxes are considerably larger than for imposed cases 1 and 4. For this case, the maximum values are one order of magnitude larger, although this concentration peaks around 2030. The modeled case shows fluxes that have values close to what was observed for imposed case 6. The main differences between this case and imposed case 6 are that the CT mass fluxes are maintained over a larger area and that the values are fairly stable between 2030 and 2107.

The simulations show that the total CT mass present for each simulation decreased gradually over time (Table ES-2). Although some CT was transported across boundaries via gas and aqueous phase transport, the vast majority of the CT mass that was originally present in the domain at 2007 is predicted to be still present in the domain by 2107. As is shown in Table ES-2, most of the mass is eventually sorbed to the porous media. This result is directly related to the imposed K_d factor of 0.2 mL/g. Table ES-2 shows that only the modeled case is predicted to have DNAPL CT present at 2107. The total CT mass in the 65-ft silt lens and the Cold Creek Unit decreased rapidly in imposed cases 1 – 5, while these zones are holding on the CT longer in imposed case 6 and the modeled case. For the modeled case, DNAPL CT remained in the Cold Creek Unit throughout 2107, while DNAPL CT is predicted to be present through 2060 for imposed case 6.

Cumulative aqueous and gas phase CT movement across the domain boundaries were considerably smaller for imposed cases 2, 3, and 5 than for cases 1 and 4 (Table ES-2). Gas CT disappeared mainly through the top and south boundaries. Dissolved aqueous phase CT moved out of the system via groundwater movement through the east boundary. The results for imposed case 4 were again similar to the results of imposed case 1. Mass flow rates and cumulative masses for imposed case 6 are approximately one order of magnitude larger than for imposed case 1. This result shows the nonlinearity of these multiphase systems because at 2007, imposed case 6 contains 33 times more CT than imposed case 1. The cumulative transported masses for the modeled case are, in turn, considerably larger than for imposed case 6. For instance, the cumulative mass transported out of the domain from 2007-2107 through moving groundwater is more than 60,000 kg for the modeled case versus about 1,800 kg for imposed case 6. Note that for the modeled case, CT was distributed in the domain following the infiltration between 1955.5 and 1962.5. In 2007, approximately 30,000 kg CT was located in the aquifer as dissolved and DNAPL CT. The 60,000 kg transported across the aquifer boundary by 2107 partly reflects the initial mass in the saturated zone. The larger difference between the two cases is related to the

fact that for the modeled case, DNAPL CT penetrated the water table and dissolved over time. For imposed case 6, no DNAPL CT was transported across the water table.

Table ES-2. CT Mass at 2007 and 2107 and CT Losses Across Boundaries

Simulation	Total CT 2007 (kg)	Total CT 2107 (kg)	Difference (kg)	Loss Due to Groundwater Transport (kg)	Loss Due to Gas Phase Transport Top Boundary (kg)	Loss Due to Gas Phase Transport Side Boundaries (kg)
IC-1	607.4	565	42.8	10.9	6.9	25.0
IC-2	90.0	81.0	9.0	7.2E-3	1.9	7.1
IC-3	9.0	8.0	1.0	3.2E-4	0.22	0.78
IC-4	585	547	38.2	10.8	5.8	21.6
IC-5	22.2	17.3	4.9	1.2E-4	1.2	3.7
IC-6	20,122	17,986	2,136	1,790	65.0	281
MC-1	388,676	299,599	89,077	60,922	518	27,537

Table ES-3. CT Phase Partitioning in 2107

Simulation	Total CT (kg) 2107	Sorbed CT (kg) 2107	Gas Phase CT (kg) 2107	Aqueous Phase CT (kg) 2107	DNAPL CT (kg) 2107
IC-1	565	453.6	71.8	39.2	-
IC-2	81.0	59.4	15.6	6.0	-
IC-3	8.0	5.8	1.6	0.6	-
IC-4	547	441.2	68.0	37.8	-
IC-5	17.3	11.7	4.1	1.5	-
IC-6	17,986	15,020	1,637	1,330	-
MC-1	299,599	231,576	22,821	19,116	26,086

The large-scale model can be considered as a base tool for subsequent numerical investigations, such as sensitivity analyses, and remediation simulations. The model configuration also allows for detailed smaller-scale flow and transport modeling in the subsurface of disposal sites of special interest, such as the 216-Z1A, 216-Z-9 and 216-18 sites.

A crucial subsequent step for the modeling effort is to reconcile the current large-scale numerical model needs with the detailed conceptual model described in DOE-RL (2006a). Model boundary and initial conditions, as well as the geological model, need to be update with the findings in this report. The main boundary conditions for consideration are disposal volume, rate, and area, and the extent of DNAPL surface volatilization. Incorporating the state-of-knowledge conceptual model described in DOE-RL (2006a) in the current model may help to improve the simulated CT distributions and SVE extraction results.

The large-scale model predicts extraction of more CT by SVE than has been observed in the field (FHI, 2006).There are several possible reasons for the discrepancy between observed and simulated results, including preferential flow paths adjacent to extraction wells, and uncertainties in flow rates, fluid-media properties, and disposal history (e.g., volumes, rates, and timing). The differences also result from the current model configuration based on equilibrium phase partitioning, meaning simulations do not account for any rate-limited (kinetic) interfacial mass transfer effects. Another reason why modeled SVE removal rates are larger than the observed rates is the assumption that the DNAPL composition remains unaltered over time. In reality, during SVE, CT is removed from the DNAPL, lowering its molar fraction and vapor pressure. The reduced vapor pressure, in turn, leads to decreasing vapor concentration and removal rates. A multicomponent version of the simulator, allowing for kinetic volatilization, is likely needed to improve simulation of SVE.

The local-scale modeling results clearly show the dominance of sorbed CT partitioning. The considerable sorption is directly related to the assumption of a constant K_d of 0.2 mL/g, which was imposed on all porous media. Additional simulations with different K_d values and values that are porous media and moisture-content dependent are needed to obtain a better understanding of the role of sorption for CT transport.

Acknowledgments

Contents

Figures

Tables

Acronyms and Abbreviations

CERCLA   *Comprehensive Environmental Response, Compensation, and Liability Act*

CT   carbon tetrachloride

DBBP   dibutyl butyl phosphonate

DNAPL   dense, nonaqueous phase liquid

DOE   U.S. Department of Energy

HWIS   Hanford Well Information System

NAPL   nonaqueous phase liquid

NP   not present

PFP   Plutonium Finishing Plant

RI/FS   remedial investigation and feasibility study

STOMP   Subsurface Transport Over Multiple Phases

SVE   soil vapor extraction

TBP   tributyl phosphate

1.0   Introduction

Plutonium recovery operations within the Z-Plant aggregate area (Plutonium Finishing Plant [PFP]) at the Hanford Site resulted in organic and aqueous wastes that were disposed of at several cribs, tile fields, and French drains. The organic wastes consisted of carbon tetrachloride (CT) mixed with lard oil, tributyl phosphate (TBP), and dibutyl butyl phosphonate (DBBP). The main disposal areas were the 216-Z-9 trench, the 216-Z-1A tile field, and the 216-Z-18 crib. The three major disposal facilities received a total of about 13,400,000 L of liquid waste containing 363,000 to 580,000 L of CT. Assuming a maximum aqueous solubility of 800 mg/L and an organic liquid density of 1.59 g/cm^3, the 13,400,000 L of liquid waste would be able to contain approximately 6,700 L of CT in dissolved form. This indicates the majority of the CT entered the subsurface as an organic liquid.

A series of three-dimensional multifluid flow simulations was conducted by Oostrom et al. (2004; 2006a) with the Subsurface Transport Over Multiple Phases (STOMP) simulator (White and Oostrom 2006) to examine the impact of parameter variation on the migration of CT in the subsurface beneath the 216-Z-9 disposal area over the period from 1954 to 1993, when soil vapor extraction (SVE) was initiated in the area. The numerical models were configured using available information regarding the hydrogeology, measured fluid properties for the likely mixtures of disposed organic liquid (e.g., mixtures of CT, lard oil, TBP, and DBBP), and estimates of hydrologic boundary conditions. The hydrogeologic setting was configured by assembling a geologic model based on interpretations of borehole geologic information at the regional and local scale. The geologic model was constructed using the EarthVision™ software to provide a means for three-dimensional interpolation of borehole geologic information, and to establish an electronic format for the geologic model that enabled porous media properties to be readily mapped to the numerical model grid. Fluid properties for relevant organic liquid mixtures were determined in the laboratory as part of the U.S. Department of Energy's (DOE's) Remediation and Closure Science Project (Oostrom et al. 2004). The multifluid flow and transport simulations for the 216-Z-9 site lead to the following adjustments of the conceptual model:

- *Where is CT expected to accumulate?* CT DNAPL accumulates in the finer-grain sediments of the vadose zone but does not appear to pool on top of these layers.

- *Where would continuing liquid CT sources to groundwater be suspected?* Migration of DNAPL CT tends to move vertically downward below the disposal area. Considerable lateral movement of DNAPL CT is not likely. However, significant lateral migration of vapor phase CT occurs.

- *What is the estimated distribution and state of CT in the vadose zone?* The majority of the CT was typically a DNAPL or in the sorbed phase in 1993. Heterogeneities, however, as shown in the results reported by Oostrom et al. (2006a) tends to increase the amount of CT present in the vapor, water, and sorbed phases compared to the DNAPL phase. The center of mass for CT in the vadose zone was typically directly beneath the disposal area and within the Cold Creek Unit.

- *How does SVE affect the distribution of CT in the vadose zone?* SVE effectively removes CT from the permeable layers of the vadose zone. SVE previously applied in the 216-Z-9 trench area has likely removed a large portion of CT initially present in the permeable layers within the large radius of influence of the extraction wells. Finer-grain porous media with larger moisture contents, such as the Cold Creek Unit sediments, are less affected by SVE.

- *Where would DNAPL contamination in groundwater be suspected?* Simulations indicate that migration of DNAPL is primarily in the vertical direction such that DNAPL, if present in the groundwater, would be most likely expected in a zone distributed around the centerline of the disposal area.

Additional three-dimensional modeling was conducted by Oostrom et al. (2006b) with layered models to refine and update the conceptual model of CT distribution in the vertical and lateral direction beneath the 216-Z-1A tile field and 216-Z-18 crib, and to investigate the effects of SVE as a CT remediation option. The simulations considered disposal of aqueous-phase waste at the 216-Z-1, Z-2, and Z-3 sites, prior to CT disposal at the 216-Z-1A and 216-Z-18 sites.

A total of 34 three-dimensional simulations were conducted based on a layered EarthVision® geologic model, which is an interpretation of available geologic data. These simulations consist of one base-case simulation and 33 sensitivity analysis simulations. These simulations examined the infiltration and redistribution of CT from 1954 through 1993, just before the SVE treatment began. A second series of simulations examined the impact of SVE on the CT in the subsurface over the time period of 1993 to 2005.

Results of the simulations for the 216-Z-1A and 216-Z-18 sites (summarized below) refer to movement of CT through the different geological layers in the subsurface beneath the disposal sites. The first geologic unit encountered is the H1a unit, a near-surface unit of the Hanford formation that is present in some locations in the 200 West Area. The next units encountered are the H1 and H2 units of the Hanford formation, respectively. The Cold Creek Unit underlies the H2 unit and is significant in that it contains a fine-grained silt layer and a caliche layer. These layers have significantly different hydraulic properties and can retain more CT than other units in the vadose zone. The Ringold E unit is below the Cold Creek Unit. The water table is located in the Ringold E unit about 20 m below the Cold Creek Unit.

Simulated DNAPL movement at the 216-Z-1A site for the base-case simulation parameter values shows DNAPL movement only as deep as the Cold Creek Unit and DNAPL does not move across the water table. CT disposal at the 216-Z-1A site impacts the groundwater only through vapor and aqueous phase migration. Similarly, simulated DNAPL movement is limited at the 216-Z-18 site with DNAPL not penetrating any deeper than the H2 unit. CT disposal at the 216-Z-18 site has a limited impact on the groundwater through vapor and aqueous phase migration. The limited movement of DNAPL at these two disposal sites is partially due to the presence of the H1a unit just below the disposal site. The properties of this unit are such that DNAPL is retained to a greater extent than in the H1 and H2 units below. The H1a unit is not present at the 216-Z-9 site where previous simulations (Oostrom et al. 2004 and 2006a) showed much more significant vertical movement of DNAPL.

Sensitivity simulations with decreased disposal site area (infiltration area) showed significantly different results than for the base case. In all three sensitivity cases, DNAPL was predicted to move across the water table beneath the 216-Z-1A site, and the DNAPL moved deeper into the H2 unit beneath the 216-Z-18 site. Increasing the DNAPL volume also increased DNAPL penetration in the subsurface. When DNAPL volume was doubled, DNAPL was predicted to move across the water table beneath the 216-Z-1A site. Sensitivity simulations where the DNAPL properties or properties related the CT (e.g., solubility, partitioning coefficient) did not result in any DNAPL movement across the water table. Some of these sensitivity cases did change the distribution of CT within the subsurface by changing the distribution of CT between the DNAPL, vapor, aqueous, and sorbed phases. Porous media properties of

the H1a unit or the Cold Creek Unit also impact the distribution of CT in the subsurface, but none of the sensitivity simulations for these units resulted in DNAPL moving across the water table. Of importance, some of the sensitivity simulations that showed DNAPL moving across the water table are the results of changes in parameters for which there is a large uncertainty in the actual value. For instance, the actual infiltration area is not well known and if this area were smaller than what was selected for the base case, DNAPL may have moved across the water table beneath the 216-Z-1A site. Similarly, there is some uncertainty in the volume of DNAPL disposed and the porous media property values.

The simulations of SVE showed similar results to what has been previously reported in Oostrom et al. (2004 and 2006a) in that the model appears to predict extraction of more CT by SVE than has been observed in the field (FHI, 2006). There are several possible reasons for the discrepancy between observed and simulated results, including preferential flow near extraction wells, and uncertainties in flow rates, fluid-media properties, and disposal history (e.g., volumes, rates, and timing). The differences may also result from the current simulations being based on equilibrium phase partitioning, meaning simulations do not account for any rate-limited (kinetic) interfacial mass transfer effects. Another reason why modeled SVE removal rates are larger than the observed rates is the assumption that the DNAPL composition remains unaltered over time. In reality, during SVE, CT is removed from the DNAPL, lowering its molar fraction and vapor pressure. The reduced vapor pressure, in turn, leads to decreasing vapor concentration and removal rates. A multicomponent version of the simulator is needed to address this kind of behavior. However, the SVE simulation results suggest that SVE will be effective for removing CT from the permeable units of the Hanford and Ringold Formations and that residual CT will be predominantly located in the Cold Creek Unit, H1a unit, or in other silt lenses. Thus, SVE can be effective at removing the driving force for future CT migration to the groundwater because this migration must occur through these permeable units. The study by Oostrom et al. (2006a) includes a sensitivity analysis of the SVE beneath the 216-Z-9.

The simulations results reported by Oostrom et al. (2006b) generally support the conclusions reported by Oostrom et al. (2004; 2006a).

- *Where is CT expected to accumulate?* CT DNAPL is predicted to accumulate in the finer-grain sediments of the vadose zone but does not pool on top of these layers.

- *Where would continuing liquid CT sources to groundwater be suspected?* Migration of DNAPL CT tends to move vertically downward below the disposal area. Considerable lateral movement of DNAPL CT is not likely. However, significant lateral migration of vapor CT occurs.

- *What is the estimated distribution and state of CT in the vadose zone?* The majority of the CT was typically a DNAPL or in the sorbed phase in 1993. Heterogeneities, however, as shown in the results reported herein, tend to increase the amount of CT present in the vapor and related water and sorbed phases compared to the DNAPL phase. The center of mass for CT in the vadose zone was typically directly beneath the disposal area and within the Cold Creek Unit. The center of mass for CT in the vadose zone was typically directly beneath the disposal area and within the Cold Creek Unit.

- *How does SVE affect the distribution of CT in the vadose zone?* The 216-Z-1A and 216-Z-18 modeling effort directly supported the conclusions of the 216-Z-9 modeling results. The simulations predicted that SVE effectively removes CT from the permeable layers of the vadose zone.

- *Where would DNAPL contamination in groundwater be suspected?* The 216-Z-1A and 216-Z-18 modeling effort directly supported the conclusions of the 216-Z-9 modeling results, although DNAPL is only predicted to move across the water table under certain sensitivity conditions for the 216-Z-1A site.

Updates to the previous conceptual model depicted in the RI/FS Work Plan (DOE-RL 2004) were consistent with conceptual model shown in the recent RI report (DOE-RL 2006a):

1. No lateral movement of DNAPL to underneath the PFP is likely.

2. The zones of persistent CT mass in the vadose zone are primarily the Cold Creek Unit and H1a geologic units.

3. Large vertical and lateral density-driven movement of vapor occurred in the past.

4. DNAPL penetration to groundwater is likely to have occurred at the 216-Z-9 site, possibly at the 216-Z-1A site, and unlikely at the 216-Z-18 site.

5. DNAPL penetration to the groundwater from undocumented releases is unlikely.

6. The phase distribution of CT changes over time due to volatilization, interaction of gas-phase CT with pore water and aqueous-phase CT with sorbed phase, DNAPL dissolution in groundwater, and the impact of SVE.

Simulation results from the 216-Z-1A and 216-Z-18 modeling effort and from Oostrom et al. (2004 and 2006a) were also compared to available field data (Oostrom et al. 2006b). Key conclusions from this comparison were as follows:

- High-soil concentrations and predicted areas with high-DNAPL saturations are spread vertically within a relatively small lateral area within about 30 m of the disposal area footprint.

- Measured groundwater concentrations are higher and the high-groundwater concentrations are spread deeper in the aquifer beneath the 216-Z-9 site compared to the 216-Z-1A and 216-Z-18 sites. This observation correlates to modeling results where the CT flux to the groundwater at the 216-Z-9 site was significantly higher than the flux at the 216-Z-1A and 216-Z-18 sites. Modeling results showing a larger number of sensitivity simulations with DNAPL flux to groundwater and deeper penetration of DNAPL within the aquifer beneath the 216-Z-9 site compared to the other two disposal areas are also consistent with these observations.

Model results were also compared to this field data to evaluate reasonable scenarios for how CT entered the groundwater. For instance, with 100,000 kg of CT that entered the aquifer (based on the estimate in Murray et al. 2006), only by combining the estimates of CT mass flux to the groundwater from simulation sensitivities (not the base cases) that show DNAPL crossing the water table predict a combined mass of CT (216-Z-9, Z-18, and Z-1A) in the aquifer similar to the estimated CT mass. The average CT mass of dissolved CT that has been transported across the water table (a measure of the impact of vapor phase transport to the groundwater table and pore water from the vadose zone entering the groundwater) for all three sites through 1993 is approximately 5,000 – 10,000 kg. The accumulated CT mass in the aquifer would be significantly lower than the mass of CT in the groundwater estimated by Murray et al. (2006) if only aqueous and vapor phase CT and no DNAPL phase entered the groundwater. This assessment indicated that it is likely that DNAPL CT has entered the groundwater. The simulation results in Oostrom et al. (2004; 2006a; 2006b) show that the most likely location of significant DNAPL movement across the water table is below the 216-Z-9 site.

As described in this section, detailed local disposal site models to provide estimates of CT distribution as a function of time and as a function of CT phase (e.g., vapor, DNAPL, etc.) were developed by Oostrom et al. (2004, 2006a, 2006b). This report documents two different efforts that build on this previous work. The detailed local disposal site models examined CT distribution over time in the subsurface with consideration of the local subsurface conditions, but because of the relatively small model domain size, did not consider potential impacts from adjacent waste and water disposal sites. Thus, a large-scale model domain was configured to include the major CT and aqueous-phase disposal sites in the 200 West Area. This report includes a description of the model configuration and a limited number of simulations with the large-scale model. As such, the primary purpose for this section of the report is to document the configuration of the large-scale model. Additionally, while the previous modeling efforts provided useful information about the distribution of CT in the subsurface over time as part of improving the conceptual model for CT, information about the CT mass flux at defined boundaries is also important. For instance, the contribution of the vadose zone as a source of CT to the groundwater over time can be quantified based on the estimated CT mass flux across the water table. This report documents simulation results for the localized model of the 216-Z-9 disposal site for seven simulation scenarios selected to support the remedial investigation and feasibility study (RI/FS) efforts that were conducted concurrently with the modeling effort. The simulation scenarios primarily examined the mass flux as a function of time resulting from a selected distribution of CT that was imposed as an initial conditions. The imposed CT distributions were selected based on available field data and input from the RI/FS efforts. Simulation results are presented in terms of the CT mass flux across the water table and other defined boundaries so that these flux estimates can be used to support analyses in the RI/FS. The 216-Z-9 site was the focus of these simulations because previous modeling had shown the largest amount of CT entering the groundwater beneath this disposal site.

This report includes a description of the STOMP simulator and EarthVision® geologic models used for the simulations (Section 2.0). Section 3.0 presents the large-scale and local model configurations and a description of the simulation scenarios. The results of the three simulation scenarios conducted using the large-scale model are presented in Section 4.0. Mass flux estimates for simulations with the 216-Z-9 local model are then presented in Section 5.0. Section 6.0 provides a summary, conclusions, and recommendations for potential future work.

2.0   Model Description

2.1   Numerical Model

The water-oil-air operational mode (STOMP-WOA) of the STOMP simulator (White and Oostrom 2006) was used to simulate multifluid flow and transport beneath the disposal sites. The fully implicit integrated finite difference code has been used to simulate a variety of multifluid systems (e.g., Hofstee et al. 1998; Oostrom et al. 1997, 1999, 2003; Oostrom and Lenhard 1998, 2003; Schroth et al. 1998; White et al. 2004). The applicable governing equations are the component mass-conservation equations for water, organic compounds, and air, expressed in Equations (2.1a through 2.1i):

$$\frac{\partial}{\partial t}\left[n_D \omega_l^w \rho_l s_l\right] = -\nabla F_l^w + \dot{m}^w \tag{2.1a}$$

$$\frac{\partial}{\partial t}\left[\sum_{\gamma=l,n,g}\left(n_D \omega_\gamma^o \rho_\gamma s_\gamma\right) + \left((1-n_T)\omega_s^o \rho_s\right)\right] = -\sum_{\gamma=l,n,g}\left\{\nabla F_\gamma^o + \nabla J_\gamma^o\right\} + \dot{m}^o \tag{2.1b}$$

$$\frac{\partial}{\partial t}\left[\sum_{\gamma=l,g}\left(n_D \omega_\gamma^a \rho_\gamma s_\gamma\right)\right] = -\sum_{\gamma=l,g}\left\{\nabla F_\gamma^a + \nabla J_\gamma^a\right\} + \dot{m}^a \tag{2.1c}$$

Where:

$$F_\gamma^w = -\frac{\omega_\gamma^w \rho_\gamma k_{rl} k}{\mu_\gamma}\left(\nabla P_\gamma + \rho_\gamma gz\right) \text{ for } \gamma = l,g, \tag{2.1d}$$

$$F_\gamma^o = -\frac{\omega_\gamma^o \rho_l k_{r\gamma} k}{\mu_\gamma}\left(\nabla P_\gamma + \rho_\gamma gz\right) \text{ for } \gamma = l,n,g \tag{2.1e}$$

$$F_\gamma^a = -\frac{\omega_\gamma^a \rho_\gamma k_{r\gamma} k}{\mu_\gamma}\left(\nabla P_\gamma + \rho_\gamma gz\right) \text{ for } \gamma = l,g \tag{2.1f}$$

$$J_\gamma^w = -\tau_\gamma n_D \rho_\gamma s_\gamma \frac{M^w}{M_\gamma} D_\gamma^w \nabla \chi_\gamma^w \text{ for } \gamma = l,g \tag{2.1g}$$

$$J_\gamma^o = -\tau_\gamma n_D \rho_\gamma s_\gamma \frac{M^o}{M_\gamma} D_\gamma^o \nabla \chi_\gamma^o \text{ for } \gamma = l,n,g \tag{2.1h}$$

$$J_\gamma^a = -\tau_\gamma n_D \rho_\gamma s_\gamma \frac{M^a}{M_\gamma} D_\gamma^a \nabla \chi_\gamma^a \text{ for } \gamma = l,g \tag{2.1i}$$

Where:

l, n, g,, s $=$ aqueous, nonaqueous phase liquid (NAPL), gas and solid phases, respectively

w, o, and a $=$ water, organic compound, and air components, respectively

t $=$ time (s)

n_D $=$ diffusive porosity

n_T $=$ total porosity

ω $=$ component mass fraction

ρ $=$ density (kg/m^3)

s $=$ actual liquid saturation

V $=$ volumetric flux (m/s)

J $=$ diffusive-dispersive mass flux vector (kg/m^{2}s)

m $=$ component mass source rate (kg/m^{3}s)

k $=$ intrinsic permeability (m^2)

$k_{r\gamma}$ $=$ relative permeability of phase γ

μ $=$ viscosity (Pa s)

P $=$ pressure (Pa)

g_z $=$ gravitational vector (m/s^2)

τ $=$ tortuosity

M $=$ molecular weight (kg/mole)

D $=$ diffusive-dispersive tensor (m^2/s)

χ $=$ component mole fraction.

The partitioning between the aqueous and solid phases is described by a linear exchange isotherm through a constant distribution coefficient.

The governing partial differential equations (Equations 2.1a, 2.1b, and 2.1c) are discretized following the integrated-volume finite difference method by integrating over a control volume. Using Euler backward time differencing, yielding a fully implicit scheme, a series of nonlinear algebraic expressions is derived. The algebraic forms of the nonlinear governing equations are solved with a multivariable, residual-based Newton-Raphson iterative technique, where the Jacobian coefficient matrix is composed of the partial derivatives of the governing equations with respect to the primary variables.

Assuming the aqueous phase never disappears, the primary variable for the water equation is always the aqueous pressure. For the oil equation, the primary variable is P_n when free NAPL is present, s_n when only entrapped NAPL is present, and the component mole fraction when no NAPL is present. For the air equation, the primary variable is P_a. The algebraic expressions are evaluated using upwind interfacial averaging for fluid density, mass fractions, and relative permeability. Specified weights (i.e., arithmetic,

harmonic, geometric, upwind) are applied to the remaining terms of the flux equations. For the simulations described in this report, harmonic averages were used and the maximum number of Newton-Raphson iterations was 16, with a convergence factor of 10^{-6}.

Secondary variables, those parameters not directly computed from the solution of the governing equations, are computed from the primary variable set through the constitutive relations. In this section, only the relations between relative permeability, fluid saturation, and capillary pressure (*k-S-P*) pertinent to the conducted simulations are described. The *k-S-P* relations consist of the Brooks and Corey (1964) S-P relations in combination with the k-S relations derived from the Burdine (1953) or Mualem (1976) model. In these relations, the effects of fluid entrapment and residual saturation formation have been included.

The *k-S-P* relations distinguish between actual, effective, and apparent saturations. Actual saturations are defined as the ratio of fluid volume to diffusive pore volume. Effective saturations represent normalized actual saturations based on the pore volumes above the irreducible or minimum saturation of the wetting fluid (i.e., aqueous-phase liquid). Effective saturations for the aqueous phase, NAPL, gas phases, and the total liquid are defined according to Equation (2.2a through 2.2d):

$$\bar{s}_l = \frac{s_l - s_{rl}}{1 - s_{rl}} \tag{2.2a}$$

$$\bar{s}_n = \frac{s_n}{1 - s_{rl}} \tag{2.2b}$$

$$\bar{s}_g = \frac{s_g}{1 - s_{rl}} \tag{2.2c}$$

$$\bar{s}_t = \frac{s_l + s_n - s_{rl}}{1 - s_{rl}} \tag{2.2d}$$

where s_{rl} is the irreducible aqueous-phase saturation. Apparent saturations are defined in terms of effective saturations. Apparent saturations represent the effective saturation of the fluid, plus the effective saturations of fluids of lesser wettability entrapped within the wetting fluid. In the simulator, it is assumed that fluid wettability follows the sequence: water > NAPL > air (Leverett 1941). Fluids of lesser wettability can potentially be trapped by NAPL or aqueous phase, and NAPL can be entrapped by the aqueous phase.

In a three-phase system, the apparent total-liquid saturation is considered to be a function of the air-NAPL capillary pressure, and the apparent aqueous-phase saturation a function of the NAPL-water capillary pressure, as seen in Equation (2.3a through 2.3d):

$$\bar{\bar{s}}_t = \left[\frac{P_d}{\beta_{gn} P_{gn}} \right]^\lambda \quad \text{for} \quad \beta_{gn} P_{gn} > P_d \tag{2.3a}$$

$$\overline{\overline{s}}_t = 1 \quad \text{for} \quad \beta_{gn} P_{gn} \leq P_d \tag{2.3b}$$

$$\overline{\overline{s}}_l = \left[\frac{P_d}{\beta_{nl} P_{nl}}\right]^{\lambda} \quad \text{for} \quad \beta_{nl} P_{nl} > P_d \tag{2.3c}$$

$$\overline{\overline{s}}_l = 1 \quad \text{for} \quad \beta_{nl} P_{nl} \leq P_d \tag{2.3d}$$

Where:

P_d = air-entry pressure

P_{gn} = gas phase – NAPL capillary pressure

P_{nl} = NAPL – aqueous-phase capillary pressure

γ = pore-size distribution factor

β_{gn} and β_{nl} = interfacial tension dependent scaling factors, defined as $\beta_{gn} = (\sigma_{gn} - \sigma_{nl})/\sigma_{gn}$ and $\beta_{nl} = (\sigma_{gn} - \sigma_{nl})/\sigma_{nl}$, respectively.

The nature of these relations is discussed by Lenhard (1994) and Lenhard et al. (1994). For aqueous-gas phase systems, Equation (2.3) is replaced by Equation (2.4a and 2.4b):

$$\overline{\overline{s}}_l = \left[\frac{P_d}{P_{gl}}\right]^{\lambda} \quad \text{for} \quad P_{gl} > P_d \tag{2.4a}$$

$$\overline{\overline{s}}_l = 1 \quad \text{for} \quad P_{gl} \leq P_d \tag{2.4b}$$

2.2 Geologic Models for Large-Scale and 216-Z-9 Simulations

The geologic models for both simulation scales were constructed using similar techniques as described in Oostrom et al. (2004; 2006a; 2006b). The first effort in developing the geologic model was to build a database of geologic contacts. To create a consistent database of geologic contacts, all pertinent data sets were mapped to a single set of stratigraphic units. These stratigraphic units have also been mapped to the new Standardized Stratigraphic Nomenclature (DOE-RL 2002). Figure 3.2 in Oostrom et al. (2004) illustrates how the various stratigraphic interpretations relate to each other and how mapping was accomplished. Where discrepancies were found between multiple data sets, and/or where large gaps existed in the spatial distribution of the data, efforts were made to determine the geologic contacts by reviewing/evaluating the raw borehole data, including driller's logs, geologist's logs, summaries of the driller's or geologist's logs in as-built drawings from the Hanford Well Information System (HWIS), particle size data, calcium carbonate data, moisture content data, and geophysical logs. Analysis of the initial EarthVision® geologic model constructed based on the geologic contact database created for this study, identified several anomalous areas where adjacent boreholes had markedly different geologic contact elevations, creating large peaks or basins of unexplained paleogeomorphologic character. Thus, efforts were made to re-evaluate the raw geologic data in these areas, make new estimates (or confirm existing estimates) of the geologic contacts, and resolve these anomalies. For the models used in this

report additional refinements to the original database were made, including analyzing data from 21 boreholes in the vicinity of the 216-Z-9 trench. Assignment of flow and transport properties to the stratigraphic units defined in the geologic model was accomplished by mapping these units to various soil/sediment classes for which hydraulic property data are available (e.g., Khaleel and Freeman 1995).

During the initial phases of this work, several observations/recommendations were made regarding uncertainties in the geologic data and interpretations. Some of the factors contributing to the uncertainty were as follows:

1. Quality of the survey control

2. Lack of geophysical logs for some key wells

3. Quality of lithologic descriptions

4. Inconsistent level of detail/scale of geologic data

5. Ad hoc methods of mapping geologic lithofacies to hydrologic property distributions.

To better resolve these uncertainties, nearly every borehole/well in the geologic domain was resurveyed using a state-of-the-art global positioning system. These new survey data were then incorporated into the geologic contacts database. Recommendations were made to incorporate borehole geophysical logging of key wells into the sampling and analysis plan for upcoming investigations. Considerable efforts were made to correlate hydraulic properties with particle size data and lithofacies.

To aid multifluid flow and transport simulations, the geologic framework was simplified into a layered sequence of five main stratigraphic units and a number of subordinate units. From oldest to youngest, the main stratigraphic units are the 1) Saddle Mountains Formation (of Miocene age), 2) Ringold Formation (of Miocene/Pliocene age), 3) Cold Creek Unit (Pliocene-Pleistocene), 4) Hanford formation (Pleistocene), and 5) undifferentiated Holocene Deposits.

1. **Saddle Mountains Formation**. The Saddle Mountains Formation forms the bedrock beneath the site. Its uppermost member, the Elephant Mountain Member, lies at a depth of approximately 161 m and slopes to southwest at a rate of about 0.015 (or 15 m/100 m). This medium- to fine-grained tholeiitic basalt essentially acts as a no-flow boundary at the floor of the unconfined aquifer

2. **Ringold Formation**. The basalt bedrock is overlain by the Ringold Formation, a sedimentary sequence of fluvial-lacustrine clay, silt, sand, and granule to cobble gravel deposited by the ancestral Columbia River. The Ringold Formation has been subdivided into three subordinate units. From oldest to youngest, these are 1) Unit A – fluvial sandy gravel, 2) the Lower Mud Unit – a sequence of paleosols and lake deposits, consisting of muddy medium to fine sand, and 3) Unit E – semi-indurated fluvial muddy sand gravel.

3. **Cold Creek Unit**. Overlying the Ringold Formation is the Cold Creek Unit. Locally, this unit is differentiated into the Cold Creek carbonate layer and the Cold Creek silt layer. The Cold Creek carbonate layer, formerly described as the caliche (or calcrete), is a fine- to coarse-grained,

calcium-carbonate cemented paleosol that developed on top of the Ringold Formation. Overlying the Cold Creek carbonate layer is the Cold Creek silt layer formerly referred to as the "Early Palouse Soil." This unit consists of cohesive, compact, massive to laminated, and stratified fine-grained sand and silt (e.g., sandy mud).

4. **Hanford formation**. The Hanford formation has been locally subdivided into three main units (from oldest to youngest) 1) a sequence of interbedded sand and mud (e.g., slightly muddy medium to fine sand to sandy mud) equivalent to the Hanford H4 unit; 2) a sequence of coarse to medium sand, equivalent to the Hanford H2 unit, and 3) a sequence of sandy gravel, equivalent to the Hanford H1 unit.

5. **Backfill**. Some of the disposal sites were excavated in to the underlying Holocene Sand and Hanford sandy gravel units. The stockpiles of these sediments have been used as backfill in pipeline trenches and other excavations. These backfill materials are described as gravelly medium sand.

To create a consistent database of geologic contacts, all pertinent data sets were mapped to a single set of hydrostratigraphic units. These hydrostratigraphic units have also been mapped to the new Standardized Stratigraphic Nomenclature (DOE-RL 2002). To enhance the level of detail need for the EarthVision® geologic modeling, the 5 main hydrostratigraphic units were subsequently divided into 13 units. Starting from ground surface and working downwards, the units are Backfill, Hanford 1A, Hanford 1, Hanford 2, Hanford Lower Gravel, Hanford Lower Sand, Cold Creek Unit silt, Cold Creek Unit carbonate, Upper Ringold, Ringold E, Ringold Lower Mud, Ringold A, and Elephant Mountain Basalt.

2.2.1   EarthVision® Geologic Models

EarthVision® software was used to create three-dimensional models of the large-scale and 216-Z-9 model. The EarthVision® models consist of a "facies" file that represents each unit as a zone within a solid three-dimensional block. A 5-m resolution digital elevation model from the U.S. Geological Survey was used to define the upper surface topography for the models. The facies file can be sampled using utilities provided in the EarthVision® software to create input files for numerical flow models.

The following procedure was used to build and revise the geologic model:

1. Grids representing the tops of extensive units (present over most of the model domain) were created based on the elevation selections from wells. Control points were added in areas where data were sparse, particularly on the edges of the model domain to control extrapolation.

2. Thickness (isopach) grids were calculated for less extensive geologic units based on the thickness measured at wells and zero thickness for the not present (NP) flags in the well data. For these less extensive units, it was assumed that the unit was not present in areas where there were no data for the unit.

3. Starting from the base of the model, grids for the top elevation of each less extensive geologic unit were calculated by adding the thickness grid to the elevation grid for whichever unit exists below it.

4. The model was examined to determine if any units had incorrectly "pinched-out" because the top of a deeper unit was being extrapolated above the elevation of the well pick. If this occurred, control points were added to control the top of the deeper unit.

Analysis of the initial EarthVision® model results identified several anomalous areas where adjacent boreholes had markedly different geologic contact elevations, creating large peaks or basins of unexplained paleogeomorphologic character. Thus, efforts were made to re-evaluate the raw geologic data in these areas, make new estimates (or confirm existing estimates) of the geologic contacts, and resolve these anomalies. As these new changes were input into the revised EarthVision® models and new results were made available, additional refinements to the database were made.

2.2.1.1 Large-Scale Geologic Model

A set of selected interpretive geologic contacts were used to develop a hydrogeologic framework model that is the basis for simulations of carbon tetrachloride movement in the ZP-1 operable unit area. This model was built by expanding on earlier work that focused on a smaller scale (Oostrom et al., 2004; 2006a; 2006b). Contact data from a total of 232 boreholes were used to build the hydrogeologic framework model for the large scale model. A top view of the model, including the major waste-water disposal sites and the location of two cross sections A-A' and B-B', are shown in Figure 2.1. Simulation results will be shown in subsequent sections for these two cross sections. Figure 2.2 shows a three-dimensional view of the hydrogeologic framework model, including locations of the major waste locations. Figures 2.3 and 2.4 show the geology for cross section A-A' and B-B', respectively. These figures indicate that the Cold Creek Unit is continuous at the large scale. Figures 2.5 – 2.13 show the top elevations of several of the geologic units. On each of these figures, borehole data showing the elevation of the top of the unit is shown as a black dot and boreholes where the unit appears to be missing are shown as a vertical magenta line. For instance, in Figure 2.10, no magenta lines are shown, indicating a continuous representation of the Cold Creek silt unit. In contrast, Figure 2.12 shows numerous magenta lines in areas where the Upper Ringold Unit was not observed in the considered wells.
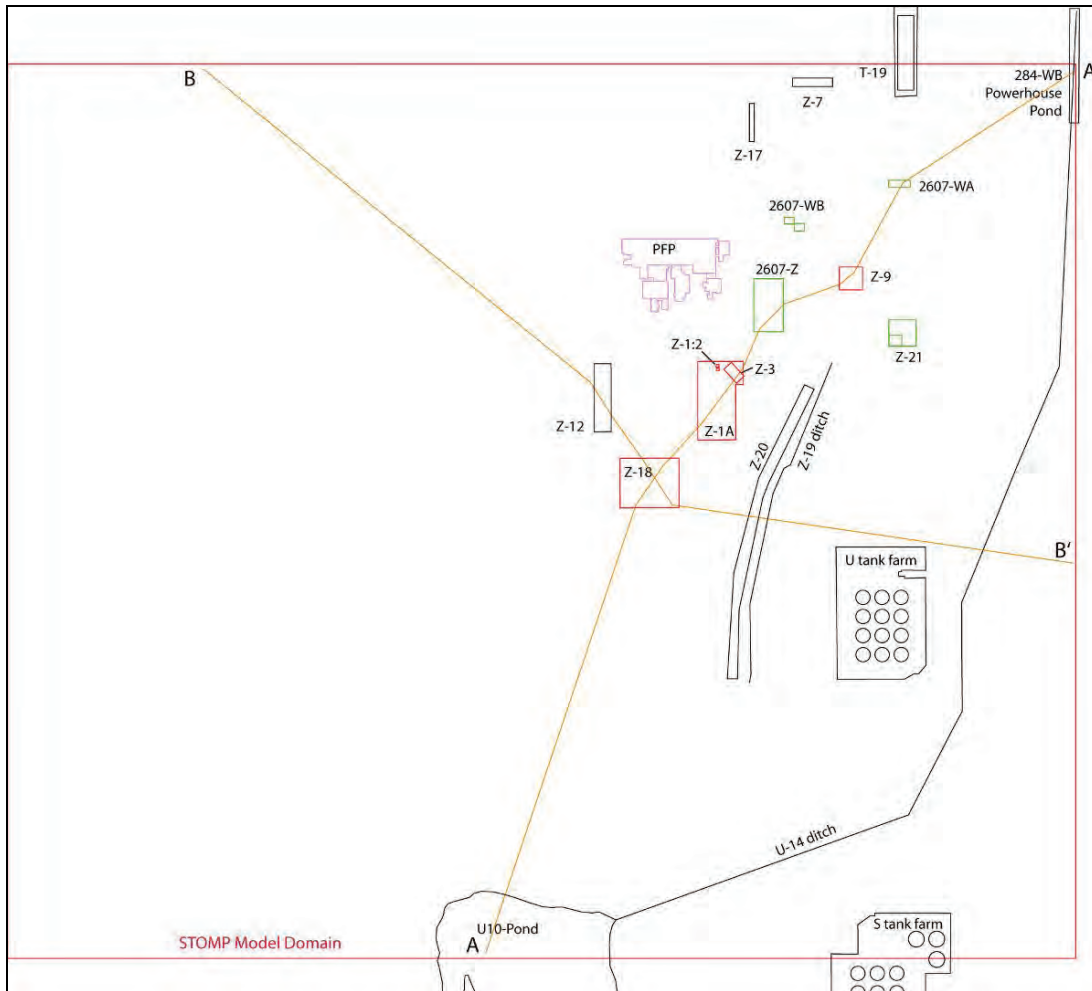
Figure 2.1. Overview of Waste Disposal Sites and Location of Cross Sections A-A' and B-B'
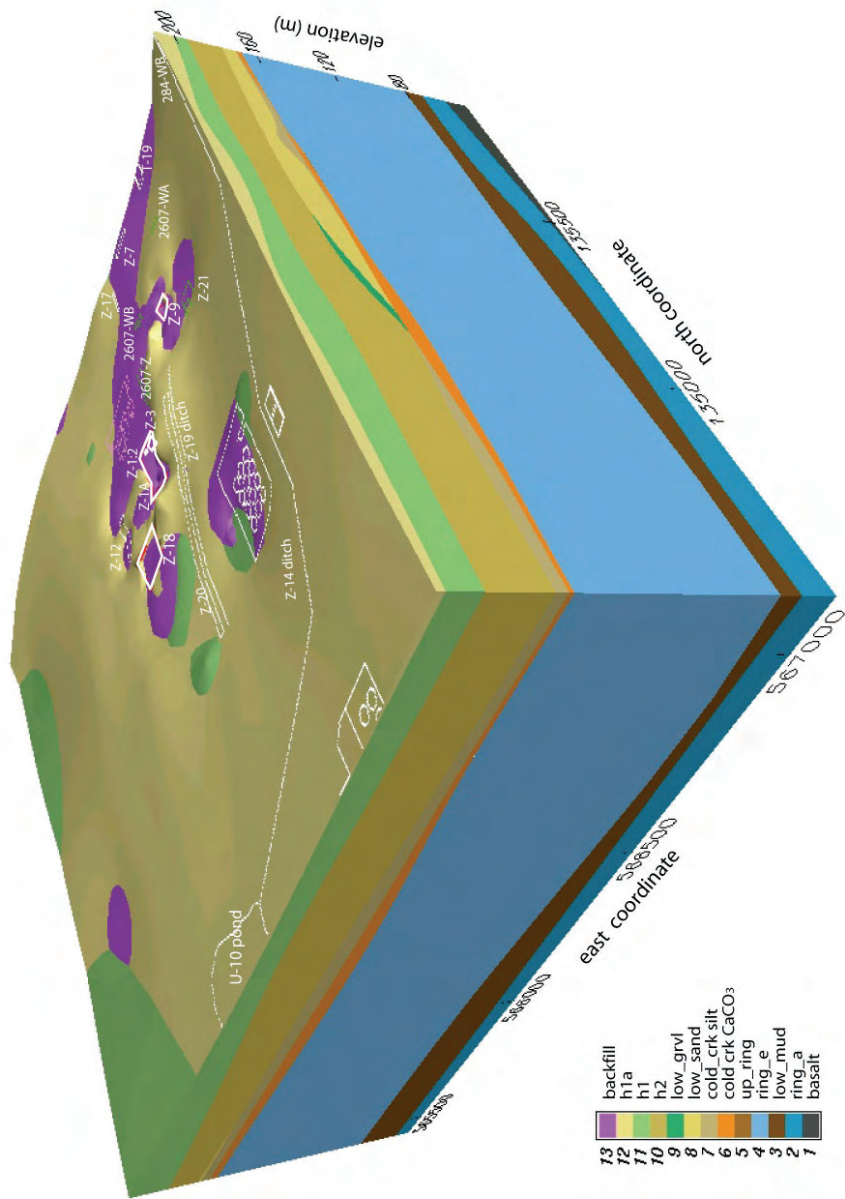
Figure 2.2. Three-Dimensional Geology of Large-Scale Model and Location of Major Waste Disposal Sites
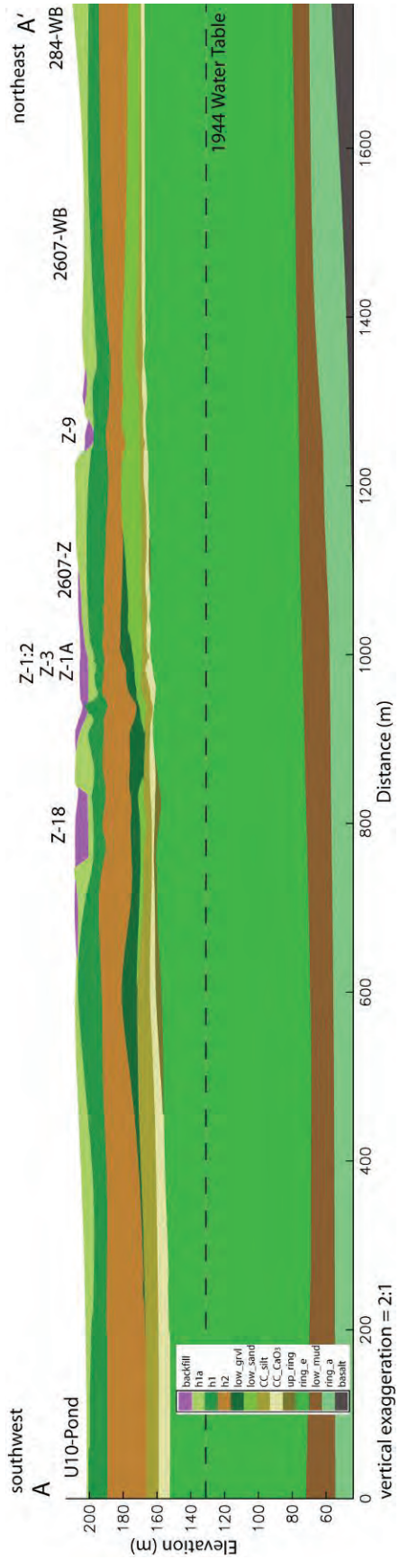
Figure 2.3. A-A' Cross Section Through the Large-Scale Model Domain
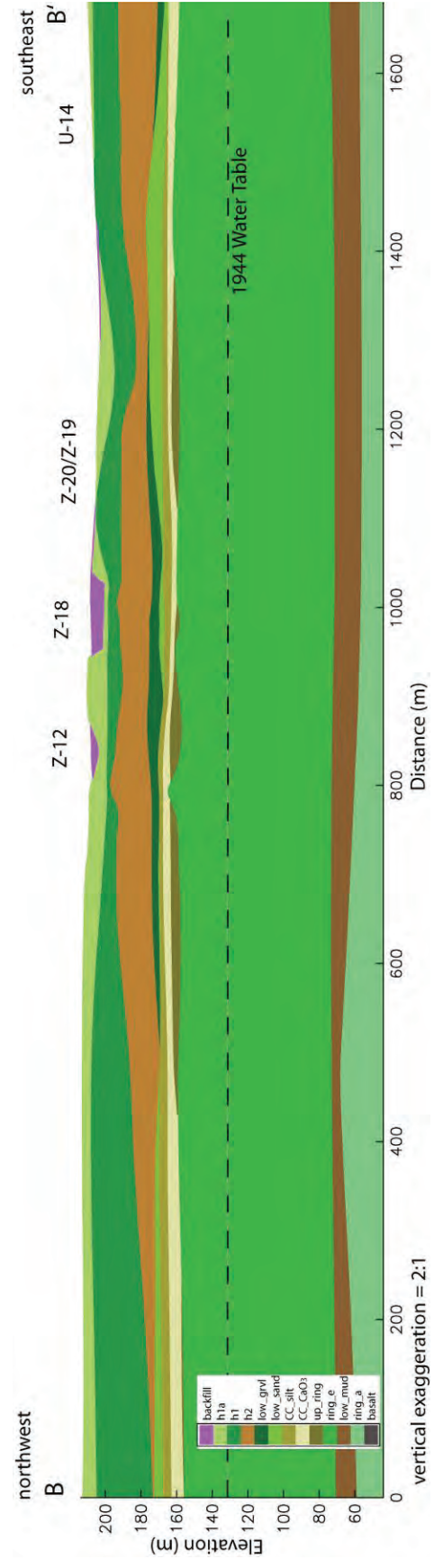
Figure 2.4. B-B' Cross Section Through the Large-Scale Model Domain

2.10
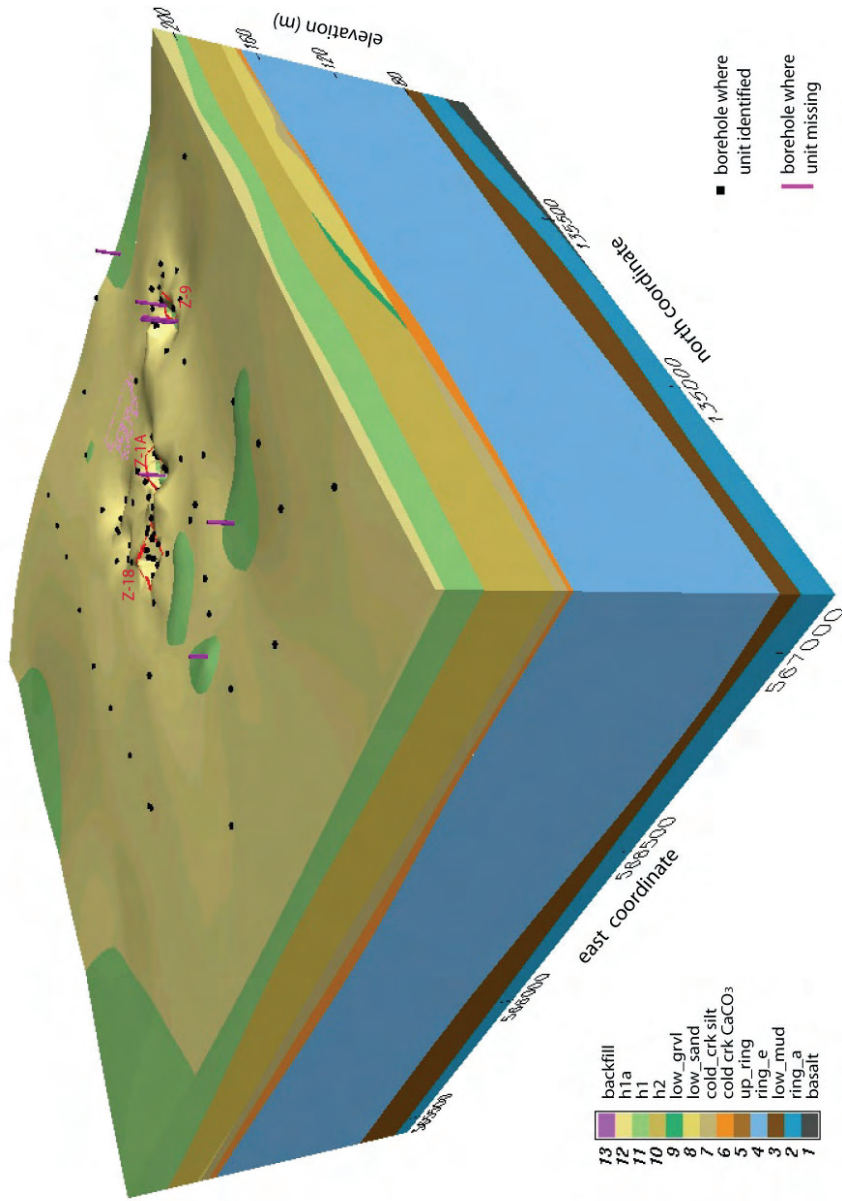
Figure 2.5. Representation of the Hanford Upper Fine (H1A) Unit in Geologic Model
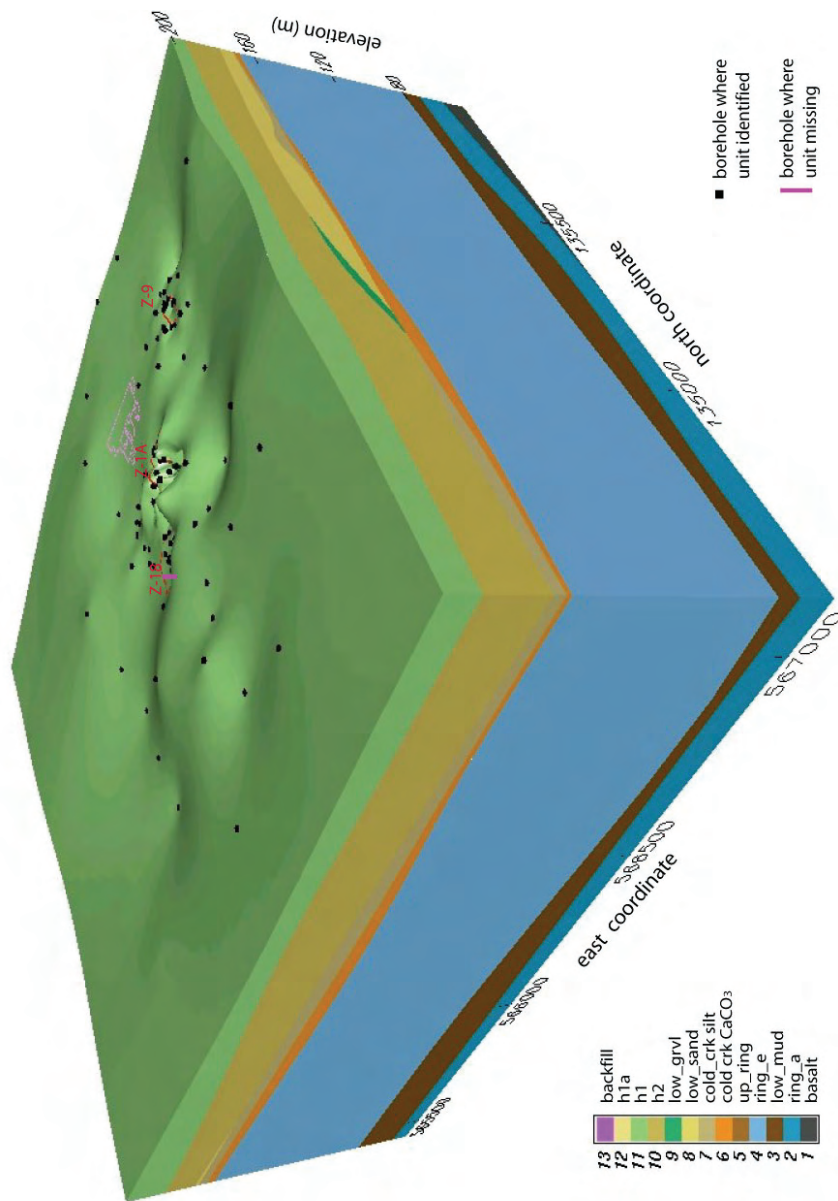
Figure 2.6. Representation of the Hanford 1 (H1) Unit in the Geologic Model
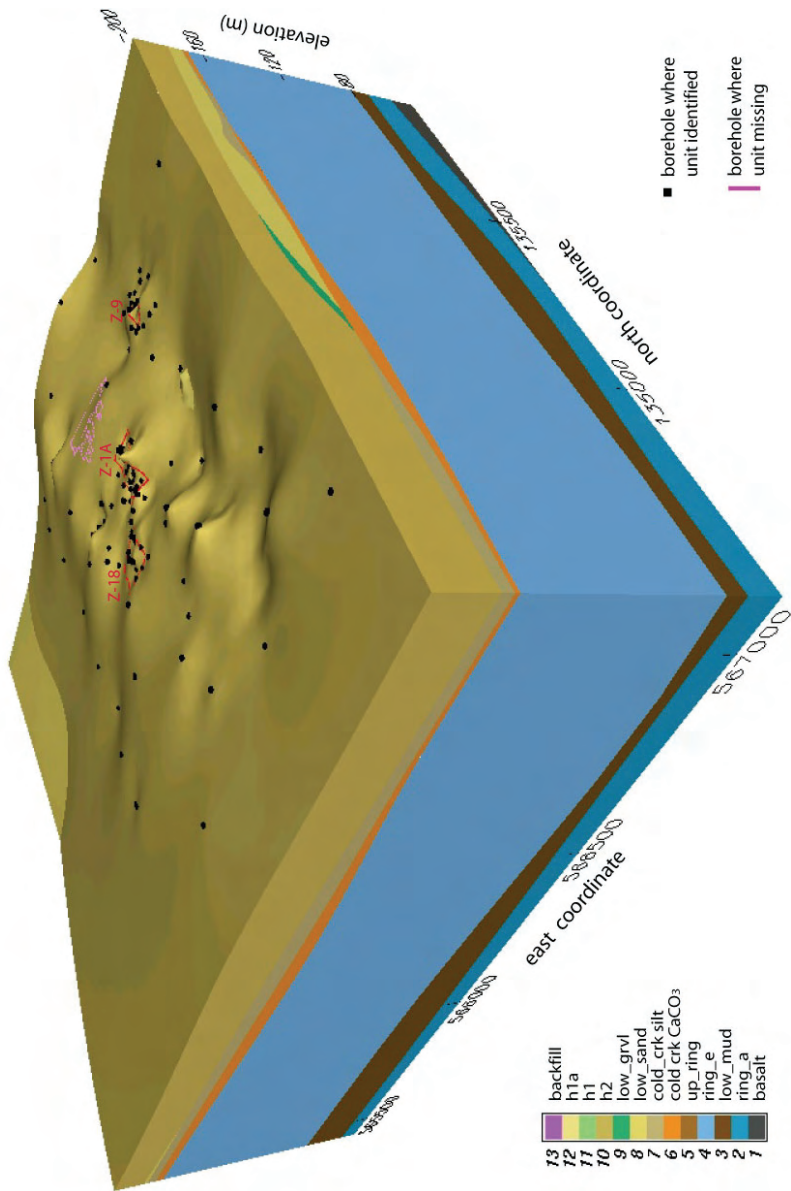
Figure 2.7. Representation of the Hanford 2 (H2) Unit in the Geologic Model

2.13
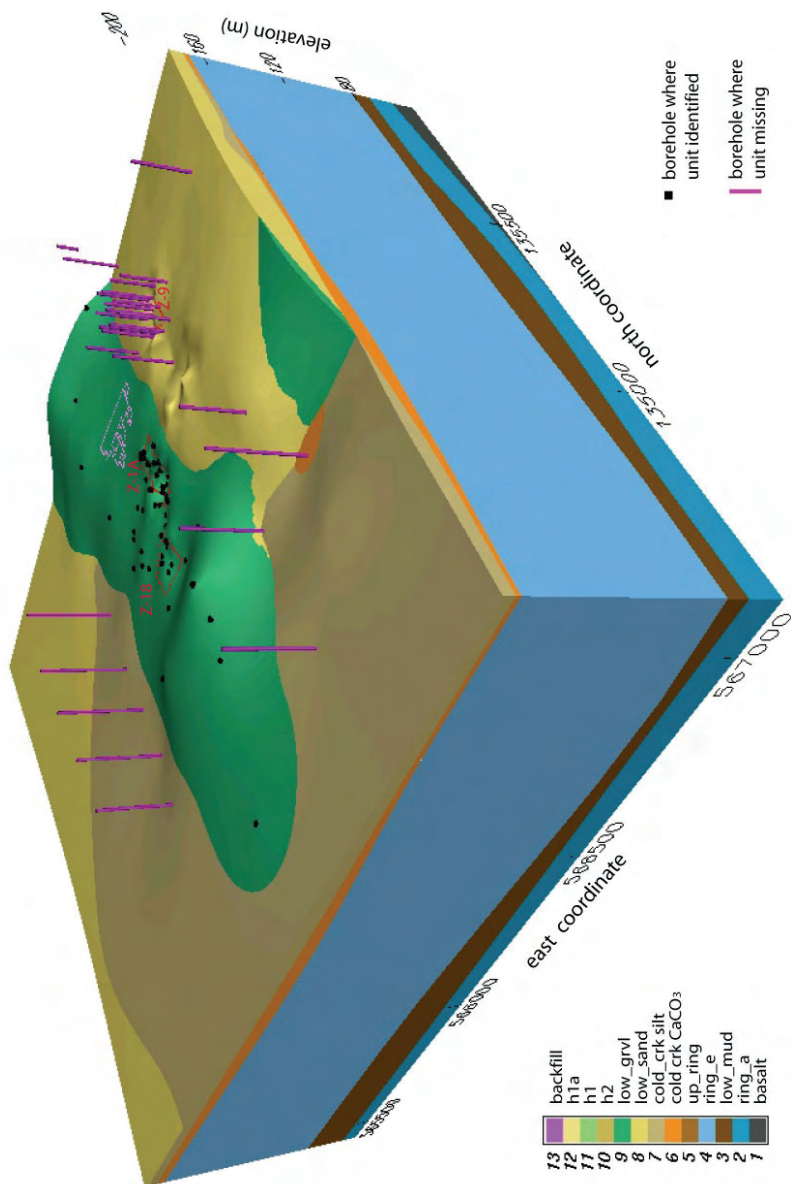
Figure 2.8. Representation of the Lower Gravel Unit in the Geologic Model

2.14
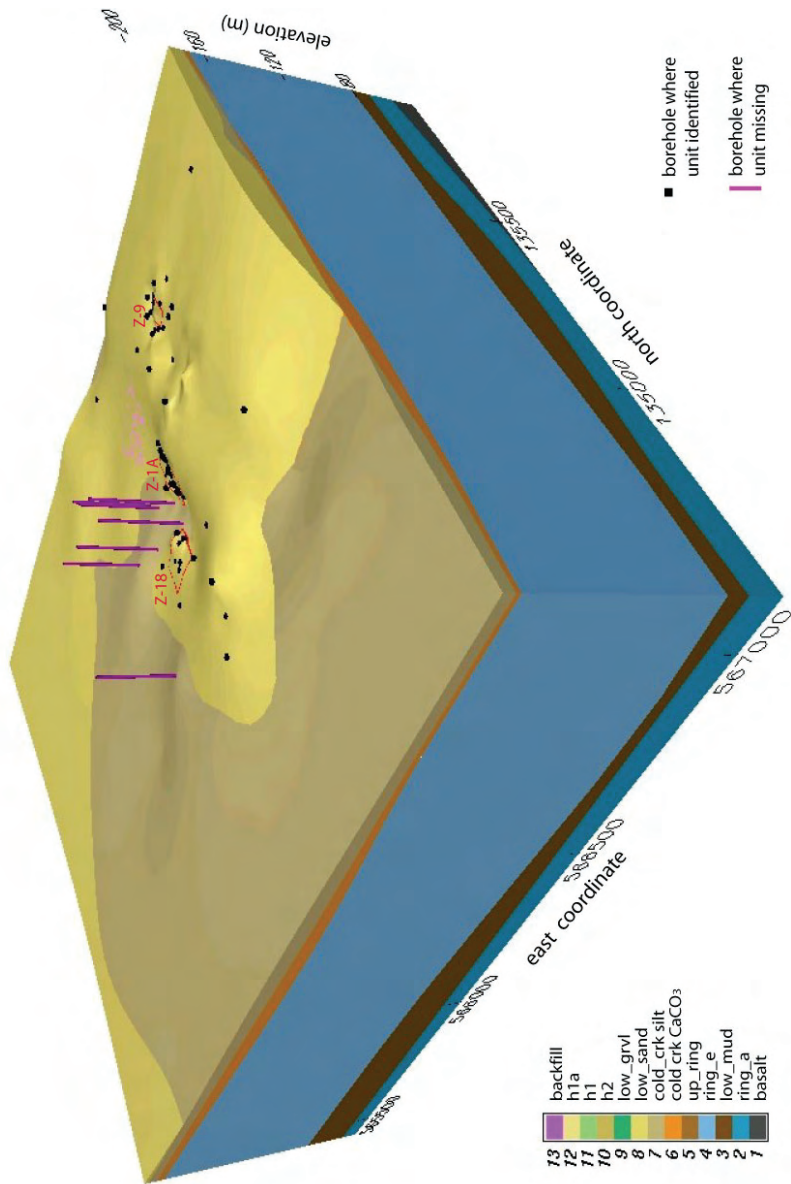
Figure 2.9. Representation of the Lower Sand Unit in the Geologic Model

2.15
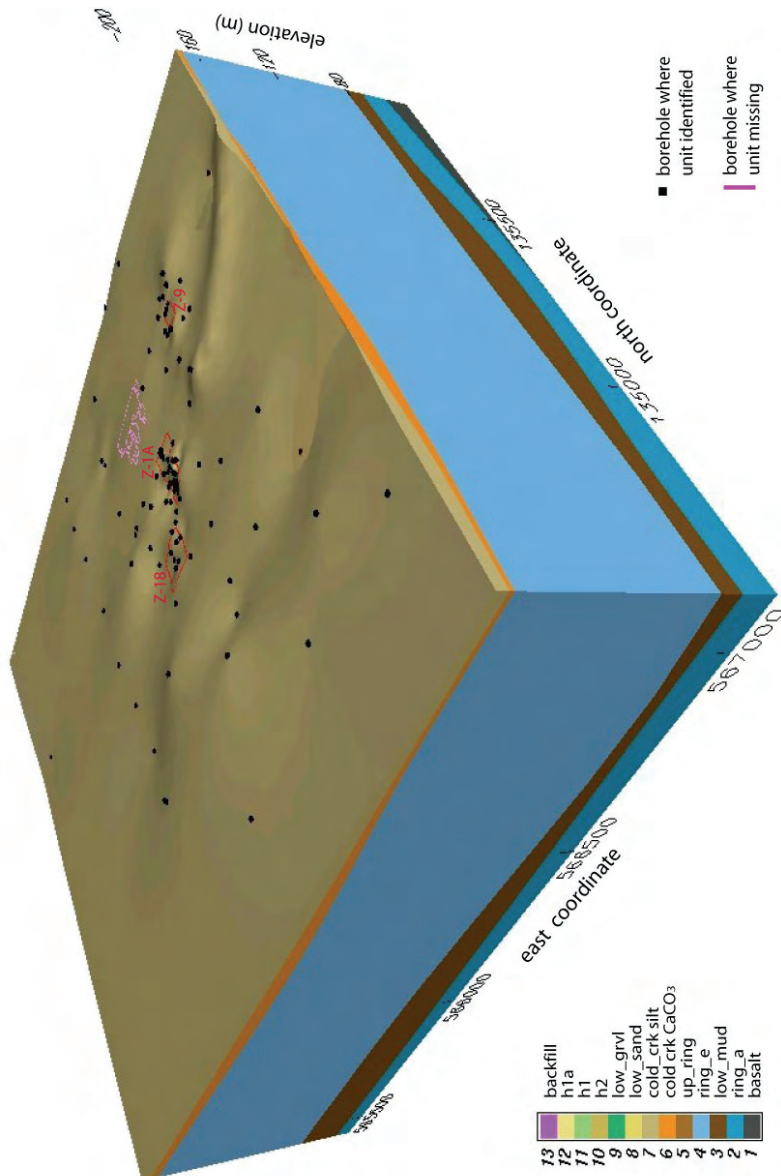
Figure 2.10. Representation of the Cold Creek Silt Unit in the Geologic Model
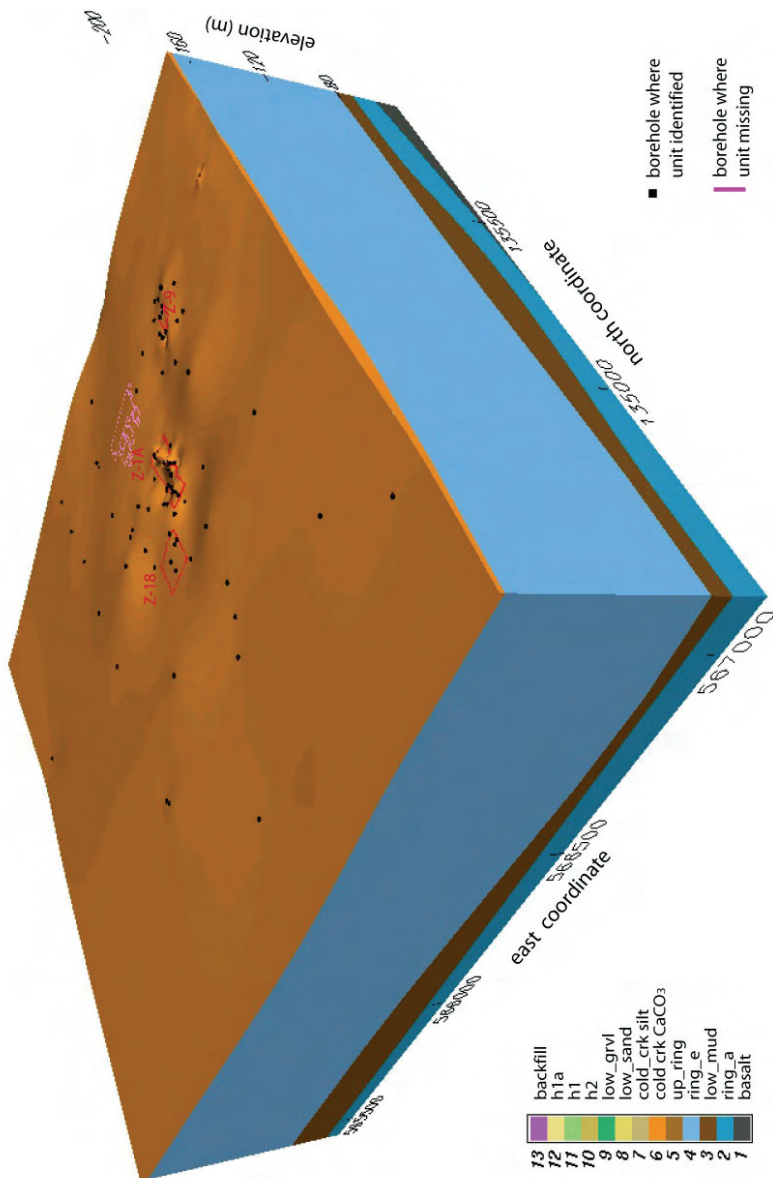
Figure 2.11. Representation of the Cold Creek Caliche Unit in the Geologic Model
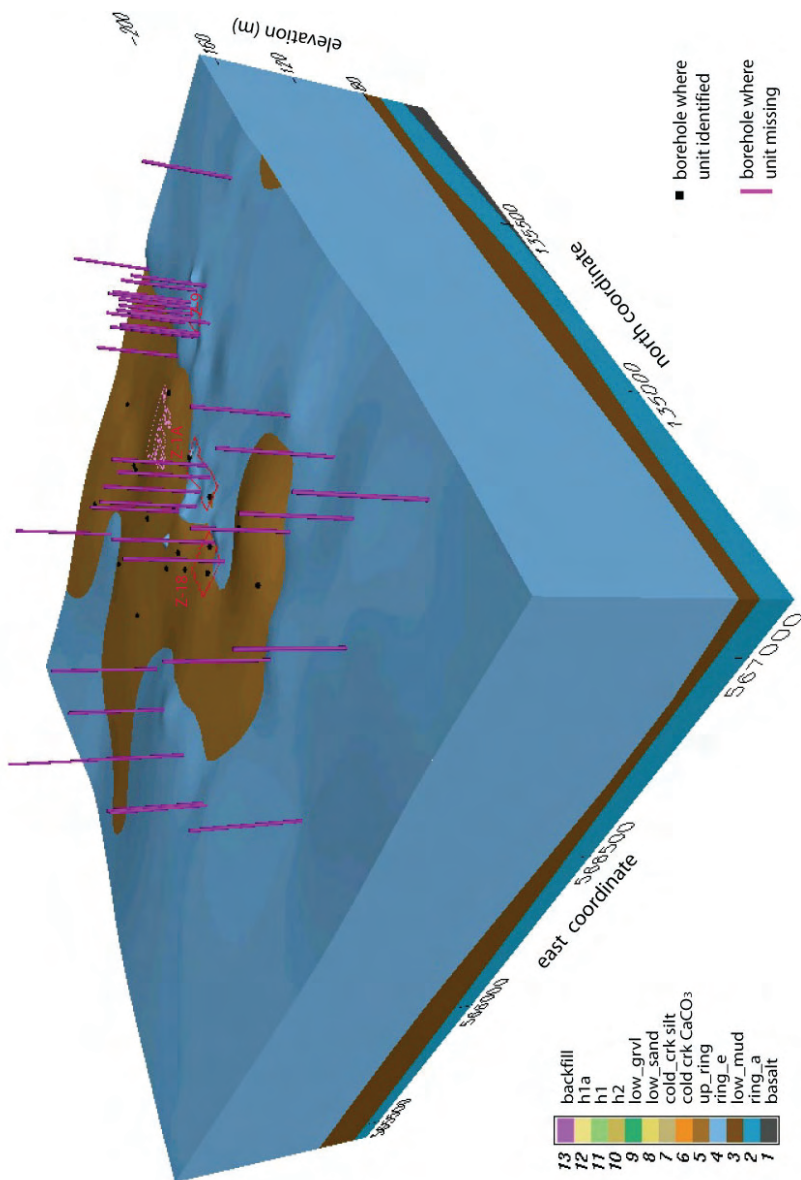
Figure 2.12. Representation of the Upper Ringold Unit in the Geologic Model

2.18
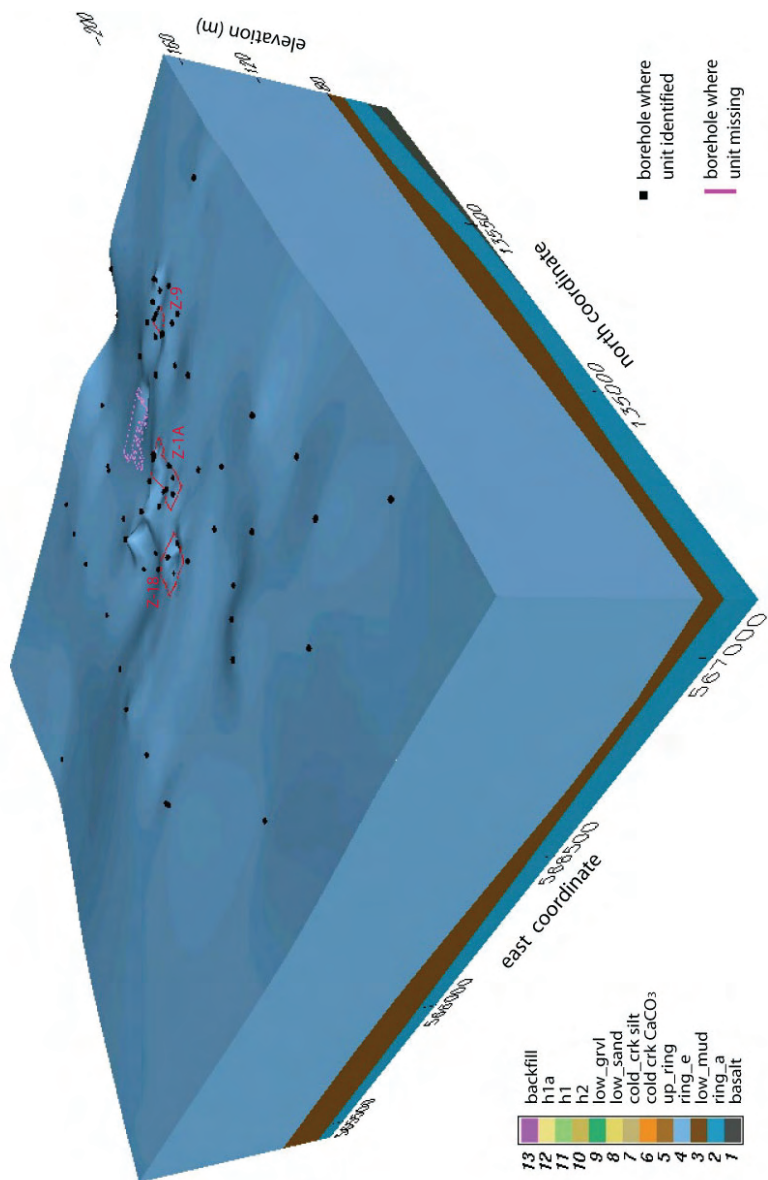
Figure 2.13. Representation of the Upper Ringold Unit in the Geologic Model

2.2.1.2   216-Z-9 Geologic Model

The geologic model for the 216-Z-9 site is similar to the model used by Oostrom et al. (2006b). The same hydrostratigraphy as for the large-scale model has been used. For the simulations in this report, a 1-ft-thick silt lens, 60-ft long in the east-west direction, and 80-ft long in the south-north direction was included. The silt layer is located approximately 65-ft below the surface, in the Hanford 2 layer. The position of this layer, referred to in this report as the "65-ft silt lens," is shown in Figure 2.14.

The EarthVision® model is displayed in Figures 2.14 through 2.16. Figure 2.14 shows the three-dimensional geologic model with a cut-out beneath the 216-Z-9 trench. Figures 2.15 and 2.16 show two dimensional north-south and east-west cross sections through the domain. The figures show that the EarthVision® interpretation yields layered system with minor undulations.
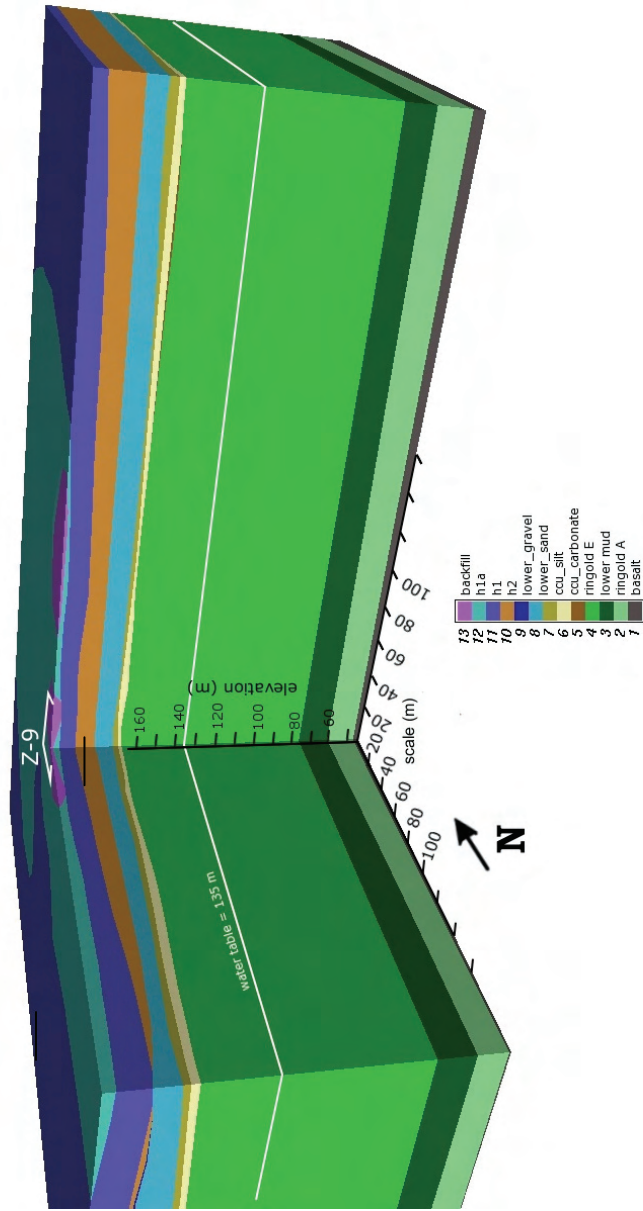
Figure 2.14. Three-Dimensional Geologic Model with a Cut-out Through the 216-Z-9 Trench. The Location of 65-ft-Silt Layer is Denoted as a Black Line in the Hanford 2 Unit Below the 216-Z-9 Disposal Site.
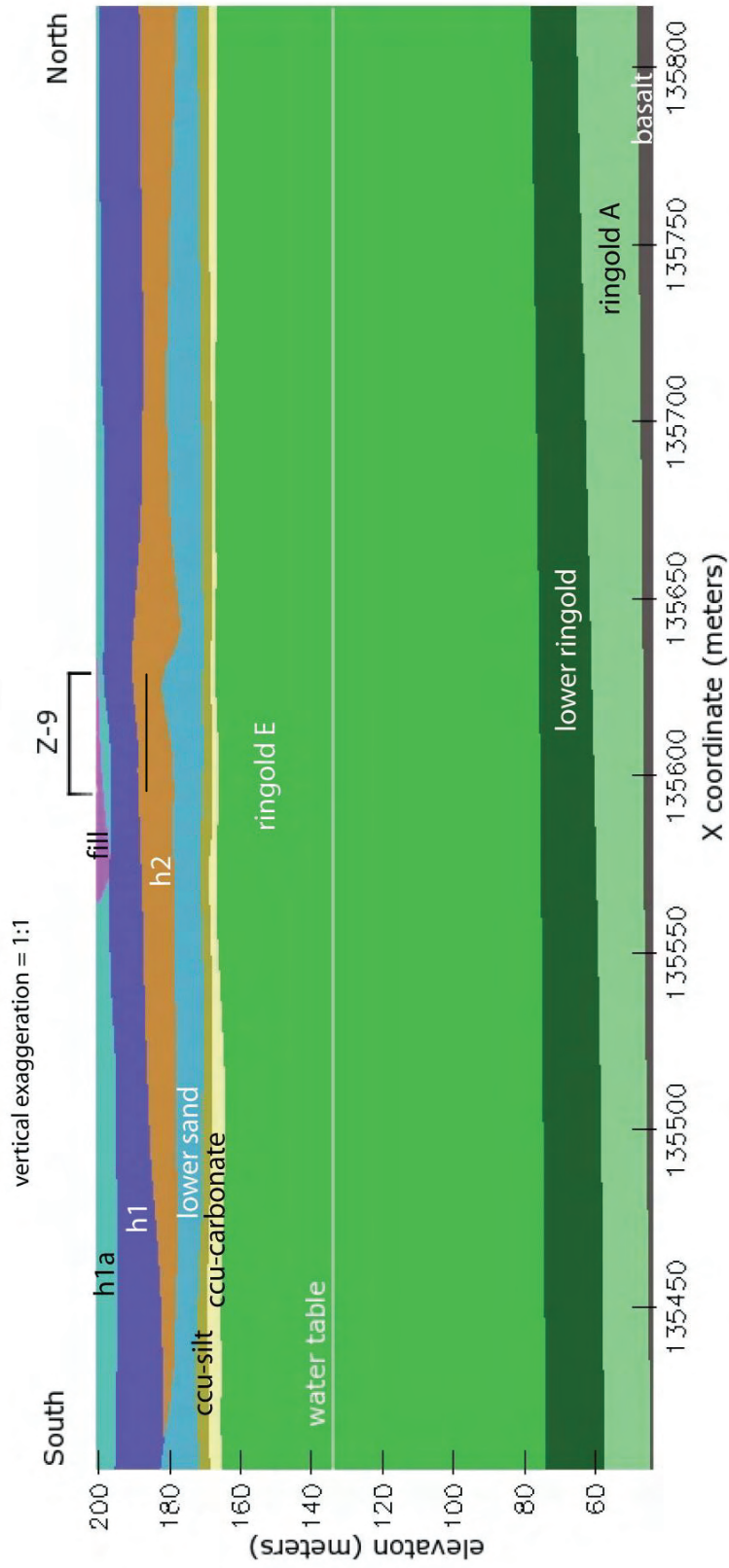
Figure 2.15. North-South Cross Section Through the 216-Z-9 Local Scale Computational Domain. The 65-ft-Silt Layer is Located in the Hanford 2 Unit Below the 216-Z-9 Disposal Site.
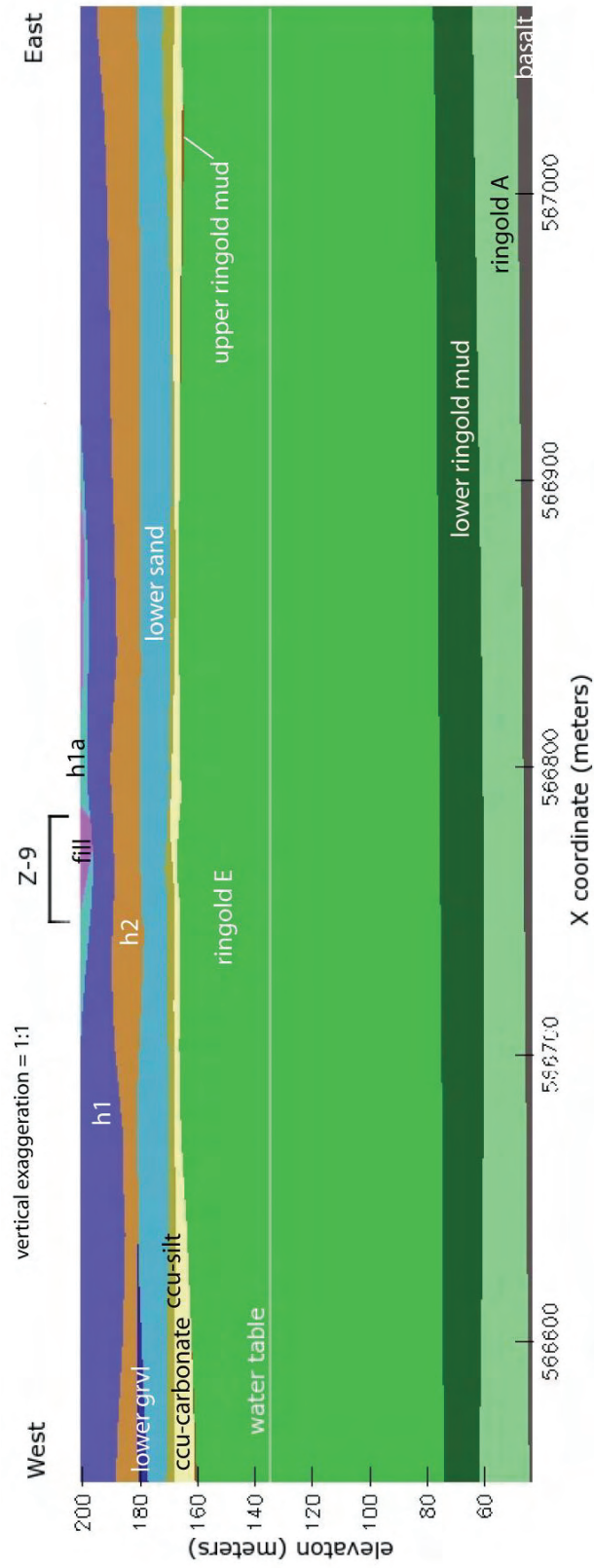
Figure 2.16. East-West Cross Section Through the 216-Z-9 Local-Scale Computational Domain. The 65-ft-Silt Layer is Located in the Hanford 2 Unit Below the 216-Z-9 Disposal Site.

2.23

3.0 Overview of Simulations

3.1 Large-Scale Model Configuration

The computational domain, with lengths in the x-, y-, and z-directions of 1429, 1711, and 159 m, respectively, was discretized into $125 \times 103 \times 60 = 772,500$ nodes. The basalt at a depth of -42 m was assumed to form an impermeable bottom boundary. Because the STOMP-WOA (water-oil-air) mode was used, this number of nodes translates into $3 \times 772,500 = 2,317,500$ unknowns.

DNAPL and Waste-Water Discharge Volumes and Times

DNAPL was assumed to originate from the 216-Z-9 (Table 3.1), 216-Z-18 (Table 3.2), and the 216-Z-1A (Table 3.3) disposal sites. DNAPL volumes reported in these tables are obtained from Anderson (1976) and Rohay et al. (1994). DNAPL mass numbers are computed by assuming on average fluid composition of 8.8% TBP, 14.7% DBBP, 2.9% lard oil, and 73.6% CT with a density of 1,426 kg/m^3. The sites with waste-water discharge only (no DNAPL) are listed in Table 3.4 (Anderson 1976, Oostrom et al. 2004). For the location of the various sites in the numerical model, the reader is referred to Figure 2.1. Half of the 216-U10 area, located in the south, and half of the 216-T-19 area, located in the north, are included in the model. The area of the 284-WB, located in the northwest, is included for 25%.

DNAPL Properties

Fluid properties were measured in the EMSL Subsurface Flow and Transport Experimental Laboratory based on an average fluid composition of 8.8% TBP, 14.7% DBBP, 2.9% lard oil, and 73.6% CT (Rohay et al. 1994).

- Density: 1,426 kg/m^3

- Viscosity: 1.11×10-3 Pa s

- Vapor pressure: 10,830 Pa

- Surface tension (air-DNAPL): 25.1 dynes/cm

- Interfacial tension (water-DNAPL): 15.2 dynes/cm

- CT aqueous-phase solubility: 720 mg/L

- CT gas phase concentration: 108,300 ppmv.

Porous Media Present In Domain (Bottom to Top)

- Ringold A
- Lower Mud
- Ringold E
- Upper Ringold
- Cold Creek C
- Cold Creek Z

- Lower Sand
- Lower Gravel
- Hanford 2
- Hanford 1
- Hanford 1a
- Backfill.

Table 3.1. Discharged Aqueous Waste and DNAPL Volumes for the 216-Z-9 Site.

Year	Aqueous Phase Volume (L)	DNAPL Volume (L)	DNAPL Mass (kg)
1955 (July–December)	2.55E5	5.12E3	7.30E3
1956	4.14E5	4.64E4	6.62E4
1957	4.94E5	4.64E4	6.62E4
1958	6.56E5	4.42E4	6.30E4
1959	5.13E5	4.73E4	6.75E4
1960	5.72E5	4.78E4	6.82E4
1961	7.07E5	6.34E4	9.04E4
1962 (January–June)	1.65E5	1.48E4	2.11E4
Total	**3.77E6**	**3.15E5**	**4.49E5**

Table 3.2. Discharged Aqueous Waste and DNAPL Volumes for the 216-Z-18 Site

Year	Aqueous Phase Volume (L)	DNAPL Volume (L)	DNAPL Mass (kg)
From 4/1969	5.50E5	2.20E4	3.14E4
1970	7.69E5	3.00E4	4.28E4
1971	8.84E5	3.40E4	4.85E4
1972	1.24E6	5.00E4	7.13E4
Through 4/1973	3.66E5	1.40E4	2.00E4
Total	**3.72E6**	**1.47E5**	**2.10E5**

Sorption

A linear equilibrium adsorption coefficient (K_d) of 0.2 mL/g was applied to all porous media (Oostrom et al. 2004; 2006a; 2006b).

Hydraulic Properties

Retention parameters, porosities, and hydraulic conductivities were obtained from Khaleel et al. 2001 and Khaleel and Freeman (1995). The published van Genuchten (1980) saturation-pressure parameters were converted to equivalent Brooks-Corey (1964) parameters using the algorithms presented by Lenhard et al. (1989). The Brooks-Corey (1964) parameter values are listed in Table 3.5.

Permeability Anisotropy Ratio

10:1

Table 3.3. Discharged Aqueous Waste and DNAPL Volumes for the 216-Z-1A Site

Year	Aqueous Phase Volume (L)	DNAPL Volume (L)	DNAPL Mass (kg)
1949	6.00E4	-	-
1950	1.00E5	-	-
1951	1.00E5	-	-
1952	1.00E5	-	-
1953	1.00E5	-	-
1954	1.00E5	-	-
1955	1.00E5	-	-
1956	1.00E5	-	-
1957	1.00E5	-	-
1958	1.00E5	-	-
1959	4.00E4	-	-
1960 - 4/1963	-	-	-
Z-1AA			
5/1964 - 12/1964	4.20E5	2.00E4	2.85E4
1965	9.20E5	4.10E4	5.85E4
1/1966 – 5/1966	5.40E5	2.52E4	3.59E4
Z-1AB			
6/1966 – 12/1966	9.60E5	4.48E4	6.39E4
1/1967 – 9/1967	9.40E5	3.94E4	5.62E4
Z-1AC			
10/1967 – 12/1967	2.53E5	1.06E4	1.51E4
1968	1.00E6	4.50E4	7.42E4
1/1969 – 4/1969	1.55E5	7.00E3	9.98E3
Total	**6.21E6**	**2.32E5**	**3.31E5**

Table 3.4. Disposal Periods and Volumes of Aqueous-Phase Disposal Sites

Site	Disposal Period	Total Volume (L)
216-T-19[a]	1951-1976	4.550E8
216-U-10[b]	1944-1985	1.628E11
216-U-14	1944-1996	3.201E9
216-Z-7	1947-1957 1965-1966	7.988E7
216-Z1:2	1949-1959	3.370E7
216-Z-3	1952-1959	1.785E8
216-Z-12	1959-1973	2.813E8
216-Z-17	1967-1968	3.679E7
216-Z-20	1979-1996	4.392E9
284-WB[c]	1979-1996	1.688E9
2607-WA	1968-2007	7.598E7
2607-WB	1963-1998	3.132E7
2607-Z	1949-1998	4.144E9
Total	--	1.774E11
Site	**Disposal Period**	**Total Volume (L)**
Total (Model)	--	9.450E10

Table 3.4 (cont.)

[a] Disposed into model: 2.28E8 L (1/2 of site area).
[b] Disposed into model: 8.14E10 L (1/2 of site area).
[c] Disposed into model: 4.22E8 L (1/4 of site area).

Boundary and Initial Conditions

On the top boundary, atmospheric gas pressure was assumed in conjunction with a 0.5 cm/yr water flux (recharge). DNAPL was allowed to move freely across all boundaries. The initial gas and aqueous-phase pressure distributions in the domain at 1944 were obtained by conducting a 10,000-yr simulation using a water table of 131.3 m for the whole domain. This level was obtained from the CFEST-SAC model, grid node 1581 (375 m × 375 m element). It was assumed that in 1944 no DNAPL was present in the domain. The DNAPL and aqueous-phase waste water were injected using Neumann-type boundary conditions. The southern and northern boundaries were zero flux boundaries for all phases. A constant water table of 131.3 m was imposed on the west and east.

A total of three simulations were completed. The base-case simulation used the hydraulic properties listed in Table 3.5. For the two sensitivity analyses the permeability of the Cold Creek Unit was decreased and the nonwetting fluid entry pressure was decreased according to Miller and Miller (1956) scaling principles. A listing of the properties used for these two simulations is presented in Table 3.6.

Table 3.5. Horizontal Saturated Hydraulic Conductivity (K_s), Porosity, and Retention Parameter Values (Brooks-Corey λ, h_d, and irreducible water saturation, s_{rl}) of Stratigraphic Units

Stratigraphic Units	K_s (cm/s)	Porosity	Brooks and Corey h_d (cm)	Brooks and Corey λ	s_{rl}
Ringold A	5.73E-3	0.0770	71.3	0.52	0.1299
Lower Mud	1.16E-8	0.0770	71.3	0.52	0.1299
Ringold E	5.73E-3	0.0770	71.3	0.52	0.1299
Upper Ringold	5.73E-3	0.0770	71.3	0.52	0.1299
Cold Creek C	6.72E-3	0.3203	36.3	0.61	0.2451
Cold Creek Z	1.48E-4	0.4238	120.0	0.79	0.0967
Lower Sand	1.87E-2	0.3359	4.7	0.78	0.0747
Lower Gravel	3.00E-2	0.2720	23.0	0.75	0.1471
Hanford 2	5.85E-3	0.3653	14.1	0.95	0.0846
Hanford 1	5.00E-2	0.1660	7.7	0.54	0.1386
Hanford 1A	5.98E-4	0.4478	58.1	0.71	0.1740
Backfill	1.5E-2	0.2620	22.0	0.36	0.3646

Table 3.6. Horizontal Saturated Hydraulic Conductivity (K_s), Porosity, and Retention Parameter Values (Brooks-Corey λ, h_d, and Irreducible Water Saturation, s_{rl}) of the Cold Creek Unit for the Base Case and Two Sensitivity Cases

Stratigraphic Units	Case	K_s (cm/s)	Brooks and Corey h_d (cm)
Cold Creek C	Base Case	6.72E-3	36.3
Cold Creek Z	Base Case	1.48E-4	120.0
Cold Creek C	Case 1	6.72E-4	114.8
Cold Creek Z	Case 1	1.48E-5	379
Cold Creek C	Case 2	6.72E-5	363
Cold Creek Z	Case 2	1.48E-6	1,200

Soil Vapor Extraction

Details of the field SVE campaigns for the 200-PW-1 Operable Unit, which includes the major Hanford CT sites (the 216-Z-9 trench, the 216-A-1A tile field, and the 216-Z-18 crib) were described by Rohay (2002) and are summarized in Oostrom et al. (2004; 2006a; 2006b). There are 46 wells available for SVE operation in this operable unit, with well diameters ranging from 5 to 20 cm. During the active SVE campaigns, each system extracted soil vapor simultaneously from multiple wells open either above and/or below the Cold Creek Unit. In addition to these SVE wells, 126 subsurface monitoring probes were installed to depths of up to 36 m below ground surface using a cone penetrometer and 87 shallow soil vapor monitoring probes were also installed at depths ranging from 1.2 to 1.8 m below ground surface.

Details regarding flow rates and extracted vapor concentrations for individual wells on selected days are given by Rohay (2002, Table B-3). Daily records of pumping rates for the well network, its hours of operation on each day, and the online well intervals were provided by Fluor Hanford, Inc.[2] These data were used in conjunction with information on the current screened intervals for each well in the well field to generate time-averaged flow rates that were applied as sink terms to represent SVE in the STOMP model.

Several modifications were made to STOMP to allow it to simulate the process of SVE more accurately and efficiently. These modifications included the addition of a fully coupled SVE well model to the code (White and Oostrom 2006) and incorporation of a model for a gas-slip phenomenon known as the Klinkenberg effect (Klinkenberg 1941). The well model partitions the volumetric air flow rates that are specified for each well or well interval such that the rate applied to each affected grid block is a fraction of the total flow rate, weighted by product of the gas permeability for the grid block and the length of the portion of the screened interval that overlaps the grid block. The Klinkenberg effect is an experimentally observed phenomenon. At low pressures, such as occur near well bores during SVE, the Klinkenberg effect results in increased gas permeability relative to the gas permeability that would be computed from the intrinsic permeability and fluid properties alone. In general, the Klinkenberg effect is more significant at lower pressures and in finer-grained porous media.

3.2   Local-Scale Simulations for 216-Z-9 Site

Six of the seven local-scale simulations, denoted with Imposed Case 1-6 in Table 3.7, have an initial CT distribution imposed in the 65-ft silt lens and/or the Cold Creek Unit. The imposed CT distributions are based on characterization data and the conceptual model in the Remedial Investigation report (DOE-RL 2006a). The seventh simulation used the local-scale model to simulate infiltration of CT at the disposal sites based on disposal inventory information, distribution in the subsurface through 1993, and the impact of SVE between 1993 and 2007. The removal of CT through SVE in this timeframe was terminated after 53,000 kg were extracted. This amount represents the CT mass that has been extracted from the subsurface of the 216-Z-9 site through 2005 (FHI 2006). All seven simulations predict future migration from 2007 through 2107. The simulation scenarios in Table 3.7 describe the specific simulations selected for prediction of future CT migration. Both types of simulation scenarios used the same hydrogeologic model, fluid and porous media properties, and numerical domain. The computational domain contains a 1-ft thick silt lens, located approximately 65 ft below the surface in the Hanford 2 formation, which was not found in the previous 216-Z-9 site simulations reported by Oostrom et al. (2004, 2006b). The approximately location of this layer is shown in Figures 2.14 – 2.16. This lens, denoted as the 65-ft silt lens, has an areal extent of ½ the area of the 216-Z-9 disposal site.

---

[2] Spreadsheet from V. J. Rohay, Fluor Hanford, Inc., Richland, Washington.

Table 3.7. Simulation Scenario Initial Conditions for the 216-Z-9 Disposal Site

Simulation and ID	Total DNAPL Input to Disposal Site (kg)	CT Imposed in Cold Creek Unit in 2007[a]	CT Imposed in 65-ft Silt Lens in 2007[b]	Total CT Mass in 2007 (kg)
Imposed Case 1 (IC-1)	Zero	350,000 µg/kg	350,000 µg/kg	607.4
Imposed Case 2 (IC-2)	Zero	35,000 µg/kg	35,000 µg/kg	90.0
Imposed Case 3 (IC-3)	Zero	3,500 µg/kg	3,500 µg/kg	9.0
Imposed Case 4 (IC-4)	Zero	350,000 µg/kg	Zero	585.2
Imposed Case 5 (IC-5)	Zero	Zero	350,000 µg/kg	22.2
Imposed Case 6 (IC-6)	Zero	5% DNAPL Saturation	5% DNAPL Saturation	20,122
Modeled Case 1 (MC-1)	450K (base case)	Zero	Zero	388,676
[a]Areal extent of imposed CT in the Cold Creek Unit is equal to the area of the 216-Z-9 disposal site.				
[b]Areal extent of imposed CT in the 65-ft silt lens is equal to one-half the area of the 216-Z-9 disposal site.				

   Cross-sections depicting the initial distribution of sorbed CT concentrations for imposed cases 1-5 are shown in Figure 3.1 – 3.5, respectively. The initial DNAPL saturations for imposed case 6 and modeled case 1 are shown in Figures 3.6 and 3.7, respectively.

   The computational domain, with lengths in the x-, y-, and z-direction of 540, 440, and 159 m, respectively, was discretized into $43 \times 42 \times 60 = 108,360$ nodes. The discretization of the local-scale and large-scale model is the same in this domain. The Basalt at a depth of -42 m was assumed to form an impermeable bottom boundary. Because the STOMP-WOA (water-oil-air) mode was used, this number of nodes translates into $3 \times 108,360 = 325,080$ unknowns.
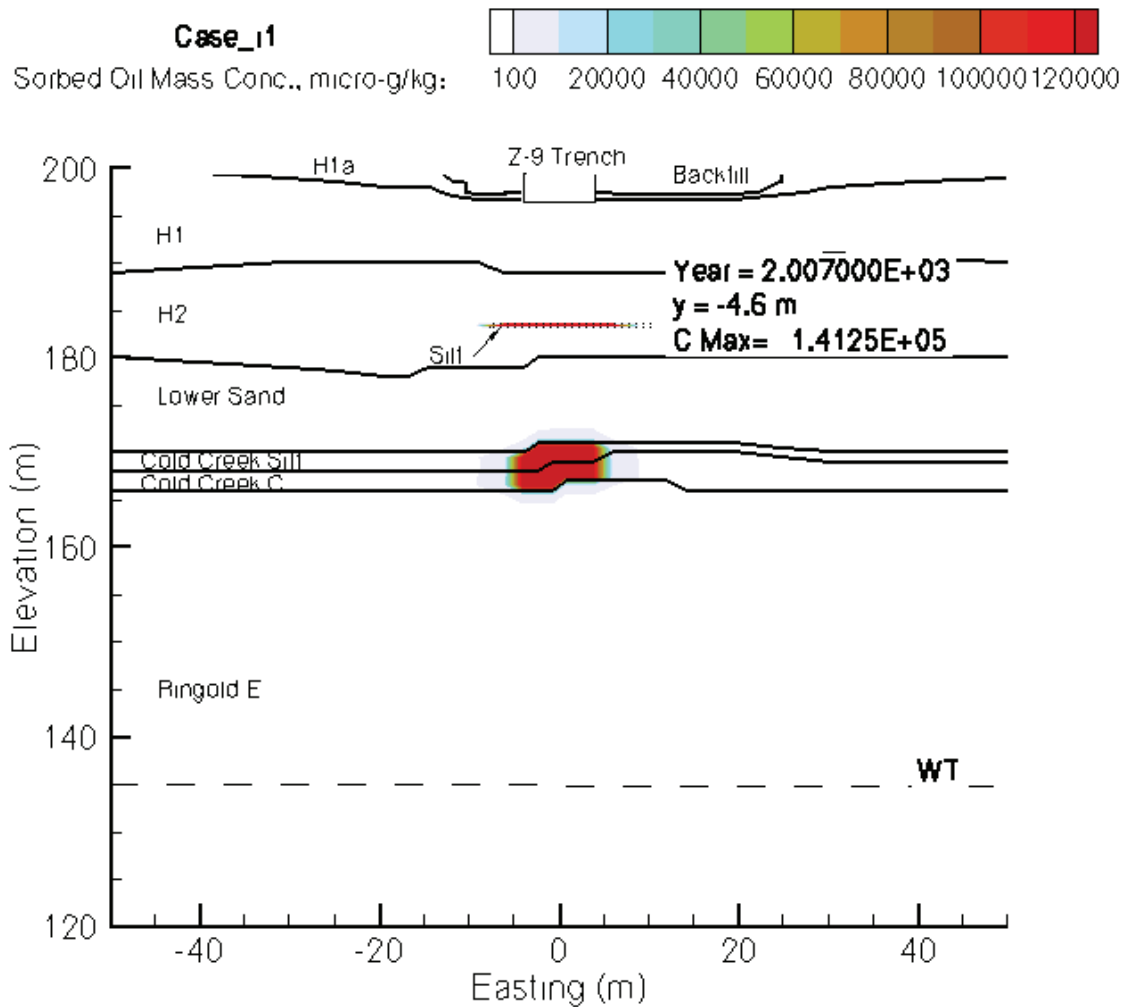
Figure 3.1. Sorbed CT Mass Concentration (μg/kg) at an Easting (y = -4.6 m) Cross-Section for Imposed Case 1. The center of the 216-Z-9 trench is located at (x, y) = (0, 0) m. The dashed line marked with WT denotes the water table.
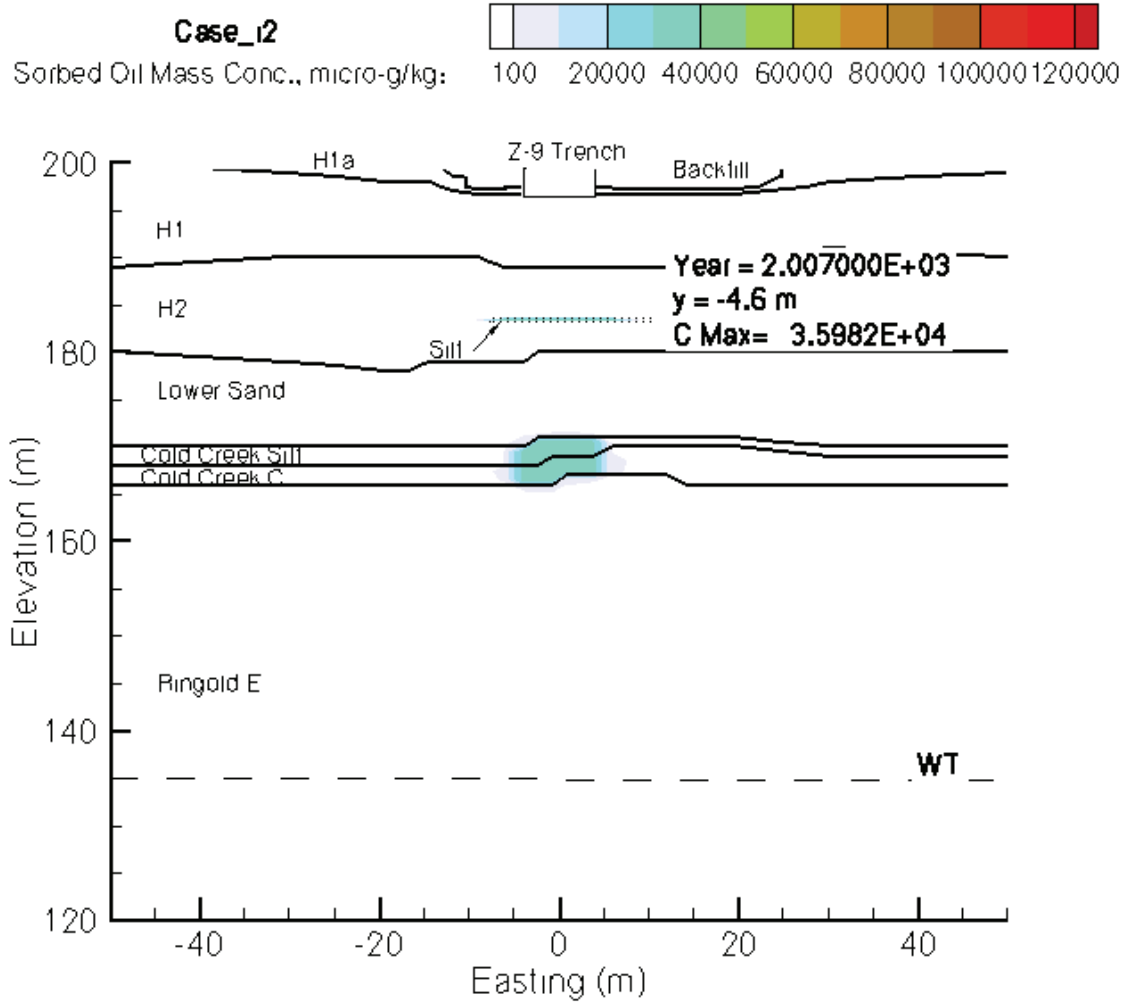
Figure 3.2. Sorbed CT Mass Concentration (μg/kg) at an Easting (y = -4.6 m) Cross-Section for Imposed Case 2. The center of the 216-Z-9 trench is located at (x, y) = (0, 0) m. The dashed line marked with WT denotes the water table.
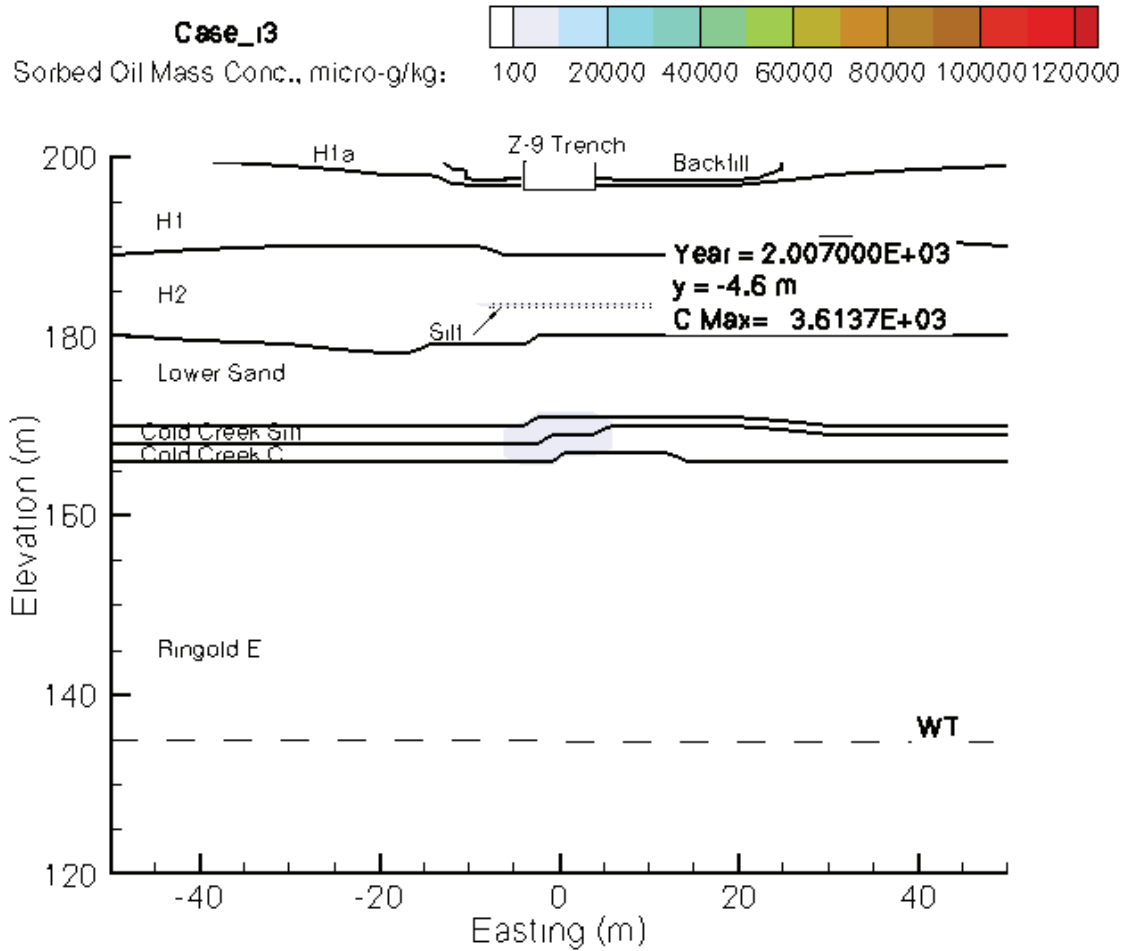
Figure 3.3. Sorbed CT Mass Concentration (µg/kg) at an Easting (y = -4.6 m) Cross Section for Imposed Case 3. The center of the 216-Z-9 trench is located at (x, y) = (0, 0) m. The dashed line marked with WT denotes for water table.
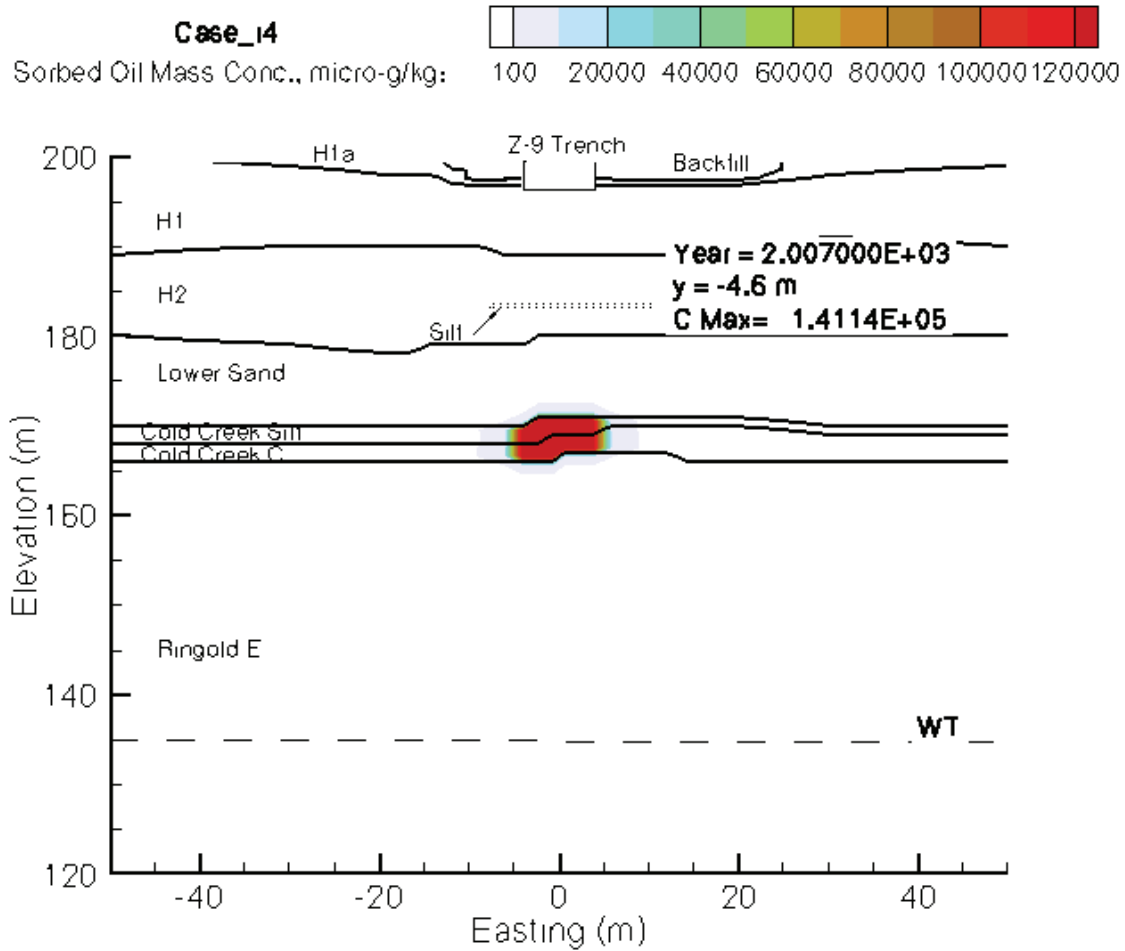
Figure 3.4. Sorbed CT Mass Concentration (μg/kg) at an Easting (y = -4.6 m) Cross-Section for Imposed Case 4. The center of the 216-Z-9 trench is located at (x, y) = (0, 0) m. The dashed line marked with WT denotes the water table.
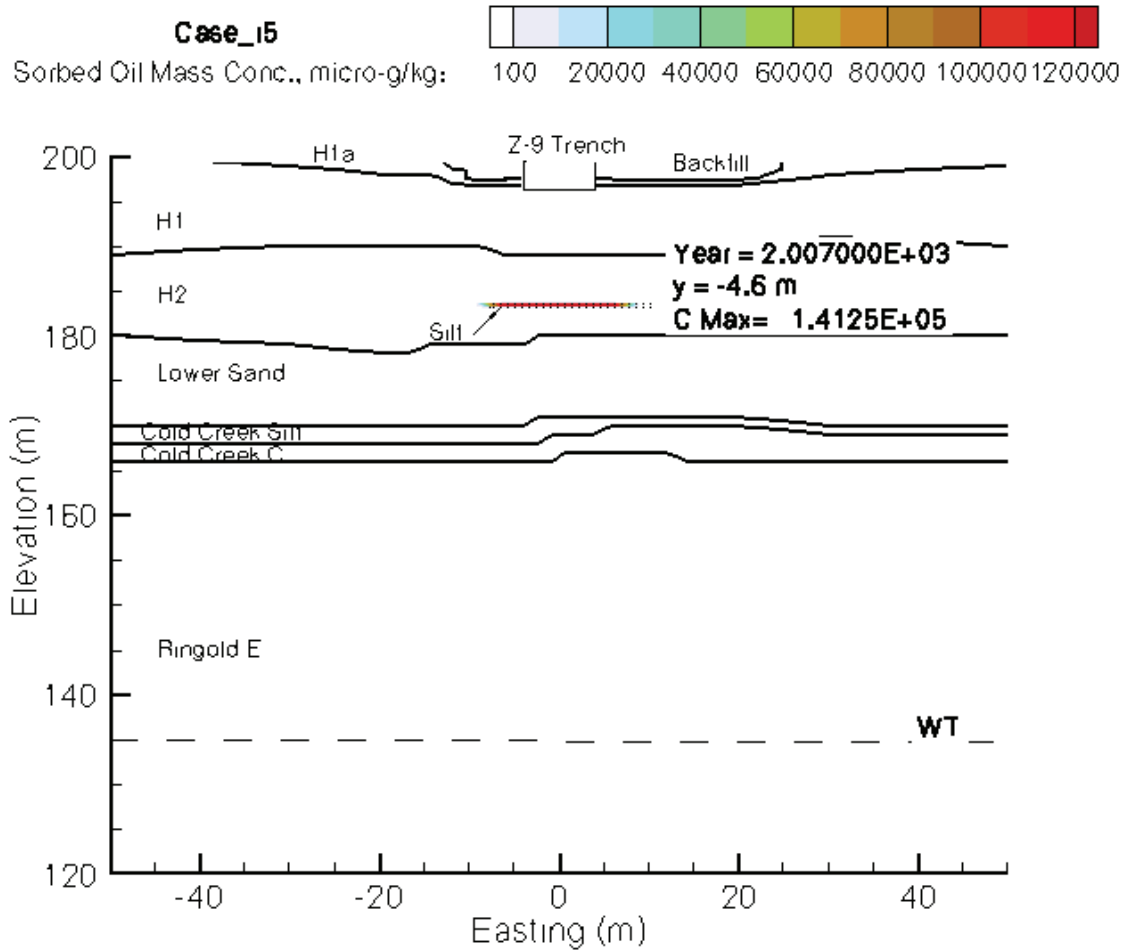
Figure 3.5. Sorbed CT Mass Concentration (µg/kg) at an Easting (y = -4.6 m) Cross-Section for Imposed Case 5. The center of the 216-Z-9 trench is located at (x, y) = (0, 0) m. The dashed line marked with WT denotes the water table.
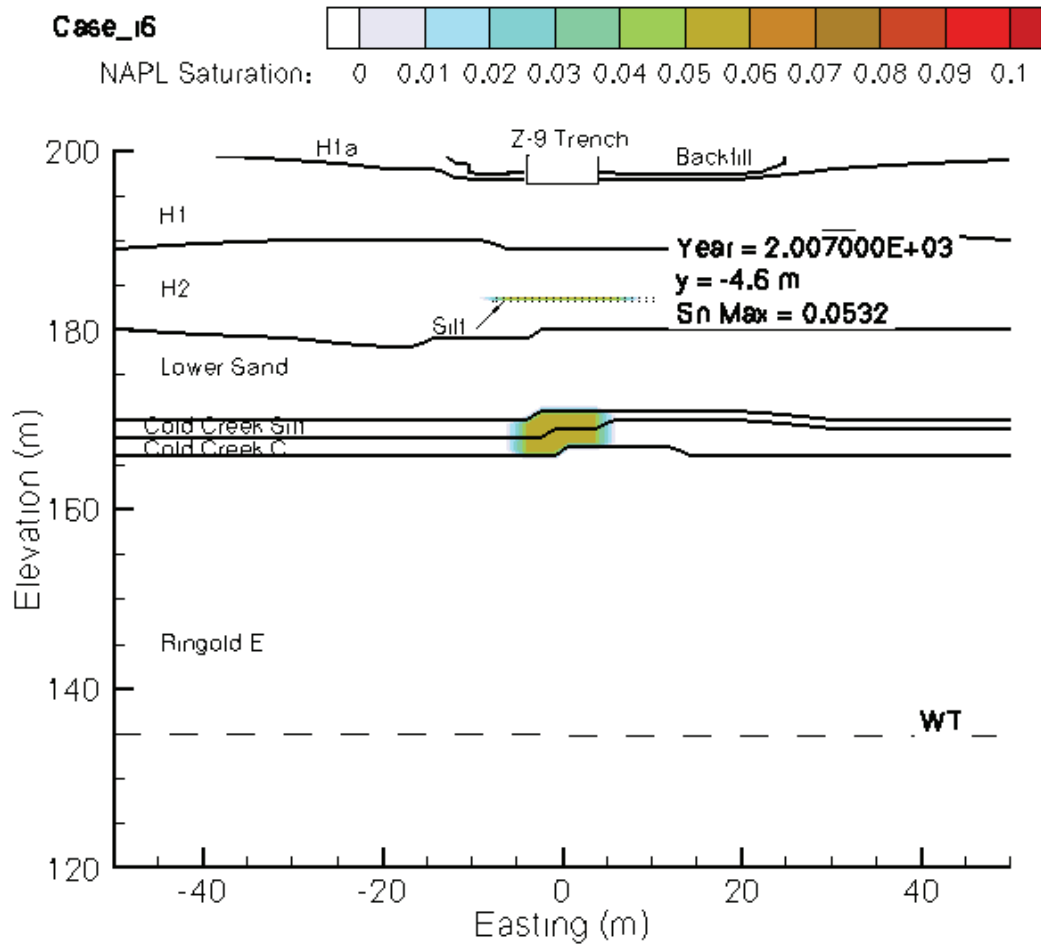
Figure 3.6. NAPL-Phase CT Saturation at an Easting (y = -4.6 m) Cross-Section for Imposed Case 6. The center of the 216-Z-9 trench is located at (x, y) = (0, 0) m. The dashed line marked with WT denotes the water table.
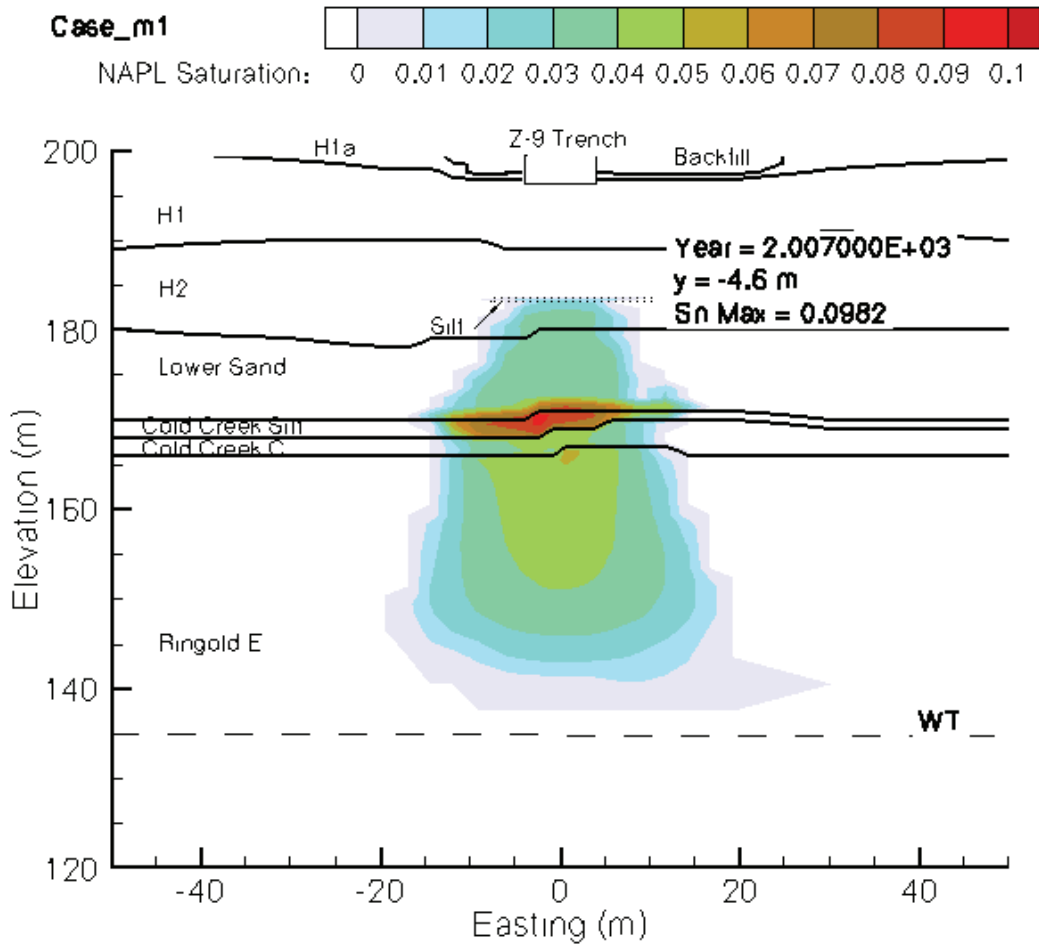
Figure 3.7. NAPL-Phase CT Saturation at an Easting (y = -4.6 m) Cross-Section for the Modeled Case. The center of the 216-Z-9 trench is located at (x, y) = (0, 0) m. The dashed line marked with WT denotes the water table.

The following characteristics are the same for all seven simulations.

216-Z-9 Trench Area

The bottom of the trench is 6.4 m below ground surface. The east-west (x), and north-south (y)-dimensions are 9.1 and 18.3 m, respectively.

DNAPL Properties

Fluid properties are measured in the laboratory based on average fluid composition of 8.8% TBP, 14.7% DBBP, 2.9% lard oil, and 73.6% CT.

- Density: 1,426 kg/m^3
- Viscosity: 1.11×10^{-3} Pa s
- Vapor pressure: 10,830 Pa

- Surface tension (air-DNAPL): 25.1 dynes/cm
- Interfacial tension (water-DNAPL): 15.2 dynes/cm.

Porous Media Present in Domain

- Ringold A
- Lower Mud
- Ringold E
- Upper Ringold
- Cold Creek C
- Cold Creek Z
- Lower Sand

- Lower Gravel
- 65-ft silt lens
- Hanford 2
- Hanford 1
- Hanford 1a
- Backfill.

Hydraulic Properties

Retention parameters, porosities, and hydraulic conductivities were obtained from Khaleel et al. 2001 and Khaleel and Freeman (1995). The published van Genuchten (1980) saturation-pressure parameters were converted to equivalent Brooks-Corey (1964) parameters using the algorithms presented by Lenhard et al. (1989). The Brooks-Corey relations were used in all simulations. The Brooks-Corey (1964) parameter values are listed in Table 3.8.

Table 3.8.   Saturated Hydraulic Conductivity (K_s), Porosity, and Retention Parameter Values (Brooks-Corey λ, h_d, and irreducible water saturation, s_{rl}) of Stratigraphic Units and 65-ft Silt Layer

Stratigraphic Units	K_s (cm/s)	Porosity	Brooks and Corey h_d (cm)	Brooks and Corey λ	s_{rl}
Ringold A	5.73E-3	0.0770	71.3	0.52	0.1299
Lower Mud	1.16E-8	0.0770	71.3	0.52	0.1299
Ringold E	5.73E-3	0.0770	71.3	0.52	0.1299
Upper Ringold	5.73E-3	0.0770	71.3	0.52	0.1299
Cold Creek C	6.72E-3	0.3203	36.3	0.61	0.2451
Cold Creek Z	1.48E-4	0.4238	120.0	0.79	0.0967
Lower Sand	1.87E-2	0.3359	4.7	0.78	0.0747
Lower Gravel	3.00E-2	0.2720	23.0	0.75	0.1471
65-ft Silt Lens	1.48E-4	0.4238	120.0	0.79	0.0967
Hanford 2	5.85E-3	0.3653	14.1	0.95	0.0846
Hanford 1	5.00E-2	0.1660	7.7	0.54	0.1386
Hanford 1A	5.98E-4	0.4478	58.1	0.71	0.1740
Backfill	1.5E-2	0.2620	22.0	0.36	0.3646

Sorption

A CT linear equilibrium partitioning coefficient (K_d) was applied to all porous media (Oostrom et al. 2004; 2006a; 2006b).

Permeability Anisotropy Ratio

10:1

For the modeled case, DNAPL and waste water were allowed to infiltrate into the domain between 1955.5 and 1962.5. The disposal characteristics are as follows:

DNAPL Volume

DNAPL volume = 3.16E5 L

DNAPL Infiltration Rates (Derived from Anderson 1976)

1955 (July-Dec) – 0.062 m/yr
1956 – 0.277 m/yr
1957 – 0.277 m/yr

1958 – 0.264 m/yr
1959 – 0.283 m/yr
1960 – 0.286 m/yr
1961 – 0.379 m/yr
1962 (Jan-Jun) – 0.178 m/yr.

Aqueous Phase Infiltration Rates (Derived from Anderson 1976):

1955 (July-Dec) – 3.04 m/yr
1956 – 2.47 m/yr
1957 – 2.95 m/yr
1958 – 3.92 m/yr
1959 – 3.07 m/yr
1960 – 4.42 m/yr
1961 – 4.23 m/yr
1962 (Jan-Jun) – 1.98 m/yr.

Boundary and Initial Conditions

The simulations for the six imposed cases lasted from 2007 – 2107. At the start of 2007, a total DNAPL mass corresponding to the amount listed in Table 3.7 was injected in the appropriate grid cells in the Cold Creek Unit and/or 65-ft silt lens in 1 hour. The boundary conditions for these simulations were not provided by the large-scale model. On the top boundary, atmospheric gas pressure was assumed in conjunction with a 0.5 cm/yr water flux. Hydraulic-gradient boundary conditions were imposed for the gas phase on all side-boundaries, allowing gas to move freely in and out of the domain. The humidity was kept at 0.54 (Hoitink et al. 2005). For the west and east boundaries, hydraulic gradient aqueous-phase boundary conditions of 1073403 and 992317 Pa were imposed. The pressures correspond to an average water table elevation was 135.4 m with a gradient of 1.40 m over the 540-m long domain (Hartman et al. 2006). To establish the 2007 conditions for these six scenarios, two preliminary simulations were conducted. First, the gas and aqueous-phase pressure distributions in the domain at 1954 were obtained by conducting a 10,000-yr simulation using the interpolated 1954 water levels (Oostrom et al. 2006b) at the south and north boundary and a recharge rate of 0.5 cm/yr. The second simulation included water infiltration at the disposal site from 1955.5 – 1962.5 according to the disposal inventory (Oostrom et al. 2006b). The simulation had a constant water table level of 143.69 m through 1993 based on the observed 1993 water table (Oostrom et al. 2006b). From 1993 until 2007, the water table was decreased linearly from the 1993 level to the observed level and gradient in 2006. Future migration of CT was simulated with a constant water table level and gradient based on the observed level and gradient in 2006. For the modeled case, boundary and initial conditions similar to those reported by Oostrom et al. (2004; 2006b) were used through 1993. Neumann boundary conditions were imposed for water and DNAPL discharges for the 216-Z-9 trench area during the years that these liquids were disposed. The flow rates are listed in the section associated with the specific input parameters for each simulation case. DNAPL was allowed to move freely across all boundaries. From 1993 through 2006, the water table was decreased in a similar fashion as for the imposed cases. During the period from 1993 to 2006, SVE was used to remove 53,000 kg CT from the subsurface. After this amount was removed, the SVE wells were turned off.

4.0   Large-Scale Model Simulation Results

4.1   Waste-water Infiltration and Redistribution

The water saturations in 1944, corresponding to the initial conditions, are shown in Figure 4.1 for cross section A-A' and in Figure 4.2 for cross section B-B'. Three-dimensional (3-D) plots of differences in water saturation (10% difference contour) at the end of 1953, 1962.5, 1974, 1985, 1993, and 2007, and the initial water saturations in 1944, are shown in Figures 4.3 through 4.8, respectively. Two-dimensional (2-D) plots of the water saturation differences for the same years and 1944 are shown in Figures 4.9 through 4.14 for cross section A-A' and in Figures 4.15 to 4.20 for cross section B-B'. As opposed to the 3-D figures that only show the 10% water difference contour, the 2-D cross section plots show the range of simulated water saturation differences. The cross section locations are shown in Figure 2.1.

In 1953, discharge at the 216-Z1:2, located in the footprint of the 216-Z-1A disposal site had stopped, while disposal at the 216-Z-3 site, also within the 216-Z-1A footprint, was initiated. As is shown in Figure 4.3, besides from the mentioned sites, disposal at this time occurred at the 216-T-19, 216-Z-7, and 2607-Z disposal sites, the 216-U-10 pond, and the 216-U14 ditch. The plot shows the large impact of the 216-U-10 pond in terms of area influenced by the high disposal volume at the site, which is at least two orders of magnitude larger than at the other sites (see Table 3.4). This figure also indicates that discharge from the sites, except for the 216-U-10 pond, is primarily vertical. Figure 4.9, for cross-section A-A', confirms the large subsurface area affected by the 216-U-10 pond and the primarily vertical movement of the aqueous waste at the other sites. The B-B' cross section at the same time (Figure 4.15) shows that water from the 216-U-10 pond has reached the water table at this location, only 9 years after discharge at the site was initiated.

In 1962.5, disposal at the 216-Z-9 trench, the primary CT disposal site, was terminated. At this time (Figure 4.4), waste was also discharged at the 216-Z-12 site, while no aqueous phase discharge occurred at the 216-Z1:2 and 216-Z-3. Figure 4.10 shows the water saturation changes below the 216-Z-9 and the drainage below the 216-Z1:2 and 216-Z-3. It is of interest to note that the water saturation differences caused by the disposal at the 216-U-10 have come to a steady-state by this time since observed differences between the situation at 1953 (Figure 4.9) and 1962.5 (Figure 4.10) are minimal. Figure 4.16 (cross section BB'), clearly shows the discharge from the 216-Z-12 site and the disposal at the 216-U-14 ditch.

In 1974, CT disposal was ended at the 216-Z-18 site (Table 3.3). CT discharge at 216-Z-1A occurred from 1964 – 1969 (Table 3.3). The 3-D water saturation differences between 1974 and 1944 (Figure 4.5) show the nearly vertical movement of water discharged from 216-Z-18 and water drainage below 216-Z-1A, 216-Z-7, and 216-Z-17. Contributions from the 2607-WA (starting in 1968) and 2607-WB (starting in 1963) are also apparent in this figure. The latter two sites stopped receiving waste in 1966 and 1968, respectively. The aqueous phase discharge from the 216-Z-18 is also observed in the 2-D plots (Figure 4.11 and 4.17).

By the next highlighted time, 1985, disposal at the 216-U-10 pond stopped. At this time, no discharges occurred anymore at 216-T-19 and 216-Z-12. In 1979, disposal operations started at 216-Z-20 and 284-WB. The effects on water saturation from these two sites are shown in Figure 4.6 (3-D),

Figure 4.12 (cross section A-A'), and Figure 4.18 (cross section B-B'). The contribution from 216-Z-20 is especially considerable.

In 1993 (Figure 4.7), the continued discharge from 216-Z-20, 284-WB, 2607-WA, 2607-WB and 2607-Z can be observed. The same plot also shows the drainage of the water that was previously disposed at the 216-U-10 pond. The drainage of that waster is also obvious in the two cross sections for this time (Figures 4.13 and 4.19).

In 2007, only discharge from 2607-WA was considered. As is shown in Figure 4.8, 4.14, and 4.20, most water previously discharged from the other sites has moved to the water table. Only some minor water saturation differences are still noticeable in the Cold Creek Unit.

Differences in water saturations for Case 2 are shown in Figures 4.21 – 4.26 for cross section A-A' and in Figures 4.27 - 4.32 for cross section B-B'. Differences in water saturations for Case 3 are shown in Figures 4.33 – 4.38 for cross section A-A' and in Figures 4.39 - 4.44 for cross section B-B'. For both cases, the plots are shown for 1953, 1962.5, 1974, 1985, 1993, and 2007, allowing for a direct comparison with the results for the base case in Figures 4.9 – 4.14 for cross section A-A' and Figures 4.15 – 4.20 for cross section B-B'. The main difference between the two sensitivity simulations and the base case is the impact of the water discharged from the 216-U-10 pond. The simulations with the lower Cold Creek Unit permeabilities and larger nonwetting fluid entry pressure caused more spreading of the discharged water and considerable higher saturations not only in the Cold Creek Units but also in the units above and below. For Case 2, the water from the 216-U-10 pond migrates into the vadose zone to below the 216-Z-9 disposal site, which is a distance of more than 1000 m. For Case 3, the water is able to move beyond 2607-WA site in the northwest of the computational domain. As for the base case, the extent of water originating from the 216-U-10 pond for each case was fairly constant over time until the discharge at this site was terminated.
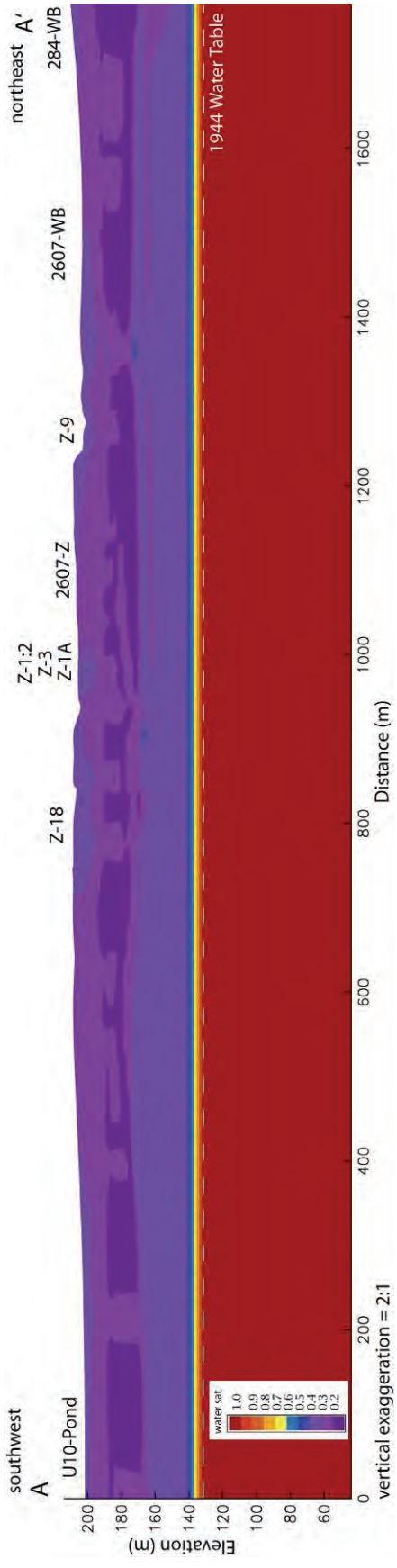
Figure 4.1. Initial Water Saturations for Cross-Section A-A'
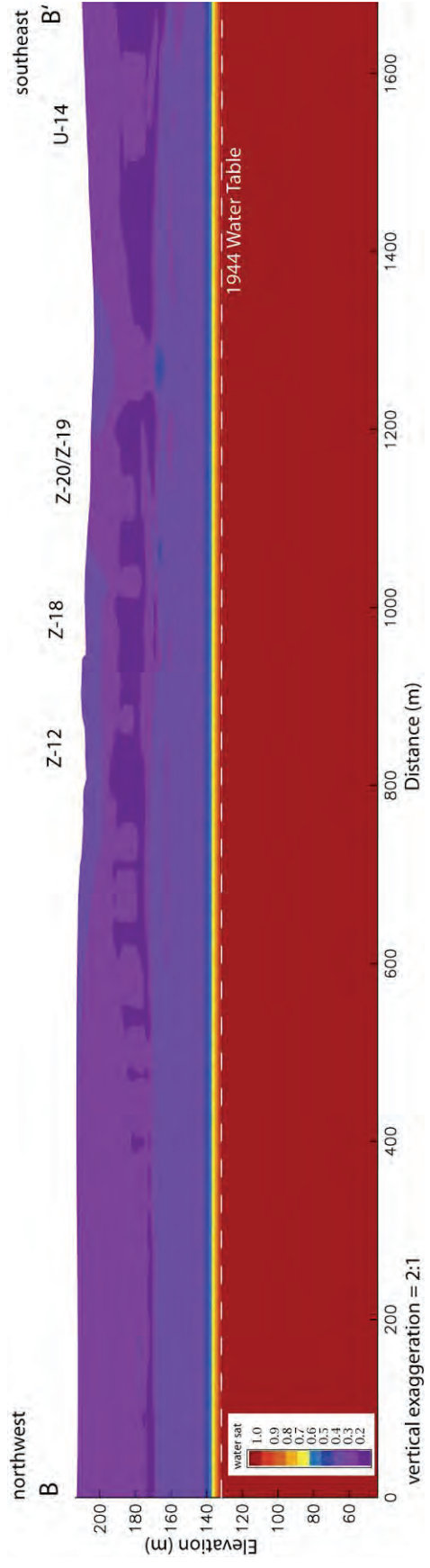
Figure 4.2. Initial Water Saturations for Cross-Section A-A'

4.3

Figure 4.3. Differences in Water Saturation (10% Contour) Between 1953 and 1944 (Initial Conditions)

4.4
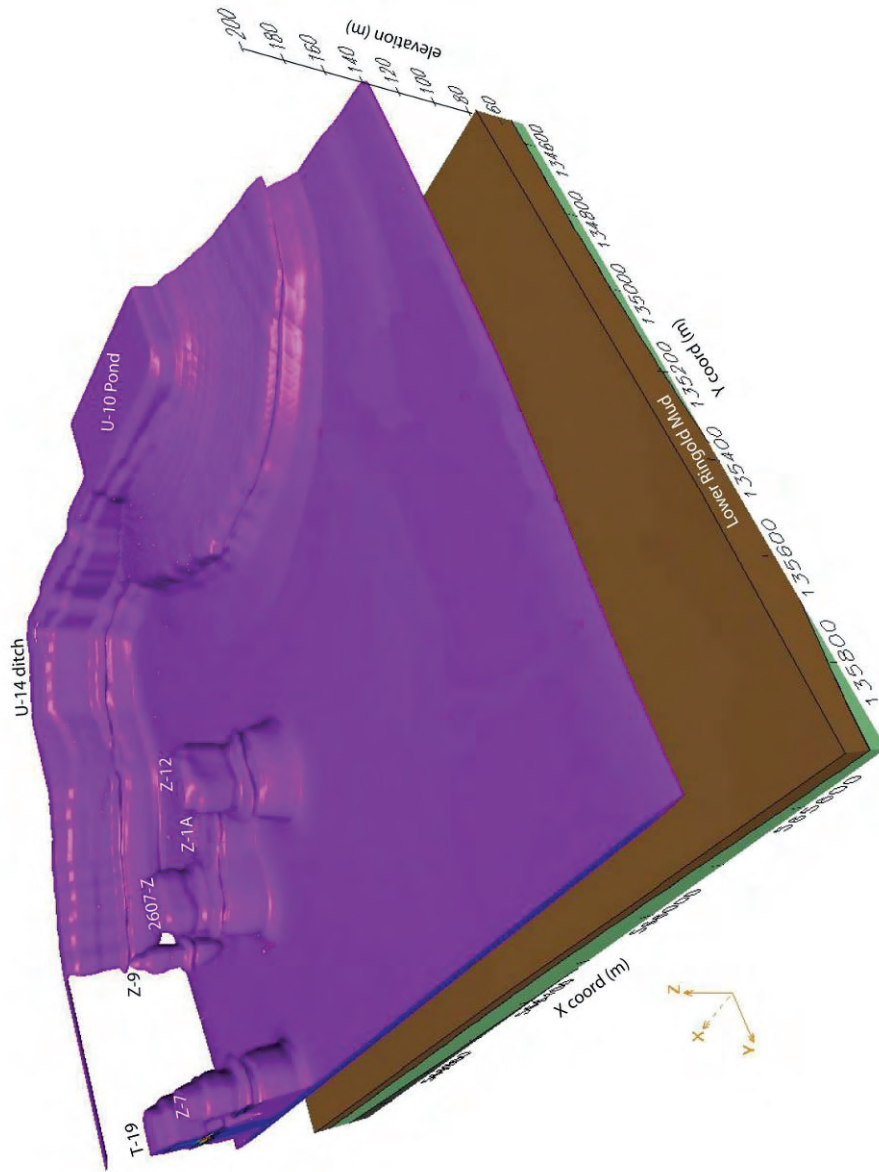
Figure 4.4. Differences in Water Saturation (10% Contour) Between 1962.5 and 1944 (Initial Conditions)

4.5
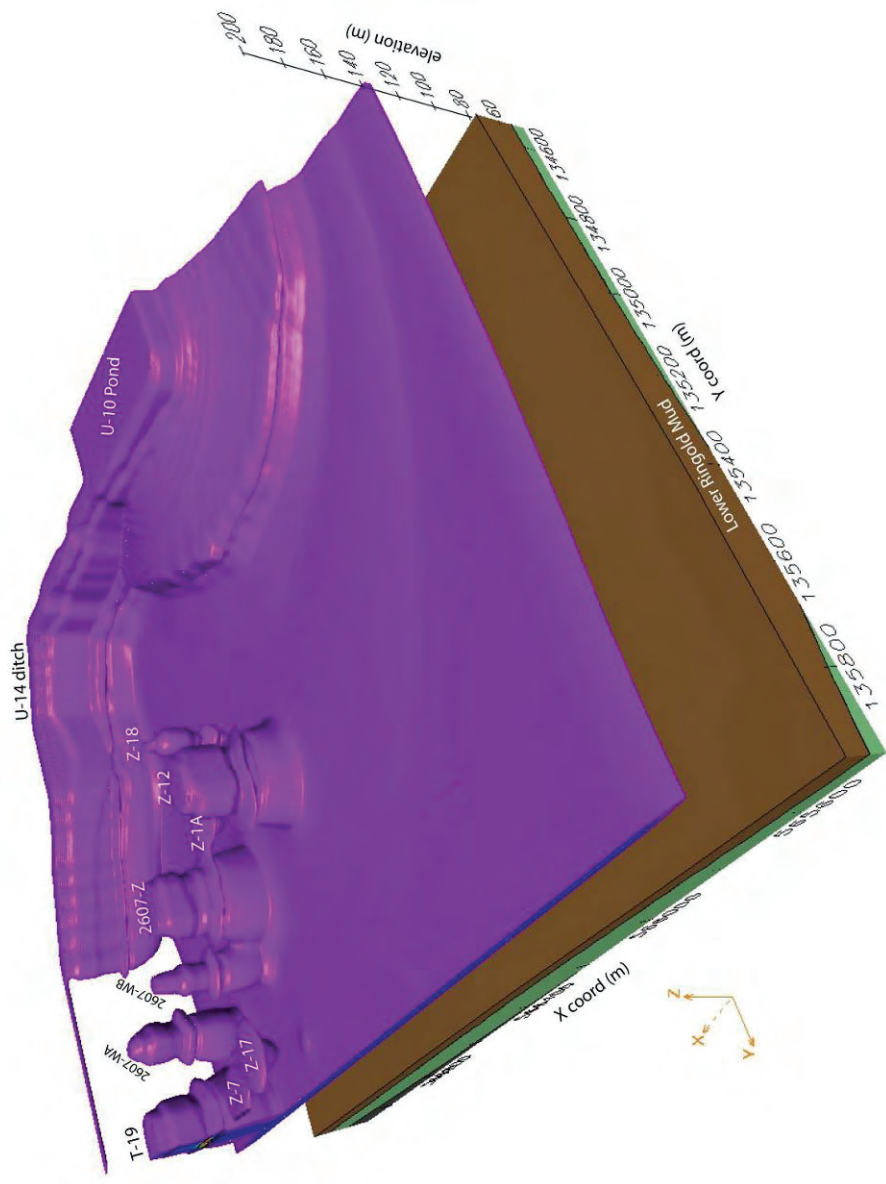
Figure 4.5. Differences in Water Saturation (10% Contour) Between 1974 and 1944 (Initial Conditions)
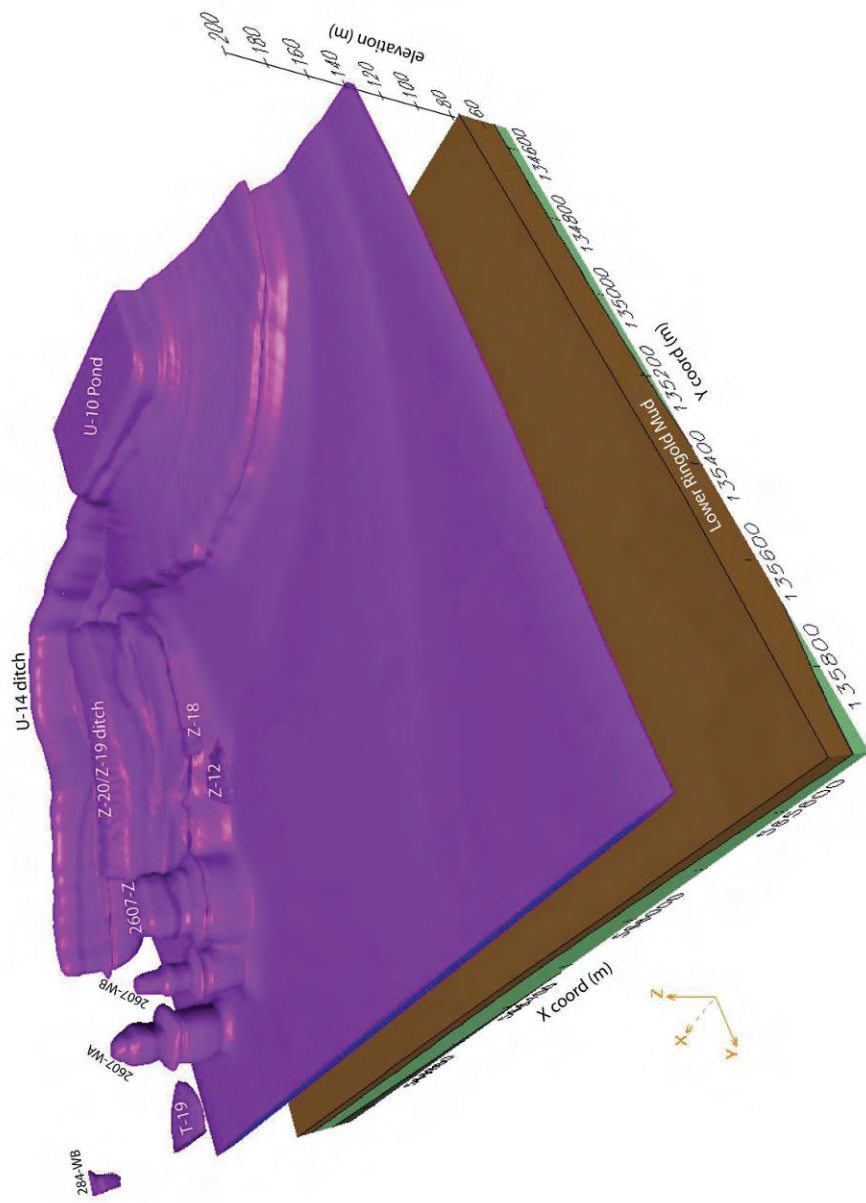
Figure 4.6. Differences in Water Saturation (10% Contour) Between 1985 and 1944 (Initial Conditions)
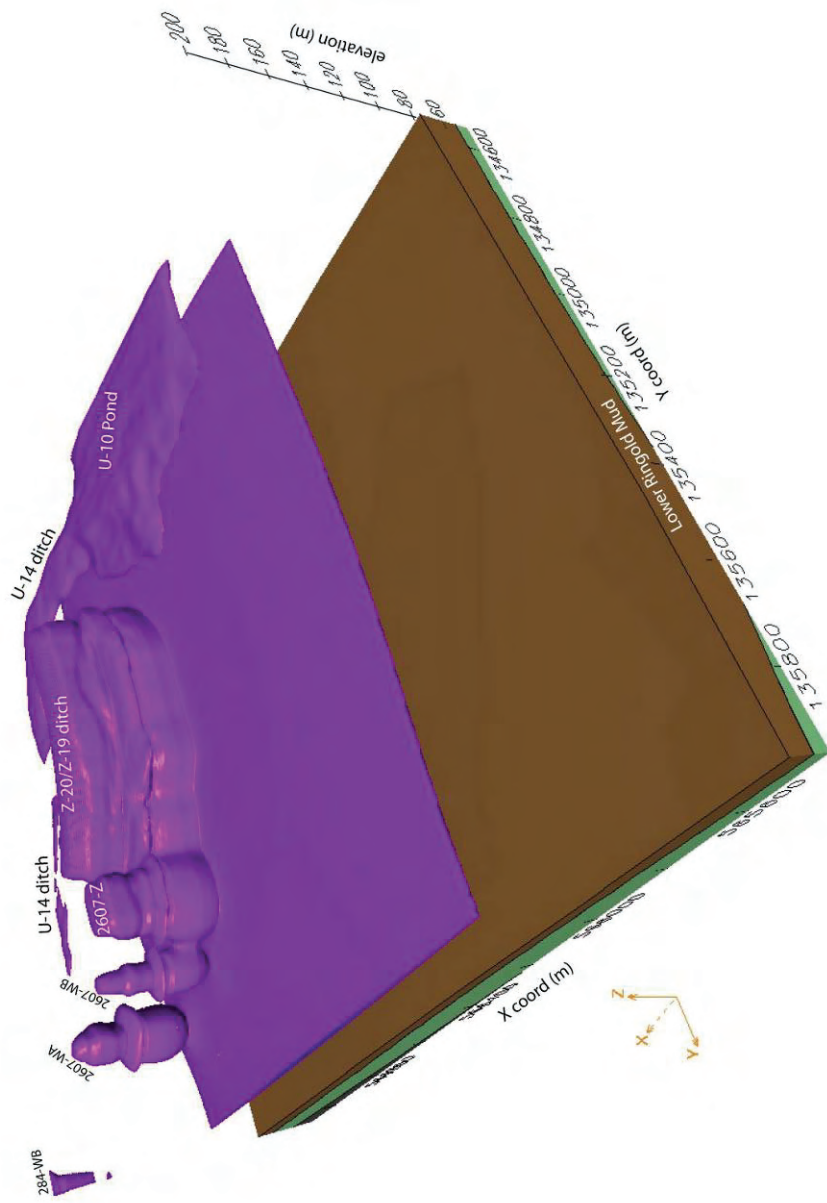
Figure 4.7. Differences in Water Saturation (10% Contour) Between 1993 and 1944 (Initial Conditions)
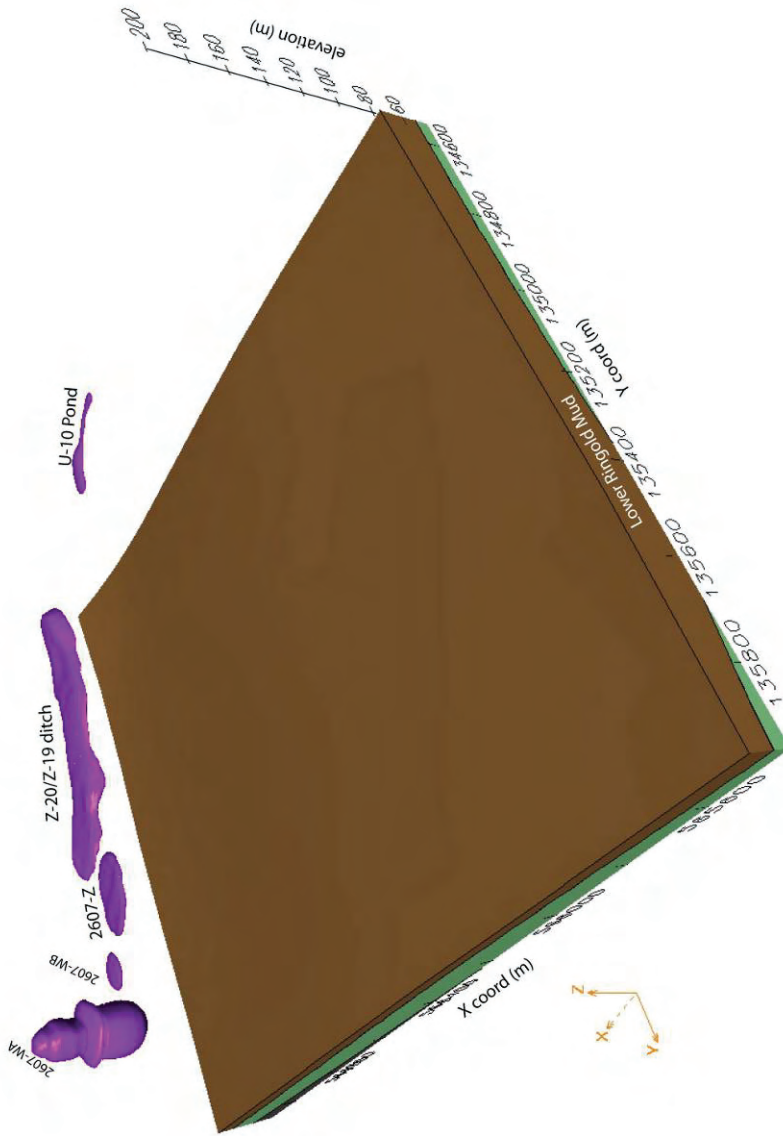
Figure 4.8. Differences in Water Saturation (10% Contour) Between 2007 and 1944 (Initial Conditions)

4.9
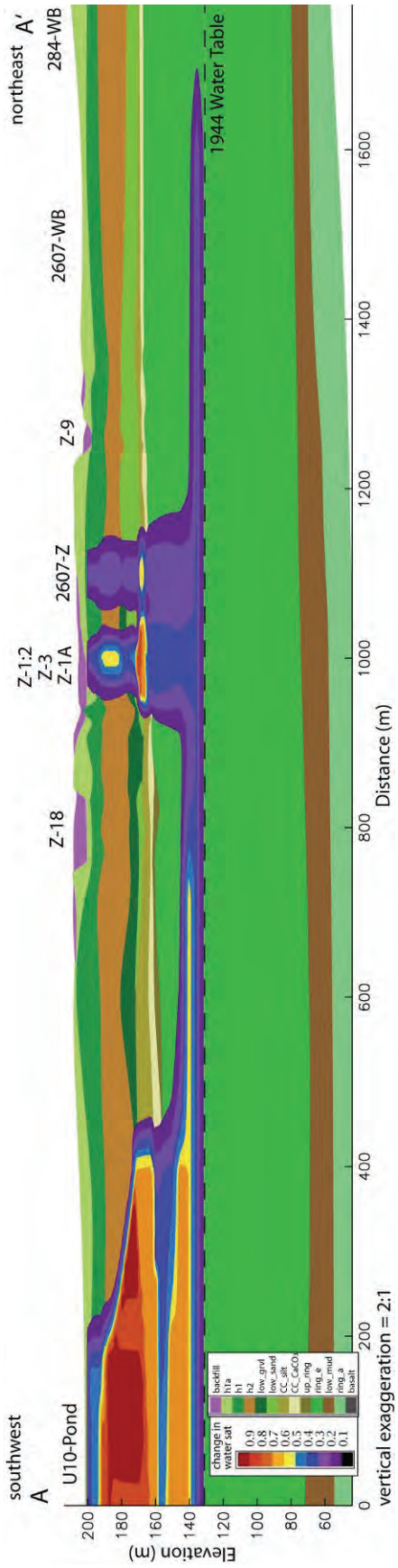
Figure 4.9. Differences in Water Saturation Between 1953 and 1944 (Initial Conditions) for Cross Section A-A' (Base Case)
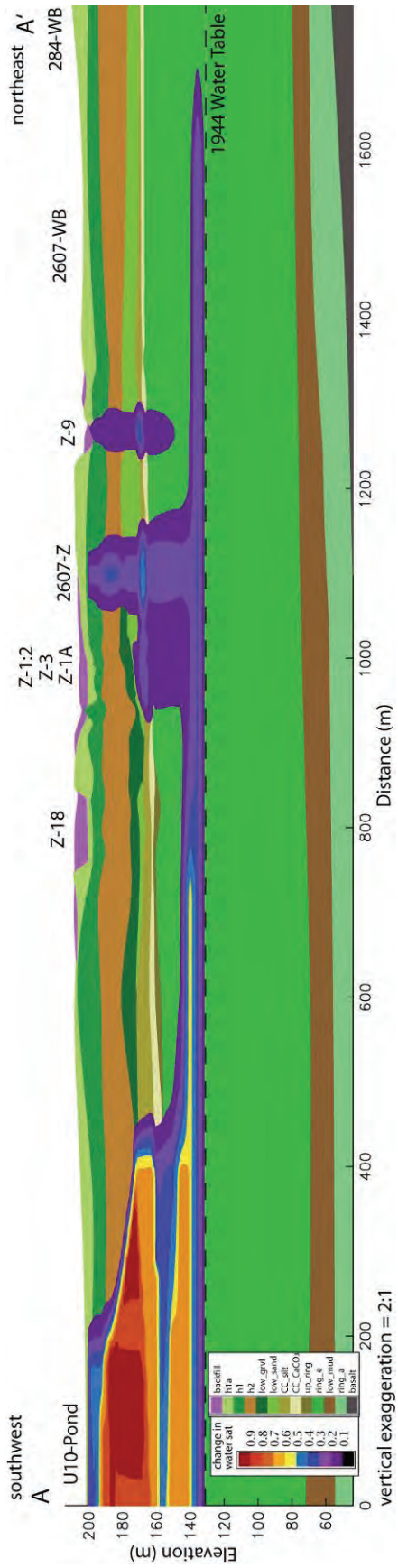
Figure 4.10. Differences in Water Saturation Between 1962.5 and 1944 (Initial Conditions) for Cross Section A-A' (Base Case)

4.10
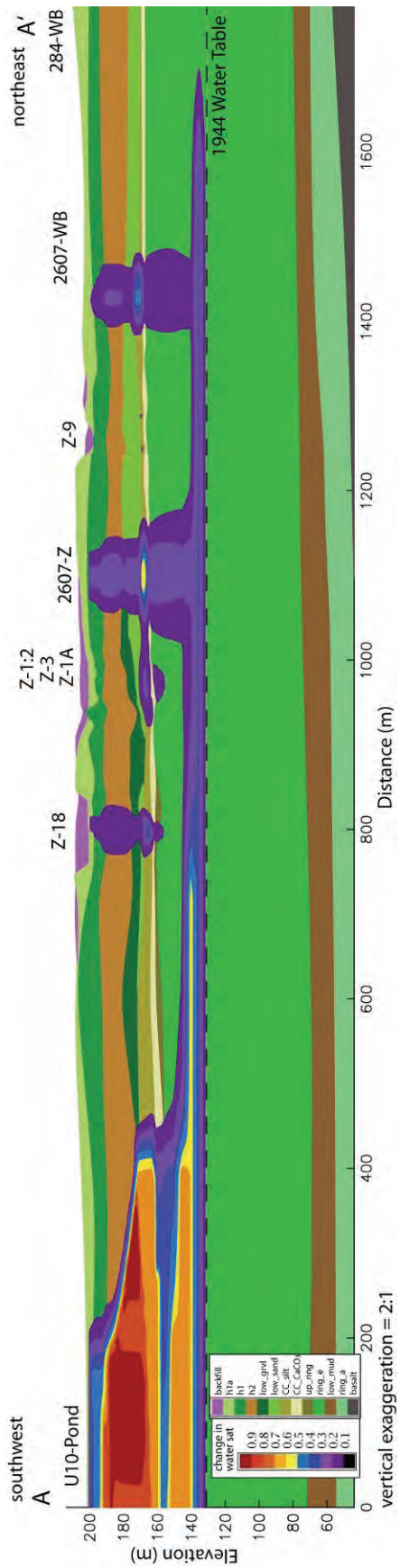
Figure 4.11. Differences in Water Saturation Between 1974 and 1944 (Initial Conditions) for Cross Section A-A' (Base Case)
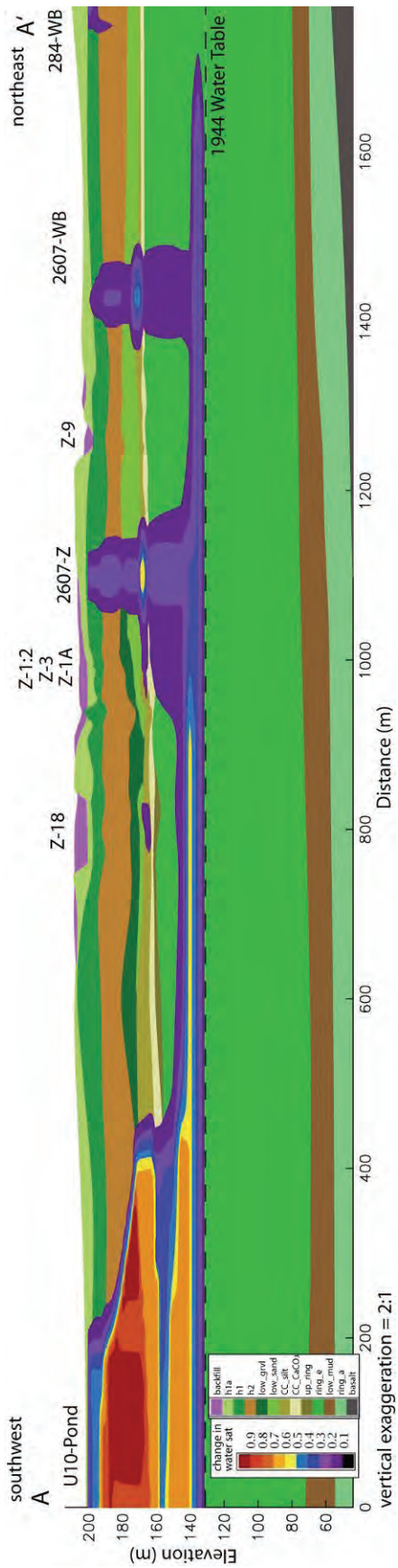
Figure 4.12. Differences in Water Saturation Between 1985 and 1944 (Initial Conditions) for Cross Section A-A' (Base Case)

4.11
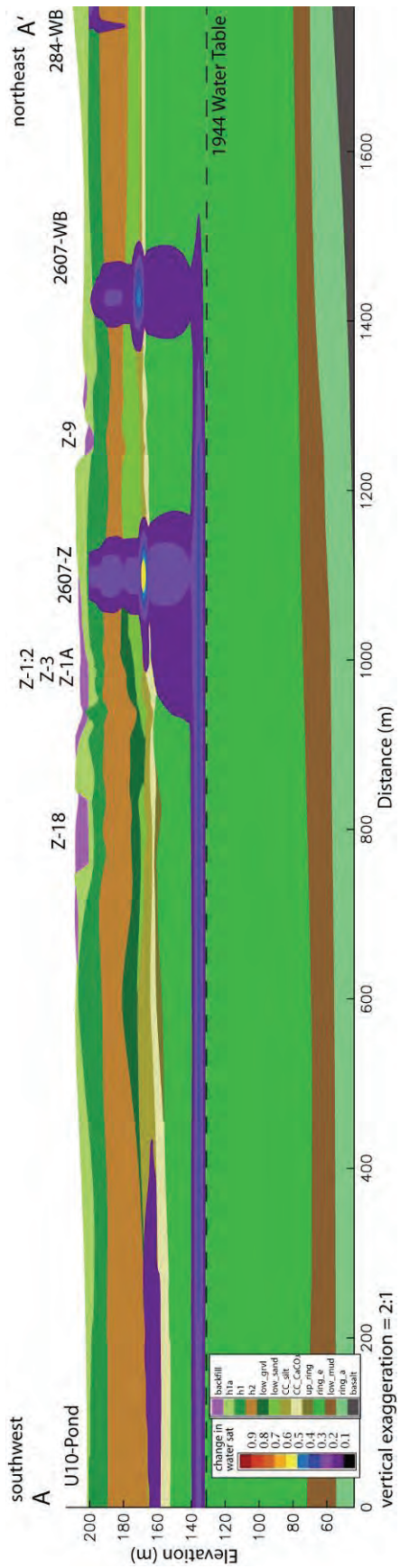
Figure 4.13. Differences in Water Saturation Between 1993 and 1944 (Initial Conditions) for Cross Section A-A' (Base Case)
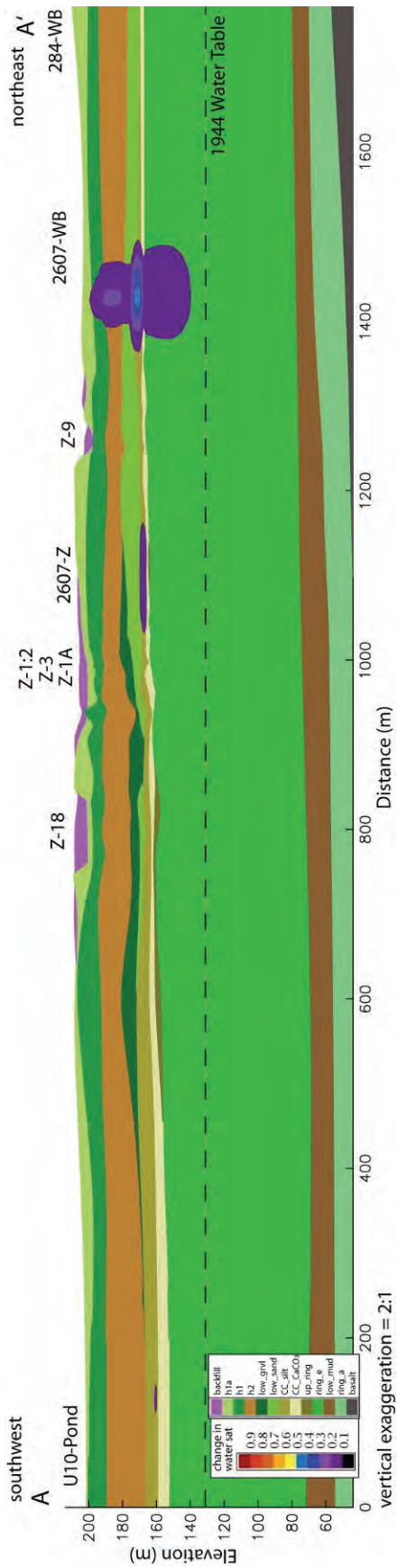
Figure 4.14. Differences in Water Saturation Between 2007 and 1944 (Initial Conditions) for Cross Section A-A' (Base Case)
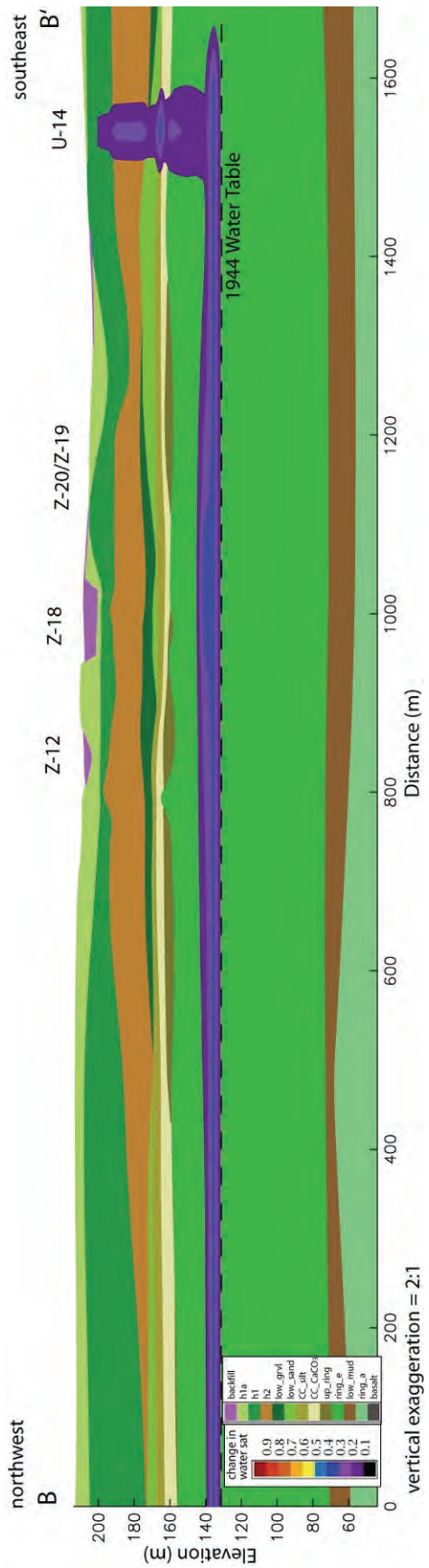
Figure 4.15. Differences in Water Saturation Between 1953 and 1944 (Initial Conditions) for Cross Section B-B' (Base Case)
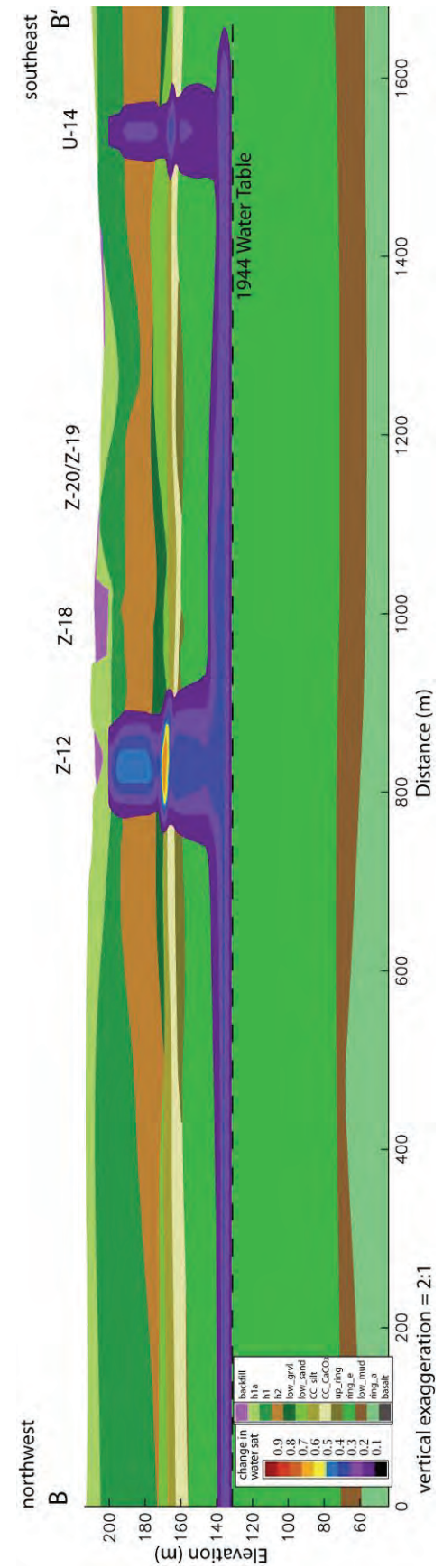
Figure 4.16. Differences in Water Saturation Between 1962.5 and 1944 (Initial Conditions) for Cross Section B-B' (Base Case)

4.13
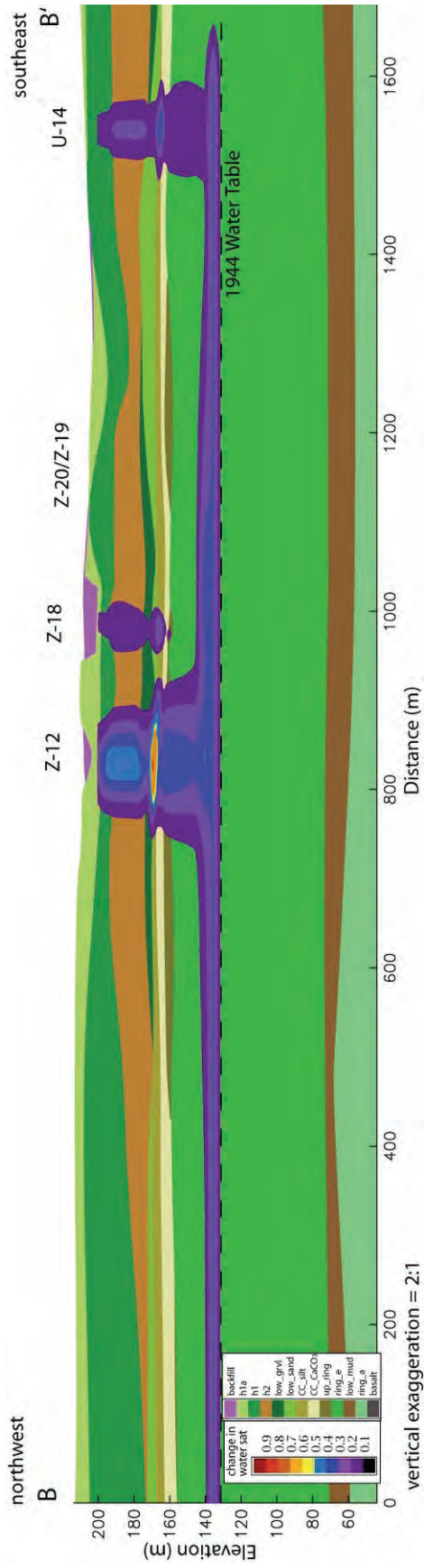
Figure 4.17. Differences in Water Saturation Between 1974 and 1944 (Initial Conditions) for Cross Section B-B' (Base Case)
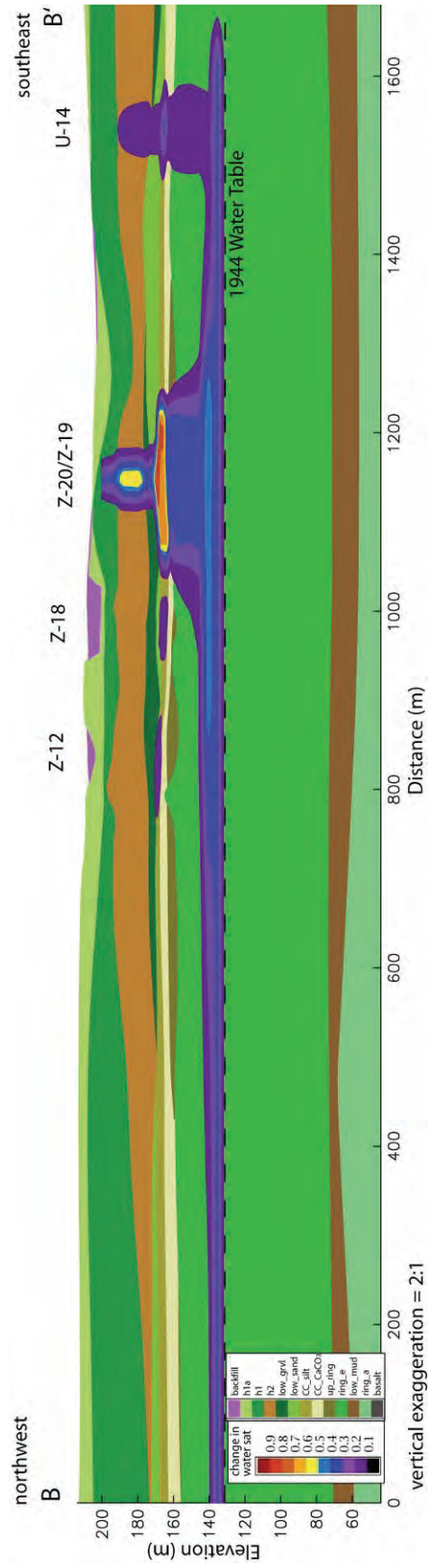
Figure 4.18. Differences in Water Saturation Between 1985 and 1944 (Initial Conditions) for Cross Section B-B' (Base Case)

4.14
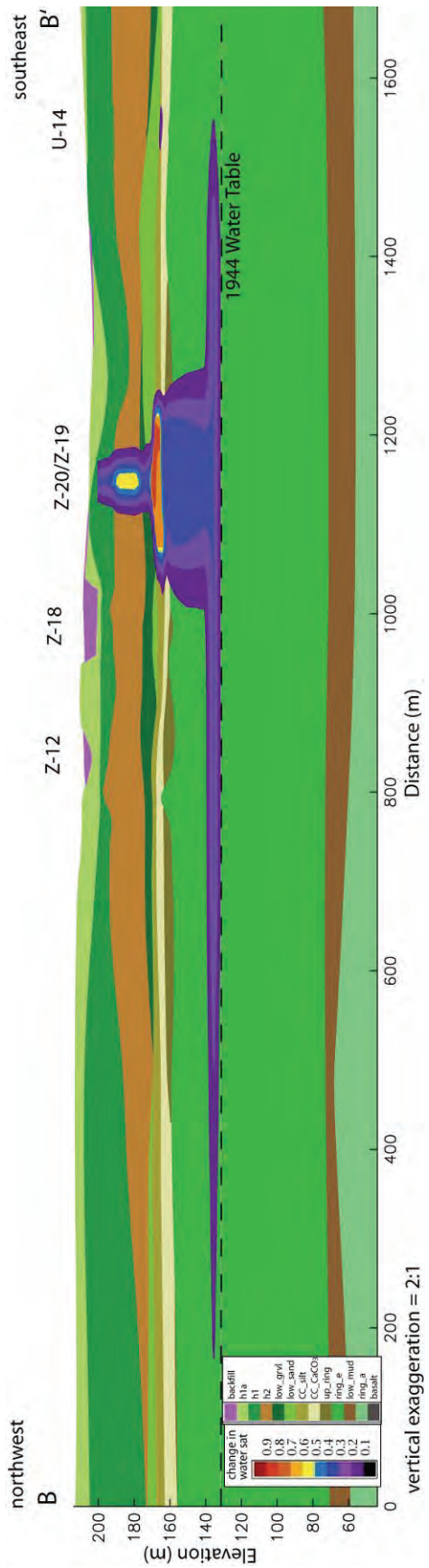
Figure 4.19. Differences in Water Saturation Between 1993 and 1944 (Initial Conditions) for Cross Section B-B' (Base Case)
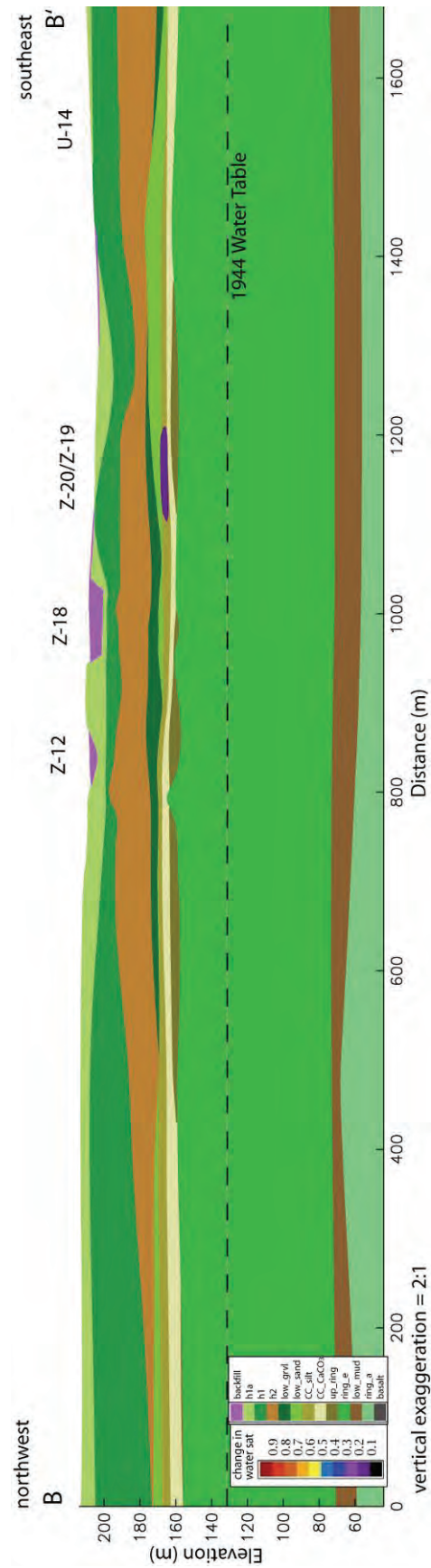
Figure 4.20. Differences in Water Saturation Between 2007 and 1944 (Initial Conditions) for Cross Section B-B' (Base Case)

4.15
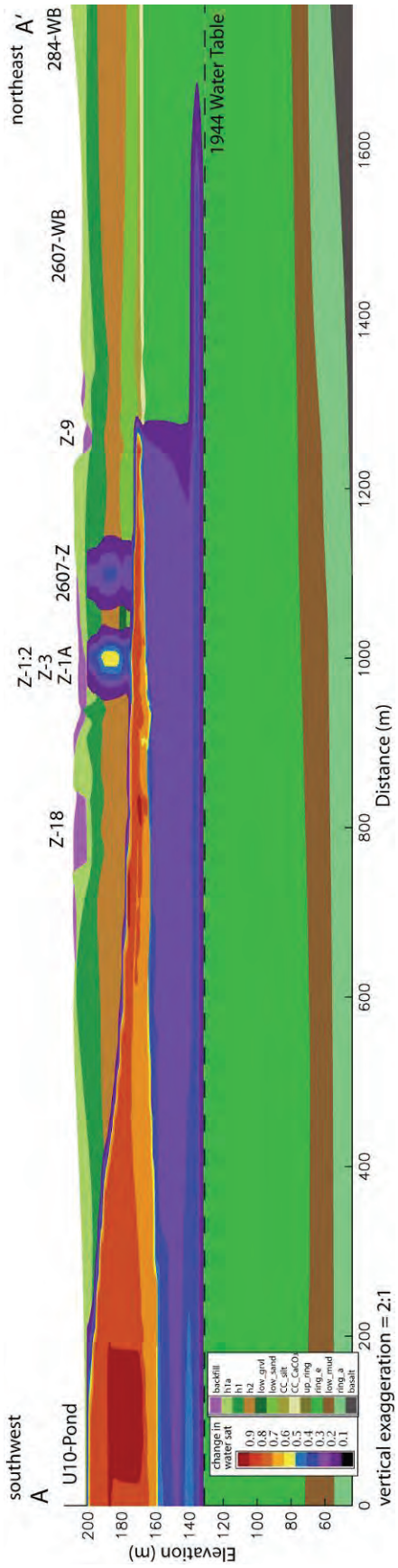
Figure 4.21. Differences in Water Saturation Between 1953 and 1944 (Initial Conditions) for Cross Section A-A' (Case 2)
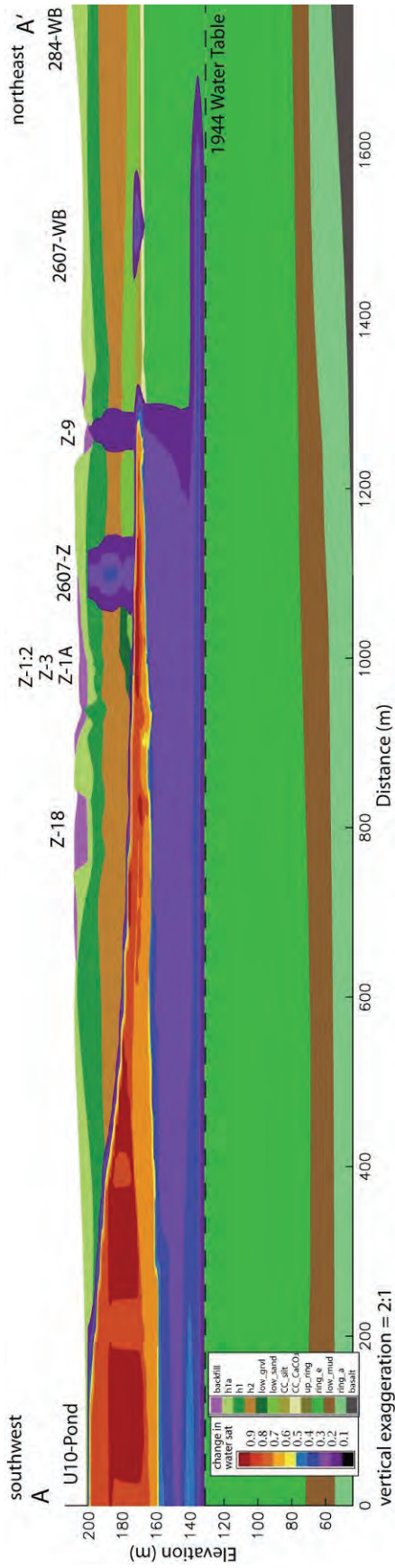
Figure 4.22. Differences in Water Saturation Between 1962.5 and 1944 (Initial Conditions) for Cross Section A-A' (Case 2)

4.16
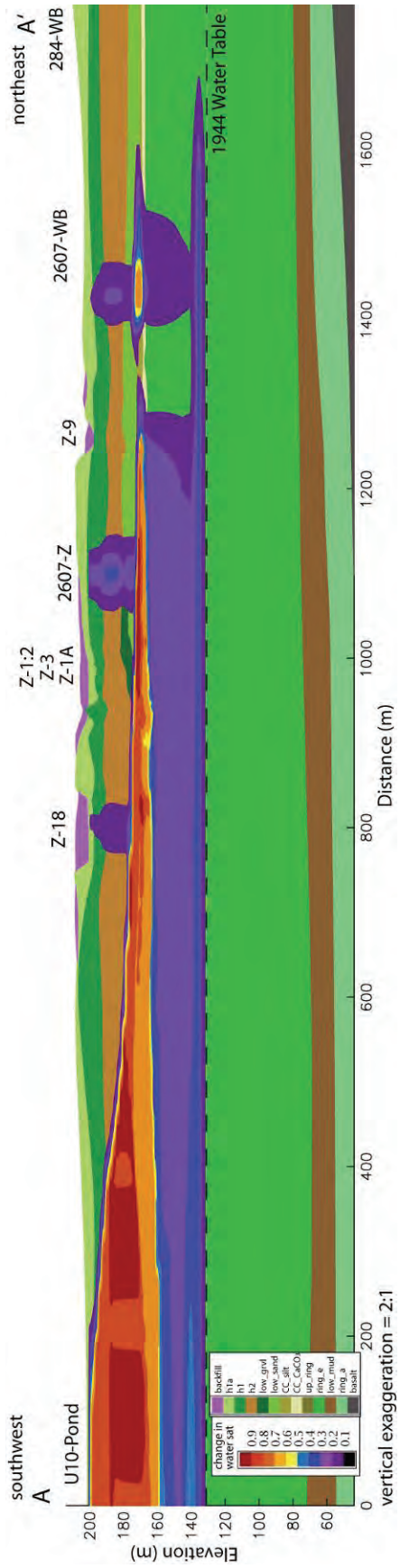
Figure 4.23. Differences in Water Saturation Between 1974 and 1944 (Initial Conditions) for Cross Section A-A' (Case 2)
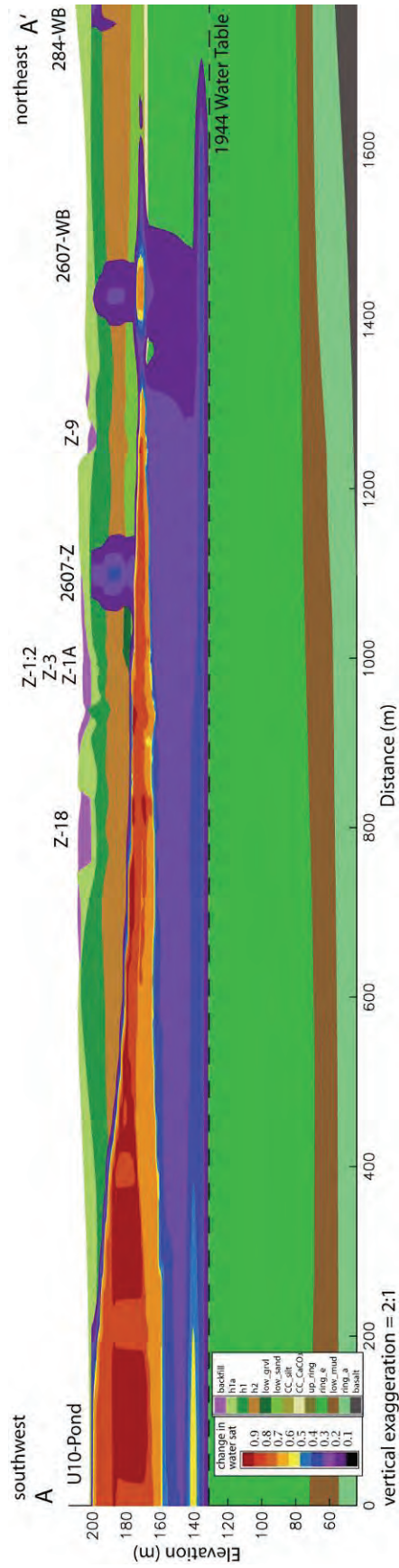
Figure 4.24. Differences in Water Saturation Between 1985 and 1944 (Initial Conditions) for Cross Section A-A' (Case 2)

4.17
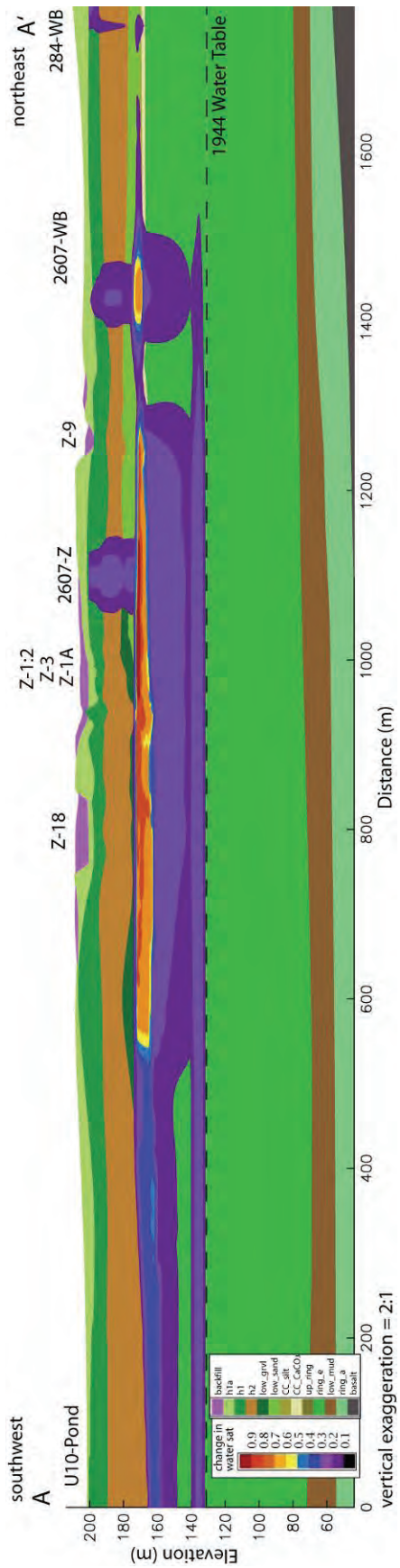
Figure 4.25. Differences in Water Saturation Between 1993 and 1944 (Initial Conditions) for Cross Section A-A' (Case 2)
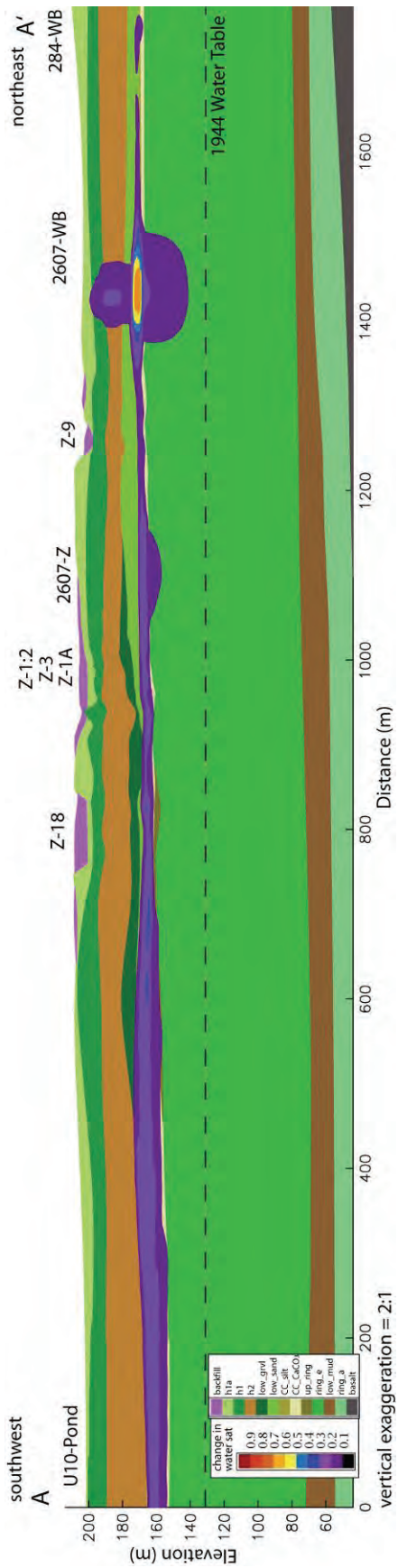
Figure 4.26. Differences in Water Saturation Between 2007 and 1944 (Initial Conditions) for Cross Section A-A' (Case 2)

4.18
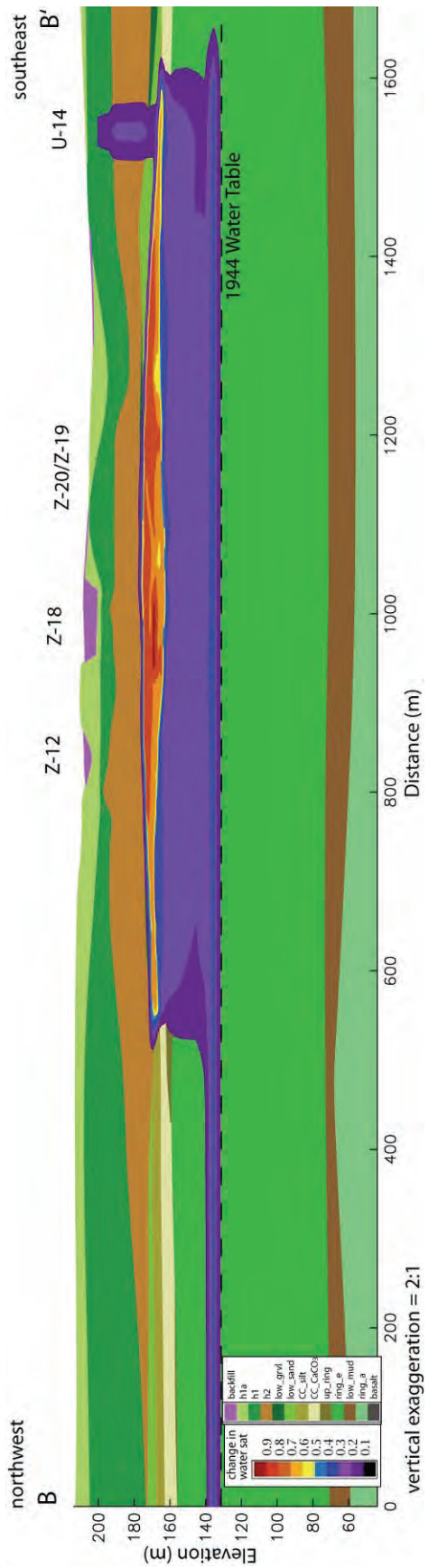
Figure 4.27. Differences in Water Saturation Between 1953 and 1944 (Initial Conditions) for Cross Section B-B' for (Case 2)
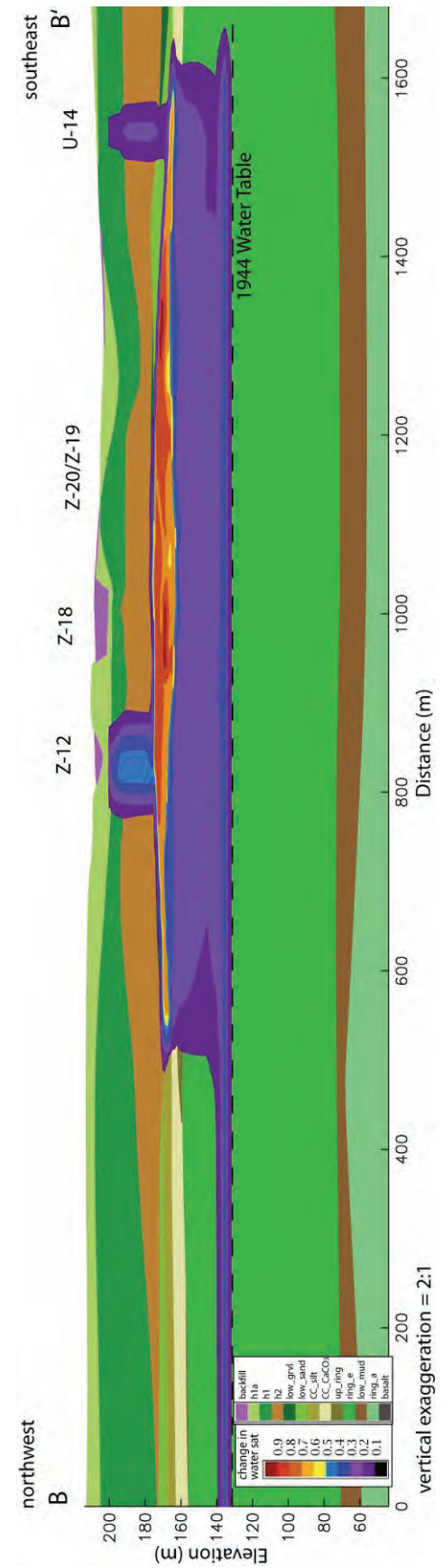
Figure 4.28. Differences in Water Saturation Between 1962.5 and 1944 (Initial Conditions) for Cross Section B-B' (Case 2)
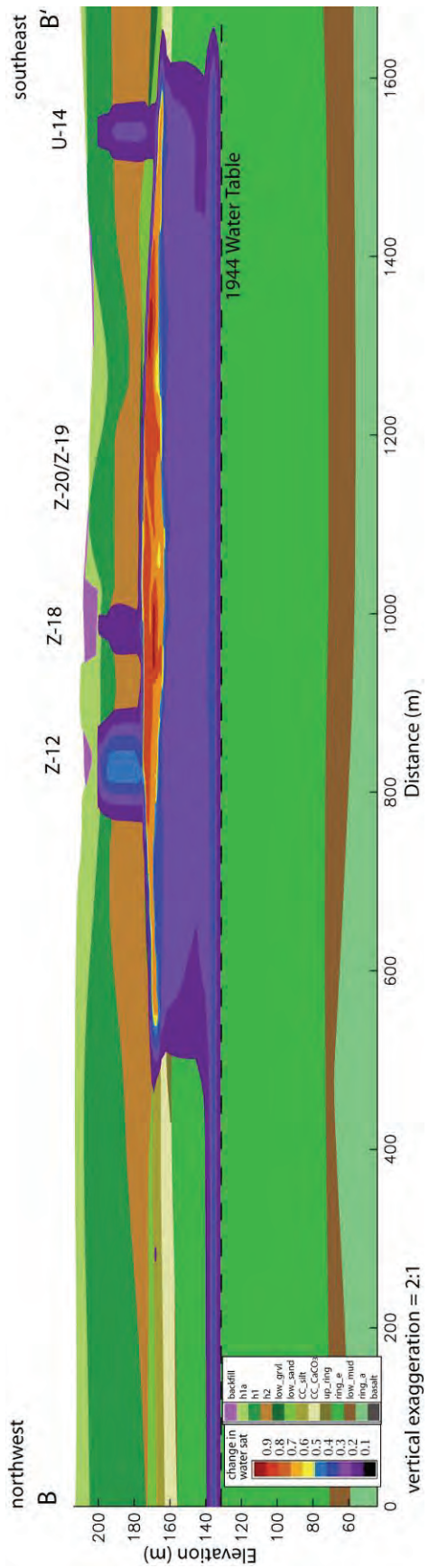
Figure 4.29. Differences in Water Saturation Between 1974 and 1944 (Initial Conditions) for Cross Section B-B' (Case 2)
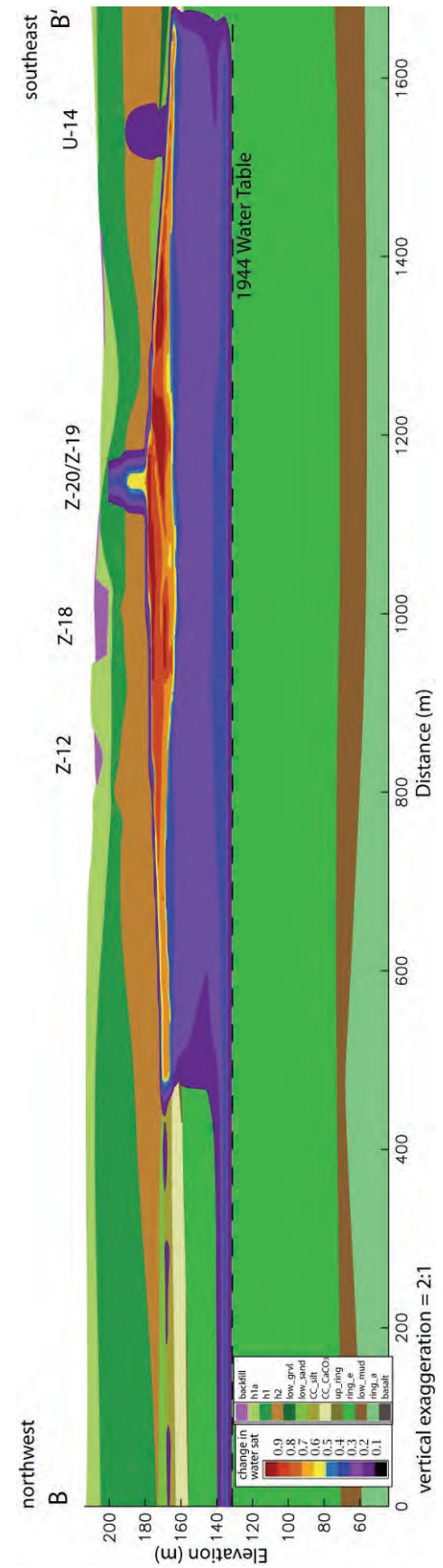
Figure 4.30. Differences in Water Saturation Between 1985 and 1944 (Initial Conditions) for Cross Section B-B' (Case 2)

4.20
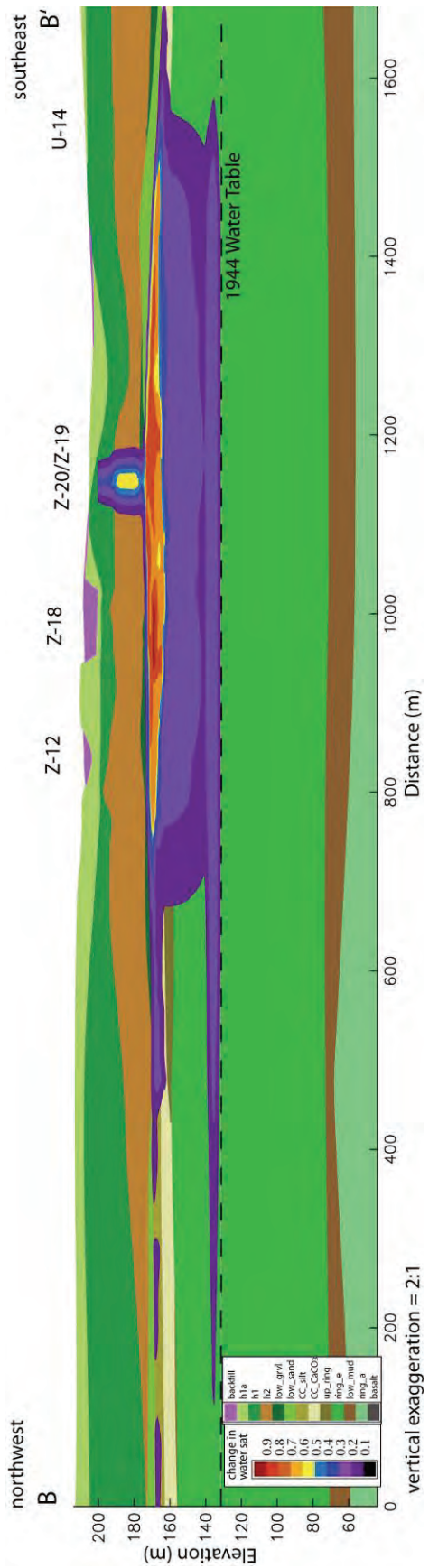
Figure 4.31. Differences in Water Saturation Between 1993 and 1944 (Initial Conditions) for Cross Section B-B' (Case 2)
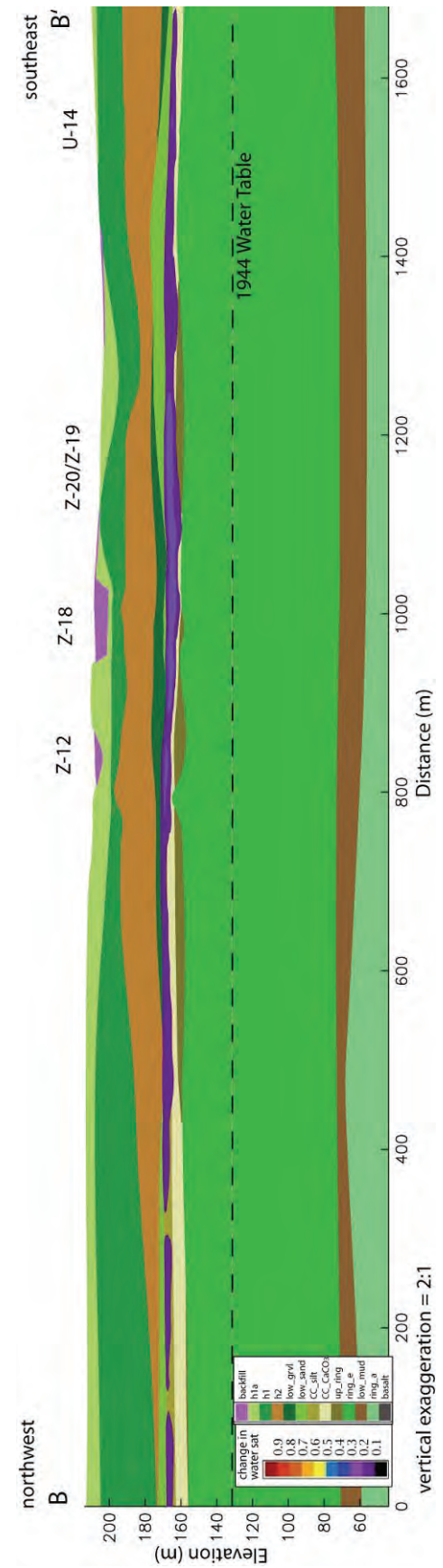
Figure 4.32. Differences in Water Saturation Between 2007 and 1944 (Initial Conditions) for Cross Section B-B' (Case 2)

4.21
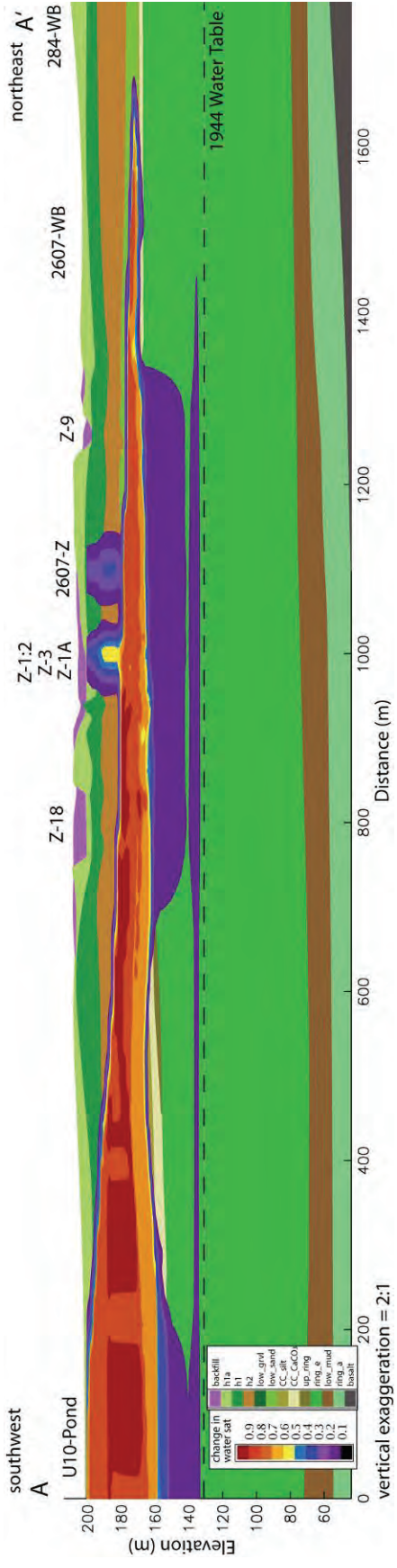
Figure 4.33. Differences in Water Saturation Between 1953 and 1944 (Initial Conditions) for Cross Section A-A' (Case 3)
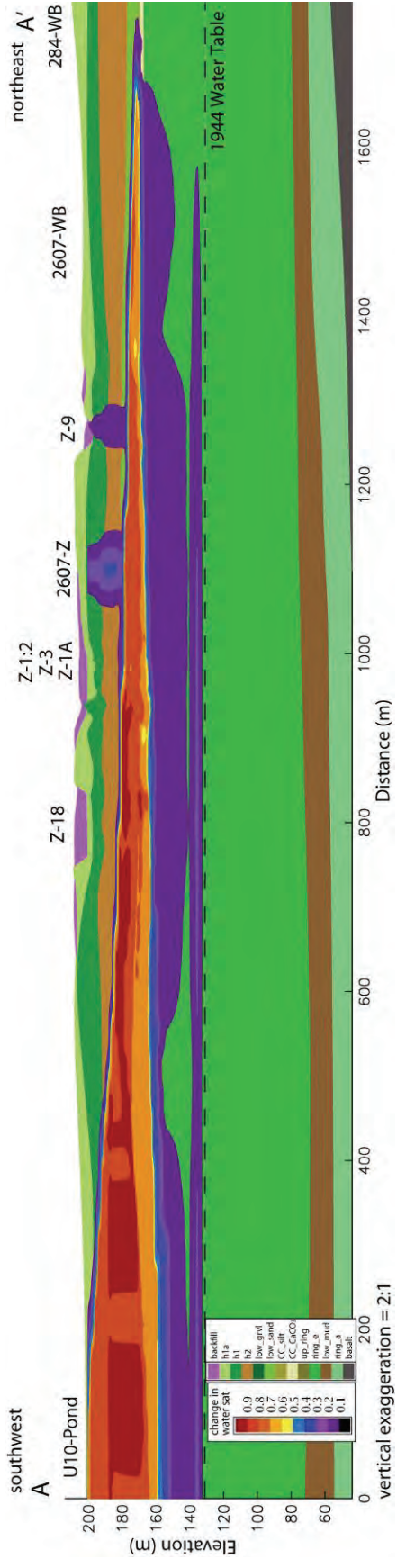
Figure 4.34. Differences in Water Saturation Between 1962.5 and 1944 (Initial Conditions) for Cross Section A-A' (Case 3)
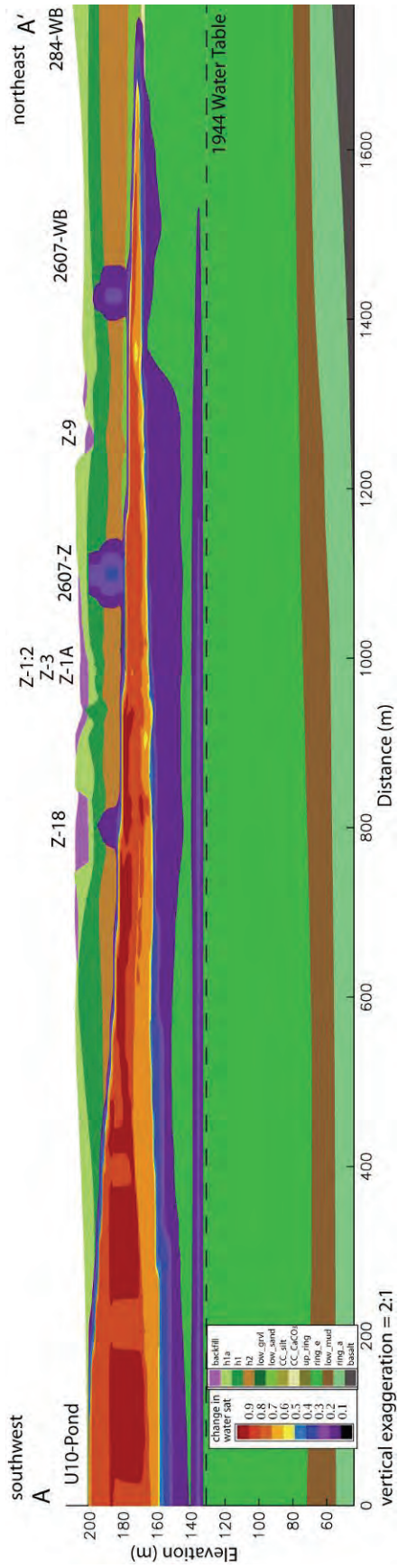
Figure 4.35. Differences in Water Saturation Between 1974 and 1944 (Initial Conditions) for Cross Section A-A' (Case 3)
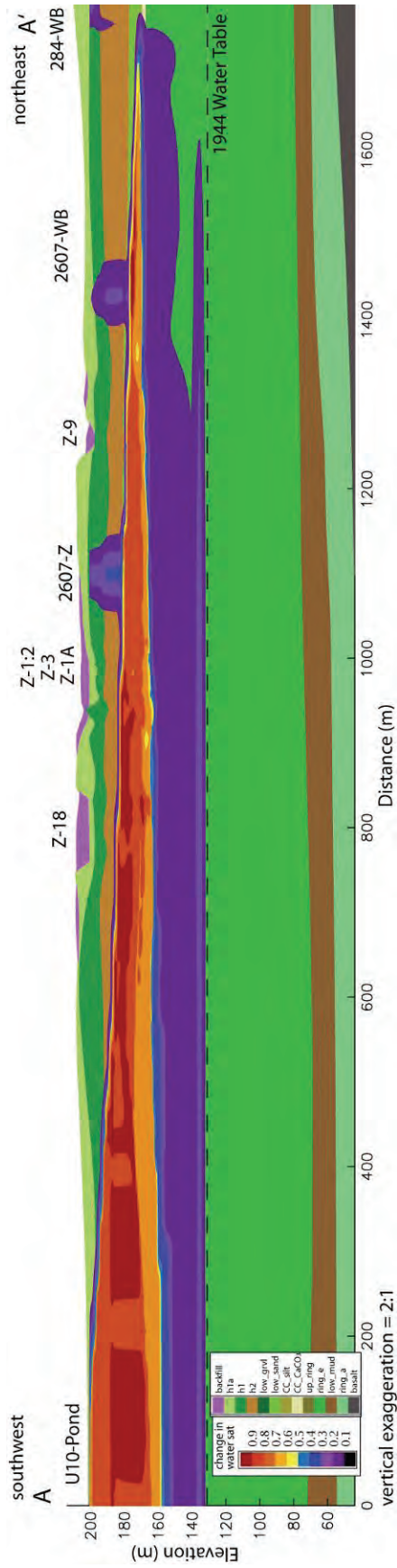
Figure 4.36. Differences in Water Saturation Between 1985 and 1944 (Initial Conditions) for Cross Section A-A' (Case 3)

4.23
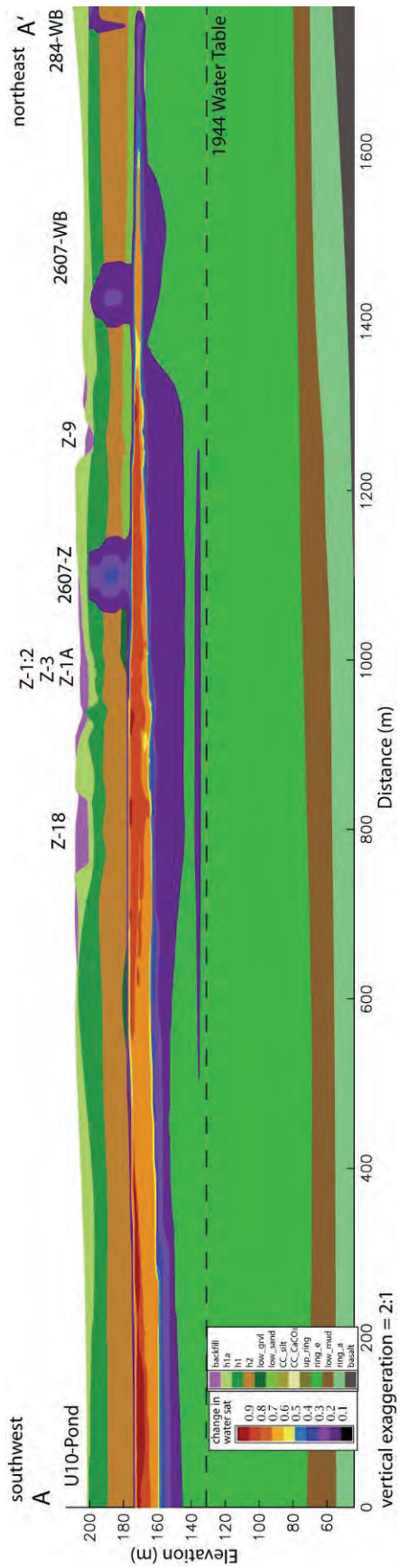
Figure 4.37. Differences in Water Saturation Between 1993 and 1944 (Initial Conditions) for Cross Section A-A' (Case 3)
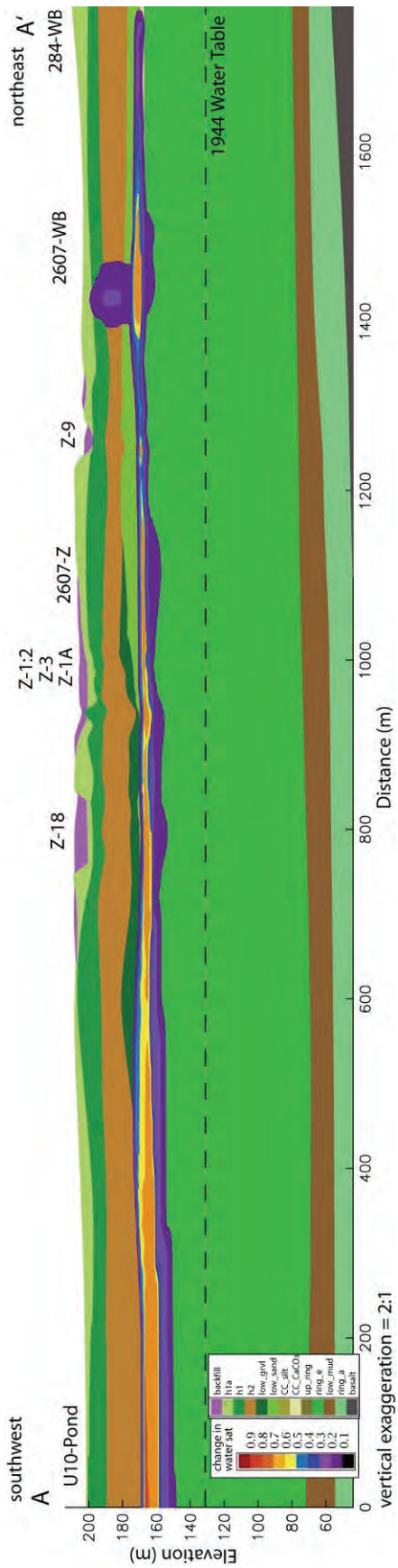
Figure 4.38. Differences in Water Saturation Between 2007 and 1944 (Initial Conditions) for Cross Section A-A' (Case 3)

4.24
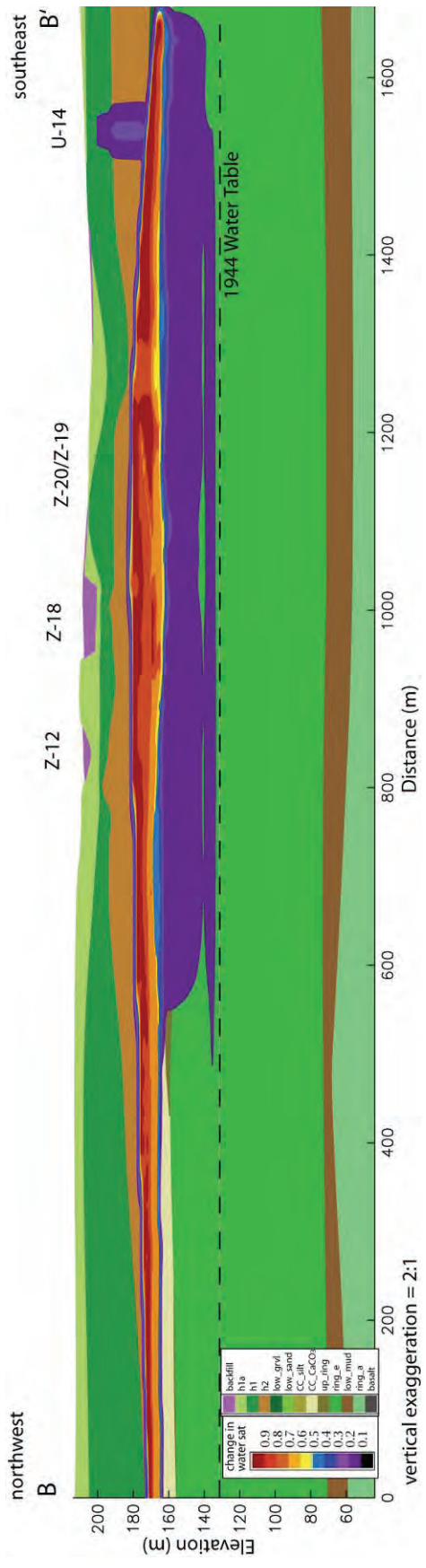
Figure 4.39. Differences in Water Saturation Between 1953 and 1944 (Initial Conditions) for Cross Section B-B' for (Case 3)
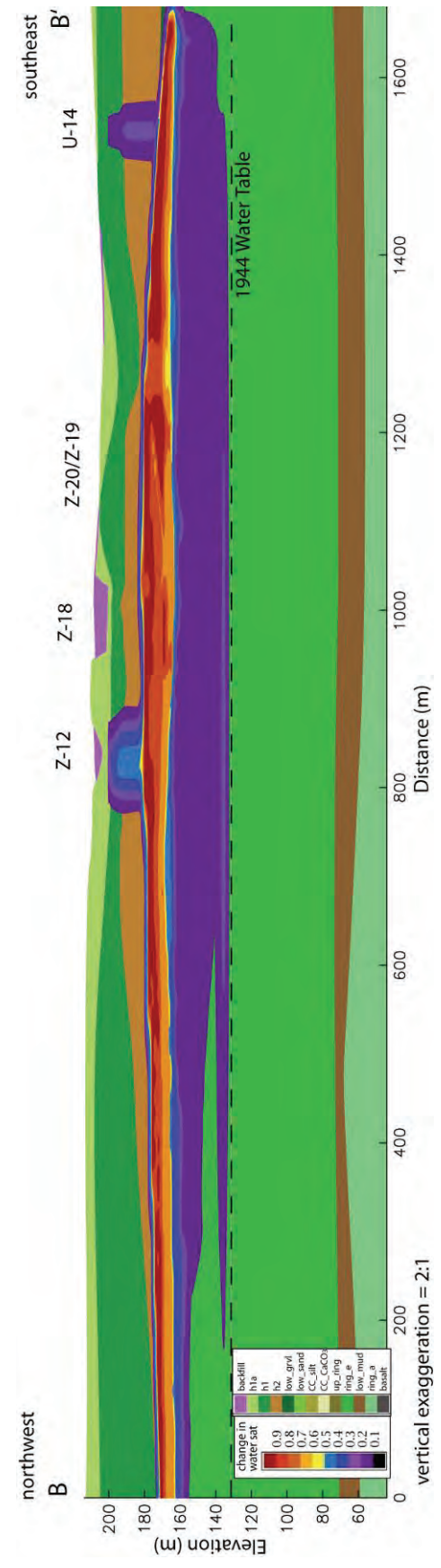
Figure 4.40. Differences in Water Saturation Between 1962.5 and 1944 (Initial Conditions) for Cross Section B-B' (Case 3)
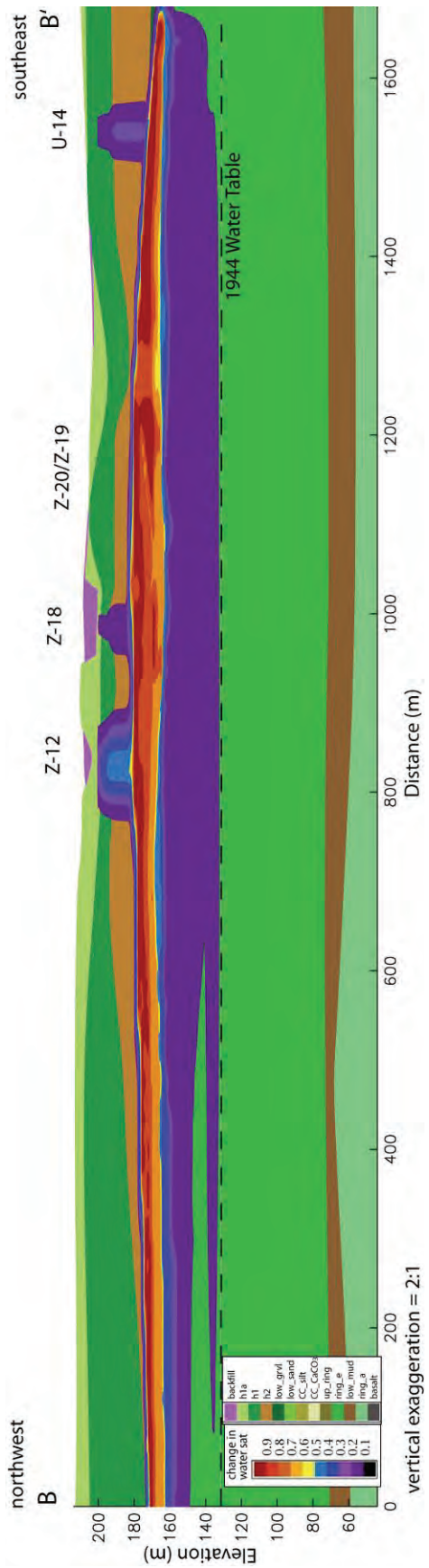
Figure 4.41. Differences in Water Saturation Between 1974 and 1944 (Initial Conditions) for Cross Section B-B' (Case 3)
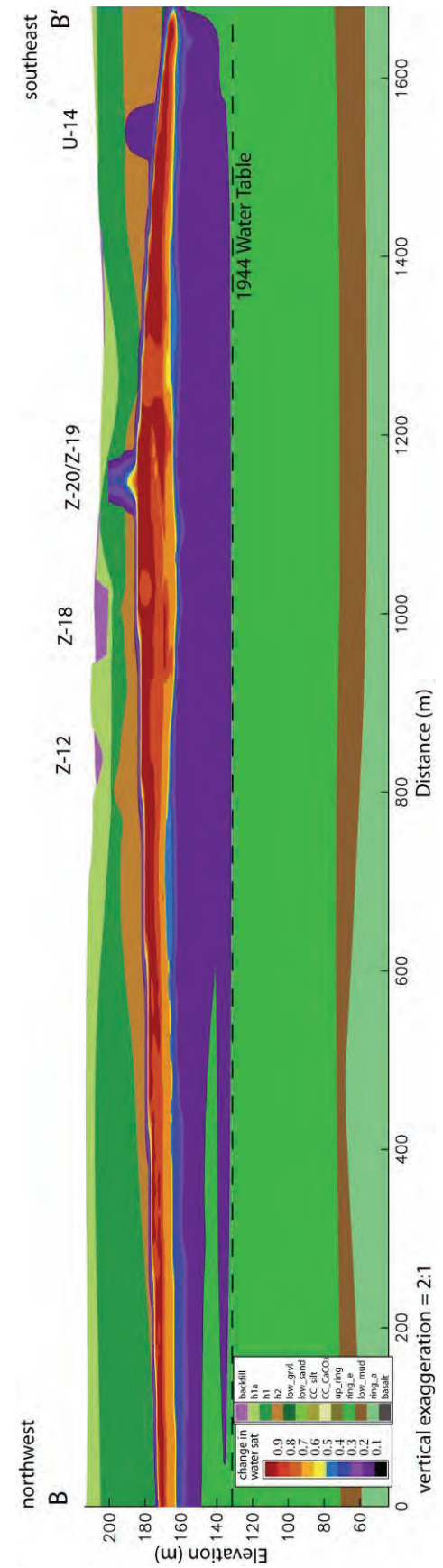
Figure 4.42. Differences in Water Saturation Between 1985 and 1944 (Initial Conditions) for Cross Section B-B' (Case 3)

4.26
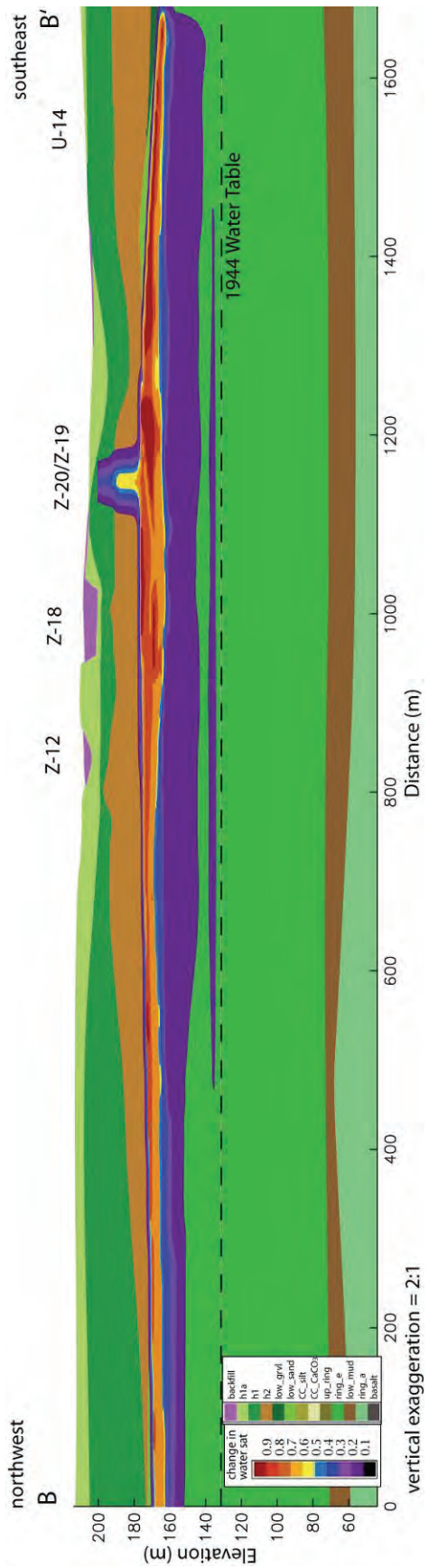
Figure 4.43. Differences in Water Saturation Between 1993 and 1944 (Initial Conditions) for Cross Section B-B' (Case 3)
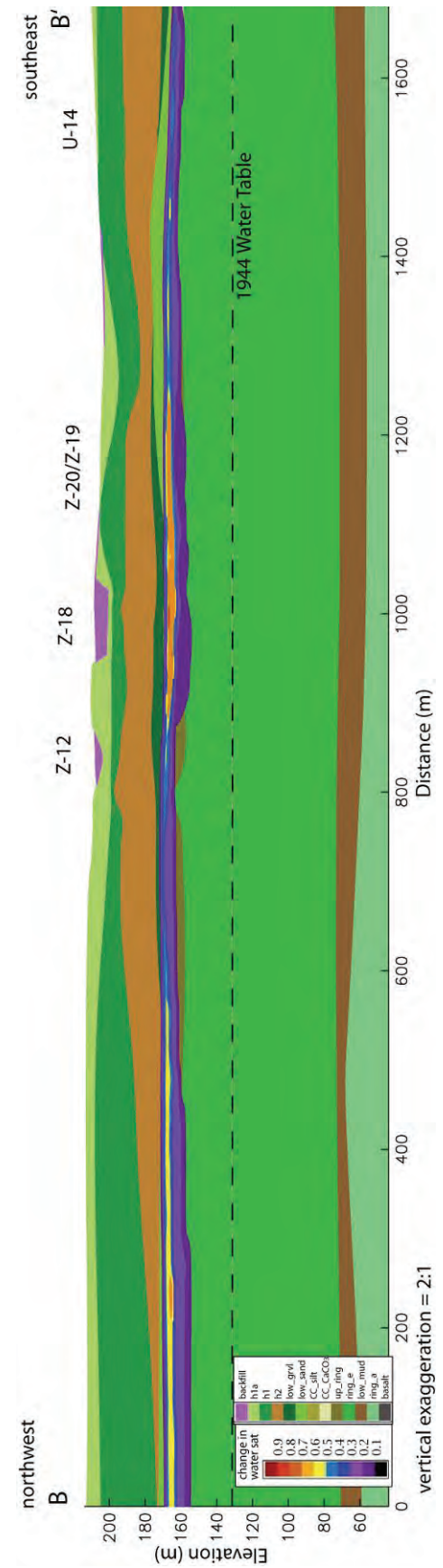
Figure 4.44. Differences in Water Saturation Between 2007 and 1944 (Initial Conditions) for Cross Section B-B' (Case 3)

4.27

4.2   NAPL Infiltration and Redistribution

In the simulations, over 900,000 kg were allowed to infiltrate into the subsurface from the 216-Z-9, 216-Z-1A, and the 216-18 disposal sites. Infiltration details are listed in Table 3.1 – 3.3. Results for the base-case simulation are shown in Figures 4.45to 4.72. The results for case 2 and case 3 are presented in Figure 4.73 to 4.80 and 4.81 - 4.88, respectively.

Pertinent mass fluxes for the base case are shown in Figure 4.45, which shows that the majority of the disposed DNAPL did not move into the Cold Creek Unit. A total of just over 22,000 kg is predicted to move across the water table by 1993 (Table 4.1). This amount is about 5,000 kg less than for the simulation reported in Oostrom et al. (2006b), where no additional water sources were considered. The additional water in the subsurface reduced the available pore space for DNAPL to move downwards. The two sensitivity cases both predicted lower DNAPL CT transfer across the water table (Table 4.1). For both cases, the reduced permeability of the Cold Creek Unit considerably lowered the ability of the DNAPL to move downwards. For case 3, with the 100-fold reduction in Cold Creek Unit permeability, no DNAPL was transported across the water table. The CT mass that moved across the water table in dissolved form is predicted to be over 6,000 kg. The dissolved CT mass that moved across the water table for these two cases was slightly higher than for the base case. Both cases show higher predictions due to the increased volume of water that moved downwards to the water table below the three DNAPL sites compared to the base case.

Table 4.1. Cumulative DNAPL and Dissolved CT Mass Fluxes Across Water Table Through 1993

Simulation	DNAPL CT Mass (kg)	Dissolved CT Mass (kg)
Base Case	22,112	6,324
Case 2	7,816	7,653
Case 3	0	7,176

The mass distribution over the phases is shown in Figure 4.46 and Figure 4.47 for the simulation with and without SVE, respectively. In the simulation with SVE, the remediation was assumed to be initiated in 1993. The difference between the two plots indicates that SVE, modeled using equilibrium volatilization and a constant vapor pressure, is very effective in removing large quantities of SVE from the system. Before 1993, a considerable fraction of the initially disposed DNAPL CT partitions into the other phases. By 1993, approximately similar quantities of CT mass are sorbed and part of the DNAPL. Figures 4.48 and 4.49 show the mass distribution over the hydrostratigraphic units as a function of time. The CT mass that is located in the Cold Creek Unit is fairly stable and is the result of the lower permeability values of this unit compared to the units above and below.

Figures 4.50 to 4.54 provide the DNAPL saturations at 1962.5 (end of 216-Z-9 infiltration), 1970 (end of 216-Z-1A infiltration), 1974 (end of 216-Z-18 simulation), 1985, and 1993. The figures show that only some DNAPL emanating from 216-Z-9 is predicted to move down to the water table. DNAPL disposed at the other two sites is not predicted to move to that depth by 1993. These results are consistent with simulations reported by Oostrom et al (2004; 2006a; 2006b). Aqueous and gaseous CT concentrations at the same times are shown in Figures 4.55 – 4.59 and in Figures 4.60 – 4.64 respectively. These plots show the rapid distribution of CT through diffusion and density driven advection of the gas phase. The similar shapes of the contaminant plumes are the result of equilibrium partitioning assumptions. Figures 4.65 – 4.68 show CT concentrations at the interface between the Cold Creek Silt

and Carbonate Units at different times. Figures 4.69 to 4.72 show the temporal growth of the CT gaseous plume at the water table. For both surfaces, growth is rapid although it is more pronounced at the water table. At this barrier, gas is forced to move horizontally, while in the Cold Creek Unit, gas is still able to move in three directions.
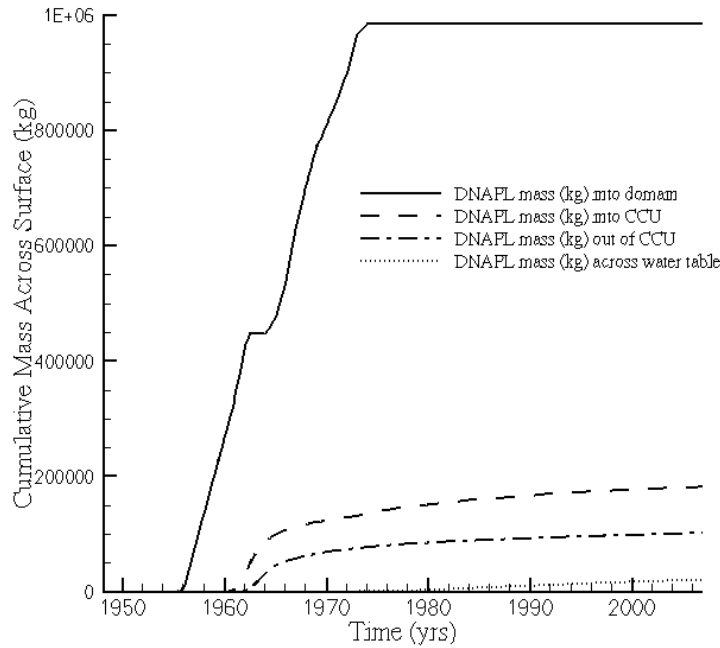
Figure 4.45. Pertinent DNAPL Mass Fluxes (Base Case)
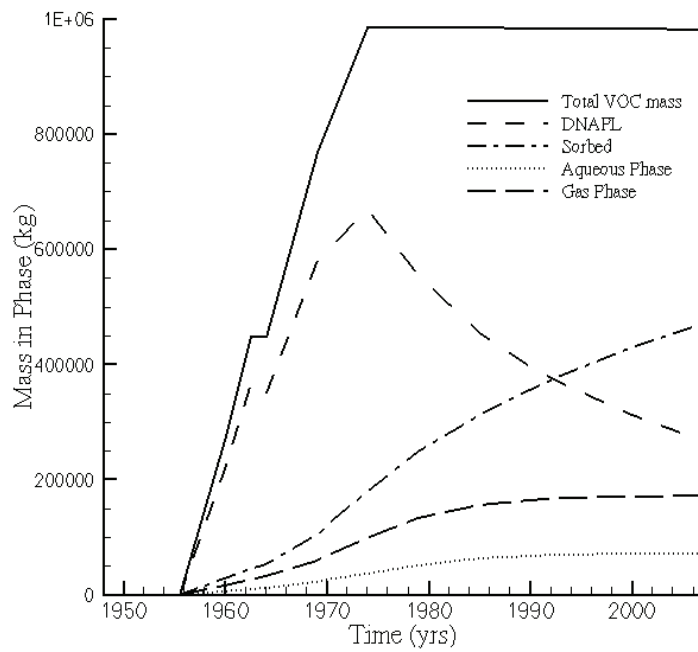
Figure 4.46.   CT Mass Distribution Over the DNAPL, Sorbed, Aqueous, and Gas Phases (Base Case; No SVE)
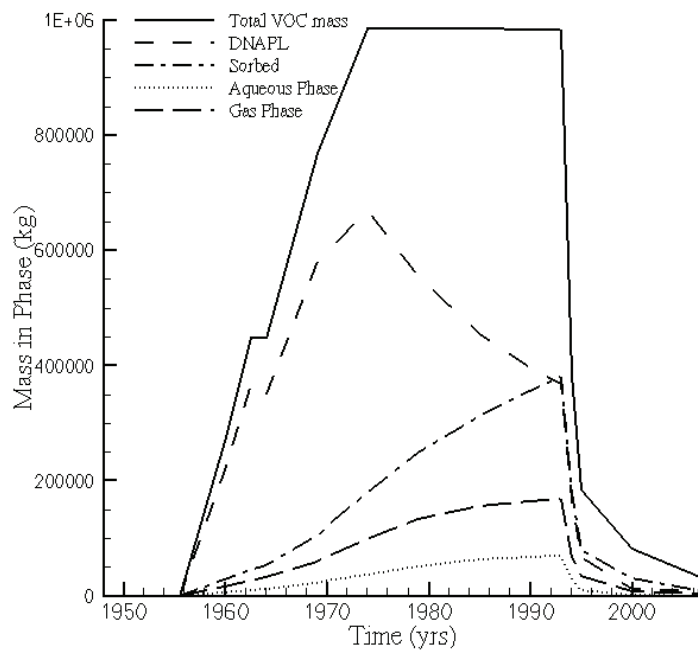
Figure 4.47.   CT Mass Distribution Over the DNAPL, Sorbed, Aqueous, and Gas Phases (Base Case; With SVE)

4.30
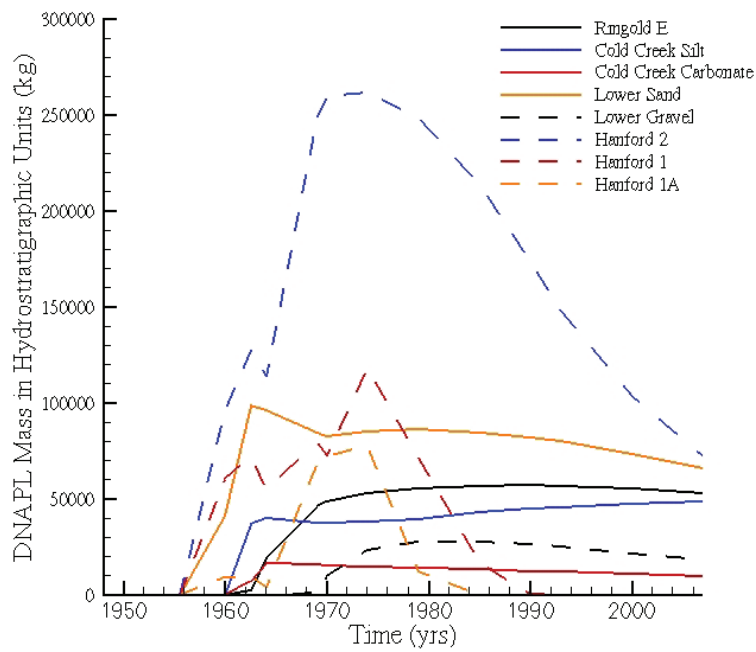
Figure 4.48. DNAPL CT Mass Distribution Over the Hydrostratigraphic Units (Base Case, No SVE)
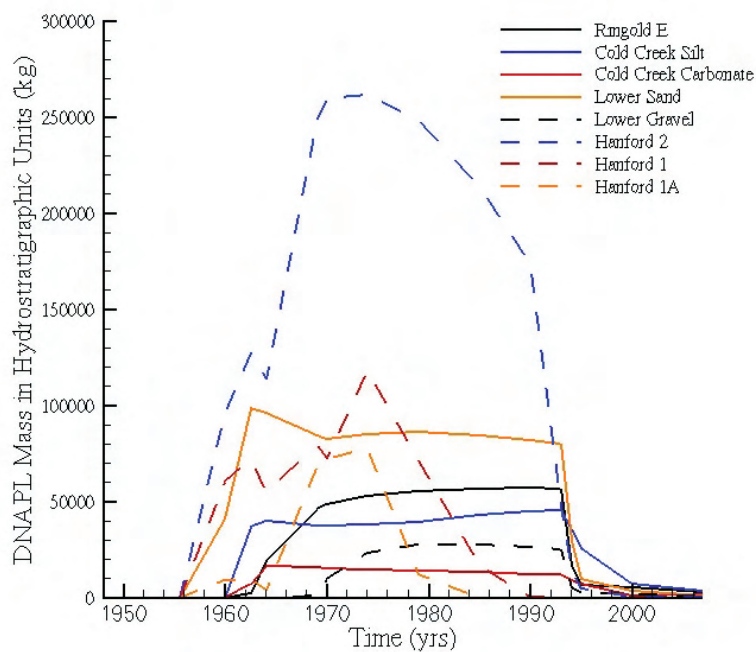
Figure 4.49. DNAPL CT Mass Distribution Over the Hydrostratigraphic Units (Base Case, With SVE)
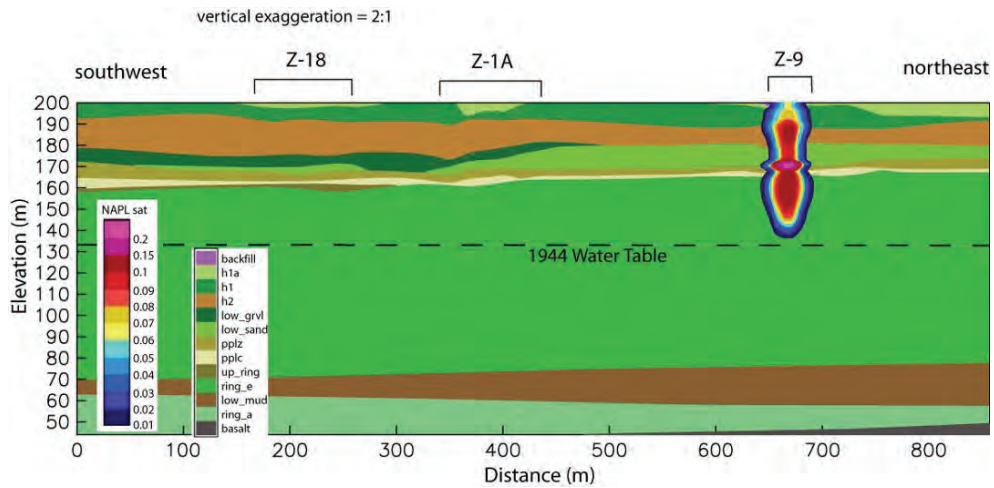
Figure 4.50. DNAPL Saturations at 1962.5 (Base Case)
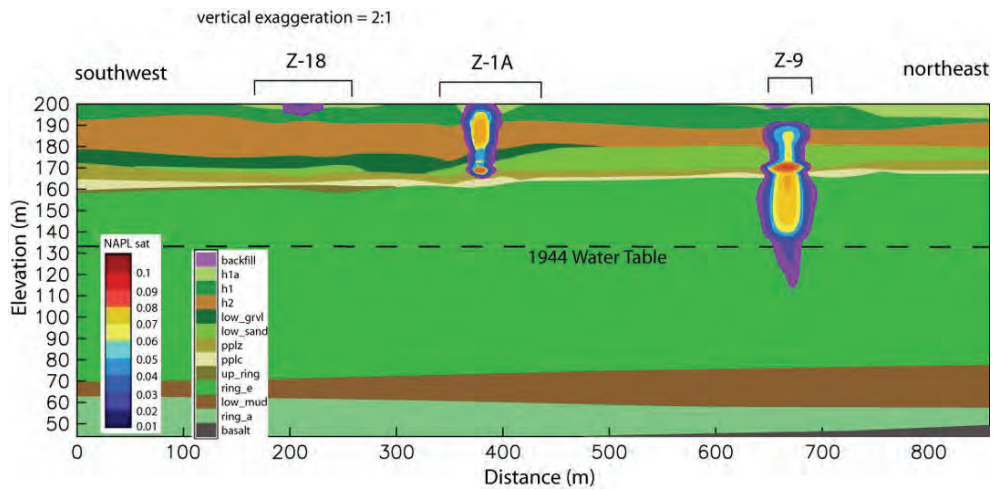
Figure 4.51. DNAPL Saturations at 1970 (Base Case)
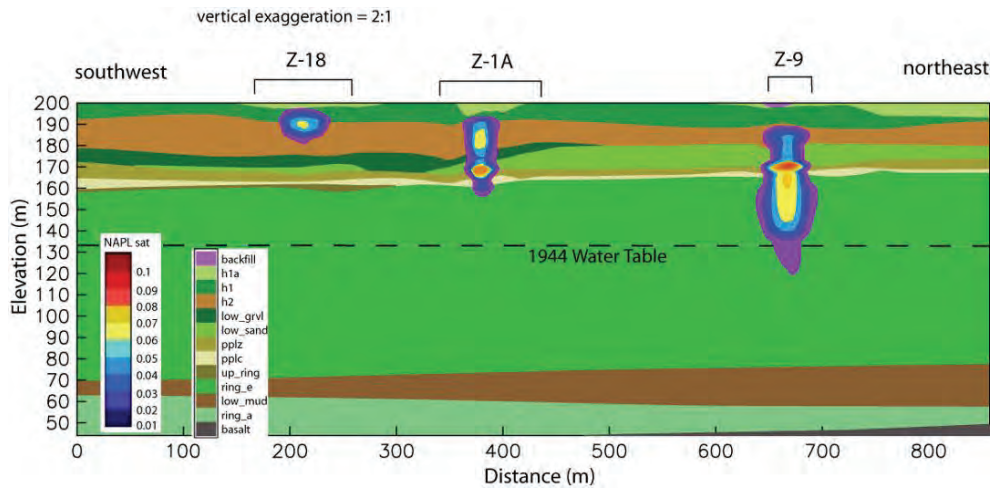
Figure 4.52. DNAPL Saturations at 1974 (Base Case)
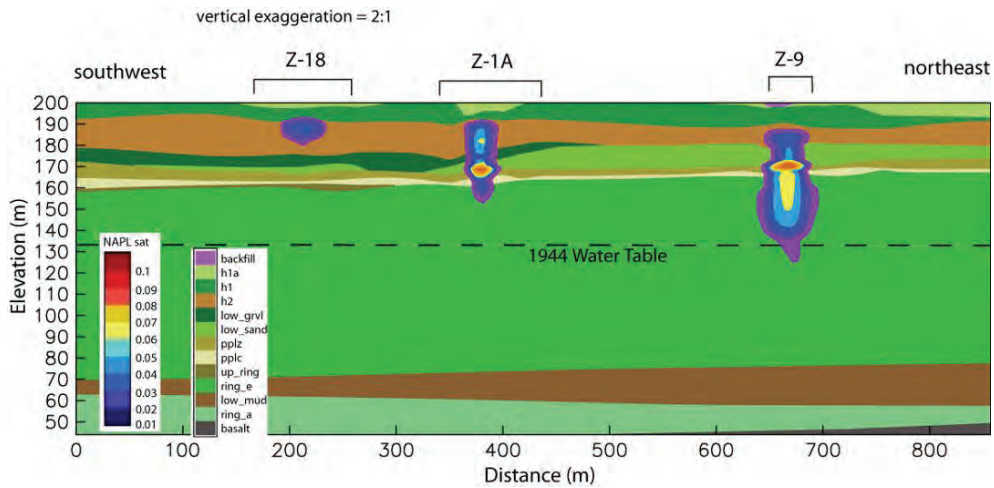
Figure 4.53. DNAPL Saturations at 1985 (Base Case)
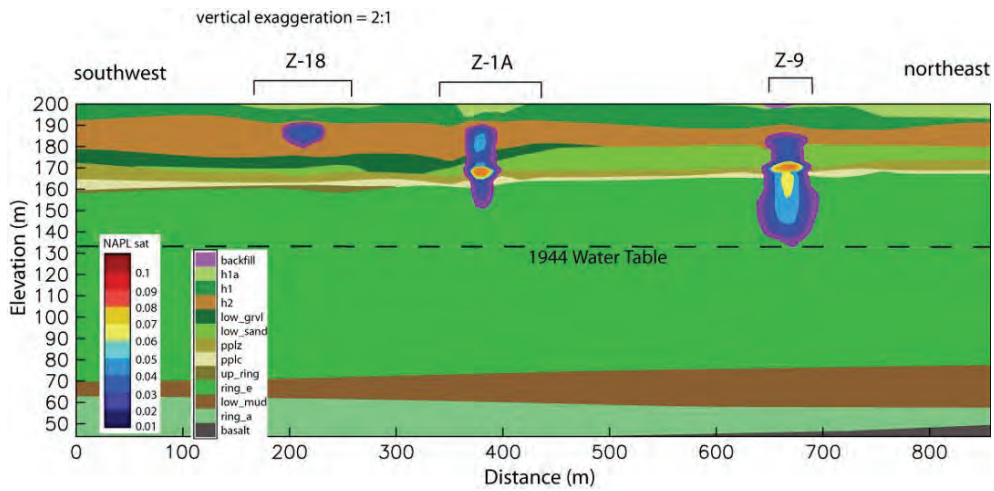
Figure 4.54. DNAPL Saturations at 1993 (Base Case)
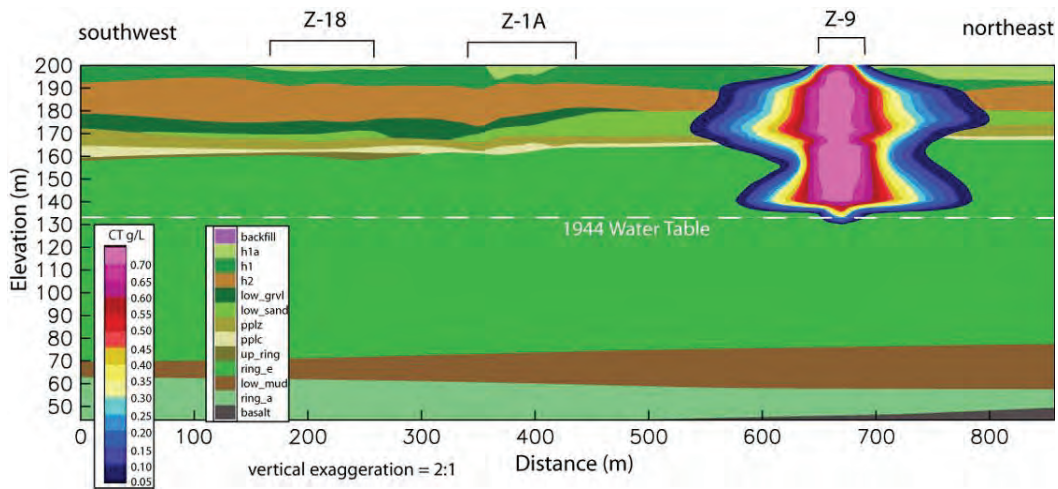
Figure 4.55. Aqueous CT Concentrations (g/L) at 1962.5 (Base Case)

4.33
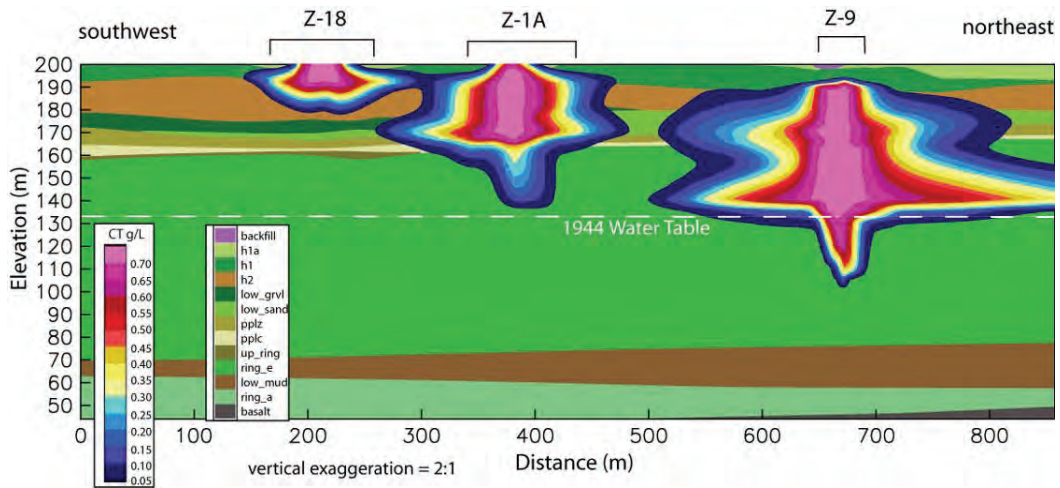
Figure 4.56. Aqueous CT Concentrations (g/L) at 1970 (Base Case)
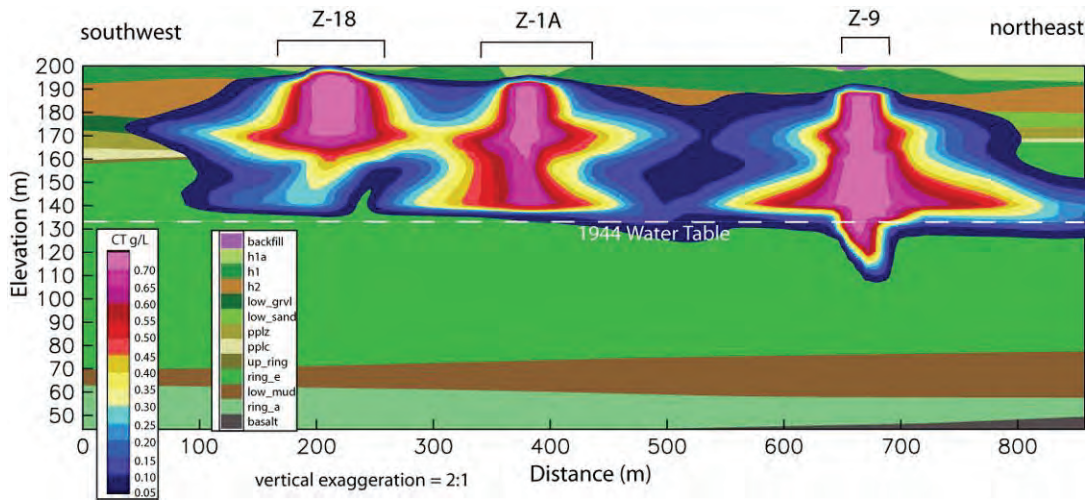
Figure 4.57. Aqueous CT Concentrations (g/L) at 1974 (Base Case)
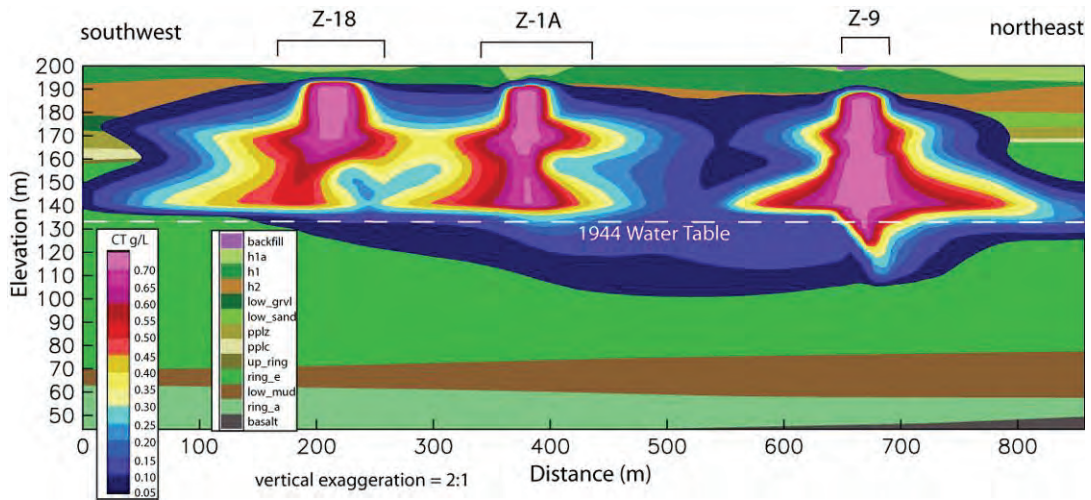
Figure 4.58. Aqueous CT Concentrations (g/L) at 1985 (Base Case)
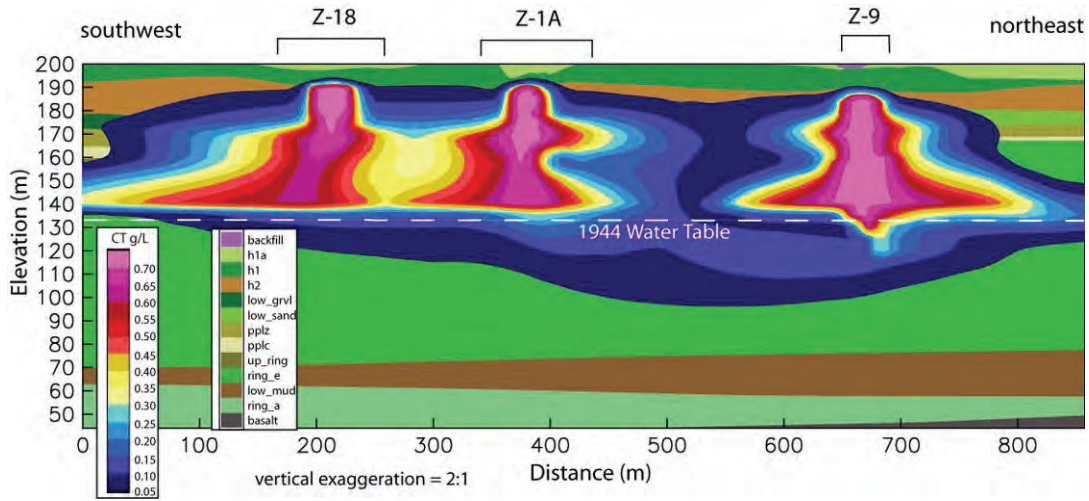
Figure 4.59. Aqueous CT Concentrations (g/L) at 1993 (Base Case)
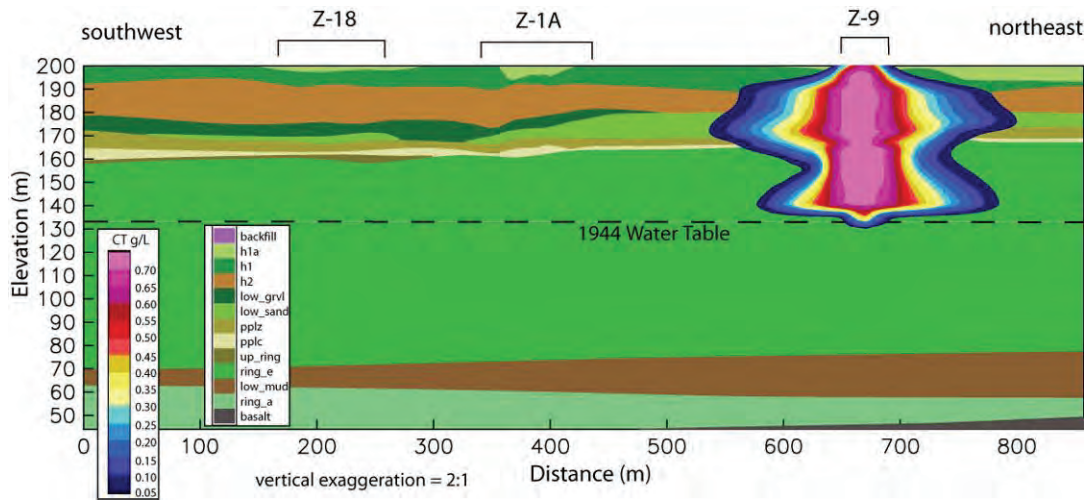
Figure 4.60. Gas CT Concentrations (g/L) at 1962.5 (Base Case)
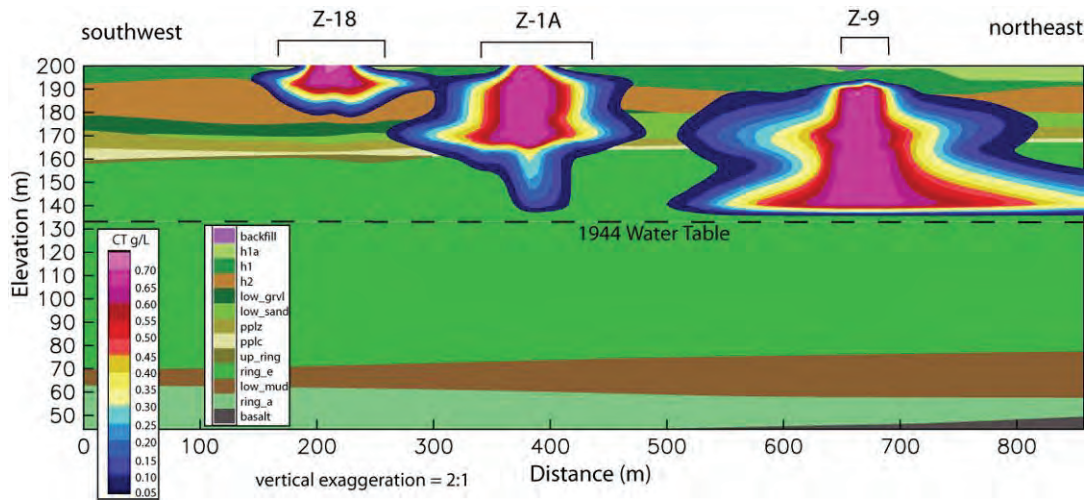
Figure 4.61. Gas CT Concentrations (g/L) at 1970 (Base Case)
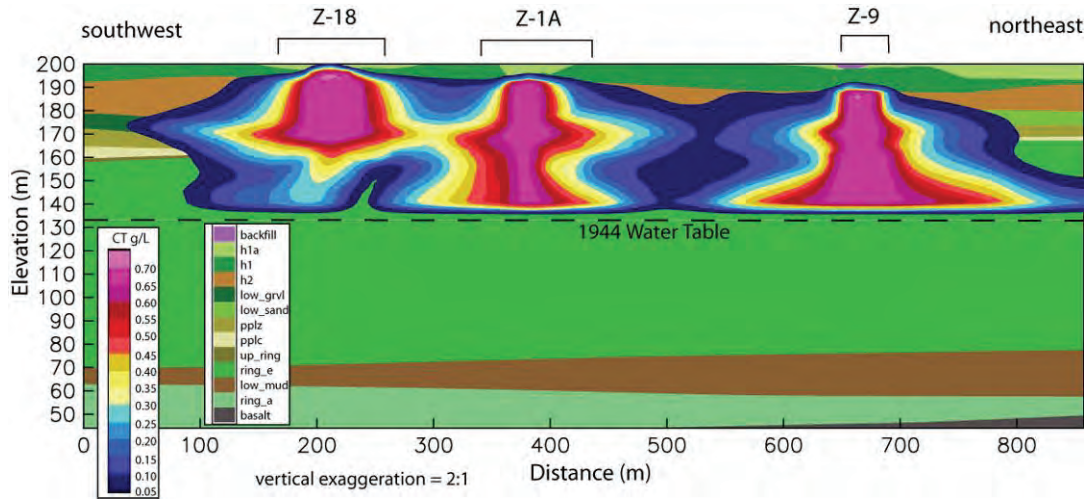
Figure 4.62. Gas CT Concentrations (g/L) at 1974 (Base Case)
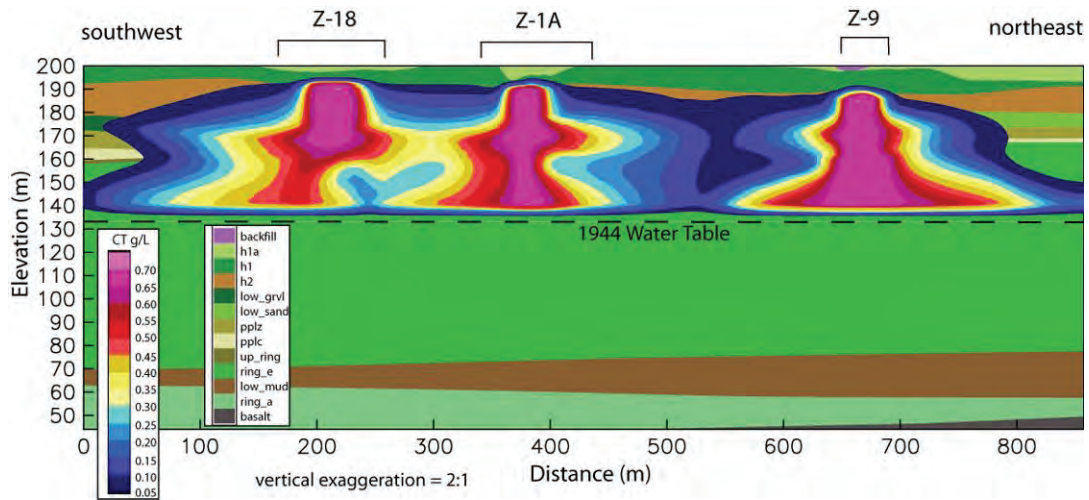
Figure 4.63. Gas CT Concentrations (g/L) at 1985 (Base Case)
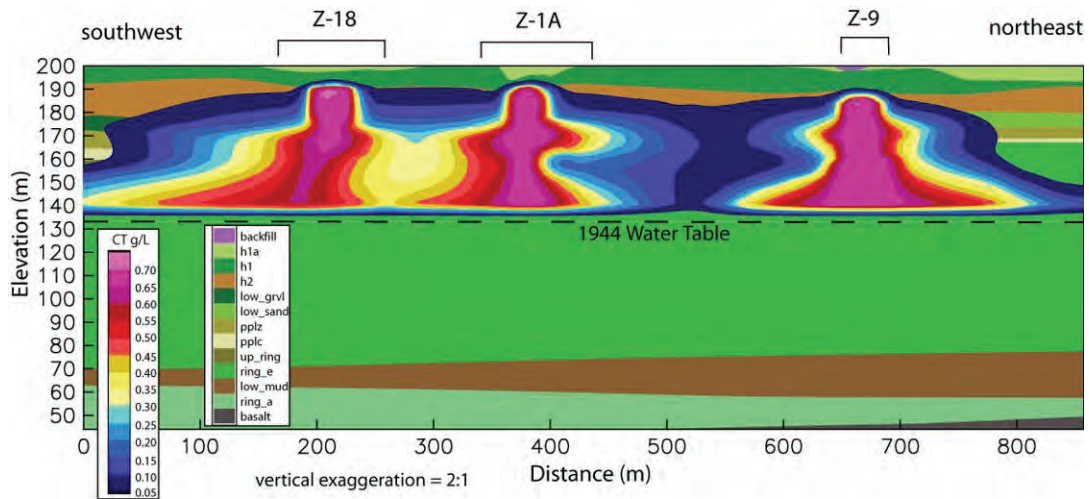
Figure 4.64. Gas CT Concentrations (g/L) at 1993 (Base Case)
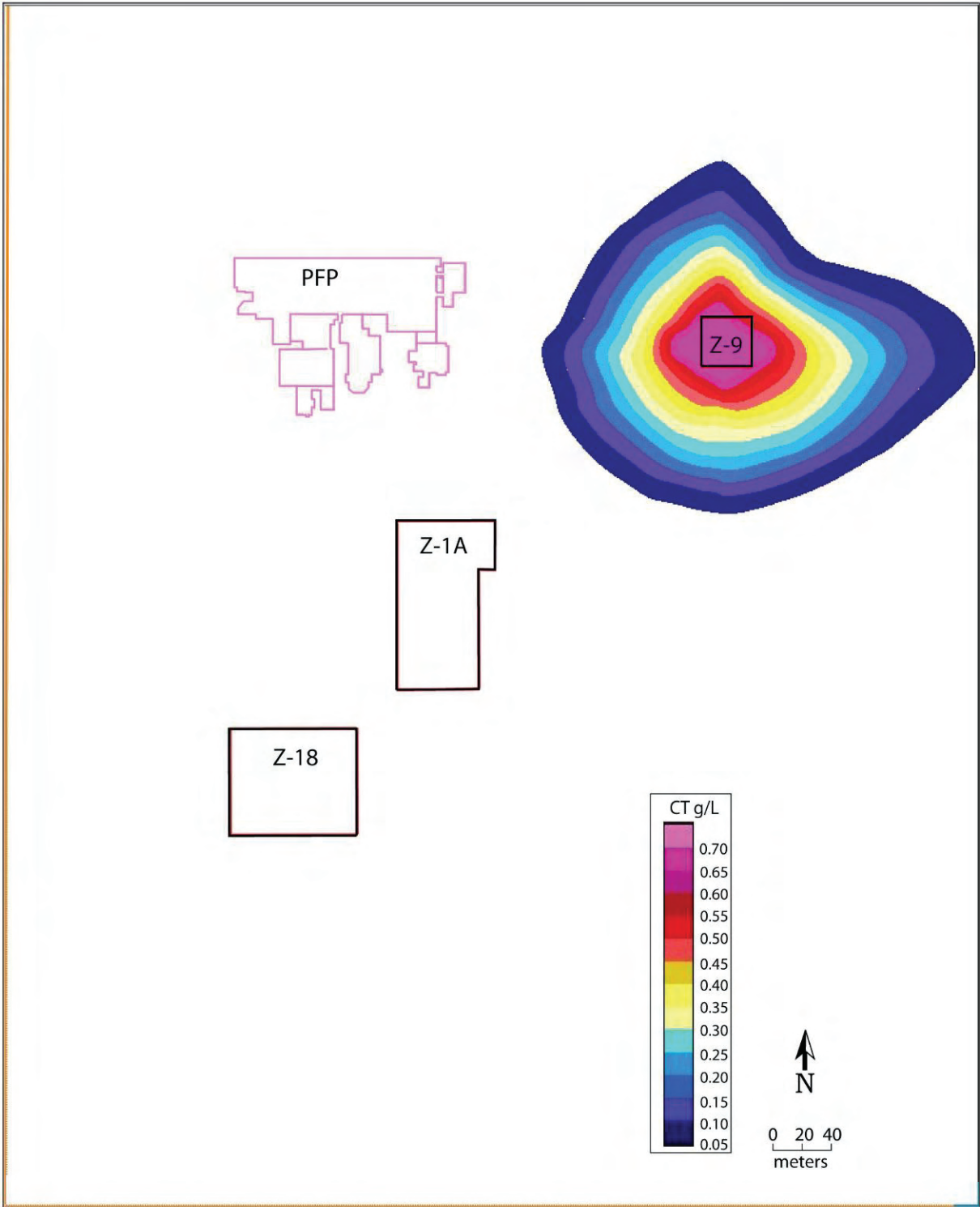
Figure 4.65.   Gas CT Concentrations at Interface Between Cold Creek Unit Silt and Carbonate (1962.5; Base Case)
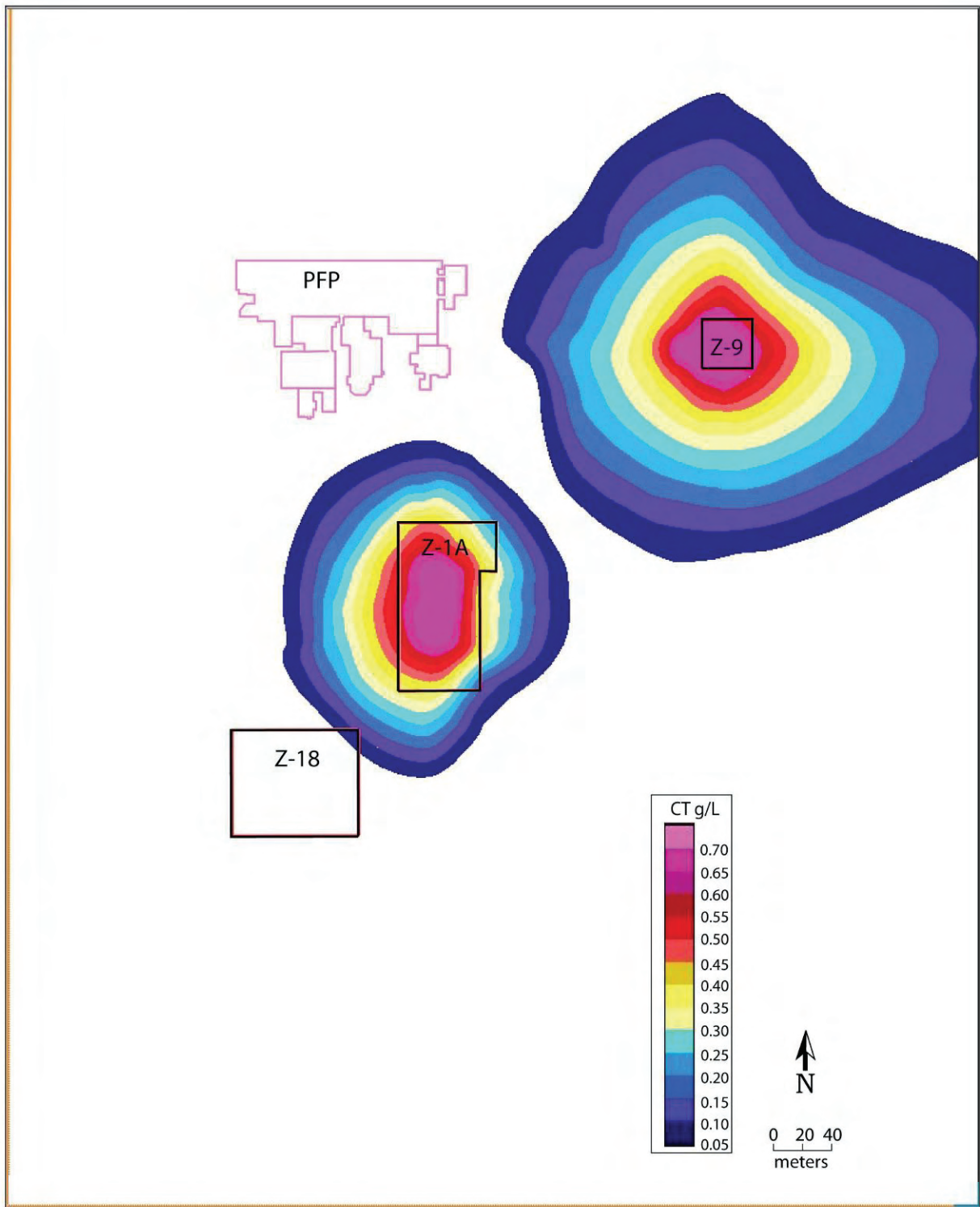
Figure 4.66.   Gas CT Concentrations at Interface Between Cold Creek Unit Silt and Carbonate (1970; Base Case)
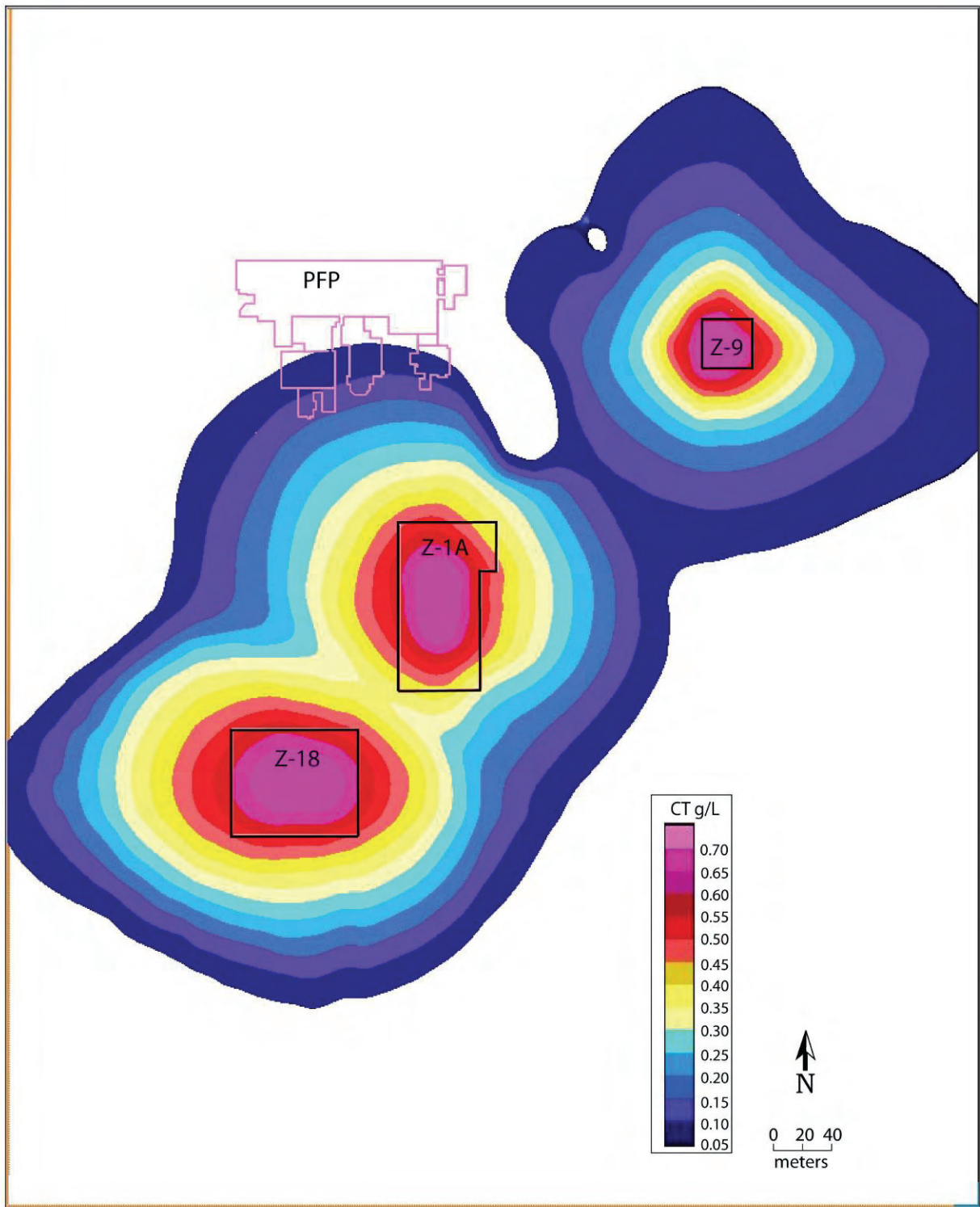
Figure 4.67.   Gas CT Concentrations at Interface Between Cold Creek Unit Silt and Carbonate (1980; Base Case)
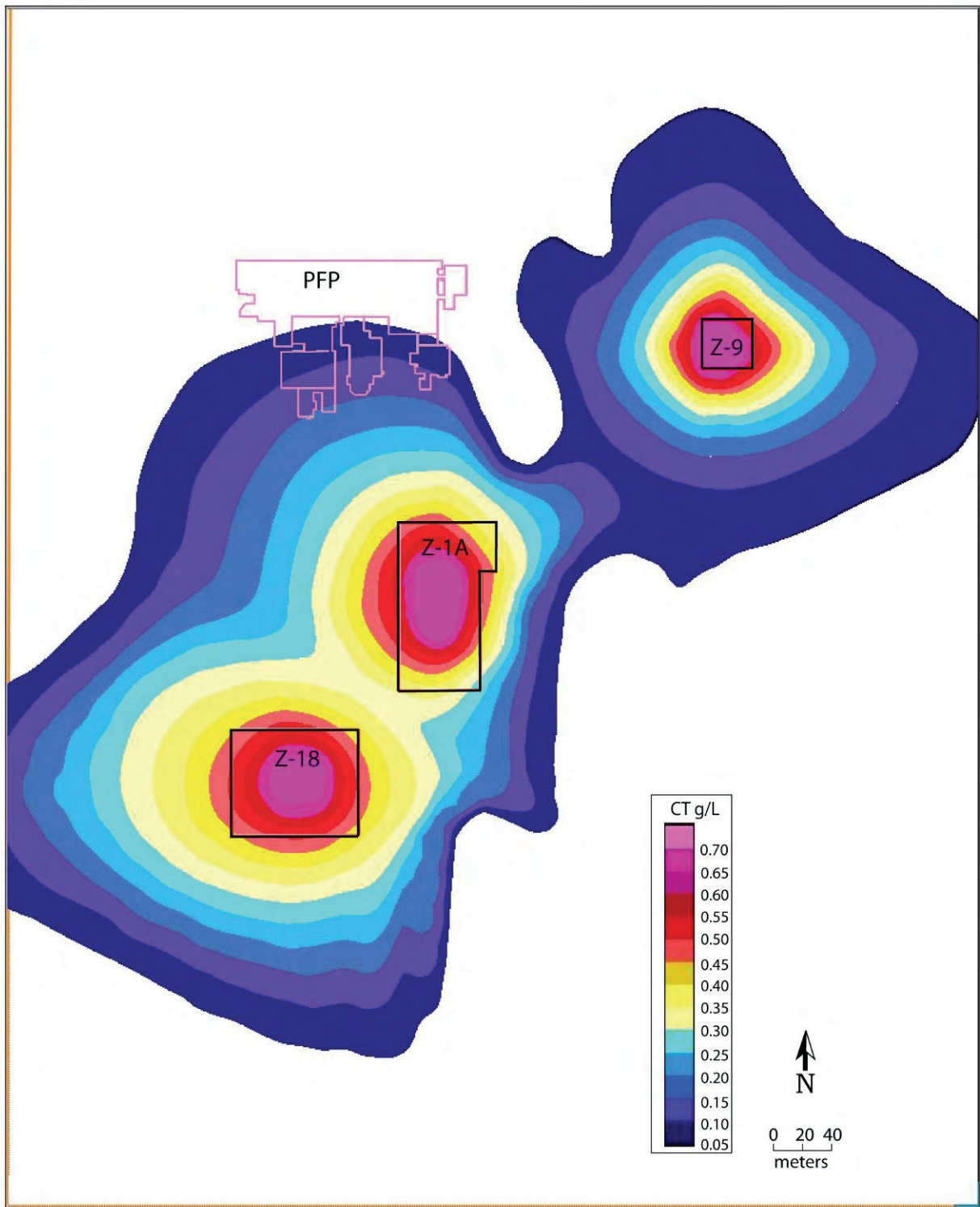
Figure 4.68.   Gas CT Concentrations at Interface Between Cold Creek Unit Silt and Carbonate (1993; Base Case)
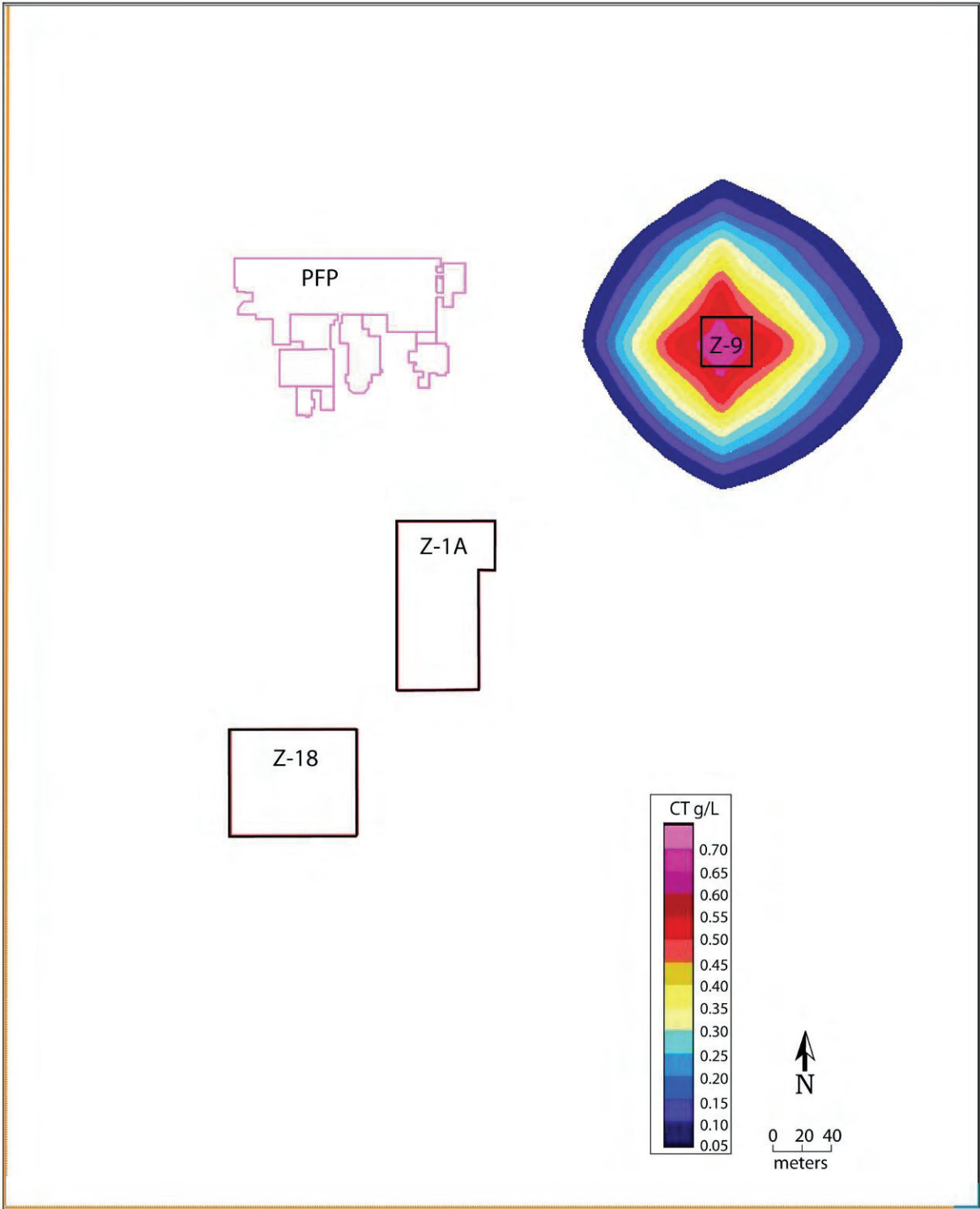
Figure 4.69. Gas CT Concentrations at Water Table (1962.5; Base Case)
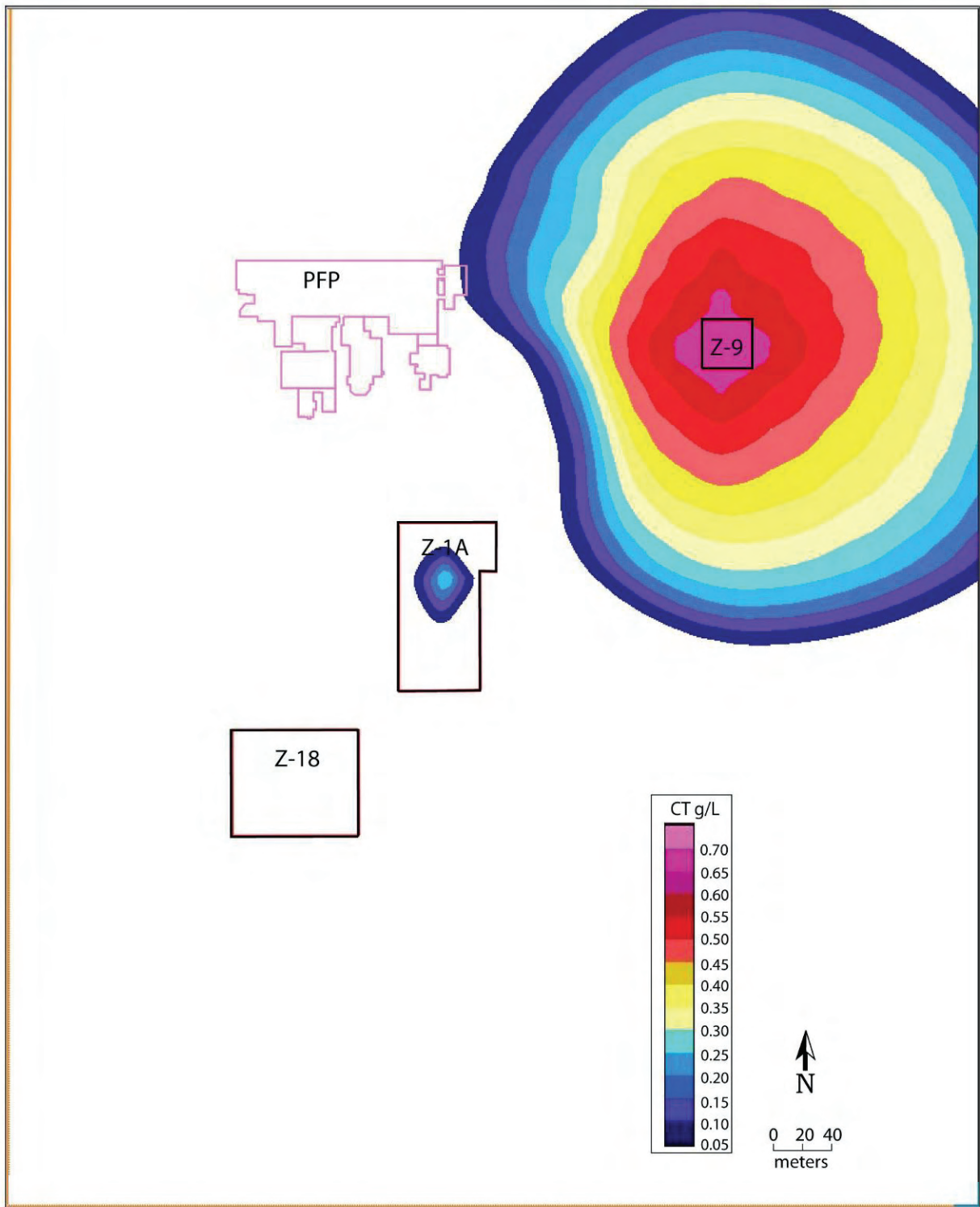
Figure 4.70. Gas CT Concentrations at Water Table (1970; Base Case)
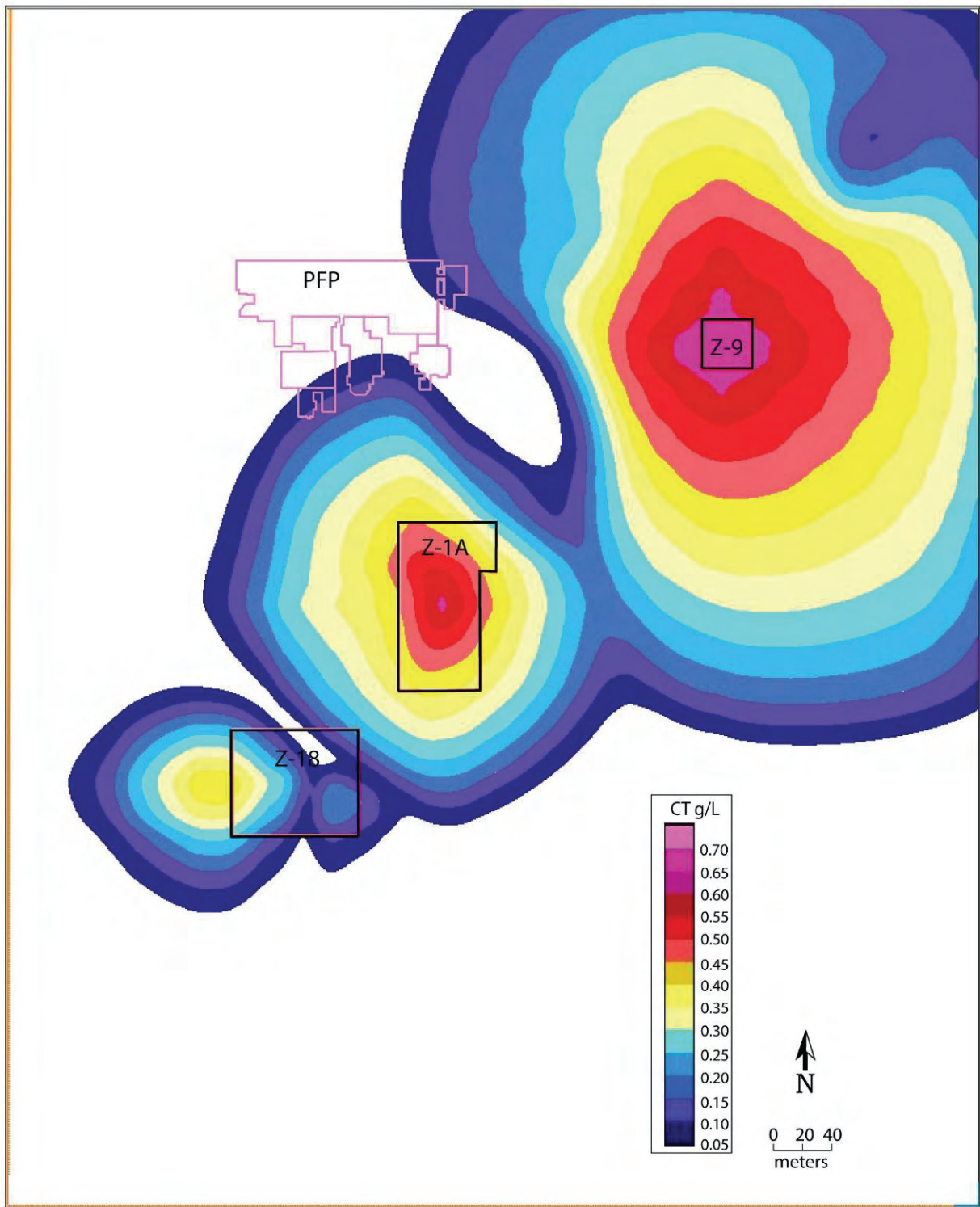
Figure 4.71. Gas CT Concentrations at Water Table (1980; Base Case)
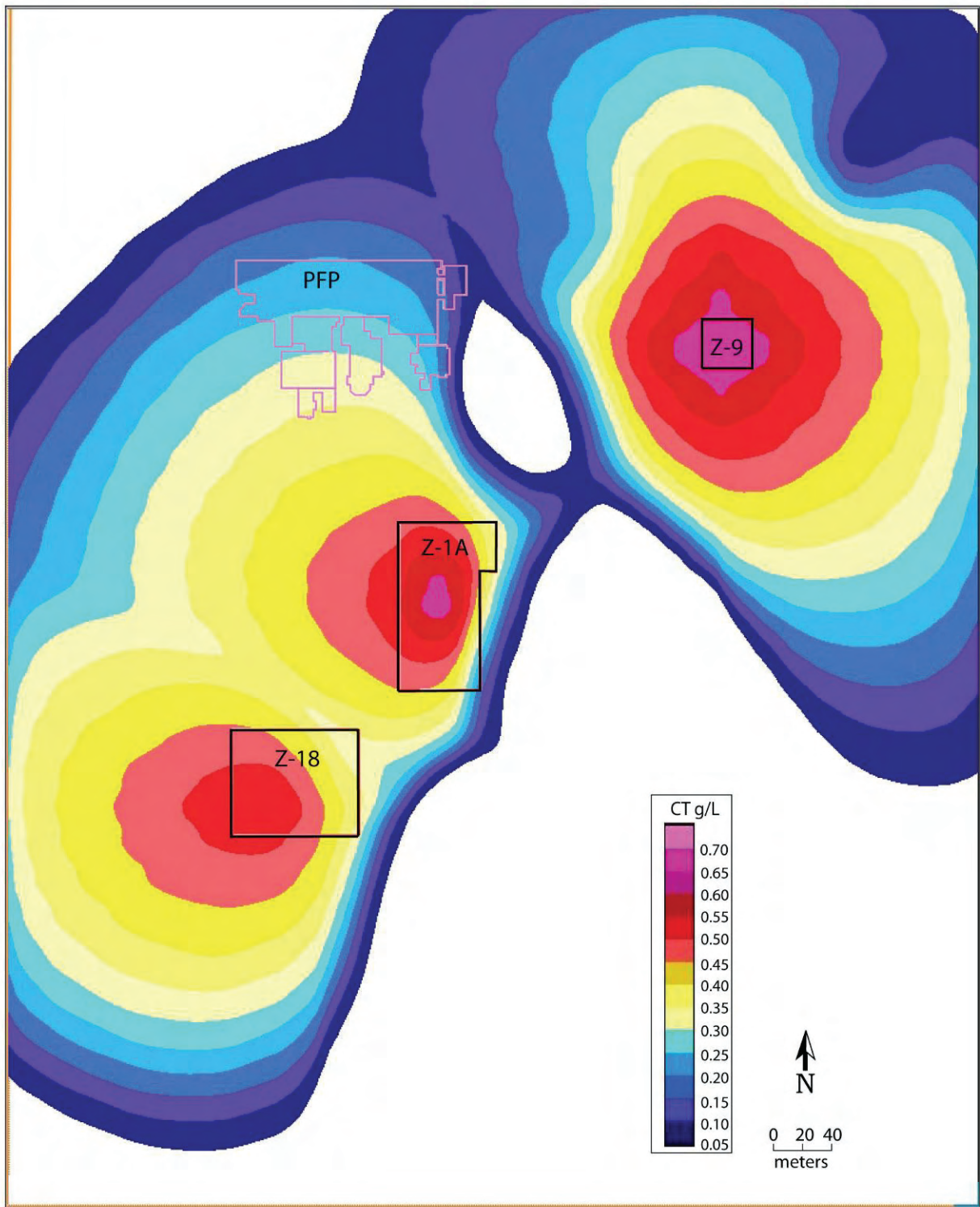
Figure 4.72. Gas CT Concentrations at Water Table (1993; Base Case)

For case 2, less DNAPL CT mass moved across the water table than for the base case (Figure 4.73). In addition, less DNAPL moved into and out of the Cold Creek Unit. This result is directly related to the decreased permeability and increased water saturations in this Unit. Figure 4.74 show that more DNAPL was able to remain in the domain compared to the base case. As less DNAPL was predicted to move vertically, less volatilization and movement in the gas phase was observed. As a result, less mass was predicted to move into the sorbed phase. Distributions into the hydrostratigraphic units are depicted in Figure 4.75. DNAPL saturations are shown at five different times in Figures 4.76 to 4.80. The plots also show that less DNAPL moved vertically downward compared to the base-case results.
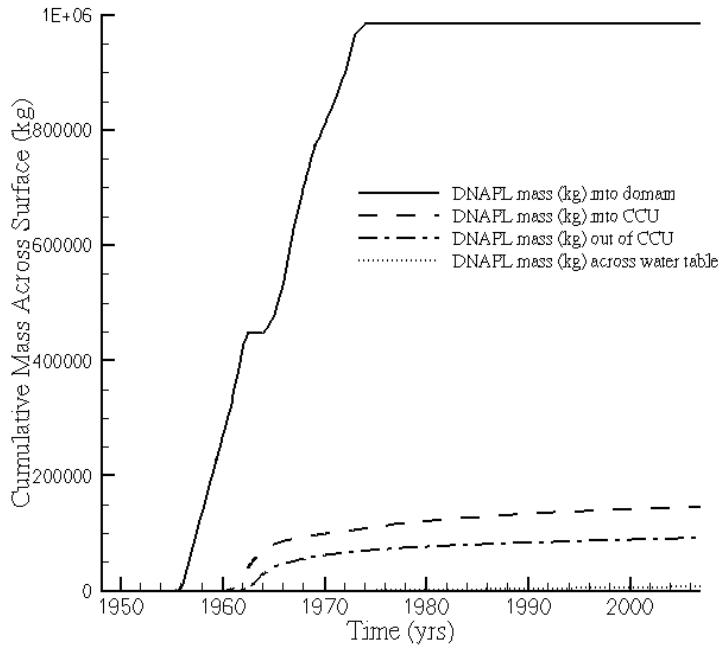
Figure 4.73. Pertinent DNAPL Mass Fluxes (Case 2)
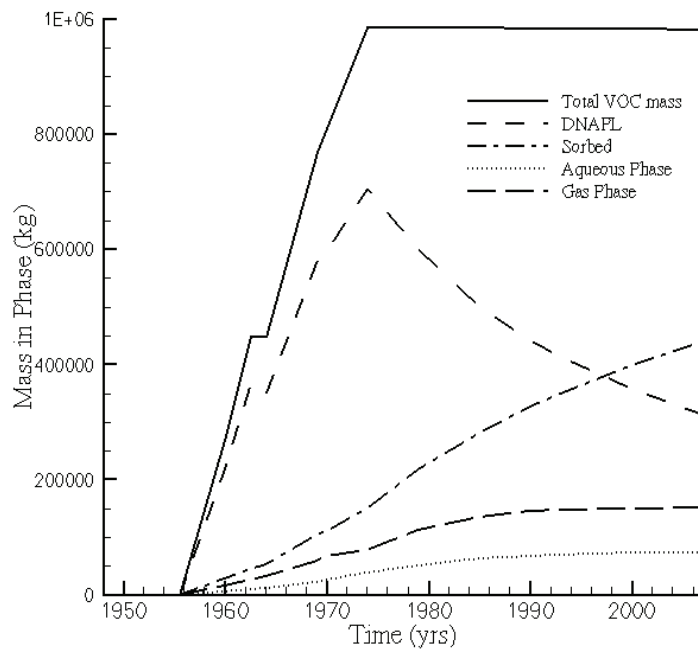
Figure 4.74.   CT Mass Distribution Over the DNAPL, Sorbed, Aqueous, and Gas Phases (Case 2; No SVE)
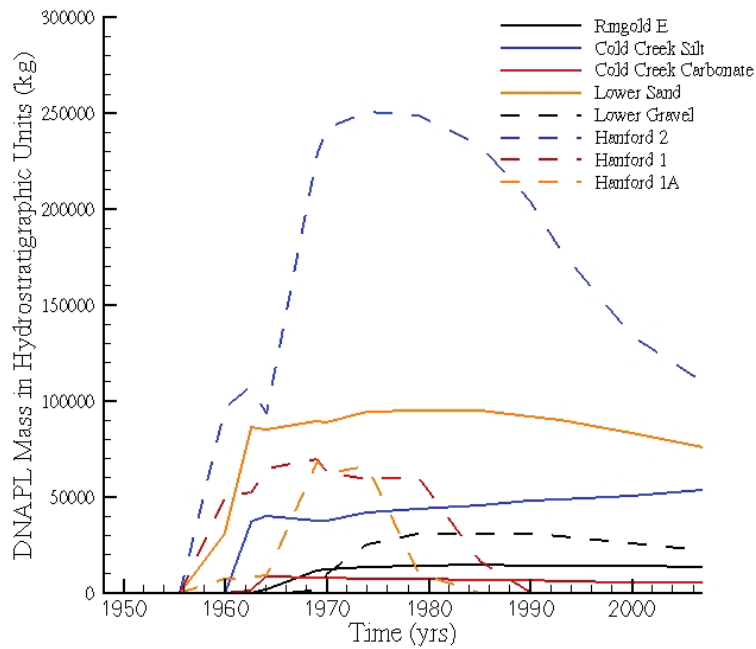
Figure 4.75. DNAPL CT Mass Distribution Over the Hydrostratigraphic Units (Case 2, No SVE)
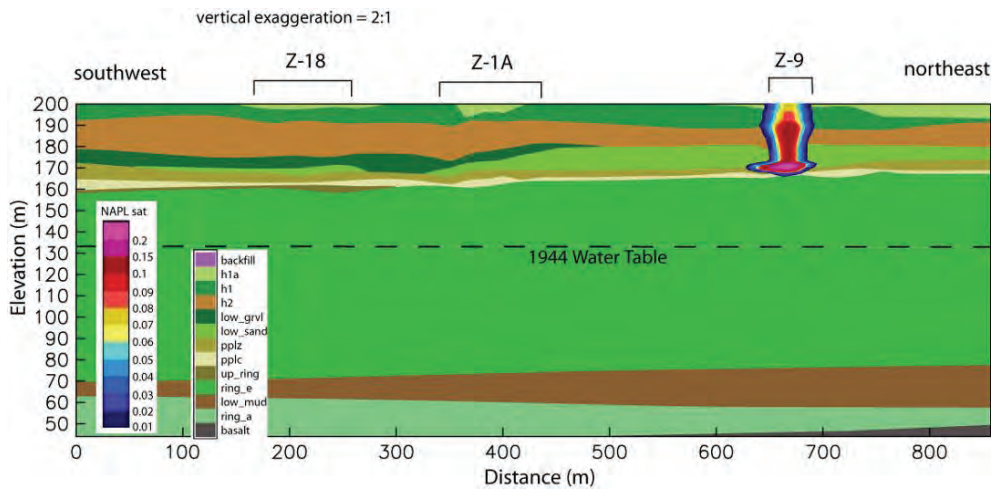
Figure 4.76. DNAPL Saturations at 1962.5 (Case 2)
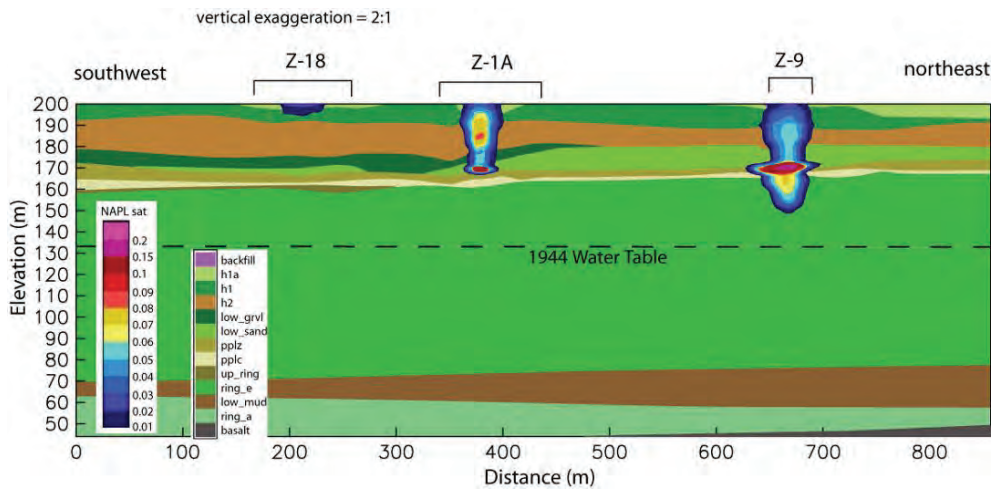
Figure 4.77. DNAPL Saturations at 1970 (Case 2)
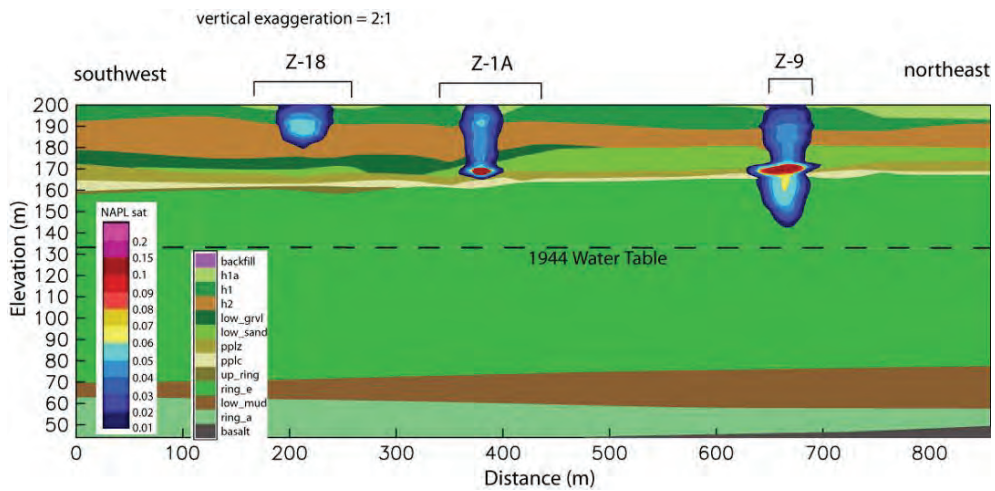
Figure 4.78. DNAPL Saturations at 1974 (Case 2)
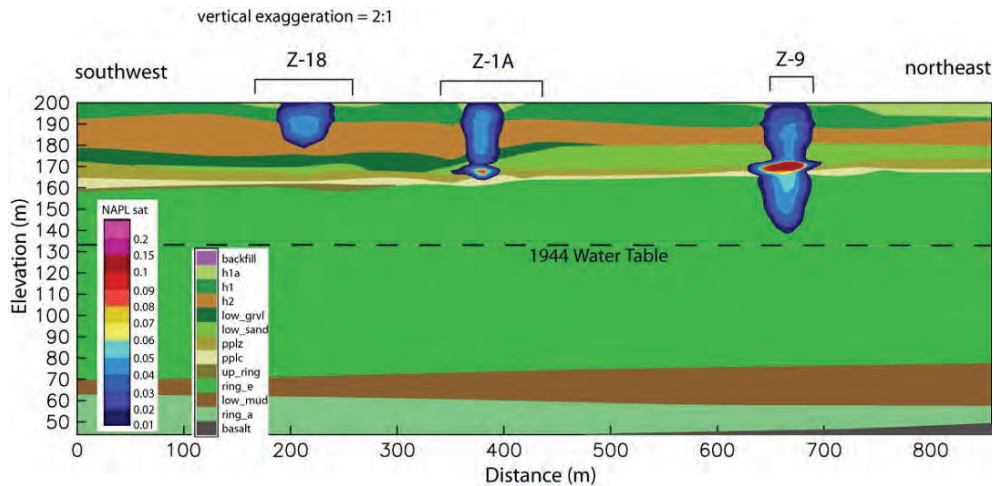
Figure 4.79. DNAPL Saturations at 1985 (Case 2)
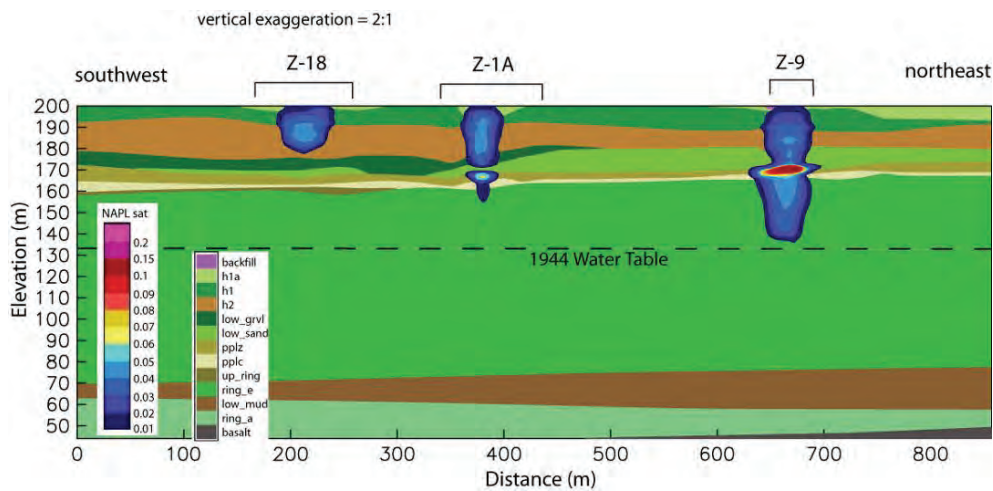
Figure 4.80. DNAPL Saturations at 1993 (Case 2)

For the case 3 simulation, no DNAPL CT mass moved across the water table (Figure 4.81). In addition, even less DNAPL moved into and out of the Cold Creek Unit than for case 2. This result is again directly related to the decreased permeability and increased water saturations in this unit. Figures 4.82 shows that more DNAPL was able to remain in the domain compared to the base case. Similar as for case 2, as less DNAPL was predicted to move vertically, less volatilization and movement in the gas phase was observed. As a result, less mass was predicted to move into the sorbed phase. Distributions of DNAPL in the hydrostratigraphic units are depicted in Figures 4.83. DNAPL saturations are shown at five different times in Figures 4.84 to 4.88. The plots show that no DNAPL moved below the Cold Creek Unit by 1993.
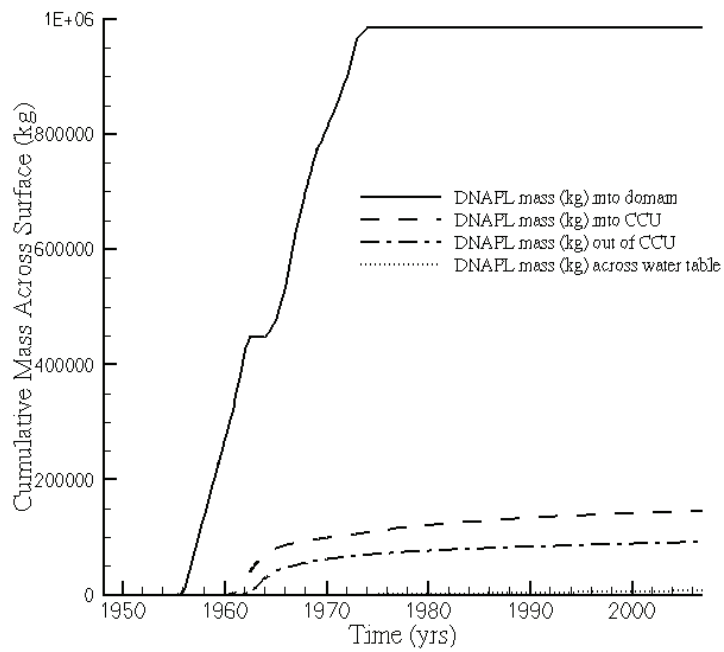
Figure 4.81. Pertinent DNAPL Mass Fluxes (Case 3)
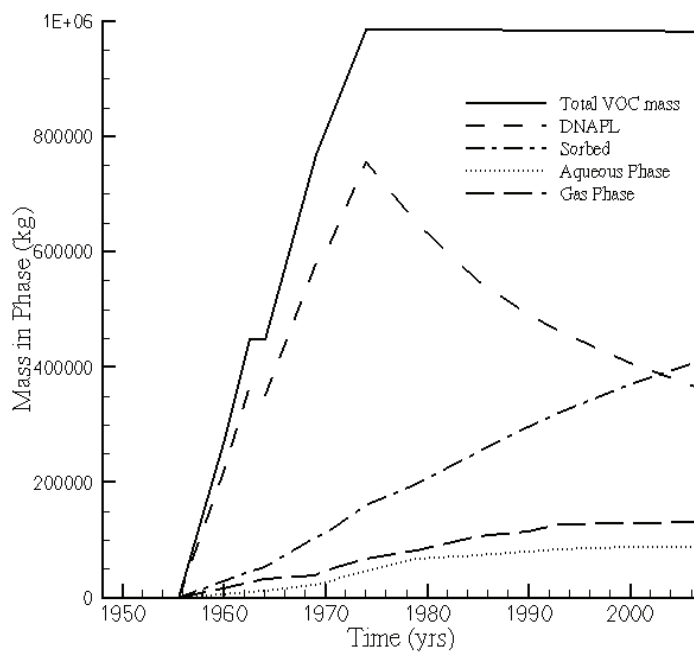
Figure 4.82. CT Mass Distribution Over the DNAPL, Sorbed, Aqueous, and Gas Phases (Case 3; No SVE)
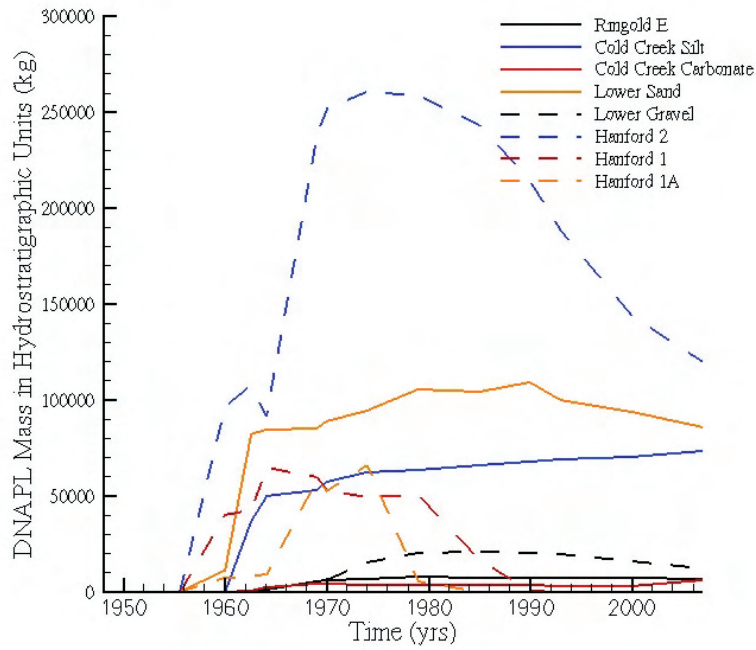
Figure 4.83. DNAPL CT Mass Distribution Over the Hydrostratigraphic Units (Case 3, No SVE)
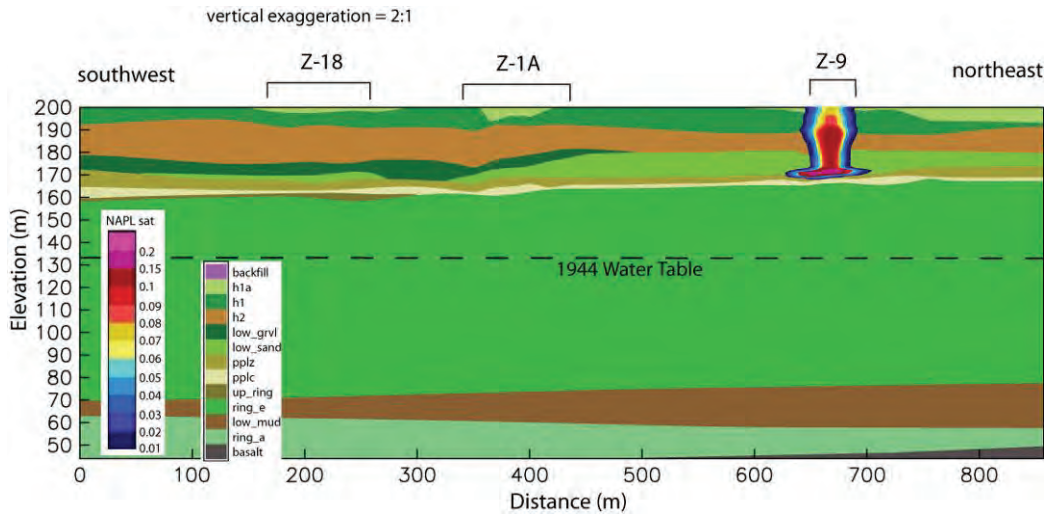
Figure 4.84. DNAPL Saturations at 1962.5 (Case 3)
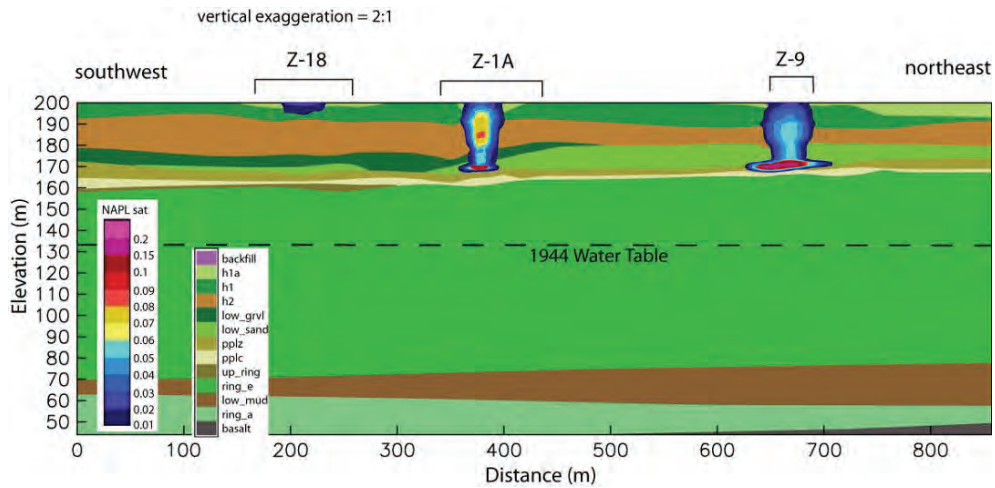
Figure 4.85. DNAPL Saturations at 1970 (Case 3)
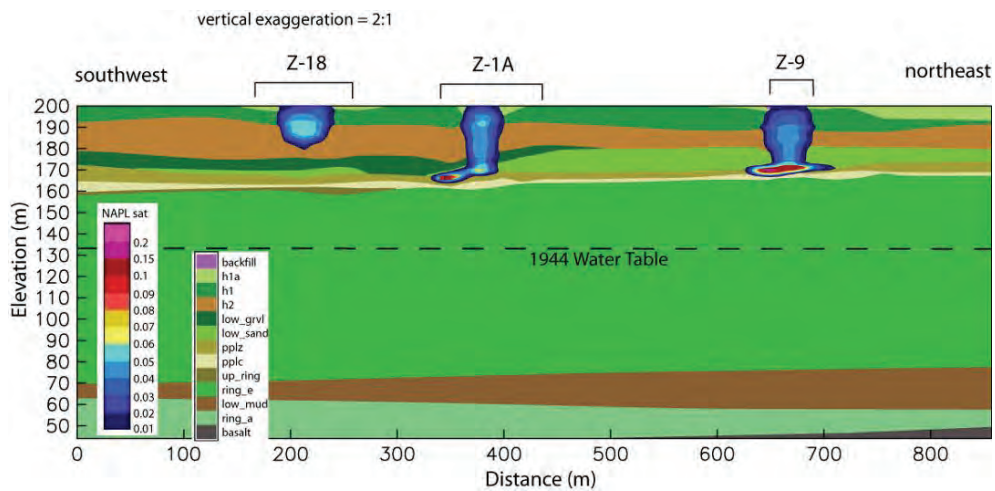
Figure 4.86. DNAPL Saturations at 1974 (Case 3)
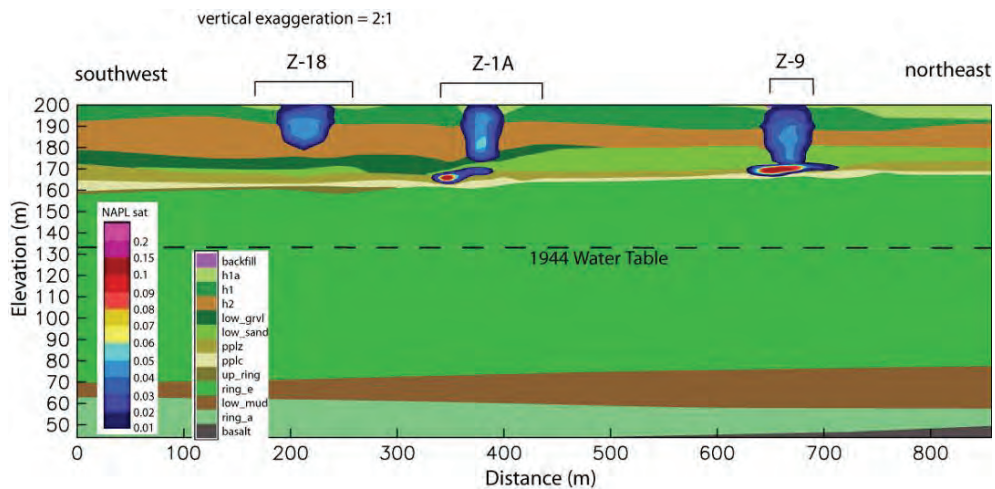
Figure 4.87. DNAPL Saturations at 1985 (Case 3)
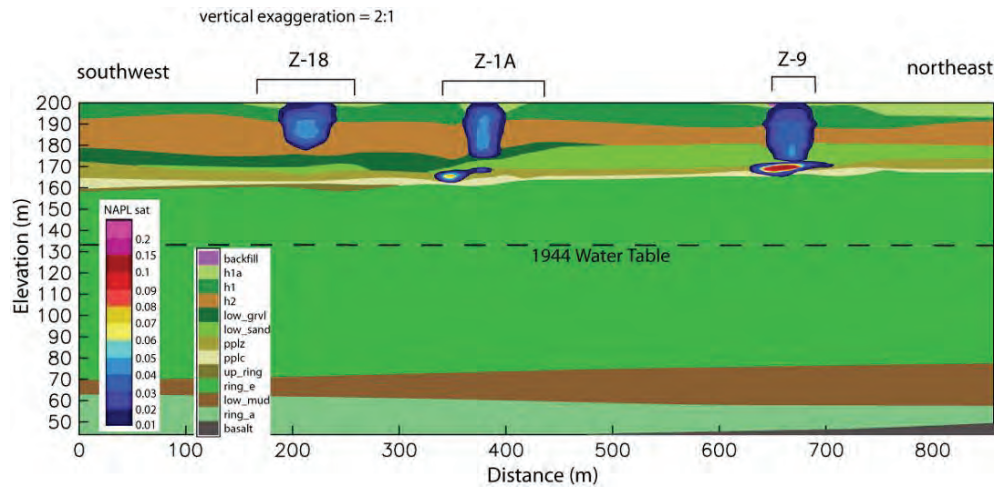
Figure 4.88. DNAPL Saturations at 1993 (Case 3)

5.0   216-Z-9 Simulation Results

A series of seven multifluid local-scale flow and transport simulations were3 completed to quantify DNAPL, aqueous, and gas CT transport in the subsurface of the 216-Z-9 disposal site. Of the three major DNAPL disposal sites, the 216-Z9 received the most DNAPL and it has the smallest footprint. CT concentrations of approximately 350,000 µg/kg were observed in a 1-ft thick lens, located at 19.8 m (65 ft) below the ground surface DOE-RL (2006). Six of the seven simulations (imposed cases 1-6) were conducted with imposed CT quantities of 100, 10 and 1% of the observed 350,000 µg/kg value in both the Cold Creek Unit and/or the 1-ft thick silt lens, located in the Hanford 2 unit below the disposal site. The simulation period for these six cases was from 2007 – 2107. The seventh case (modeled case) simulated flow and transport following aqueous phase and DNAPL disposal at the site using inventory data and SVE of 53,000 kg after 1993. The simulation period for this case was from 1955 – 2107. The computational domain of was 540, 440, and 159 m in the x-, y-, and z-direction, respectively (Oostrom et al. 2004; 2006a).

For the first five imposed cases, the imposed CT sorbed concentrations were either 3,500, 35,000, and 350,000 µg/kg (Table 3.7). Assuming a K_d value of 0.2 mL/g, the maximum sorbed CT concentration for porous media in the 65-ft silt lens and the Cold Creek Unit, is approximately 141,000 µg/kg. For the simulations where 350,000 µg/kg was imposed (imposed cases 1, 4, and 5), the excess of 209,000 µg/kg entered the system as a DNAPL, corresponding to a saturation of approximately 7 x 10^{-4}. For the imposed cases 1, 4, and 5, the small DNAPL volume was rapidly transformed into dissolved gas-phase, aqueous-phase, and sorbed CT.

Sorbed CT mass concentrations (µg/kg) at various times, as a function of elevation directly underneath the 216-Z-9 disposal site, are presented in Figures 5.1 through 5.7 for the seven cases. Since equilibrium conditions are assumed in the simulations, aqueous and gas CT concentrations will show the same trends as depicted for the sorbed CT mass concentrations. The results for the imposed cases 1 – 5, with none or small amounts of initial DNAPL present, show that the concentrations in the zones where the CT was emplaced decrease rapidly with time. These figures also show that most of the CT is transported in a downward direction. A comparison of imposed case 1 (Figure 5.1), imposed case 4 (Figure 5.4) and imposed case 5 (Figure 5.5) indicates that the contribution of the CT originally emplaced in the 65-ft silt layer is rather small. The similarity between Figures 5.1 and 5.4 clearly demonstrates that the majority of the CT at various times originates from the Cold Creek Unit. Only above an elevation of 180 m are the concentrations affected by 65-ft silt layer CT.

Transport across the water table of dissolved CT in the gas and aqueous phase appears to occur after 2025 for imposed case 1 and 4 (Figures 5.1 and 5.4, respectively). For the two cases with reduced CT emplacement (imposed case 2 and 3), and the case where CT was emplaced in the 65-ft silt layer only, the figures indicated that no or only small amounts of CT in the gas or aqueous phase were transported across the water table. The actual computed amounts are presented in Section 5.1.

The sorbed concentration versus elevation plots for imposed case 6 (Figure 5.6) and the modeled case (Figure 5.7) are more complex. Both cases have considerable amounts of DNAPL initially present in the system. As is shown in Section 5.3, DNAPL is predicted to be present in imposed case 6 until approximately 2060, while for the modeled case, DNAPL will be in the system through 2107. For imposed case 6, the zone with maximum sorbed concentration expands beyond the 65-ft silt layer and the

Cold Creek Unit through at least 2025. After that, the concentrations slowly decrease until a condition is obtained at 2107 where the concentration gradually increases from 0 at the top of the domain, to approximately 35,000 µg/kg directly above the saturated zone. For the modeled case, the sorbed concentrations remain high throughout the simulation period due to the persistence of DNAPL in the domain (Figure 5.7).

In the remainder of this section the following simulation output will be discussed:

- Section 5.1 - CT mass flow rate and cumulative mass transport across the water table and model boundaries

- Section 5.2 - Aqueous phase mass fluxes across the water table

- Section 5.3 - CT phase partitioning over time.
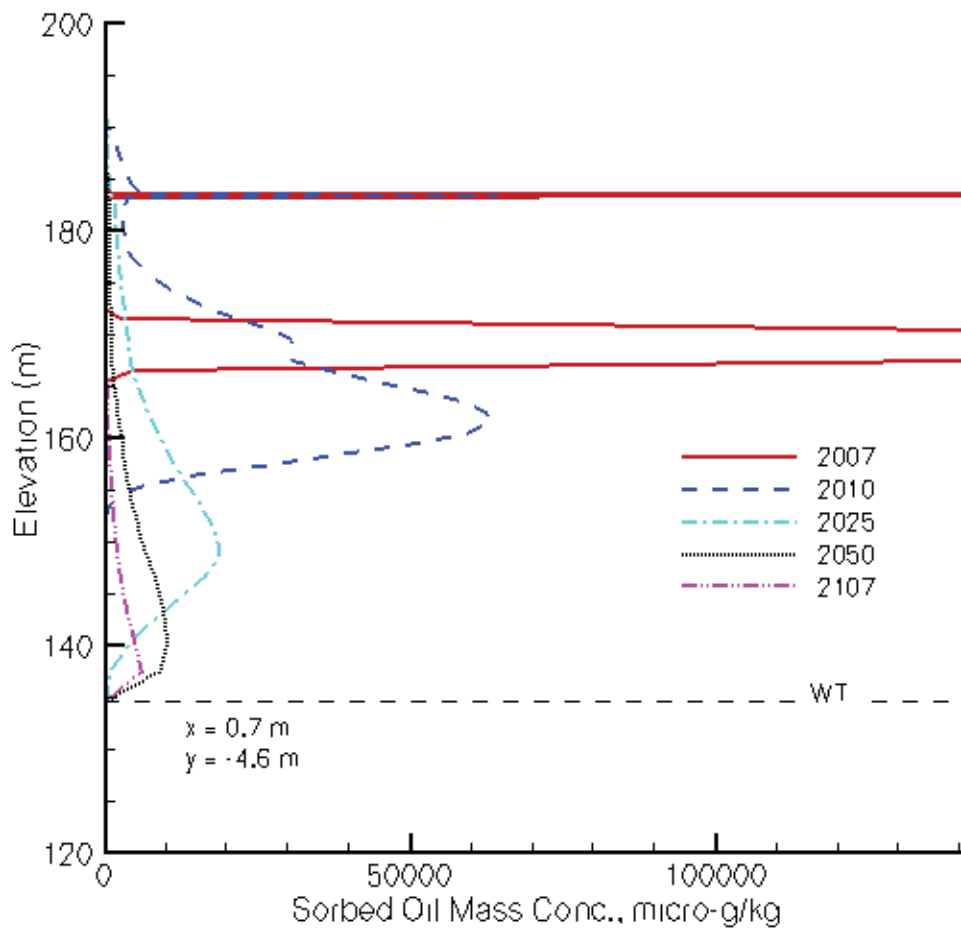
Figure 5.1.   Sorbed CT Mass Concentration (µg/kg) Profile at Different Times at (x, y) = (0.7, -4.6) m for Imposed Case 1. The center of the Z-9 trench is located at (x, y) = (0, 0) m. The dashed line marked with WT denotes the water table.
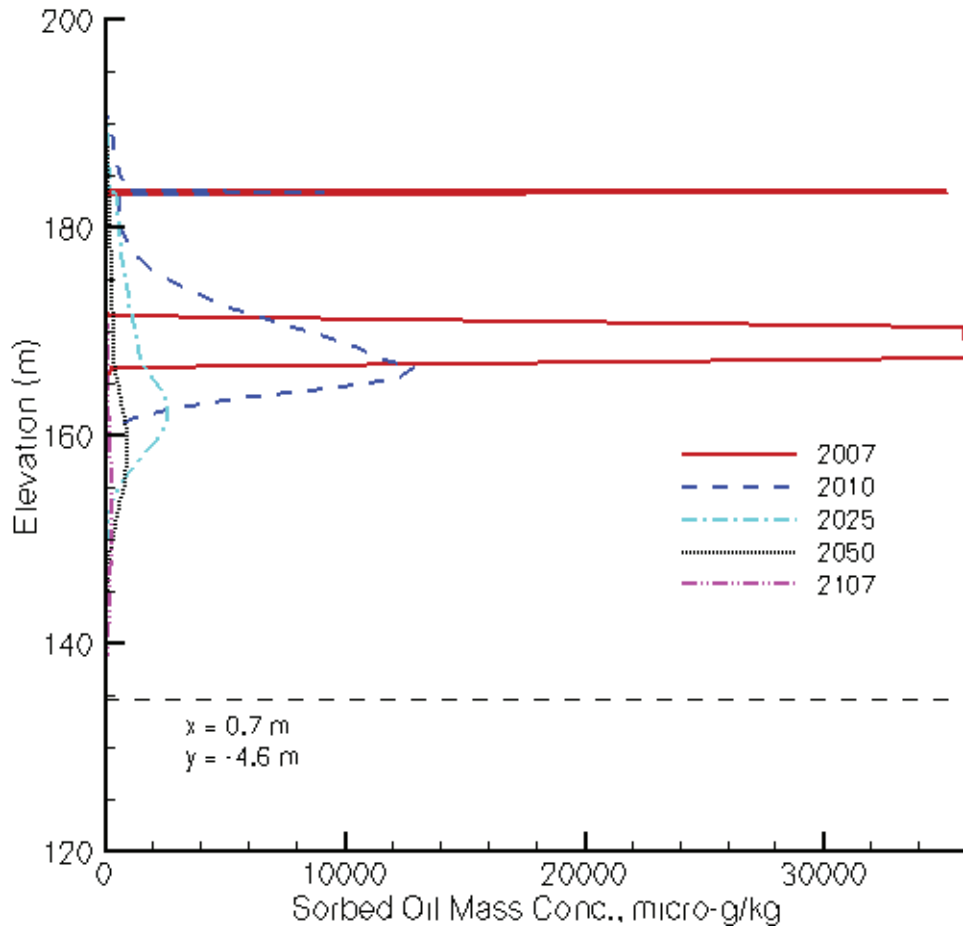
Figure 5.2. Sorbed CT Mass Concentration (μg/kg) Profile at Different Times at (x, y) = (0.7, -4.6) m for Imposed Case 2. The center of the Z-9 trench is located at (x, y) = (0, 0) m. The dashed line marked with WT denotes the water table.
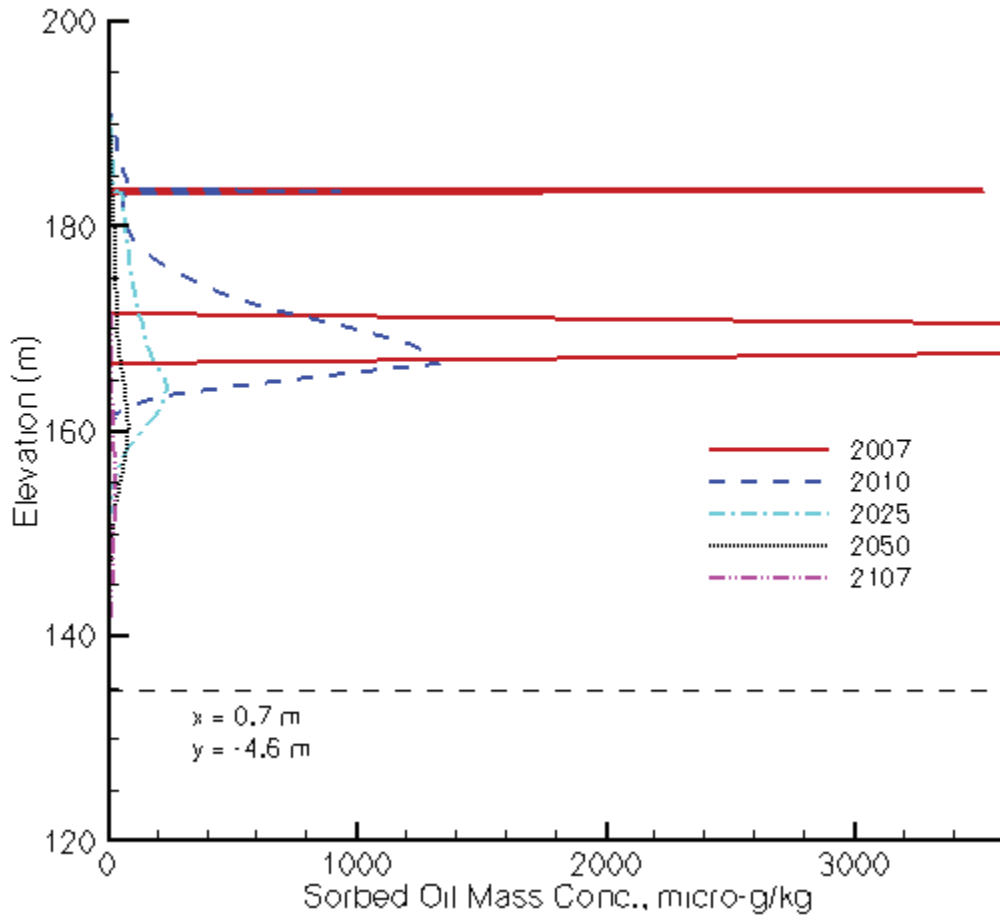
Figure 5.3.   Sorbed CT Mass Concentration (μg/kg) Profile at Different Times at (x, y) = (0.7, -4.6) m for Imposed Case 3. The center of the Z-9 trench is located at (x, y) = (0, 0) m. The dashed line marked with WT denotes the water table.
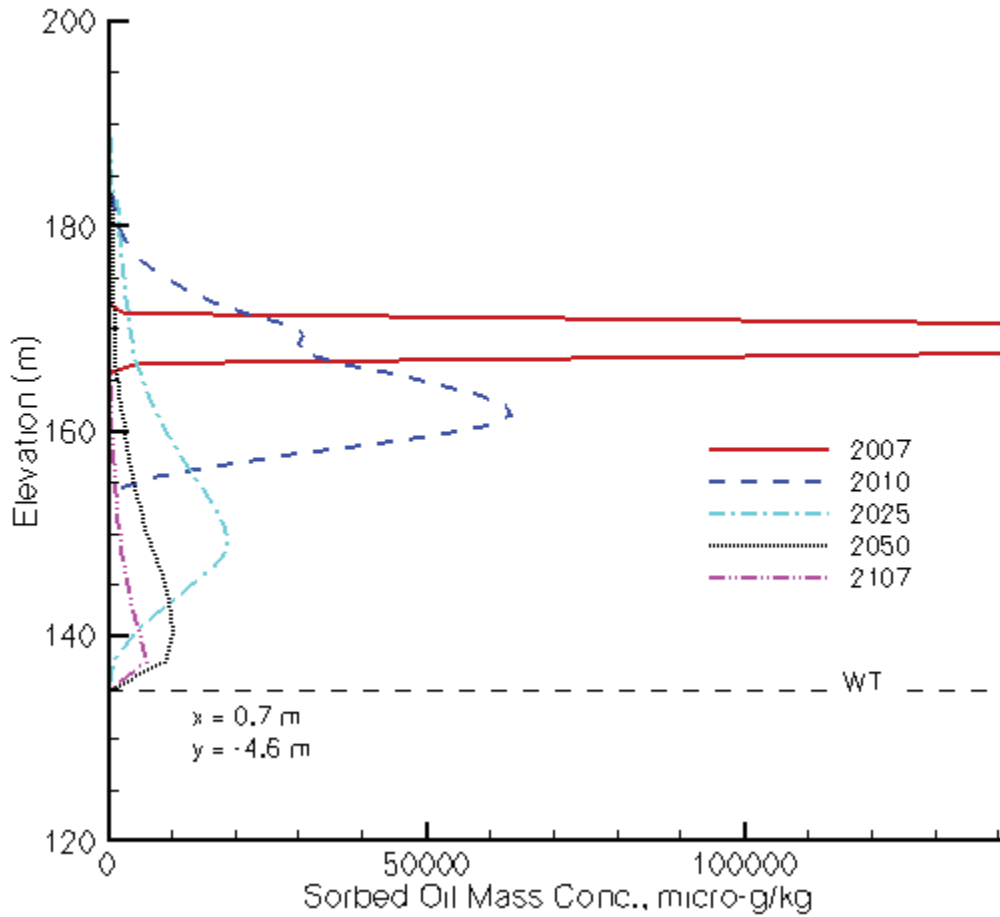
Figure 5.4.   Sorbed CT Mass Concentration (μg/kg) Profile at Different Times at (x, y) = (0.7, -4.6) m for Imposed Case 4. The center of the Z-9 trench is located at (x, y) = (0, 0) m. The dashed line marked with WT denotes the water table.
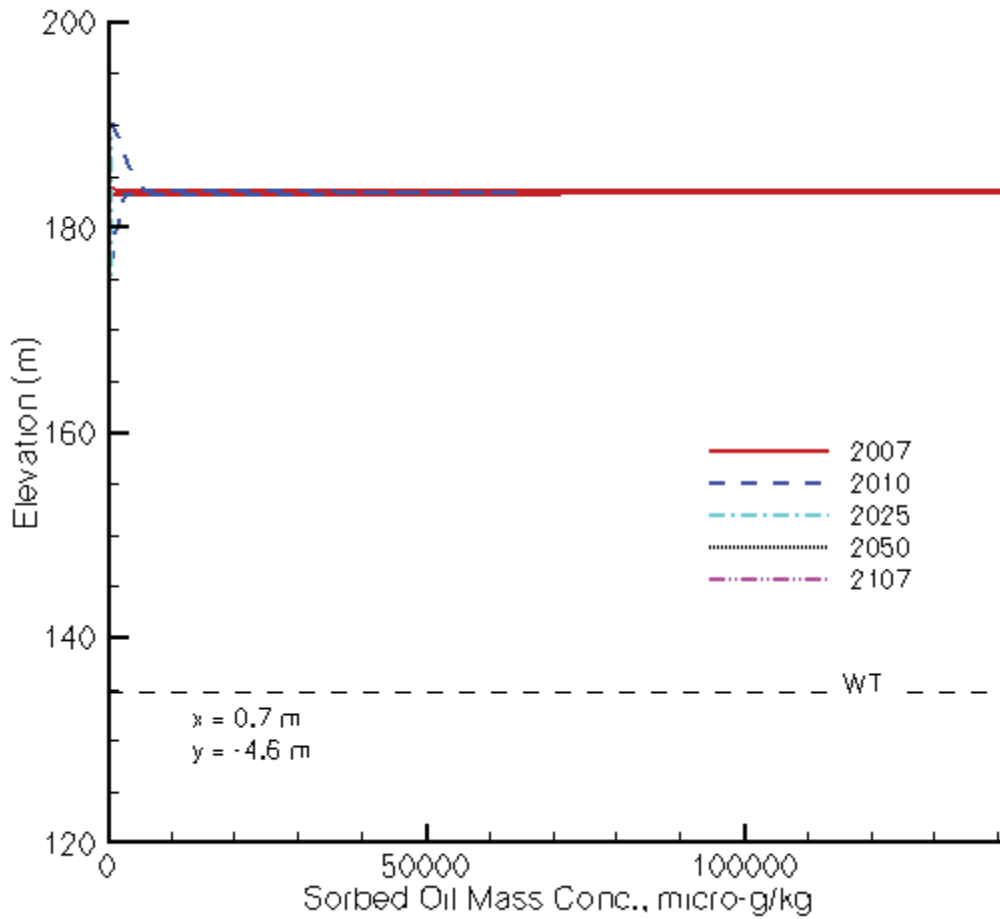
Figure 5.5.   Sorbed CT Mass Concentration (μg/kg) Profile at Different Times at (x, y) = (0.7, - 4.6) m for Imposed Case 5. The center of the Z-9 trench is located at (x, y) = (0, 0) m. The dashed line marked with WT denotes the water table.
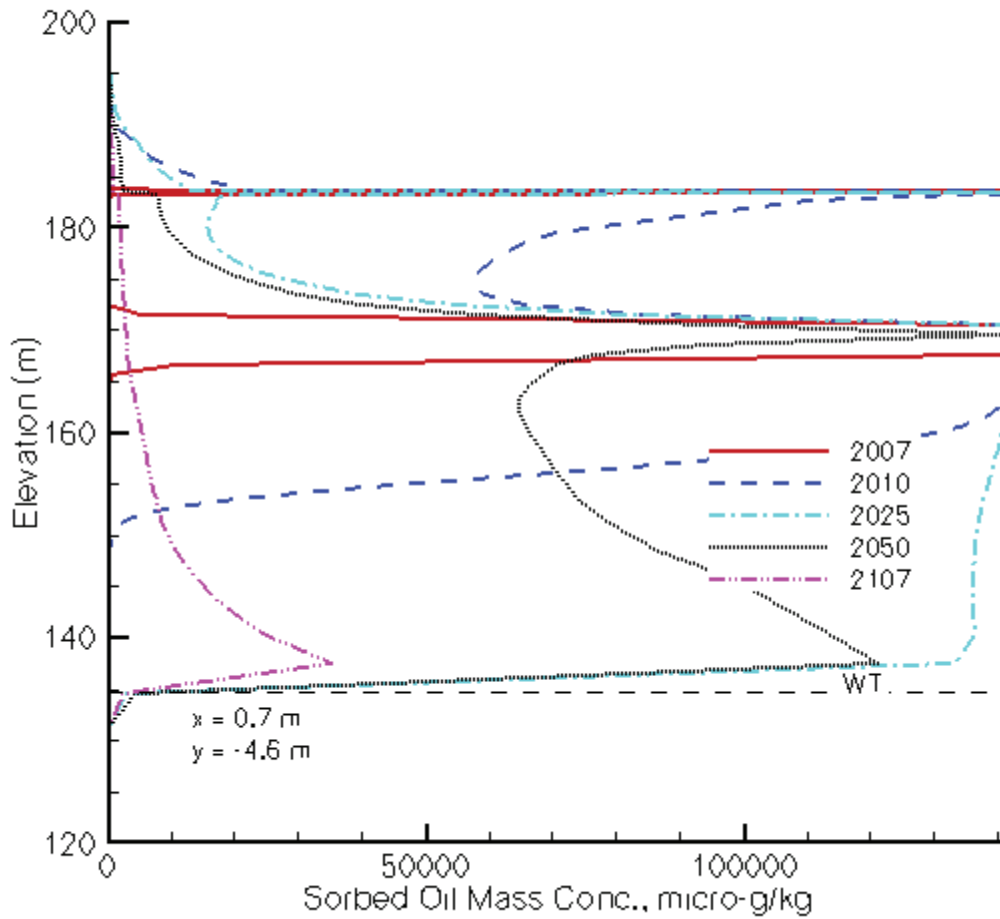
Figure 5.6.   Sorbed CT Mass Concentration (µg/kg) Profile at Different Times at (x, y) = (0.7, -4.6) m for Imposed Case 6. The center of the Z-9 trench is located at (x, y) = (0, 0) m. The dashed line marked with WT denotes the water table.
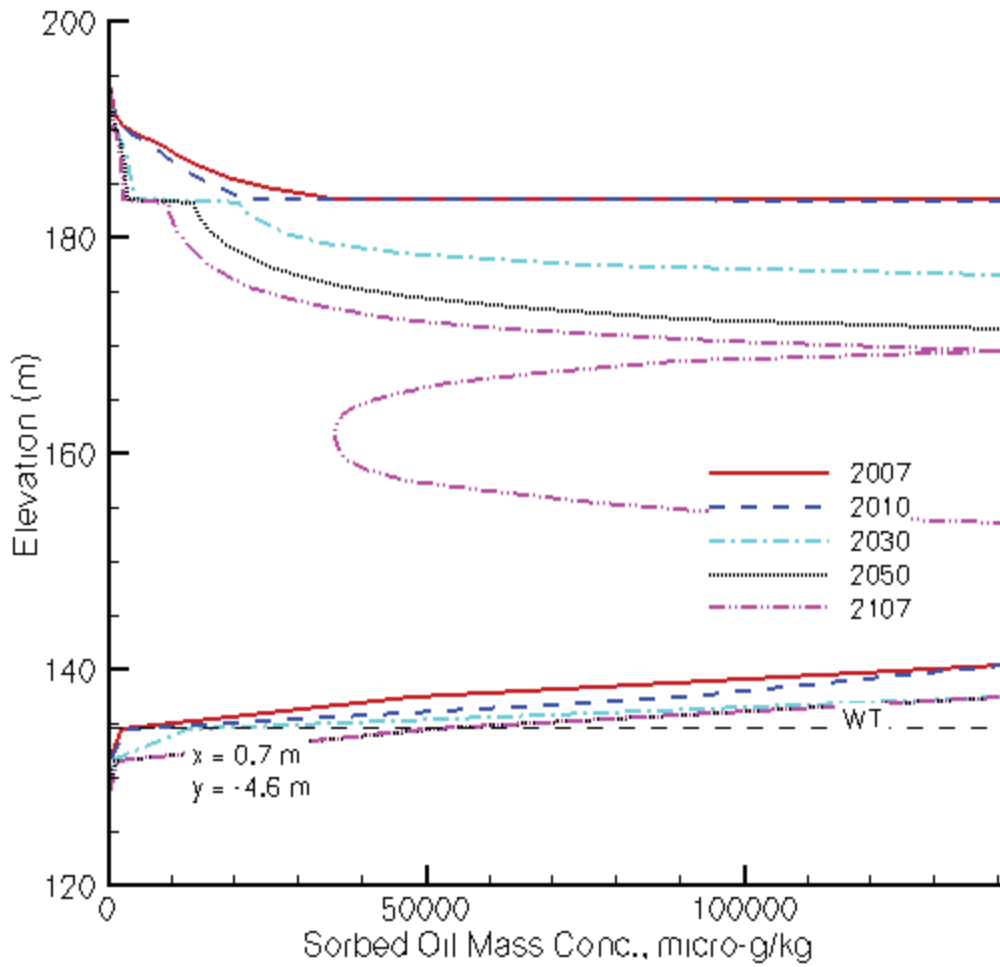
Figure 5.7.   Sorbed CT Mass Concentration (µg/kg) Profile at Different Times at (x, y) = (0.7, -4.6) m for the Modeled Case. The center of the Z-9 trench is located at (x, y) = (0, 0) m. The dashed line marked with WT denotes the water table.

5.1 Mass Flow Rates and Cumulative Mass Transport Across the Water Table and Model Boundaries

In this section, plots are provided of CT mass flow rate and cumulative mass transport across the water table and domain boundaries. An overview of the figures in this section is presented in Table 5.1. Note that DNAPL CT movement across the water table was only observed for the modeled case (Figure 5.57).

Table 5.1.   Overview of Mass Flow Rate and Cumulative Mass Transport Figure Numbers for the Seven Simulations

	IC-1	IC-2	IC-3	IC-4	IC-5	IC-6	MC
Section	*5.1.1.*	*5.1.2.*	*5.1.3.*	*5.1.4*	*5.1.5*	*5.1.6*	*5.1.7.*
Aqueous CT Across Water Table	5.8	5.15	5.22	5.29	5.36	5.43	5.50
Aqueous CT Out of Aquifer	5.9	5.16	5.23	5.30	5.37	5.44	5.51
Gas CT Across Top Domain	5.10	5.17	5.24	5.31	5.38	5.45	5.52
Gas CT Out of West Boundary	5.11	5.18	5.25	5.32	5.39	5.46	5.53
Gas CT Out of East Boundary	5.12	5.19	5.26	5.33	5.40	5.47	5.54
Gas CT Out of South Boundary	5.13	5.20	5.27	5.34	5.41	5.48	5.55
Gas CT Out of North Boundary	5.14	5.21	5.28	5.35	5.42	5.49	5.56
DNAPL CT Across Water Table	-	-	-	-	-	-	5.57

The computed aqueous CT mass flow rates across the water table for imposed case 6 (Figure 5.43) and the modeled case (Figure 5.50) are considerably larger than for imposed cases 1 – 5. The maximum mass flow rate for imposed case 6 is 45 kg/yr (at 2065) while for the modeled case the maximum rate is about 469 kg/yr (at 2107). The maximum rate for the other five cases is 0.56 kg/yr for imposed case 1 (at 2107). The maximum rates for the imposed cases 2, 3, and 5, are several orders of magnitude smaller than the value for imposed case 1. The results for imposed case 4 are similar than form imposed case 1, again indicating the limited effect of the emplaced CT in the 65-ft silt lens.

Aqueous CT mass flow rates across the water table at selected times are shown in Table 5.2. These data are extracted from the same data files that were used to create the mass flow rate figures. Water table NAPL phase mass fluxes are shown in Table 5.3. The only simulation with DNAPL CT transport across the water was the modeled case. For this case, the maximum rate is 450 kg/yr (at 2007). It is of interest that the aqueous phase and DNAPL CT fluxes for this case are of the same order of magnitude for the duration of the simulations.

Table 5.2.   Water Table Aqueous CT Mass Flow Rate (kg/yr) at Selected Times

Time (yr)	IC-1	IC-2	IC-3	IC-4	IC-5	IC-6	MC
2007	0.000E+00	0.000E+00	0.000E+00	0.000E+00	0.000E+00	0.000E+00	1.908E+02
2010	0.000E+00	0.000E+00	0.000E+00	0.000E+00	0.000E+00	2.049E-10	2.043E+02
2020	7.977E-04	4.307E-09	1.142E-10	7.965E-04	0.000E+00	7.418E+00	2.488E+02
2030	3.933E-02	8.237E-07	2.715E-08	3.926E-02	1.288E-09	2.407E+01	2.907E+02
2040	1.521E-01	1.076E-05	3.914E-07	1.518E-01	3.780E-08	3.502E+01	3.287E+02
2050	2.818E-01	5.787E-05	2.289E-06	2.811E-01	3.593E-07	4.166E+01	3.624E+02
2060	3.877E-01	1.934E-04	8.261E-06	3.866E-01	1.889E-06	4.482E+01	3.918E+02
2070	4.625E-01	4.802E-04	2.201E-05	4.611E-01	6.814E-06	4.490E+01	4.166E+02
2080	5.113E-01	9.743E-04	4.769E-05	5.095E-01	1.892E-05	4.297E+01	4.367E+02
2090	5.409E-01	1.712E-03	8.902E-05	5.389E-01	4.342E-05	4.048E+01	4.524E+02
2100	5.571E-01	2.706E-03	1.487E-04	5.548E-01	8.627E-05	3.798E+01	4.640E+02
2107	5.629E-01	3.549E-03	2.022E-04	5.604E-01	1.301E-04	3.632E+01	4.694E+02

Table 5.3.   Water Table DNAPL-Phase CT Mass Flow Rate (kg/yr) at Selected Times

Time (yr)	IC-1	IC-2	IC-3	IC-4	IC-5	IC-6	MC
2007	0.000E+00	0.000E+00	0.000E+00	0.000E+00	0.000E+00	0.000E+00	4.493E+02
2010	0.000E+00	0.000E+00	0.000E+00	0.000E+00	0.000E+00	0.000E+00	4.280E+02
2020	0.000E+00	0.000E+00	0.000E+00	0.000E+00	0.000E+00	0.000E+00	3.644E+02
2030	0.000E+00	0.000E+00	0.000E+00	0.000E+00	0.000E+00	0.000E+00	3.137E+02
2040	0.000E+00	0.000E+00	0.000E+00	0.000E+00	0.000E+00	0.000E+00	2.730E+02
2050	0.000E+00	0.000E+00	0.000E+00	0.000E+00	0.000E+00	0.000E+00	2.392E+02
2060	0.000E+00	0.000E+00	0.000E+00	0.000E+00	0.000E+00	0.000E+00	2.104E+02
2070	0.000E+00	0.000E+00	0.000E+00	0.000E+00	0.000E+00	0.000E+00	1.850E+02
2080	0.000E+00	0.000E+00	0.000E+00	0.000E+00	0.000E+00	0.000E+00	1.618E+02
2090	0.000E+00	0.000E+00	0.000E+00	0.000E+00	0.000E+00	0.000E+00	1.402E+02
2100	0.000E+00	0.000E+00	0.000E+00	0.000E+00	0.000E+00	0.000E+00	1.199E+02
2107	0.000E+00	0.000E+00	0.000E+00	0.000E+00	0.000E+00	0.000E+00	1.063E+02

The rest of the figures in Section 5.1.1 through 5.1.7 depict the mass flow rates and cumulative masses across the model boundaries for the seven simulations (Table 5.1). For instance, for imposed case 1, the various mass flow rates and cumulative masses across boundaries as a function of time are shown in Figures 5.9 – 5.14 in Section 5.1.1. The cumulative mass transfer across the various boundaries should be considered in conjunction with the computed CT mass at 2007 and 2107, as listed in Table 5.4. The amounts listed in the "Difference" column indicate the mass that was transported out of the domain. For example for imposed case 1, the difference of 42.8 kg between 2007 and 2107 was transported out of the domain as dissolved CT in the groundwater (Figure 5.9), gas phase CT across the top surface (Figure 5.10), and gas phase CT across the west (Figure 5.11), east (Figure 5.12), south (Figure 5.13) and north (Figure 5.14) boundaries. For this particular case, approximately 11 kg was transported out of the domain through moving groundwater, 7 kg as gas phase CT through the top boundary, and 25 kg as gas phase CT

across the south boundary. Gas phase CT movement across the other 3 boundaries was considerably smaller. As can be inferred from the figures in Section 5.1., aqueous and gas phase CT movement across the domain boundaries were orders of magnitude smaller for imposed case 2, 3, and 5. The results for imposed case 4 (Section 5.1.4) were similar to the results of imposed case 1.

Mass flow rates and cumulative masses for imposed case 6 (Section 3.1.6) are approximately one order of magnitude larger than for imposed case 1. This result shows the nonlinearity of these systems since at 2007 imposed case 6 contains 33 times more CT than imposed case 1. The cumulative masses for the modeled case are, in turn, considerably larger than for imposed case 6 (Section 5.1.7). For instance, the cumulative mass transported out of the domain from 2007-2107 through moving groundwater is more than 60,000 kg for the modeled case versus about 1,800 kg for imposed case 6. Note that for the modeled case, CT was distributed in the domain following the infiltration between 1995.5 and 1962.5. In 2007, approximately 30,000 kg CT was located in the aquifer as dissolved and DNAPL CT. The ~60,000 kg transported across the aquifer boundary by 2107 partly reflects the initial mass in the saturated zone. The larger difference between the two cases is related to the fact that for the modeled case, DNAPL CT penetrated the water table and dissolved over time. For imposed case 6, no DNAPL CT was transported across the water table.

Table 5.4.   CT Mass Differences in Computational Domain Between 2007 and 2107 and CT Losses Across Boundaries

Simulation	Total CT 2007 (kg)	Total CT 2107 (kg)	Difference (kg)	Loss Due to Groundwater Transport (kg)	Loss Due to Gas Phase Transport Top Boundary (kg)	Loss Due to Gas Phase Transport Side Boundaries (kg)
IC-1	607.4	565	42.8	10.9	6.9	25.0
IC-2	90.0	81.0	9.0	7.2E-3	1.9	7.1
IC-3	9.0	8.0	1.0	3.2E-4	0.22	0.78
IC-4	585	547	38.2	10.8	5.8	21.6
IC-5	22.2	17.3	4.9	1.2E-4	1.2	3.7
IC-6	20,122	17,986	2,136	1,790	65.0	281
MC-1	388,676	299,599	89,077	60,922	518	27,537

5.1.1   Imposed Case 1
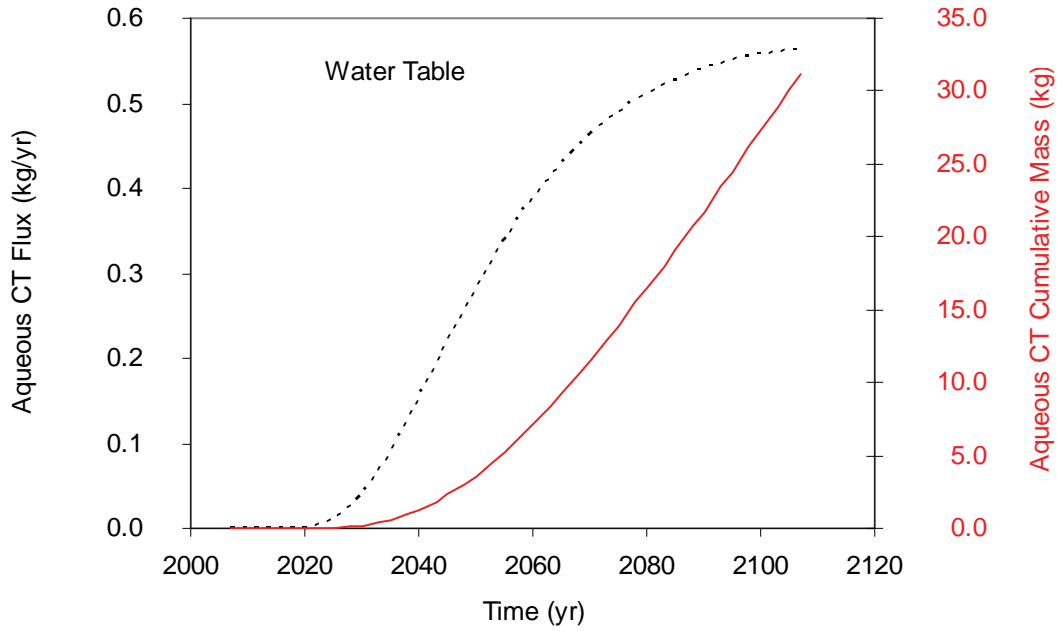
Figure 5.8.   Aqueous CT Mass Flow (kg/yr) (dashed line) and Aqueous CT Cumulative Mass Transport (kg) (solid line) Across Water Table for Imposed Case 1
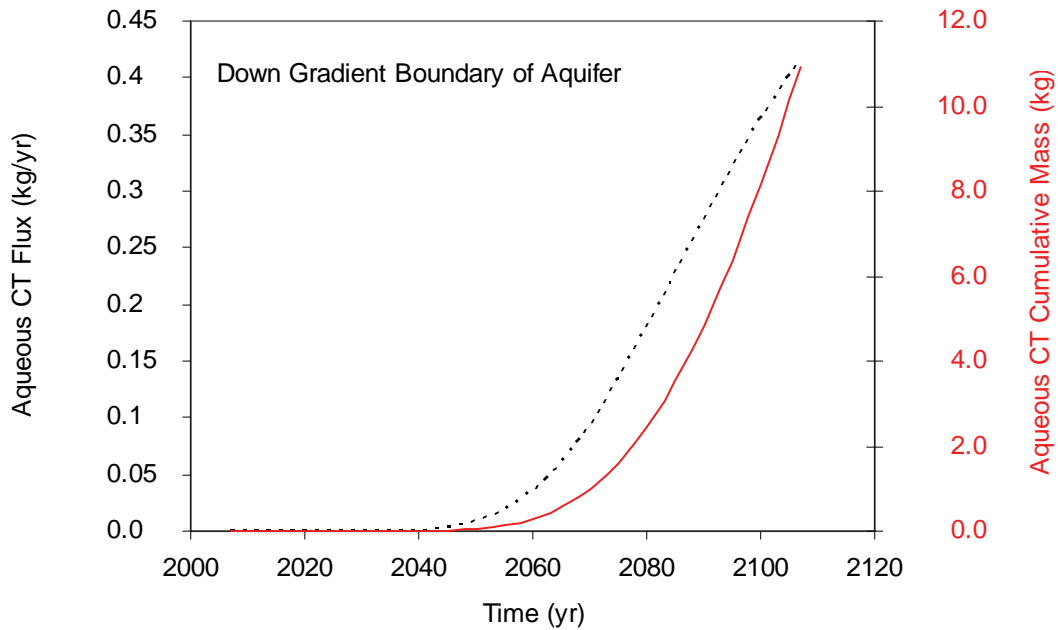
Figure 5.9.   Aqueous CT Mass Flow Rate (kg/yr) (dashed line) and Aqueous CT Cumulative Mass Transport (kg) (solid line) Across Down Gradient Aquifer Boundary for Imposed Case 1
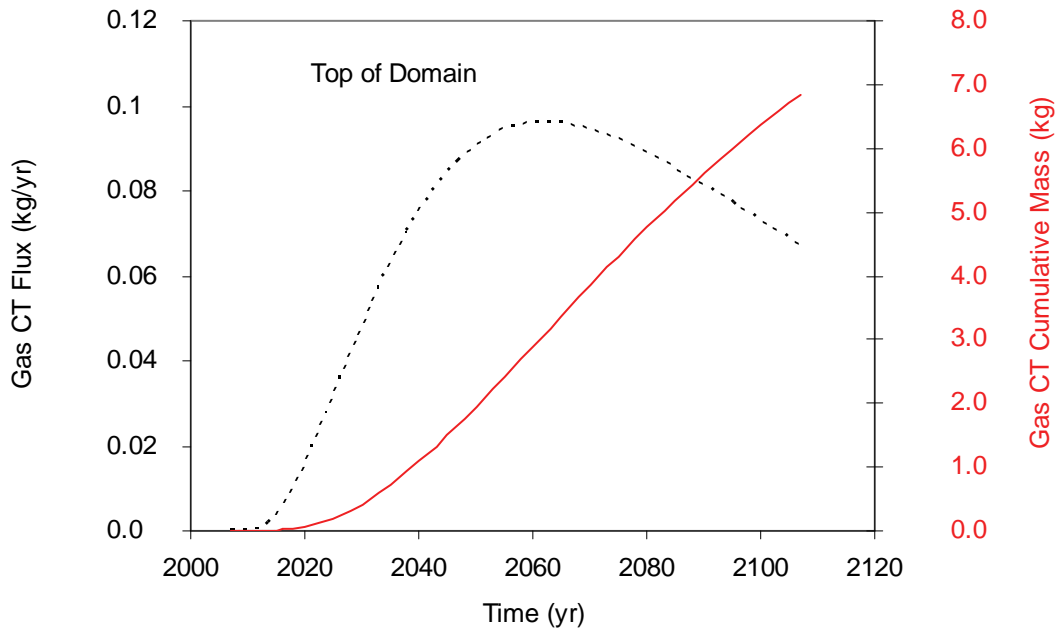
Figure 5.10. Gas CT Mass Flow Rate (kg/yr) (dashed line) and Gas CT Cumulative Mass Transport (kg) (solid line) Across Top of Domain for Imposed Case 1
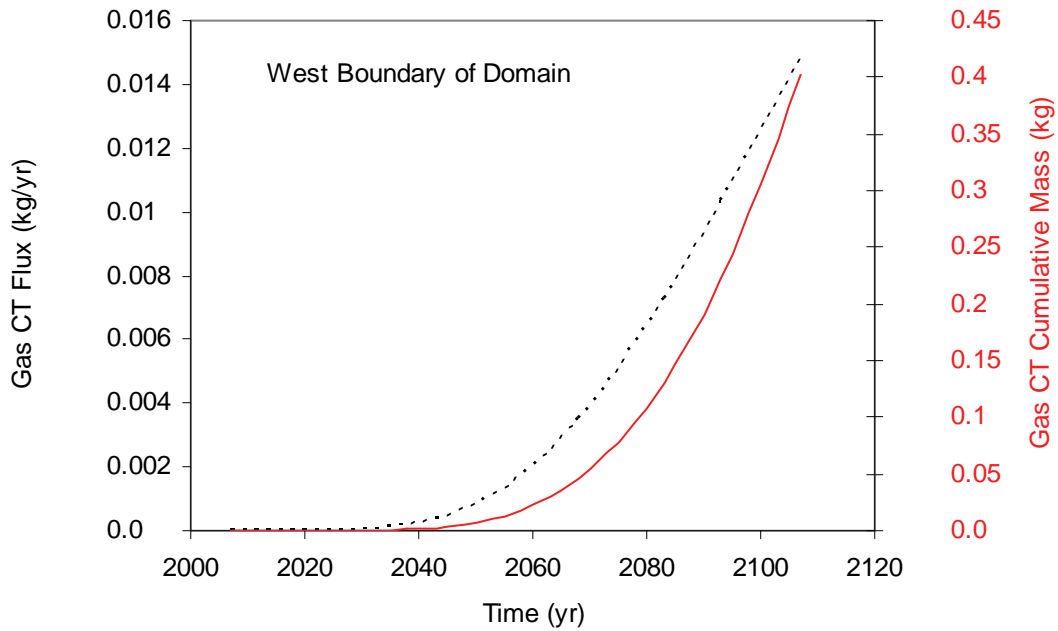
Figure 5.11. Gas CT Mass Flow Rate (kg/yr) (dashed line) and Gas CT Cumulative Mass Transport (kg) (solid line) Across West Boundary of Domain for Imposed Case 1
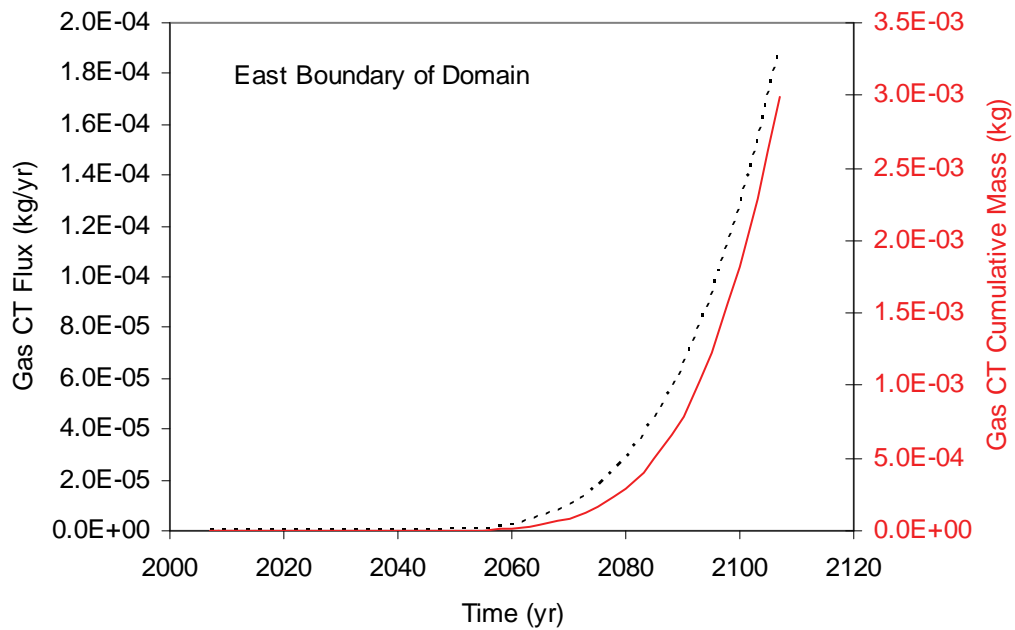
Figure 5.12. Gas CT Mass Flow Rate (kg/yr) (dashed line) and Gas CT Cumulative Mass Transport (kg) (solid line) Across East Boundary of Domain for Imposed Case 1
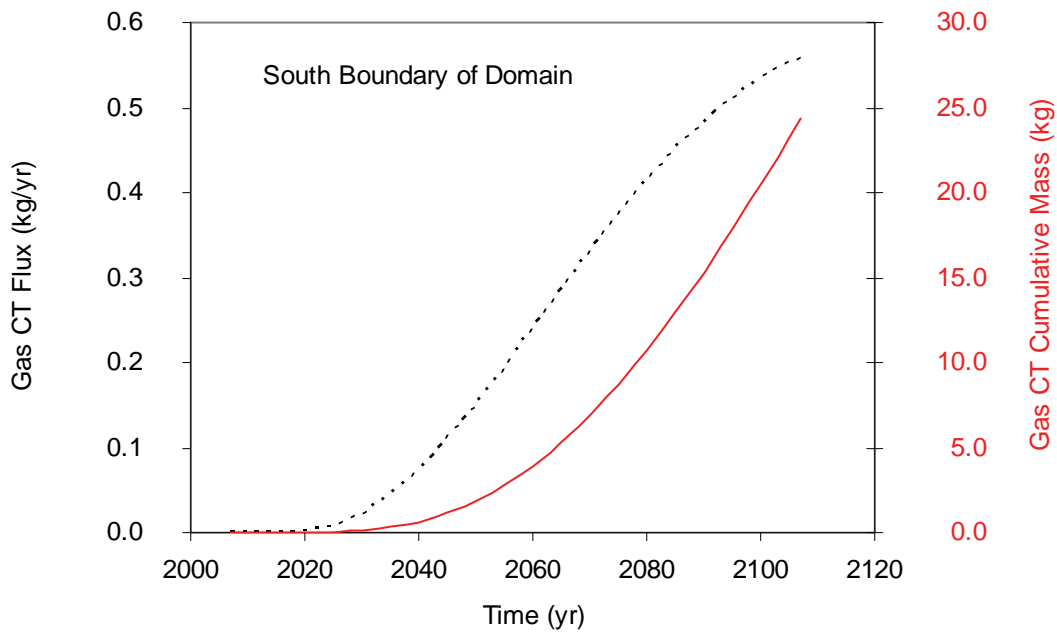
Figure 5.13. Gas CT Mass Flow Rate (kg/yr) (dashed line) and Gas CT Cumulative Mass Transport (kg) (solid line) Across South Boundary of Domain for Imposed Case 1
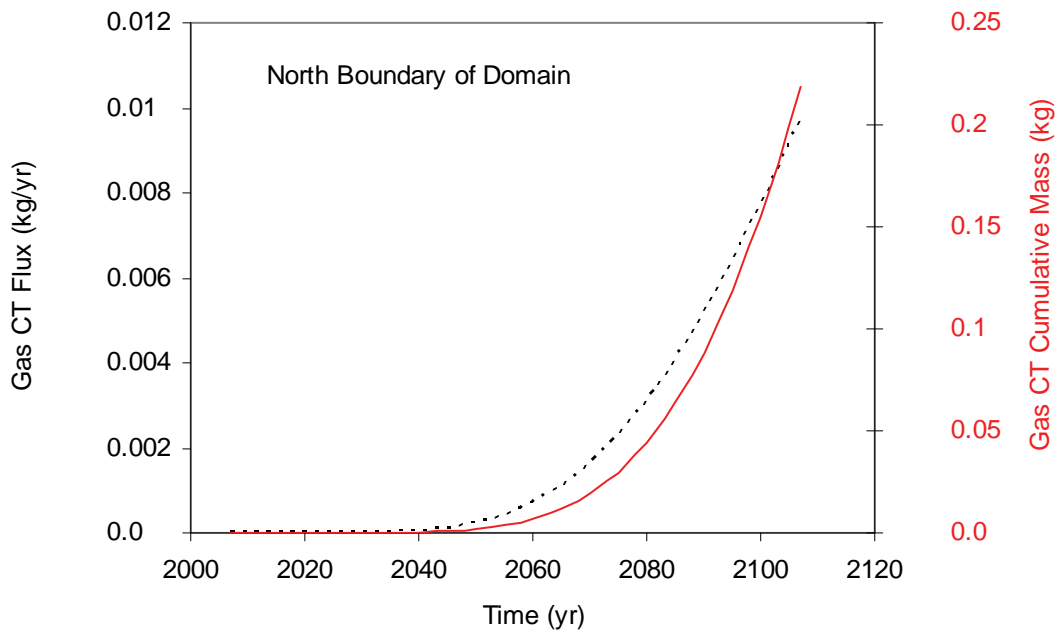
Figure 5.14.   Gas CT Mass Flow Rate (kg/yr) (dashed line) and Gas CT Cumulative Mass Transport (kg) (solid line) Across North Boundary of Domain for Imposed Case 1

5.1.2   Imposed Case 2
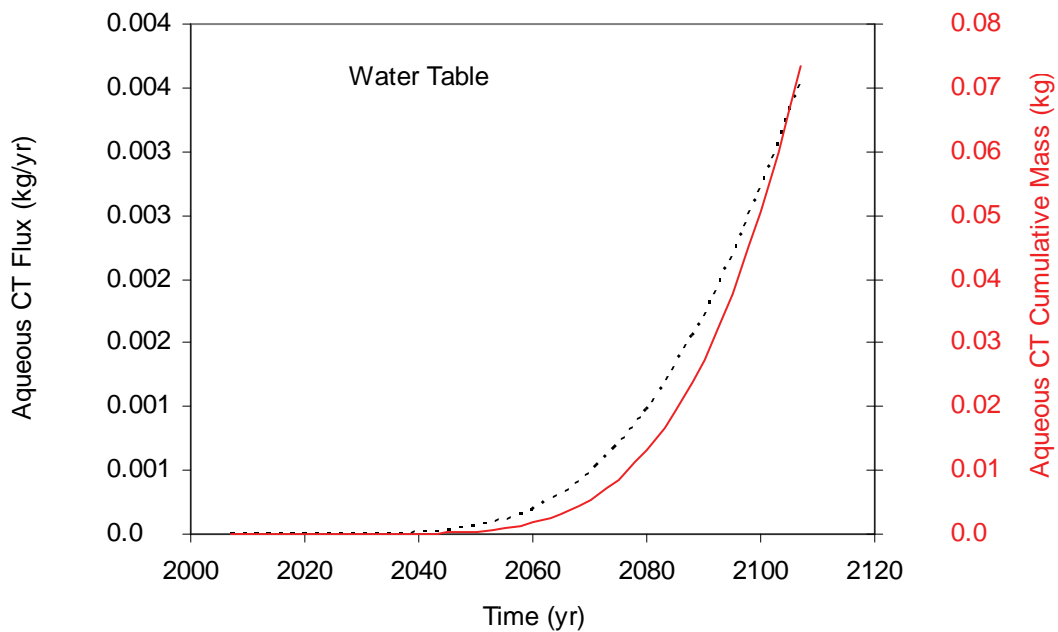
Figure 5.15.   Aqueous CT Mass Flow Rate (kg/yr) (dashed line) and Aqueous CT Cumulative Mass Transport (kg) (solid line) Across Water Table for Imposed Case 2
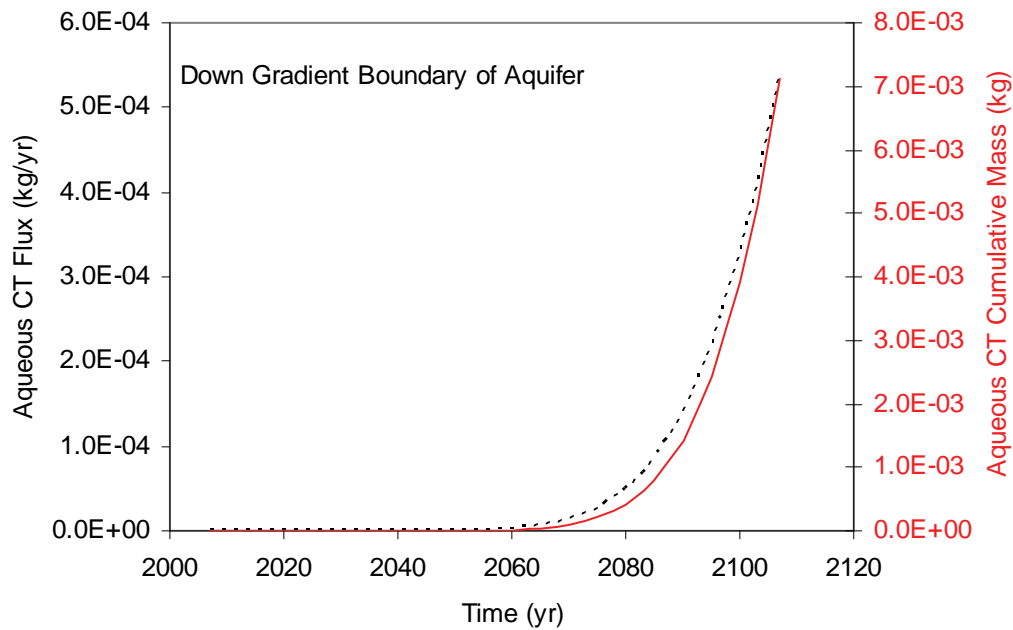
Figure 5.16.   Aqueous CT Mass Flow Rate (kg/yr) (dashed line) and Aqueous CT Cumulative Mass
Transport (kg) (solid line) Across Down Gradient Aquifer Boundary for Imposed Case 2
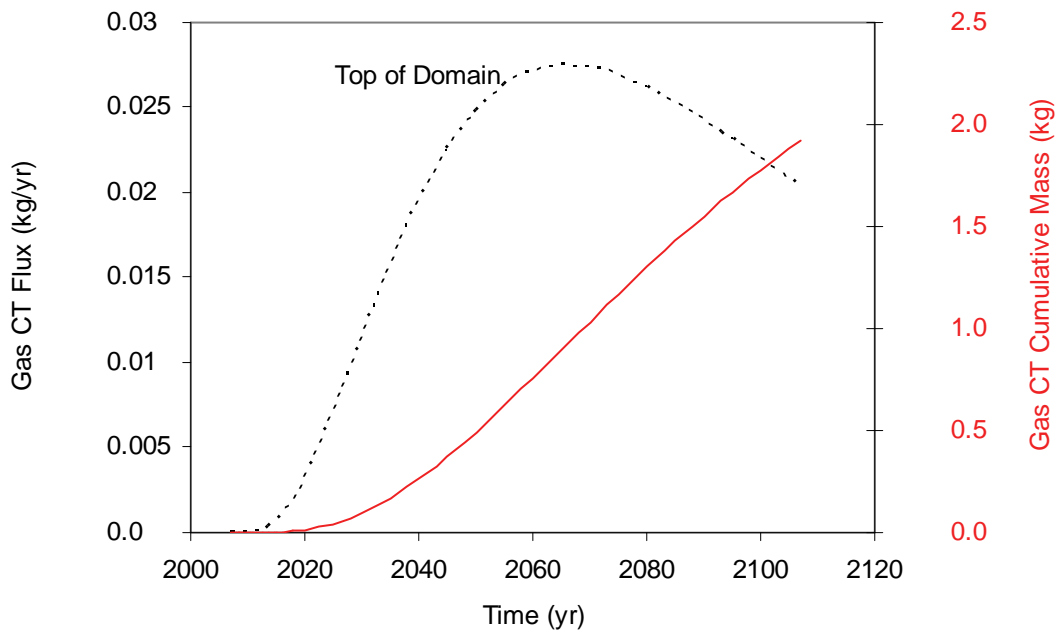
Figure 5.17.   Gas CT Mass Flow Rate (kg/yr) (dashed line) and Gas CT Cumulative Mass Transport
(kg) (solid line) Across Top of Domain for Imposed Case 2
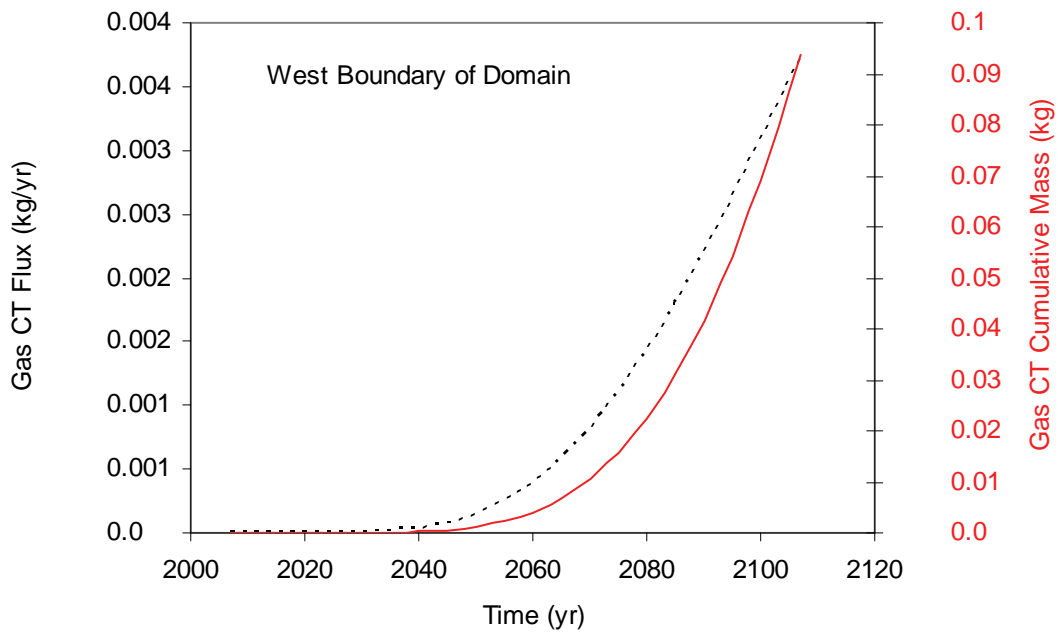
Figure 5.18.   Gas CT Mass Flow Rate (kg/yr) (dashed line) and Gas CT Cumulative Mass Transport (kg) (solid line) Across West Boundary of Domain for Imposed Case 2
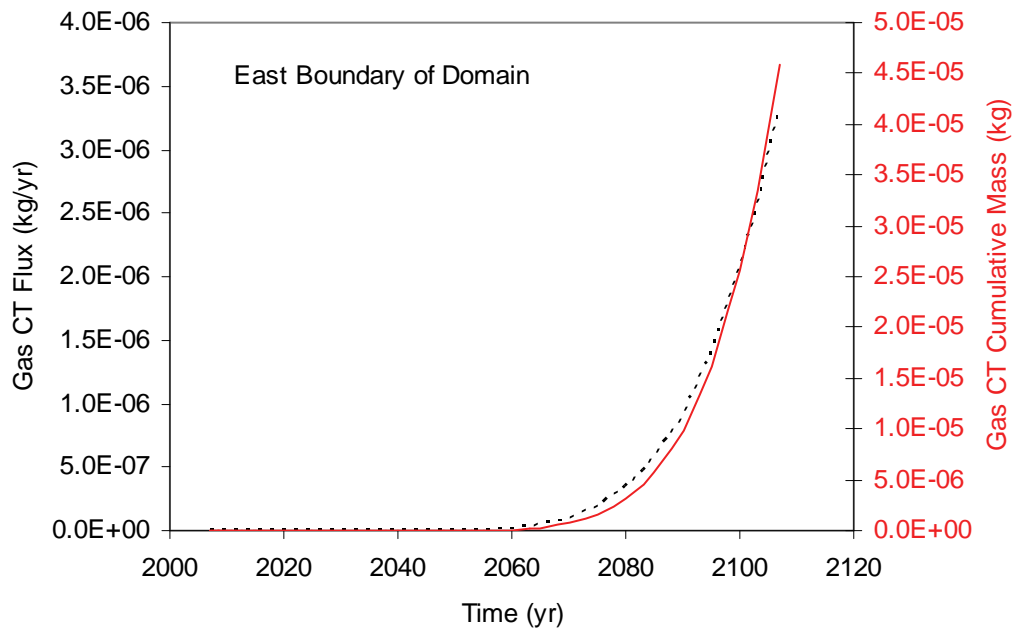
Figure 5.19.   Gas CT Mass Flow Rate (kg/yr) (dashed line) and Gas CT Cumulative Mass Transport (kg) (solid line) Across East Boundary of Domain for Imposed Case 2
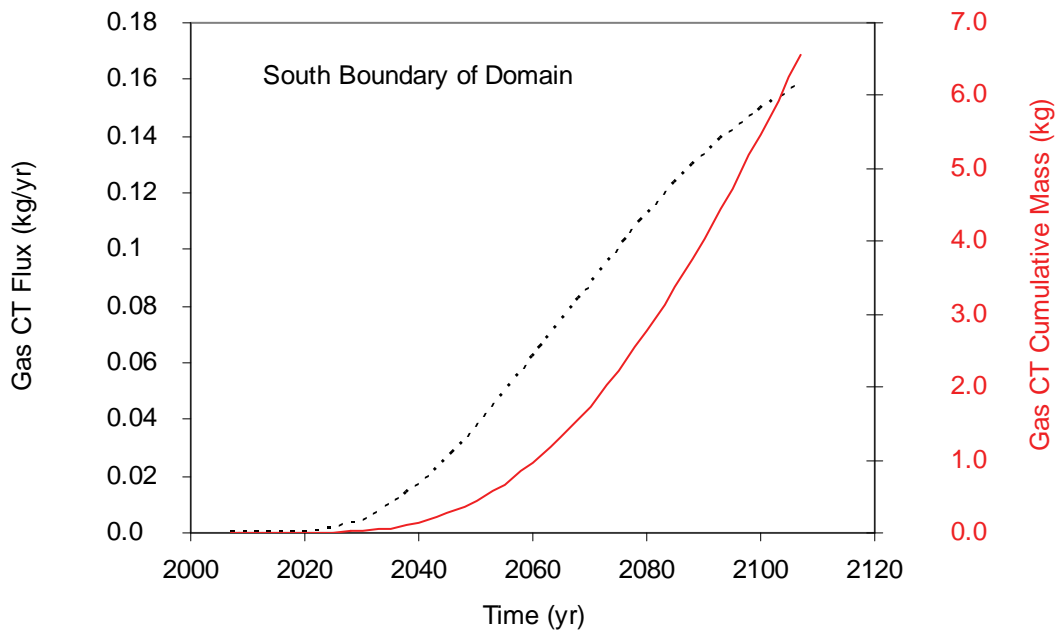
Figure 5.20.   Gas CT Mass Flow Rate (kg/yr) (dashed line) and Gas CT Cumulative Mass Transport (kg) (solid line) Across South Boundary of Domain for Imposed Case 2
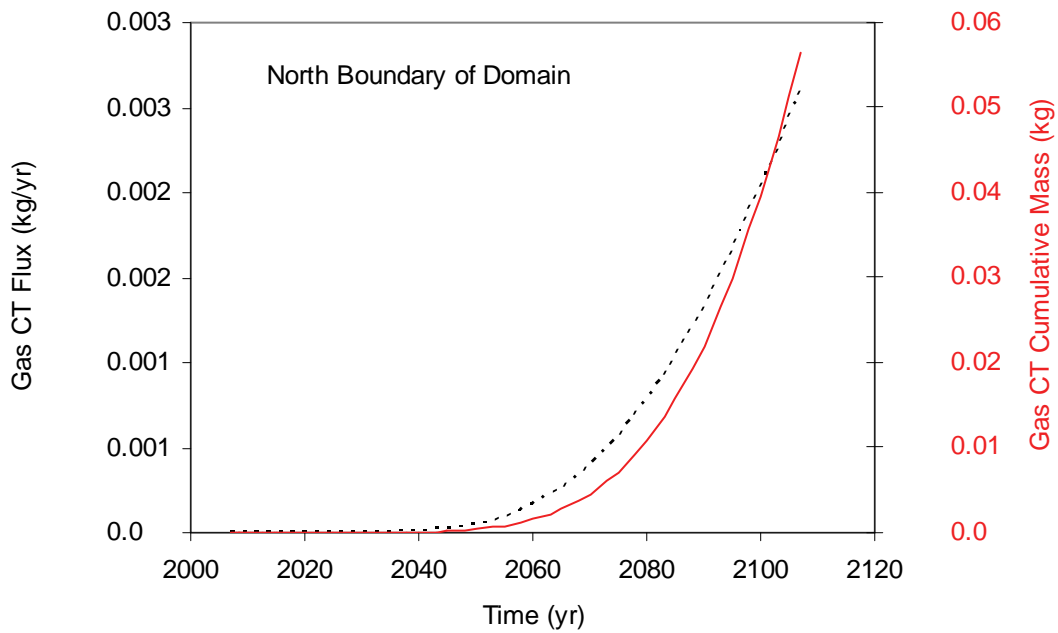
Figure 5.21.   Gas CT Mass Flow Rate (kg/yr) (dashed line) and Gas CT Cumulative Mass Transport (kg) (solid line) Across North Boundary of Domain for Imposed Case 2

5.1.3   Imposed Case 3
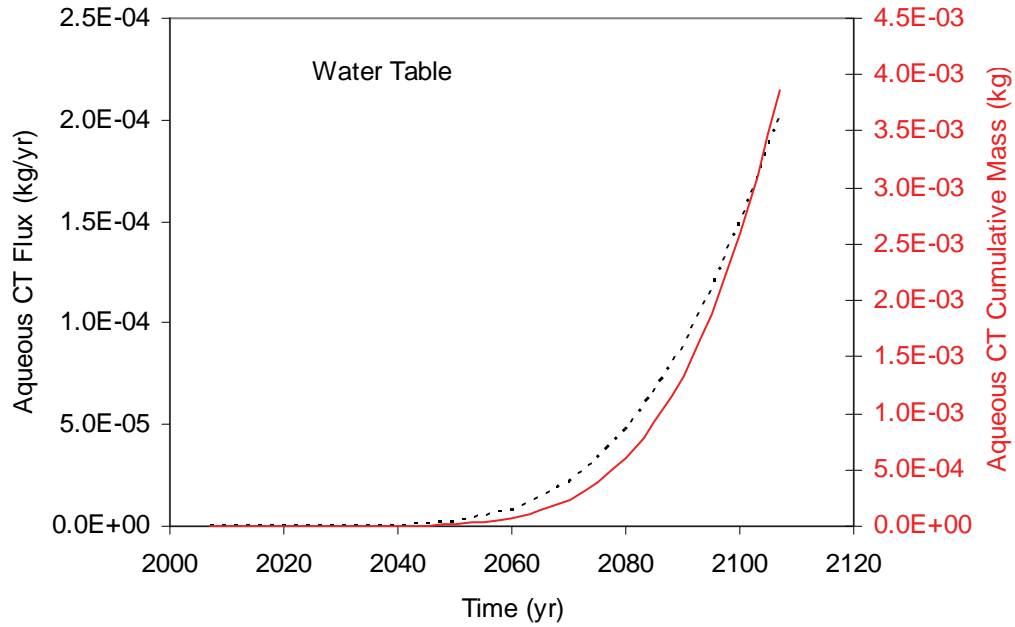
Figure 5.22.   Aqueous CT Mass Flow Rate (kg/yr) (dashed line) and Aqueous CT Cumulative Mass Transport (kg) (solid line) Across Water Table for Imposed Case 3
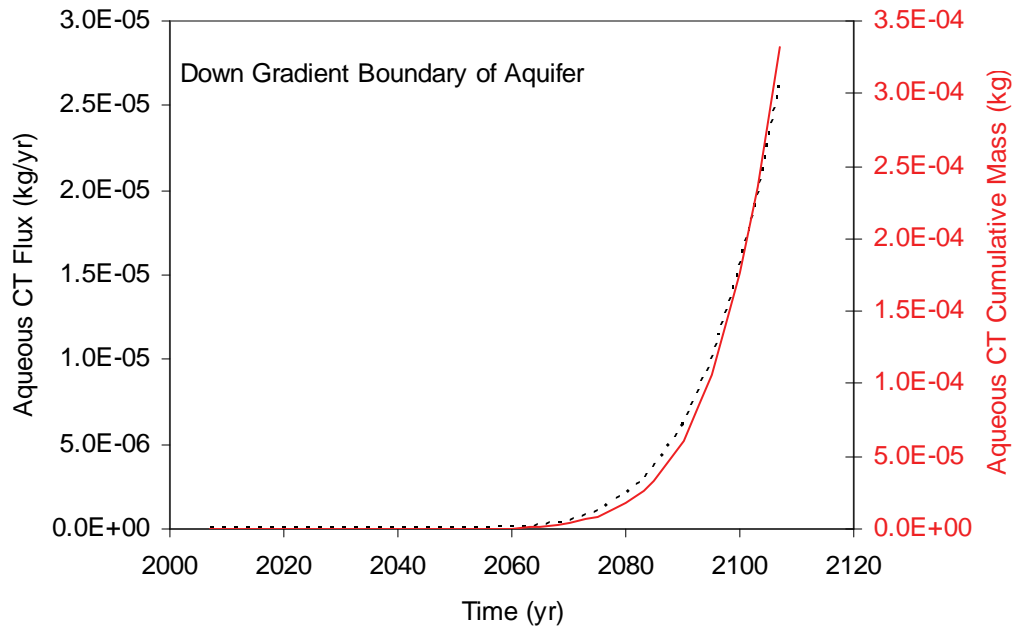
Figure 5.23.   Aqueous CT Mass Flow Rate (kg/yr) (dashed line) and Aqueous CT Cumulative Mass Transport (kg) (solid line) Across Down Gradient Aquifer Boundary for Imposed Case 3
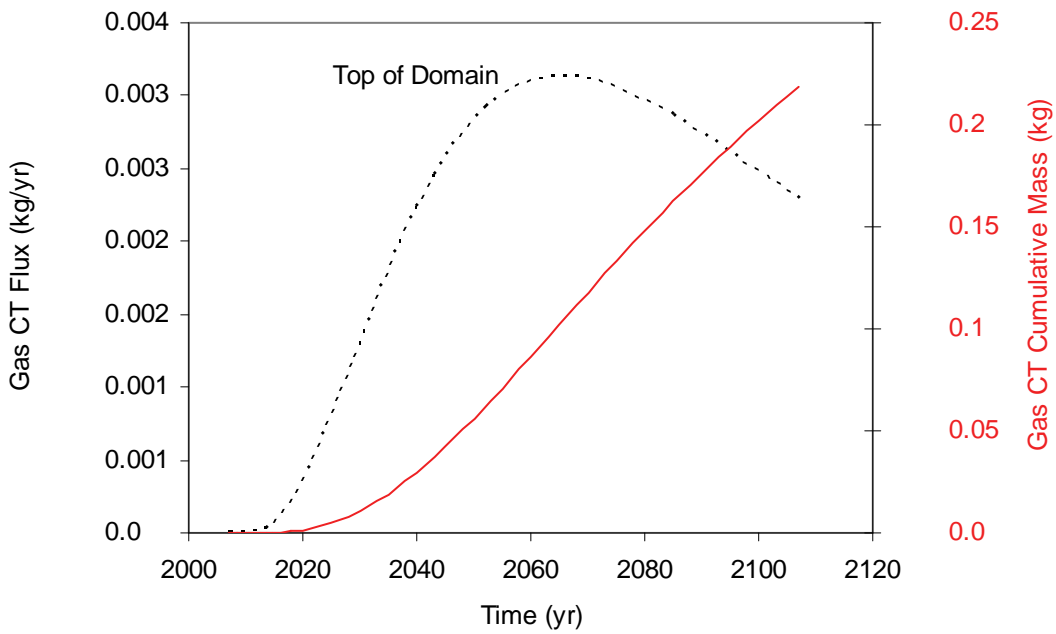
Figure 5.24. Gas CT Mass Flow Rate (kg/yr) (dashed line) and Gas CT Cumulative Mass Transport (kg) (solid line) Across Top of Domain for Imposed Case 3
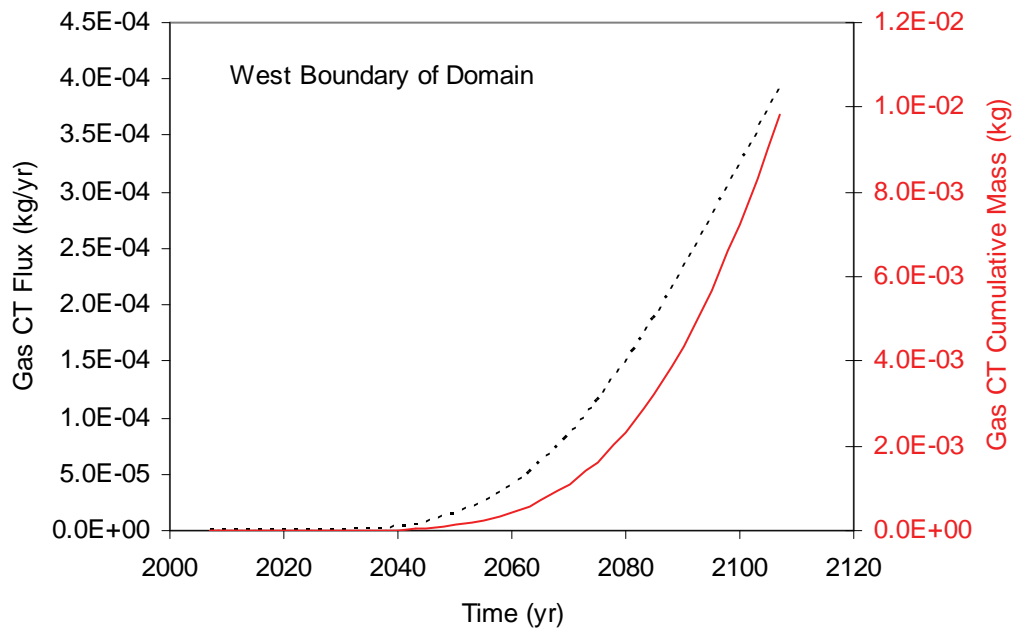
Figure 5.25. Gas CT Mass Flow Rate (kg/yr) (dashed line) and Gas CT Cumulative Mass Transport (kg) (solid line) Across West Boundary of Domain for Imposed Case 3
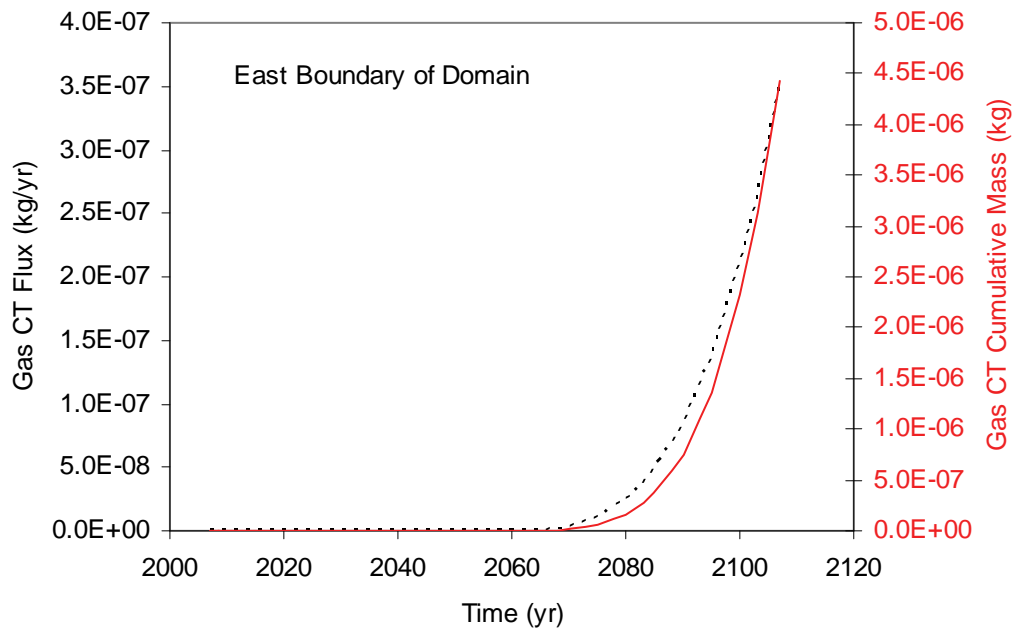
Figure 5.26. Gas CT Mass Flow Rate (kg/yr) (dashed line) and Gas CT Cumulative Mass Transport (kg) (solid line) Across East Boundary of Domain for Imposed Case 3
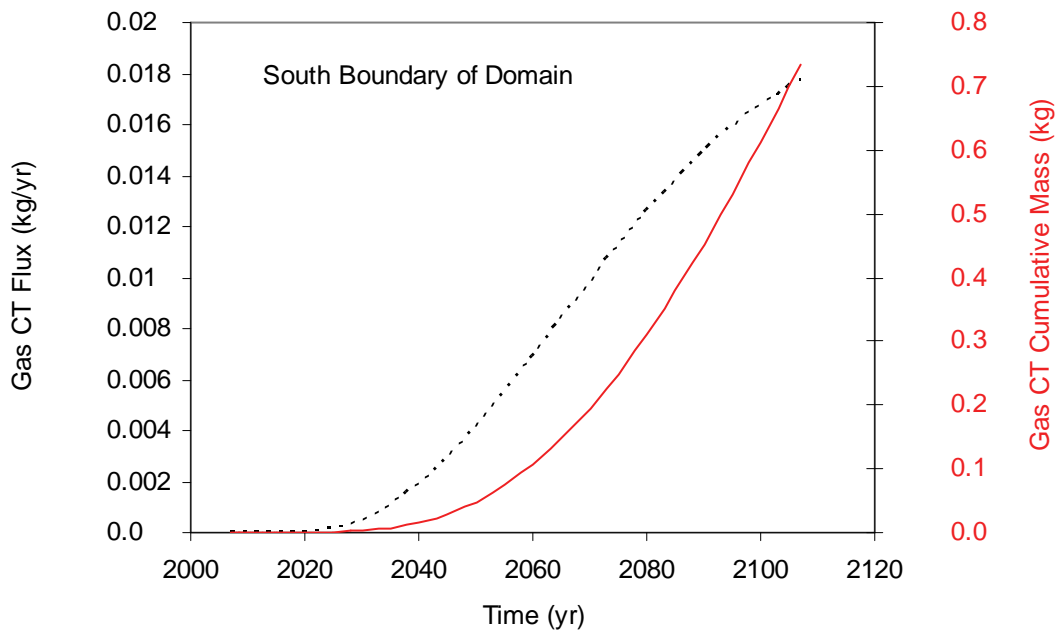
Figure 5.27. Gas CT Mass Flow Rate (kg/yr) (dashed line) and Gas CT Cumulative Mass Transport (kg) (solid line) Across South Boundary of Domain for Imposed Case 3
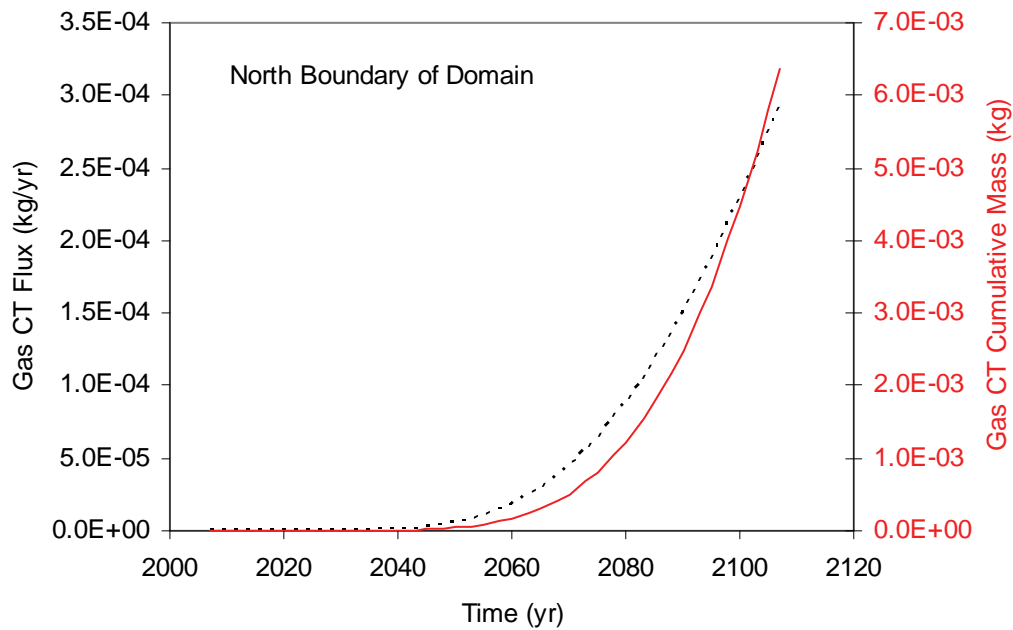
Figure 5.28.   Gas CT Mass Flow Rate (kg/yr) (dashed line) and Gas CT Cumulative Mass Transport (kg) (solid line) Across North Boundary of Domain for Imposed Case 3

5.1.4   Imposed Case 4
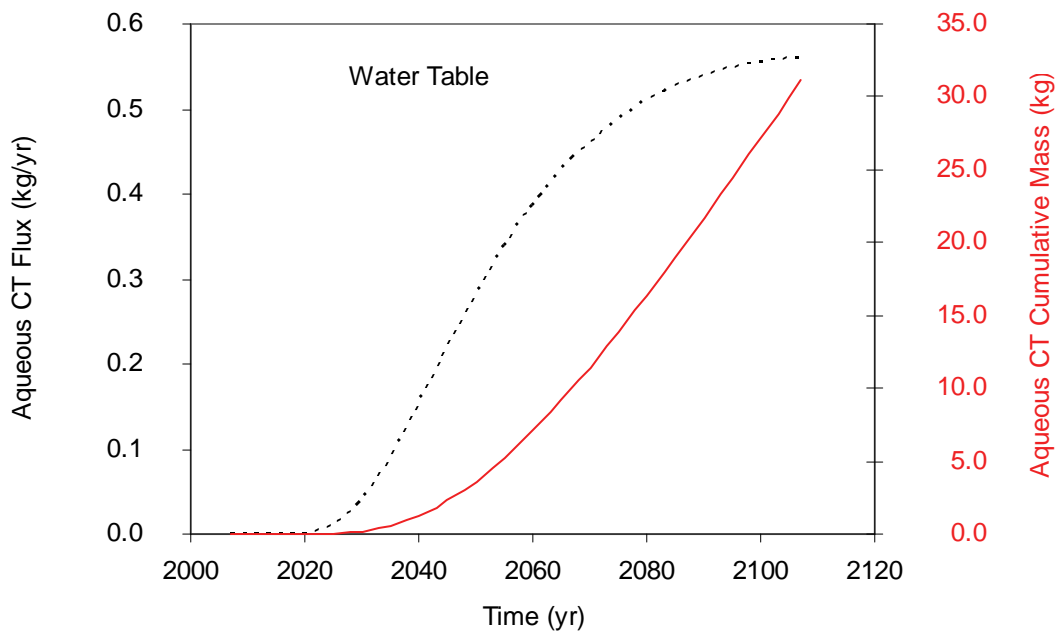
Figure 5.29.   Aqueous CT Mass Flow Rate (kg/yr) (dashed line) and Aqueous CT Cumulative Mass Transport (kg) (solid line) Across Water Table for Imposed Case 4
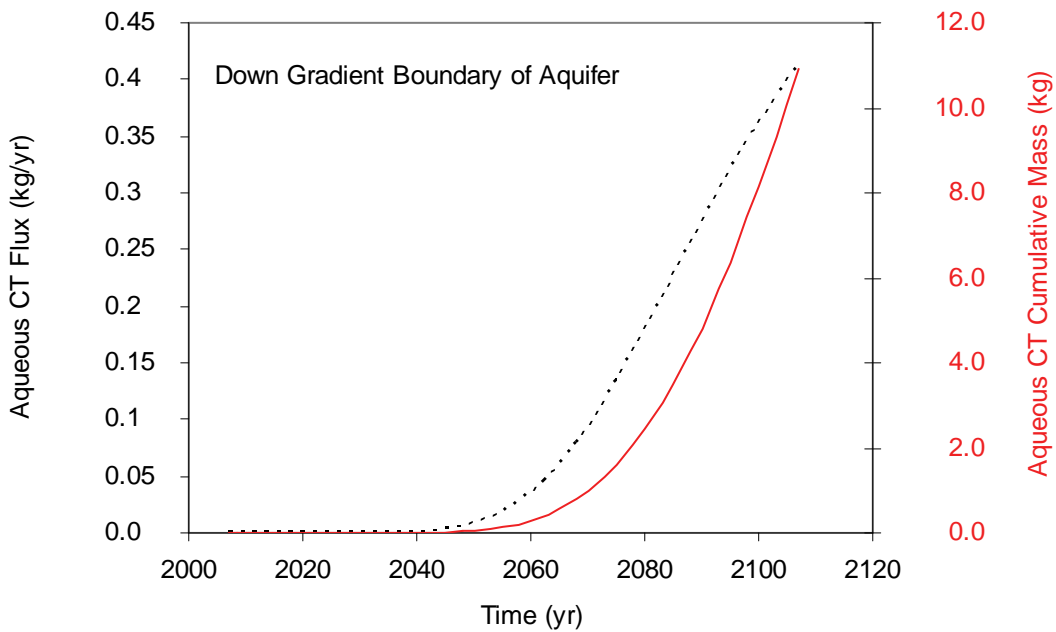
Figure 5.30. Aqueous CT Mass Flow Rate (kg/yr) (dashed line) and Aqueous CT Cumulative Mass Transport (kg) (solid line) Across Down Gradient Aquifer Boundary for Imposed Case 4
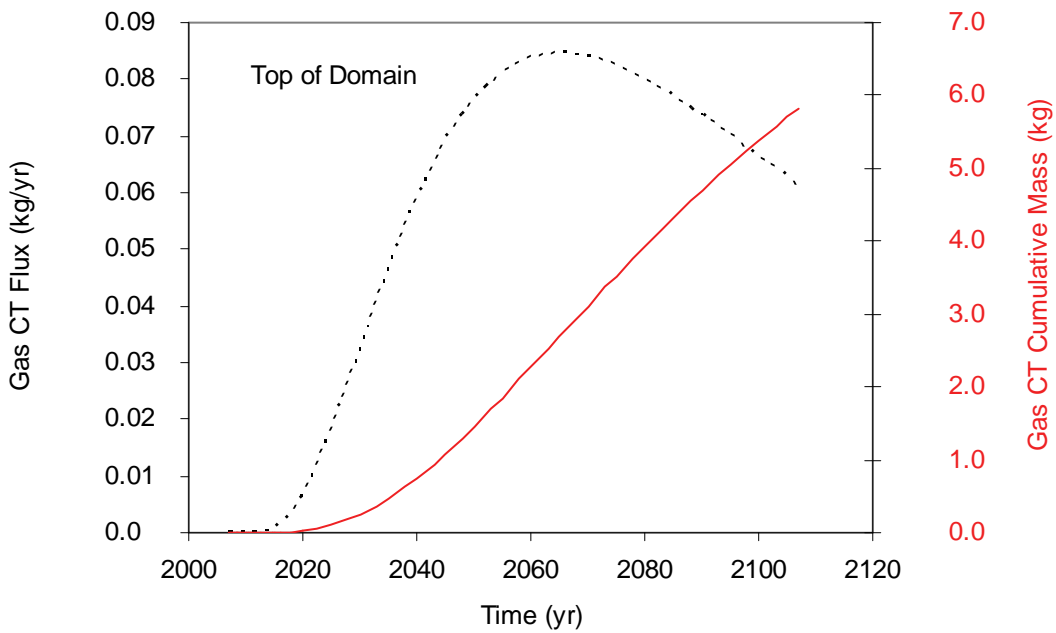
Figure 5.31. Gas CT Mass Flow Rate (kg/yr) (dashed line) and Gas CT Cumulative Mass Transport (kg) (solid line) Across Top of Domain for Imposed Case 4
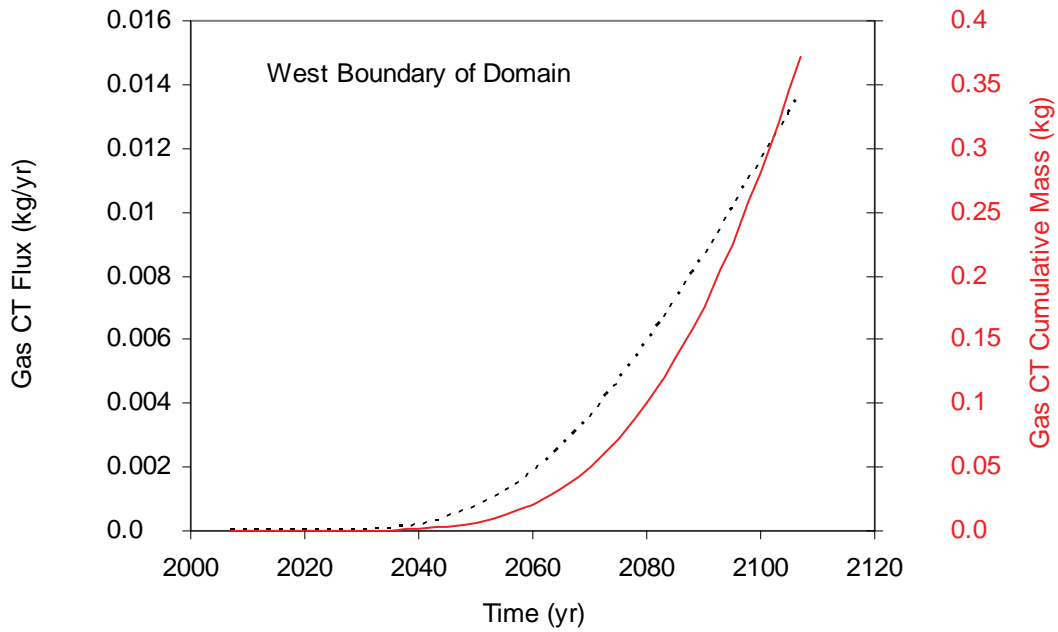
Figure 5.32. Gas CT Mass Flow Rate (kg/yr) (dashed line) and Gas CT Cumulative Mass Transport (kg) (solid line) Across West Boundary of Domain for Imposed Case 4
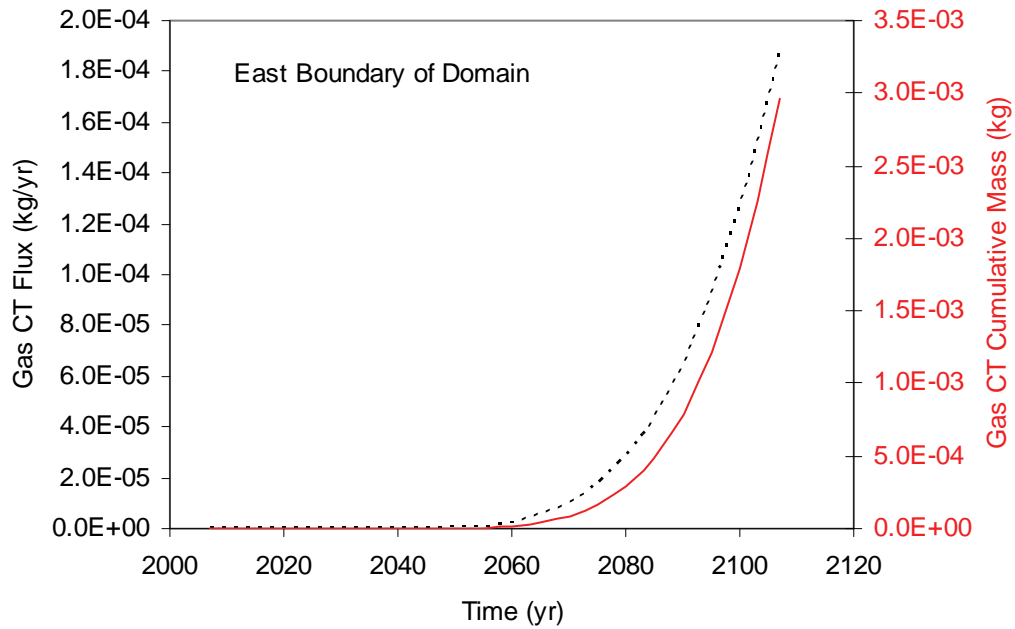
Figure 5.33. Gas CT Mass Flow Rate (kg/yr) (dashed line) and Gas CT Cumulative Mass Transport (kg) (solid line) Across East Boundary of Domain for Imposed Case 4
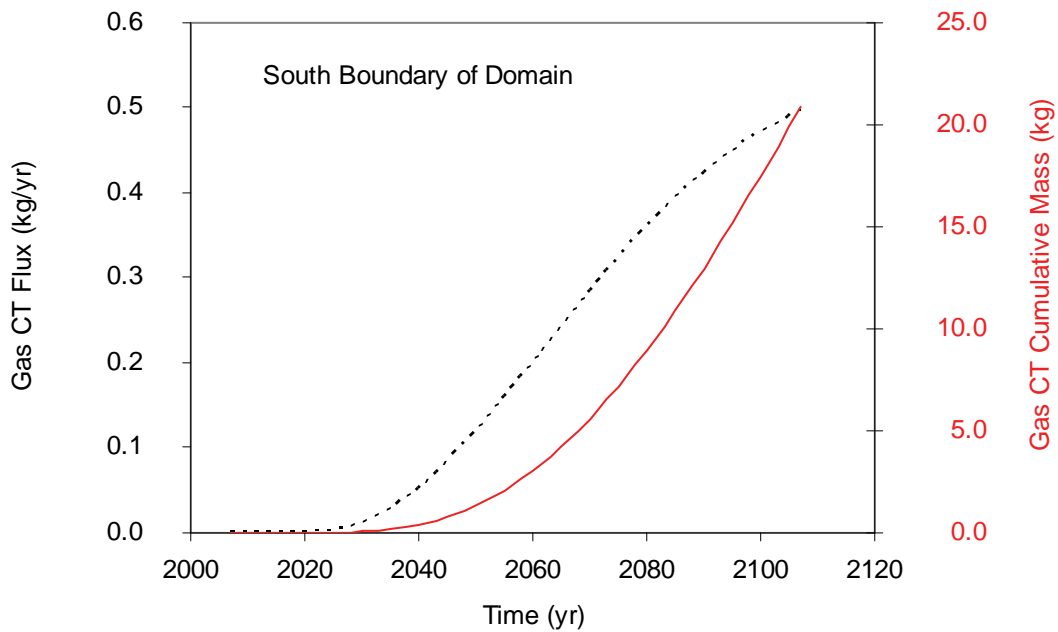
Figure 5.34.   Gas CT Mass Flow Rate (kg/yr) (dashed line) and Gas CT Cumulative Mass Transport (kg) (solid line) Across South Boundary of Domain for Imposed Case 4
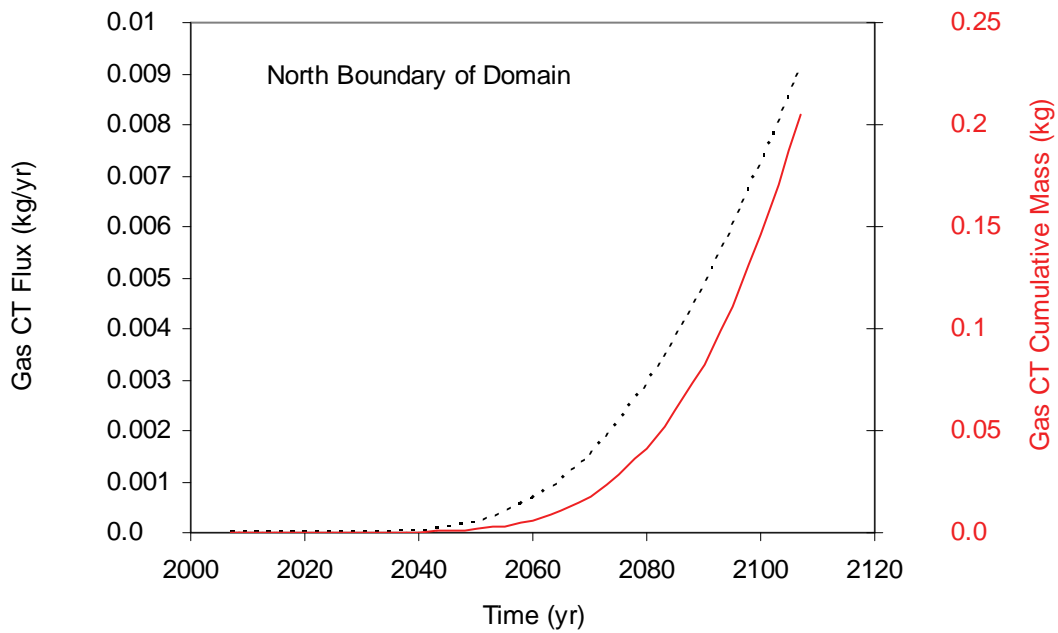
Figure 5.35.   Gas CT Mass Flow Rate (kg/yr) (dashed line) and Gas CT Cumulative Mass Transport (kg) (solid line) Across North Boundary of Domain for Imposed Case 4

5.1.5   Imposed Case 5
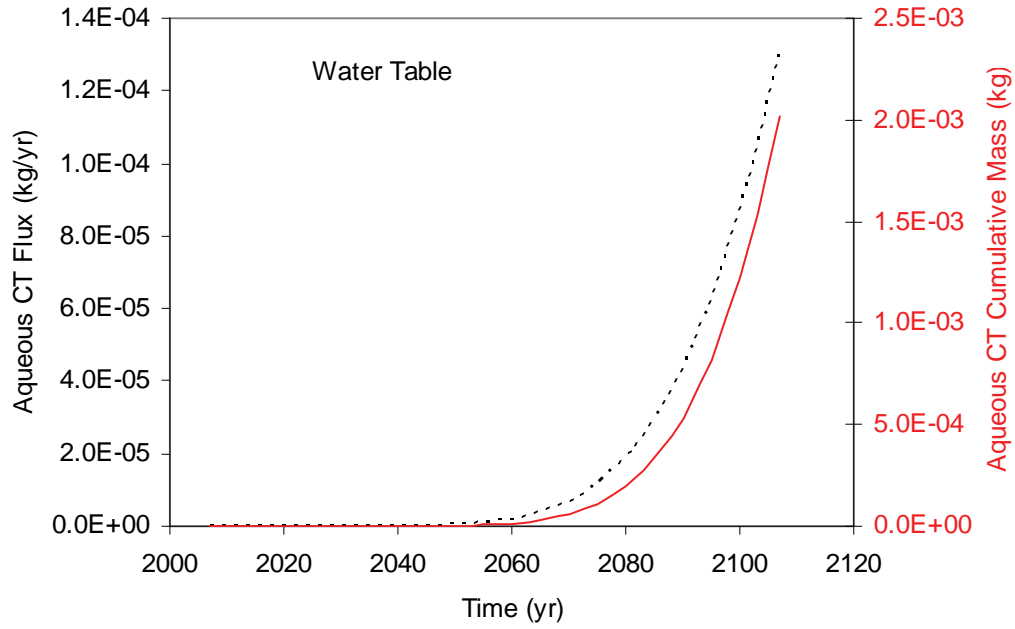
Figure 5.36.   Aqueous CT Mass Flow Rate (kg/yr) (dashed line) and Aqueous CT Cumulative Mass Transport (kg) (solid line) Across Water Table for Imposed Case 5
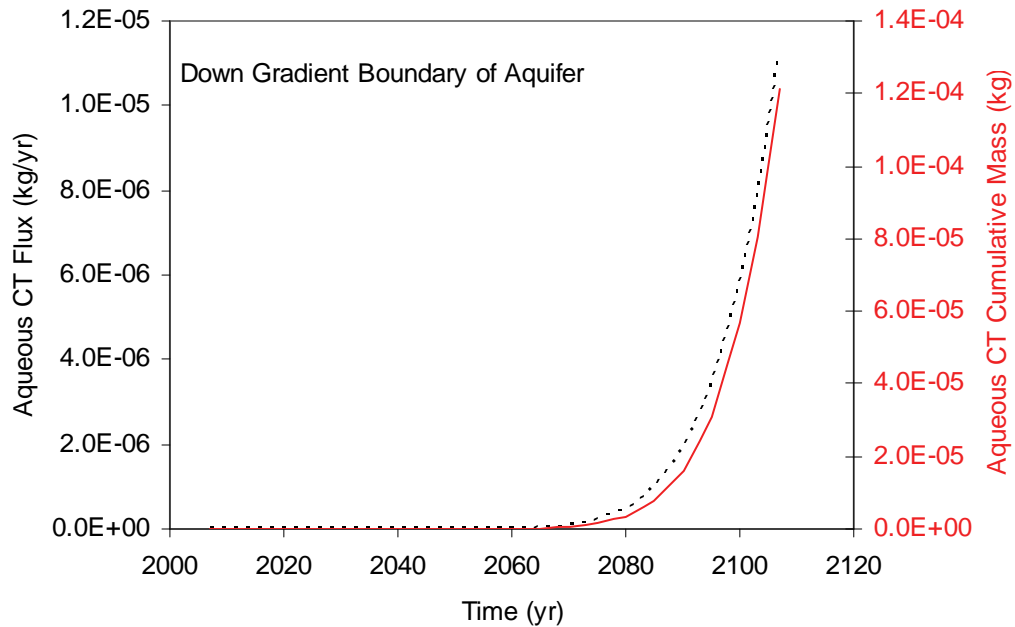
Figure 5.37.   Aqueous CT Mass Flow Rate (kg/yr) (dashed line) and Aqueous CT Cumulative Mass Transport (kg) (solid line) Across Down Gradient Aquifer Boundary for Imposed Case 5
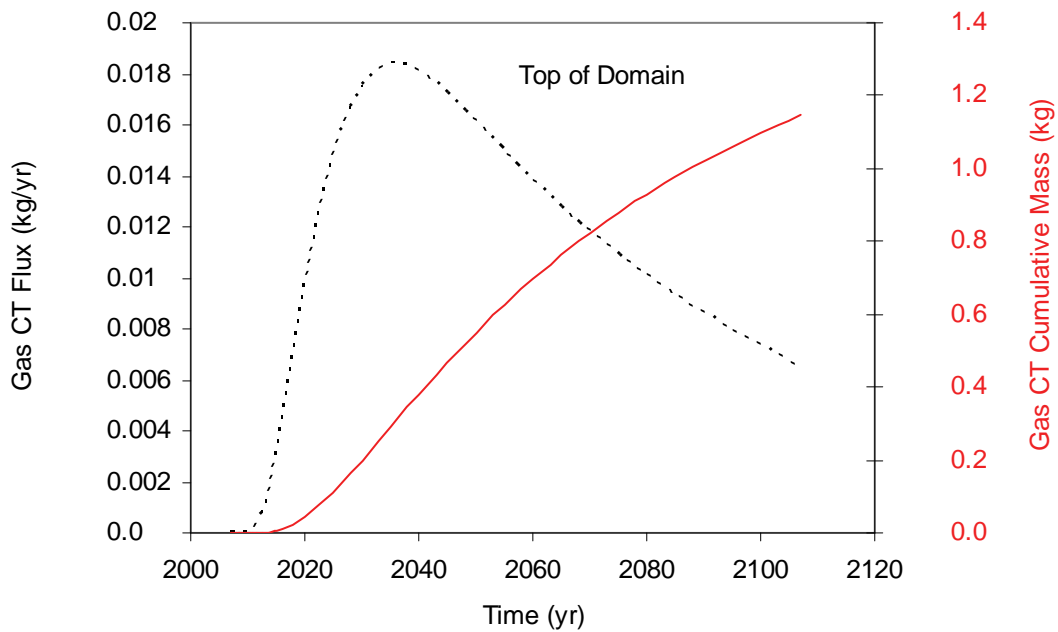
Figure 5.38.   Gas CT Mass Flow Rate (kg/yr) (dashed line) and Gas CT Cumulative Mass Transport (kg) (solid line) Across Top of Domain for Imposed Case 5
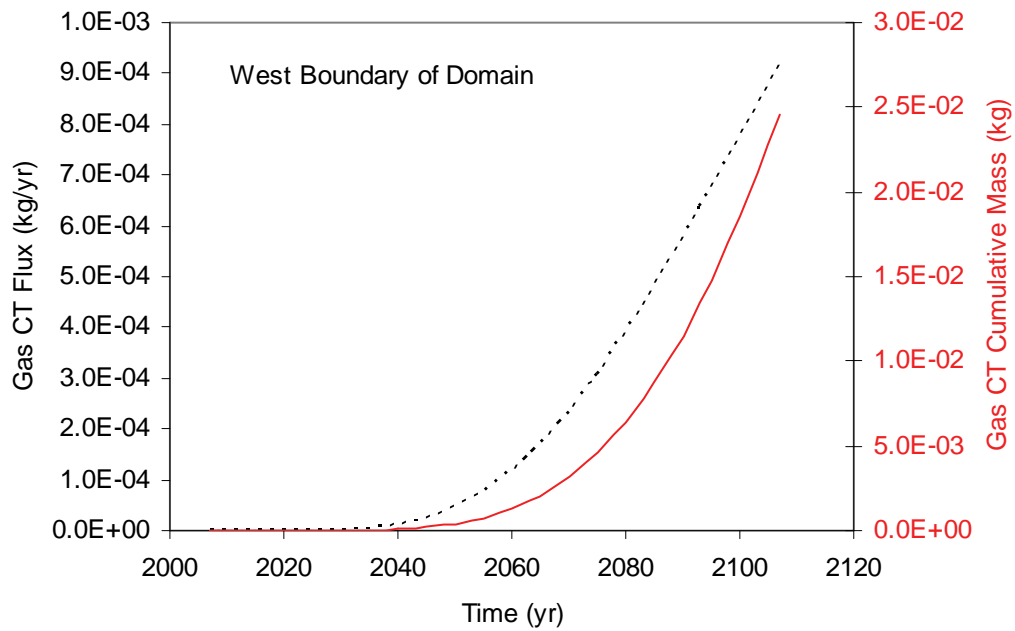
Figure 5.39.   Gas CT Mass Flow Rate (kg/yr) (dashed line) and Gas CT Cumulative Mass Transport (kg) (solid line) Across West Boundary of Domain for Imposed Case 5
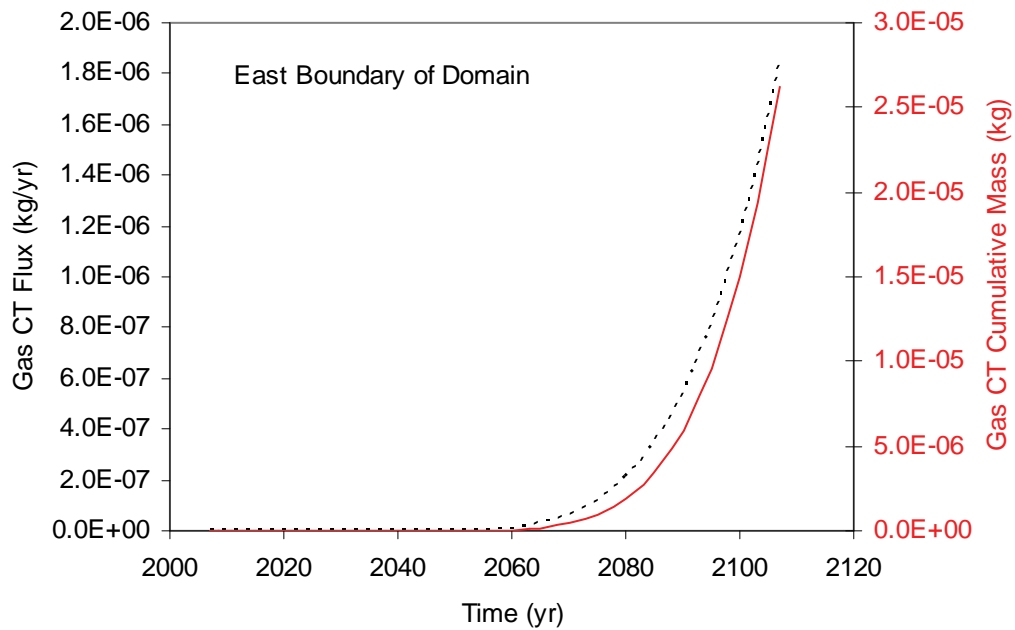
Figure 5.40. Gas CT Mass Flow Rate (kg/yr) (dashed line) and Gas CT Cumulative Mass Transport (kg) (solid line) Across East Boundary of Domain for Imposed Case 5
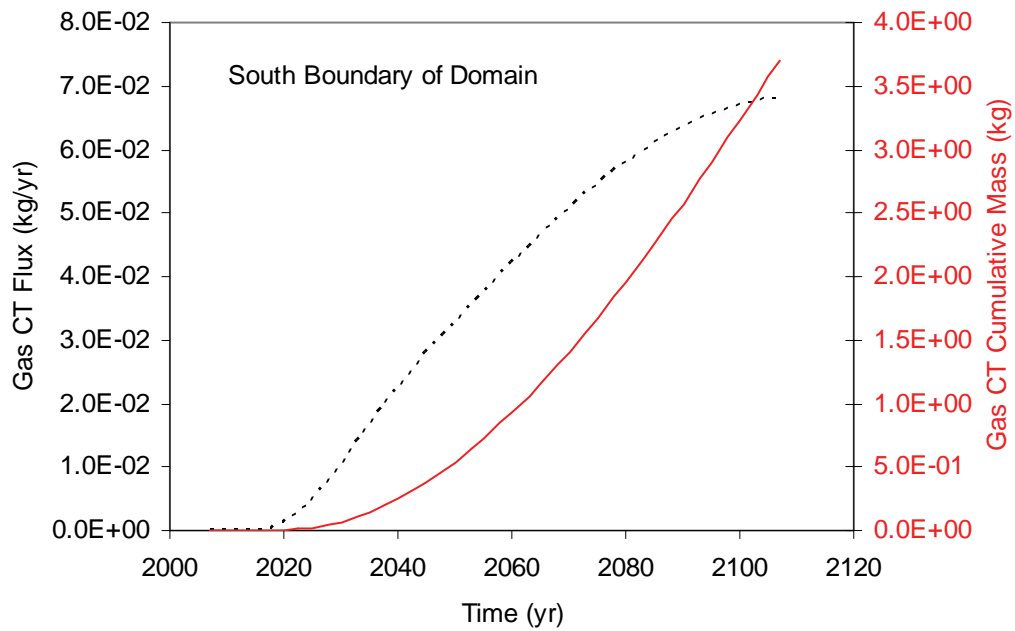
Figure 5.41. Gas CT Mass Flow Rate (kg/yr) (dashed line) and Gas CT Cumulative Mass Transport (kg) (solid line) Across South Boundary of Domain for Imposed Case 5
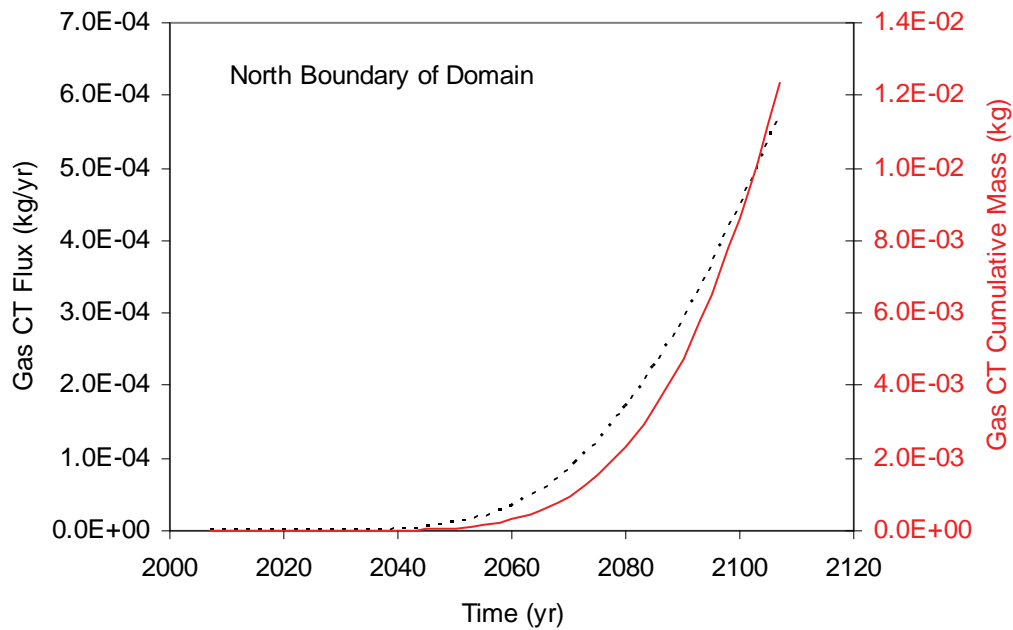
Figure 5.42.   Gas CT Mass Flow Rate (kg/yr) (dashed line) and Gas CT Cumulative Mass Transport
(kg) (solid line) Across North Boundary of Domain for Imposed Case 5

5.1.6   Imposed Case 6
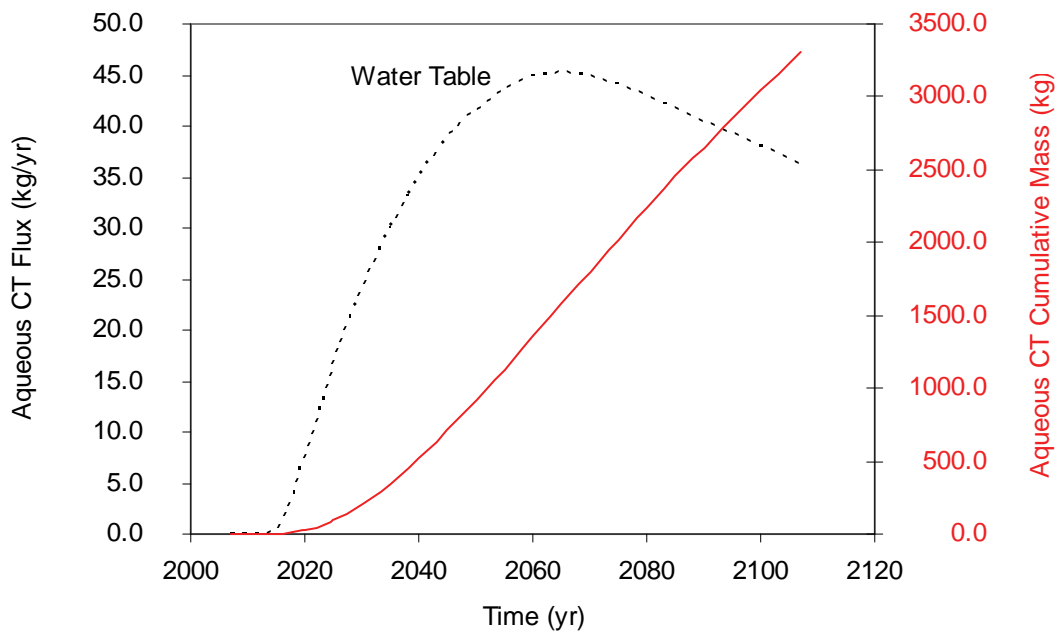
Figure 5.43.   Aqueous CT Mass Flow Rate (kg/yr) (dashed line) and Aqueous CT Cumulative Mass
Transport (kg) (solid line) Across Water Table for Imposed Case 6
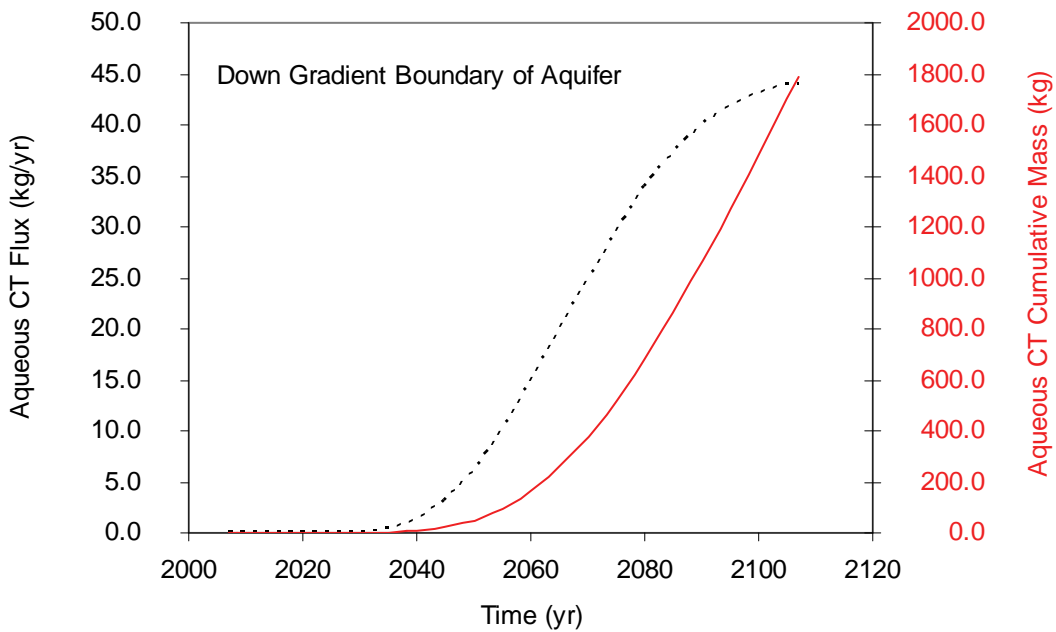
Figure 5.44. Aqueous CT Mass Flow Rate (kg/yr) (dashed line) and Aqueous CT Cumulative Mass Transport (kg) (solid line) Across Down Gradient Aquifer Boundary for Imposed Case 6
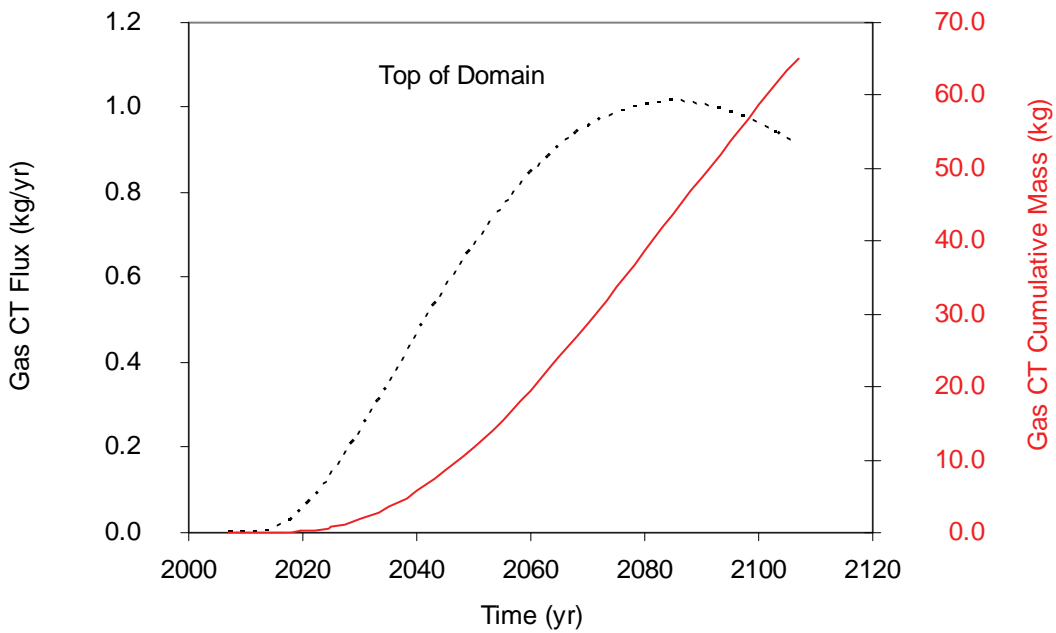
Figure 5.45. Gas CT Mass Flow Rate (kg/yr) (dashed line) and Gas CT Cumulative Mass Transport (kg) (solid line) Across Top of Domain for Imposed Case 6
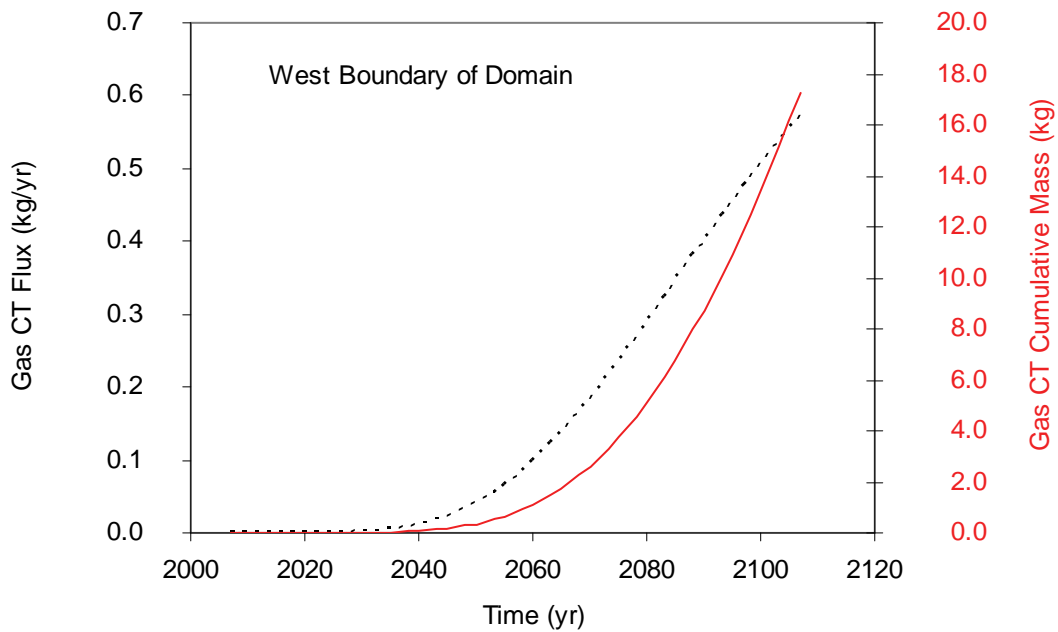
Figure 5.46. Gas CT Mass Flow Rate (kg/yr) (dashed line) and Gas CT Cumulative Mass Transport (kg) (solid line) Across West Boundary of Domain for Imposed Case 6
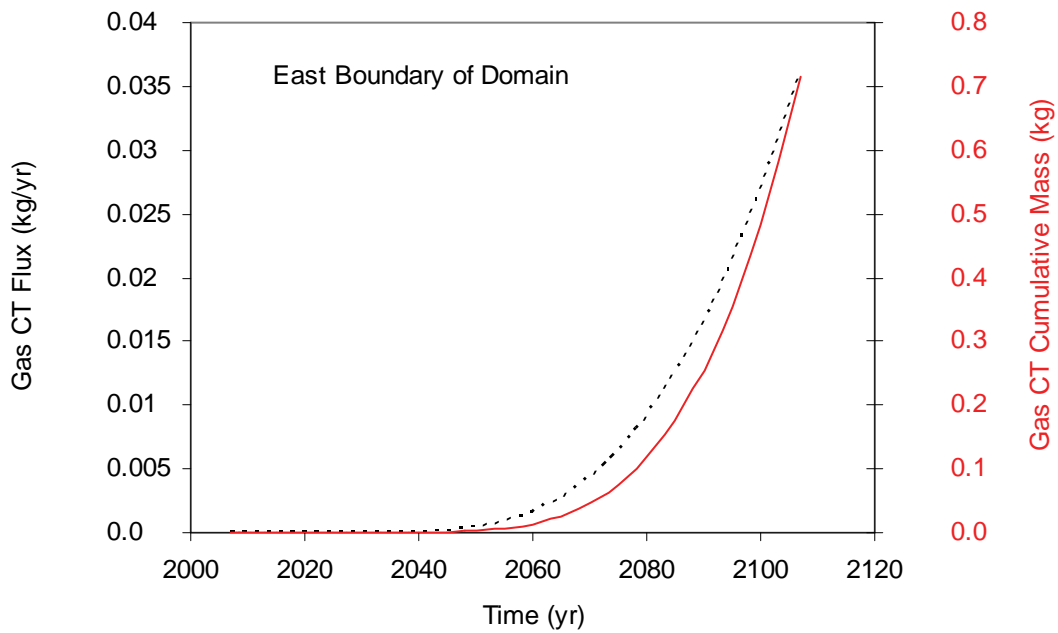
Figure 5.47. Gas CT Mass Flow Rate (kg/yr) (dashed line) and Gas CT Cumulative Mass Transport (kg) (solid line) Across East Boundary of Domain for Imposed Case 6
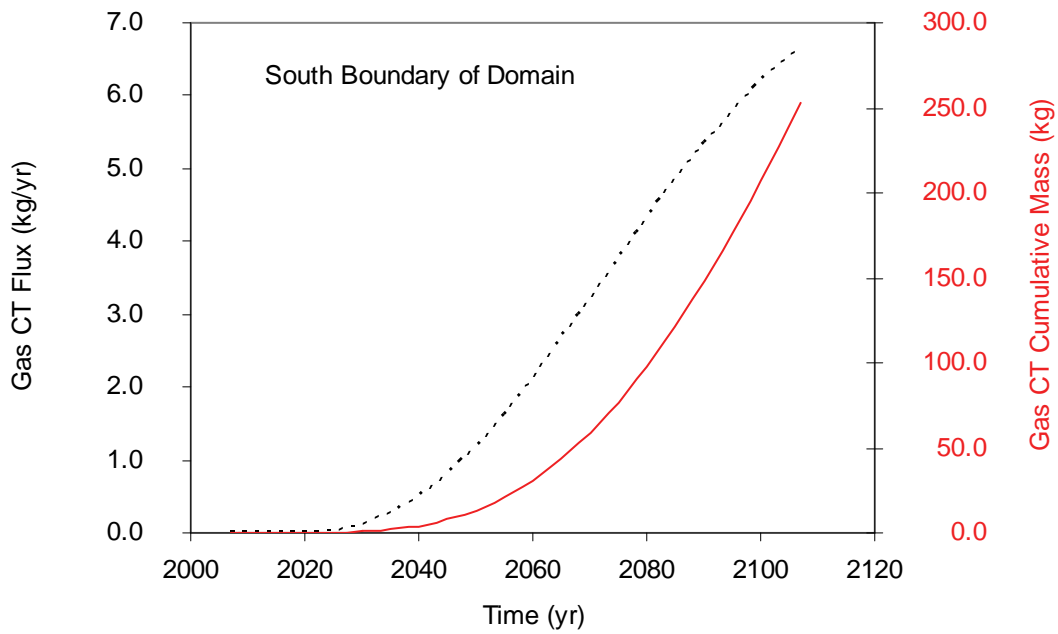
Figure 5.48. Gas CT Mass Flow Rate (kg/yr) (dashed line) and Gas CT Cumulative Mass Transport (kg) (solid line) Across South Boundary of Domain for Imposed Case 6
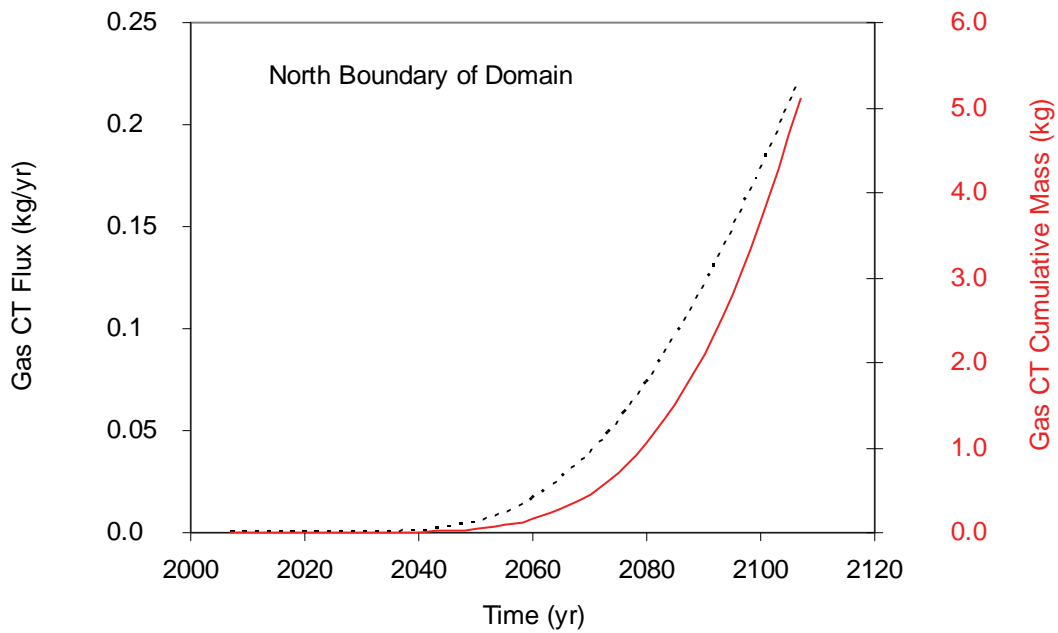
Figure 5.49. Gas CT Mass Flow Rate (kg/yr) (dashed line) and Gas CT Cumulative Mass Transport (kg) (solid line) Across North Boundary of Domain for Imposed Case 6

5.1.7 Modeled Case
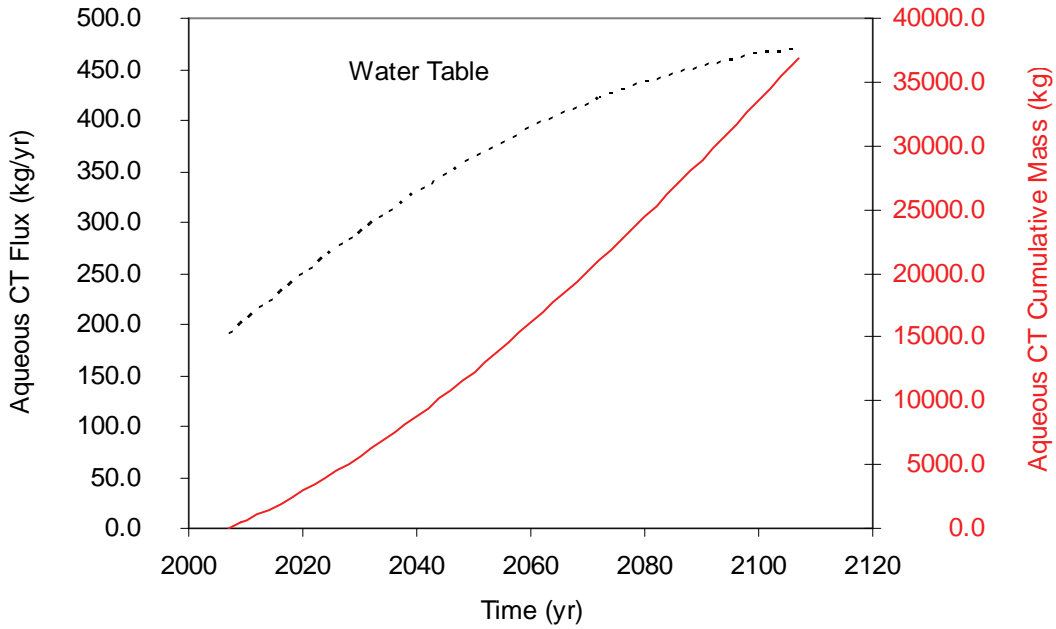
Figure 5.50. Aqueous CT Mass Flow Rate (kg/yr) (dashed line) and Aqueous CT Cumulative Mass Transport (kg) (solid line) Across Water Table for the Modeled Case
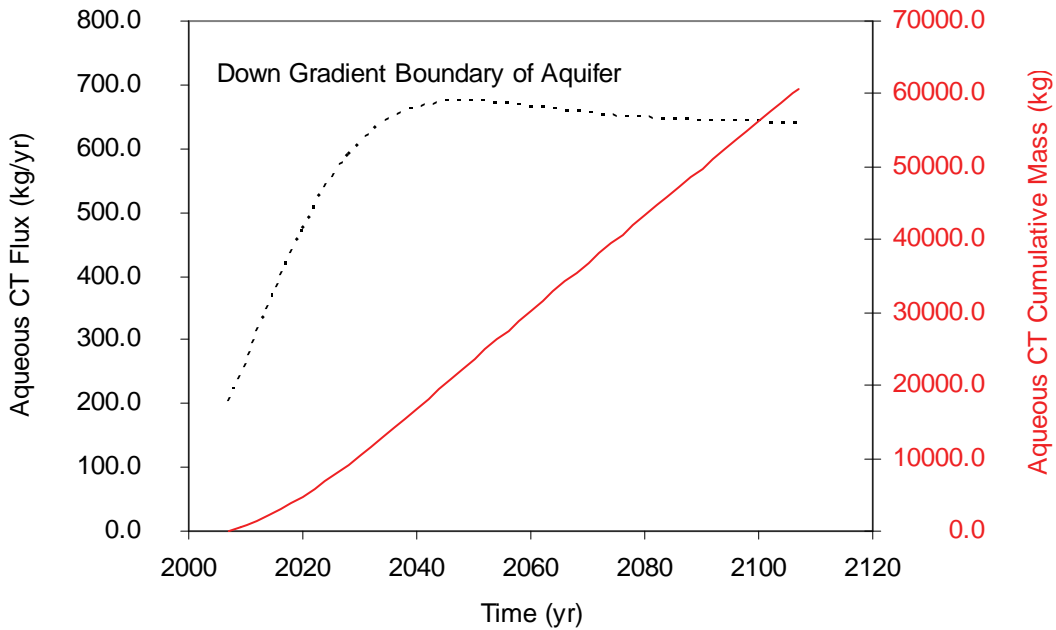
Figure 5.51. Aqueous CT Mass Flow Rate (kg/yr) (dashed line) and Aqueous CT Cumulative Mass Transport (kg) (solid line) Across Down Gradient Aquifer Boundary for the Modeled Case
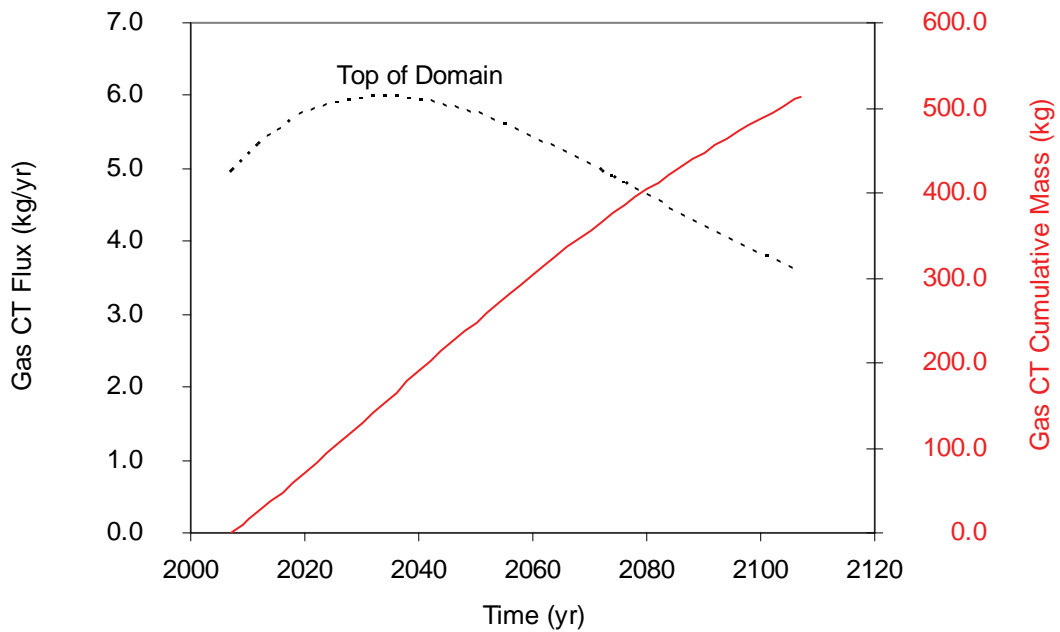
Figure 5.52. Gas CT Mass Flow Rate (kg/yr) (dashed line) and Gas CT Cumulative Mass Transport (kg) (solid line) Across Top of Domain for the Modeled Case
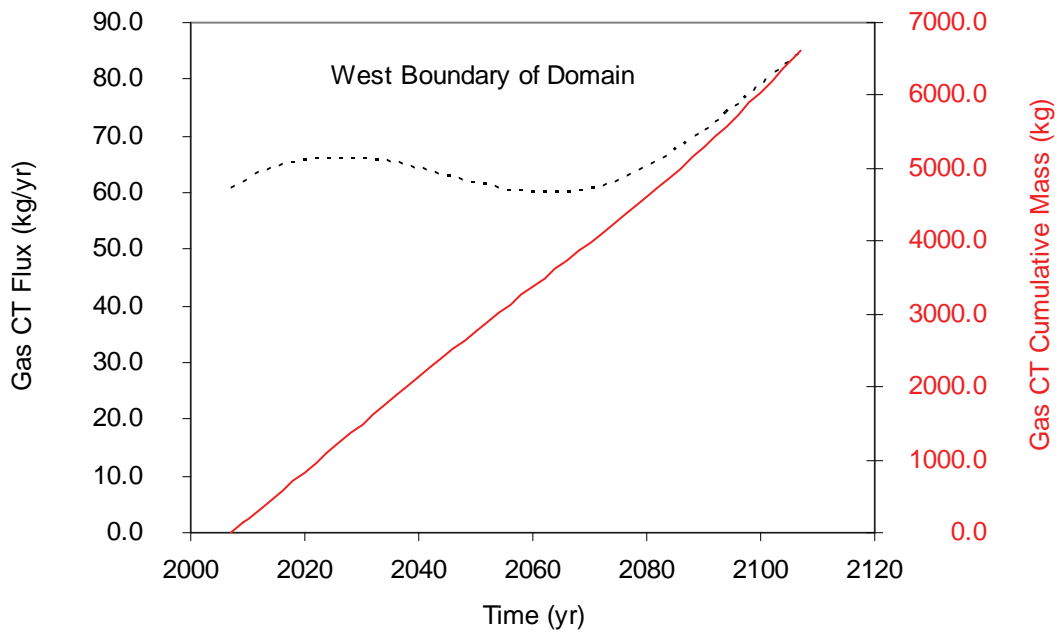
Figure 5.53. Gas CT Mass Flow Rate (kg/yr) (dashed line) and Gas CT Cumulative Mass Transport (kg) (solid line) Across West Boundary of Domain for the Modeled Case
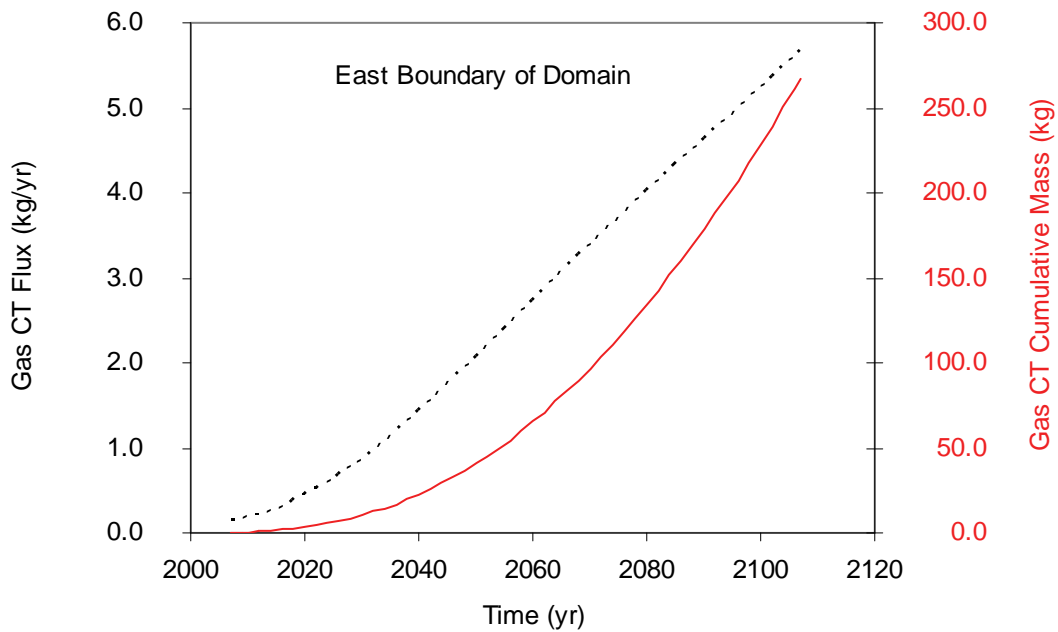
Figure 5.54.   Gas CT Mass Flow Rate (kg/yr) (dashed line) and Gas CT Cumulative Mass Transport (kg) (solid line) Across East Boundary of Domain for the Modeled Case
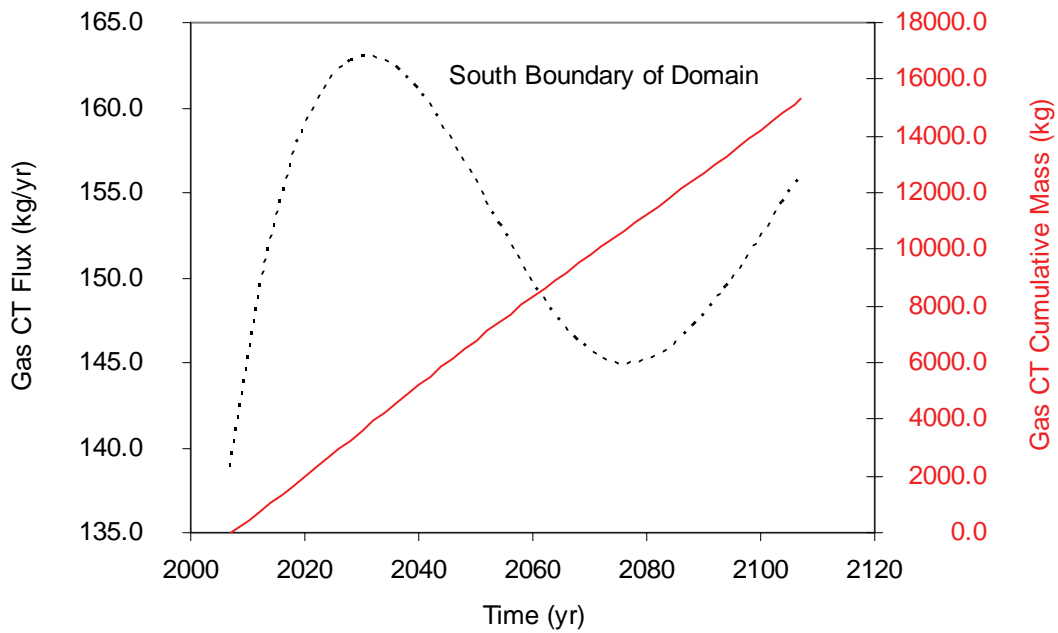
Figure 5.55.   Gas CT Mass Flow Rate (kg/yr) (dashed line) and Gas CT Cumulative Mass Transport (kg) (solid line) Across South Boundary of Domain for the Modeled Case
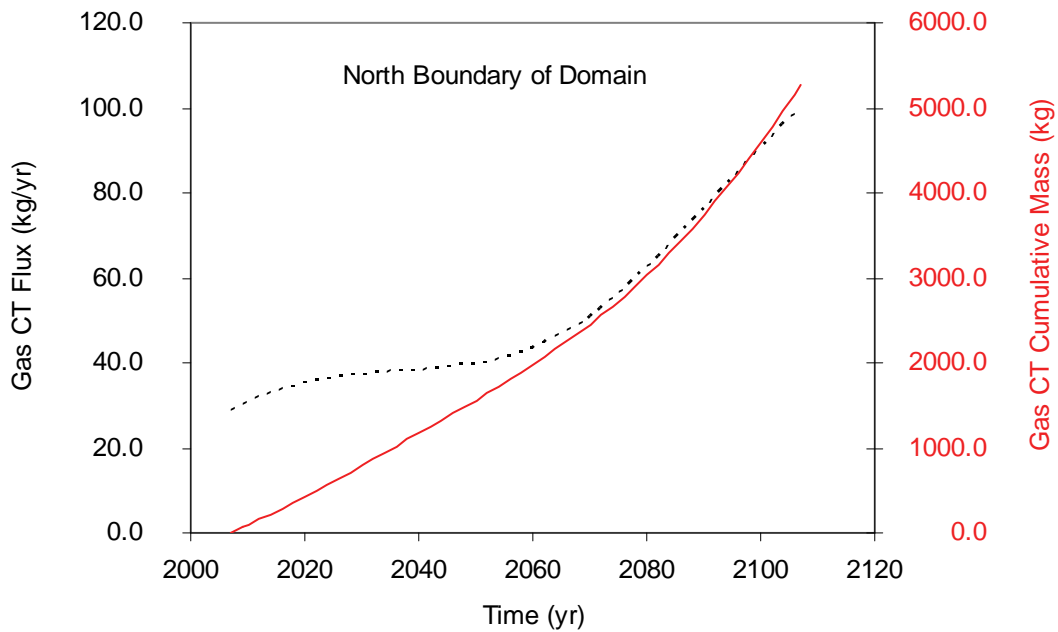
Figure 5.56. Gas CT Mass Flow Rate (kg/yr) (dashed line) and Gas CT Cumulative Mass Transport (kg) (solid line) Across North Boundary of Domain for the Modeled Case
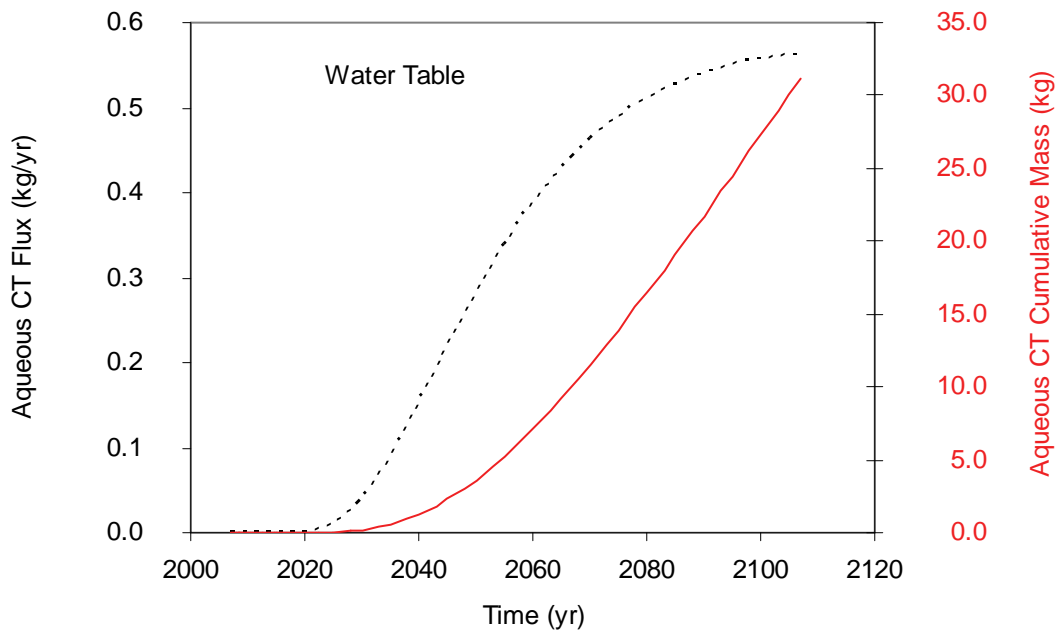
Figure 5.57. NAPL-Phase Mass Flow Rate (kg/yr) (dashed line) and NAPL CT Cumulative Mass Transport (kg) (solid line) Across Water Table for the Modeled Case

5.2   Aqueous Phase CT Mass Flux Across the Water Table

In this section, aqueous phase mass fluxes (in kg m^{-2} yr^{-1}) across the water table at selected locations on a west-east and south-north cross-section are computed and plotted in Figure 5.58 through 3.64 for the seven simulations. The computed values, based on aqueous phase flux and dissolved CT concentration in the first unsaturated node above the water table, are listed in Appendix A. The fluxes all have negative values because, by convention, upward movement is positive. The figures demonstrate results that are consistent with the figures shown in Section 5.1. For imposed cases 1 through 5, the maximum flux is approximately directly below the disposal site. This result is expected because the emplaced CT was in areas directly underneath the disposal site. The fluxes for imposed cases 1 (Figure 5.58) and 4 (Figure 5.61) are considerably larger than for imposed cases 2 (Figure 5.59), 3 (Figure 5.60), and 5 (Figure 5.62). Although the fluxes for these three cases are smaller, they increase over time. For imposed cases 1 and 4, maximum values are obtained between 2050 and 2070, before the values decrease.

For imposed case 6 (Figure 5.63), the computed fluxes are considerably larger than for imposed cases 1 and 4. For this case, the maximum values are one order of magnitude larger, although this concentration peaks around 2030. The modeled case (Figure 5.64) shows fluxes that have values close to what was observed for imposed case 6. The main differences between this case and imposed case 6 are that the fluxes are maintained over a larger area and that the values are fairly stable between 2030 and 2107. The behavior shown in Figure 5.64 almost resembles a steady-state transport system.
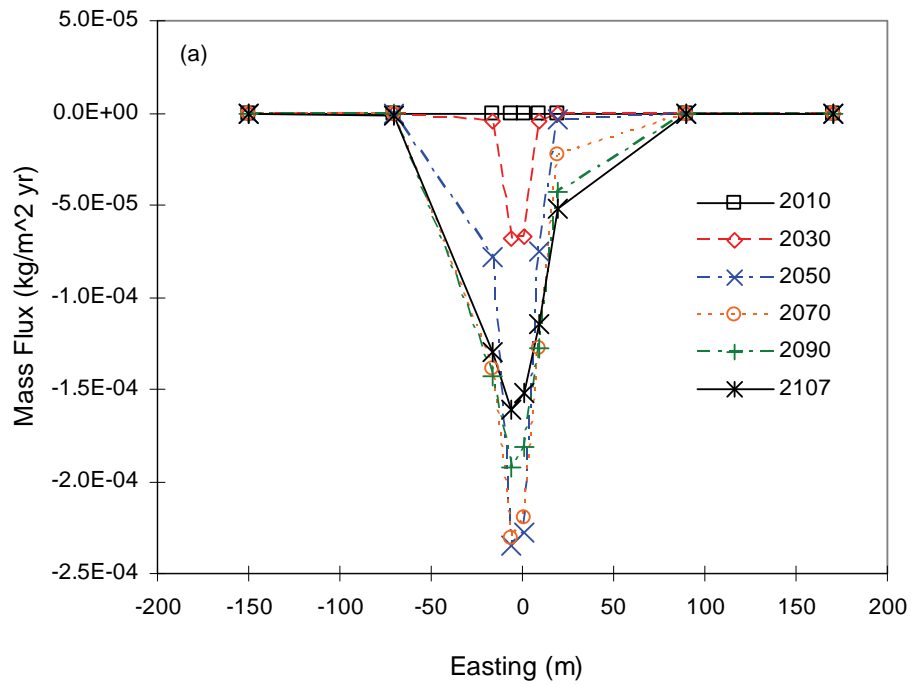
(a)
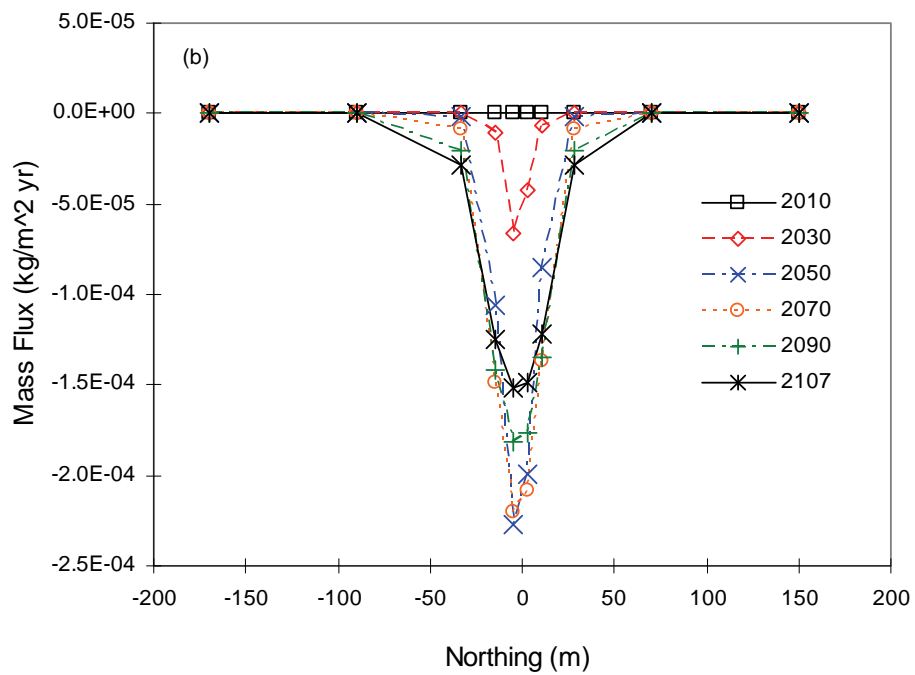
(b)

Figure 5.58.   Aqueous Phase CT Flux Distribution at the Water Table at (a) an Easting (y = -4.6 m) and
(b) a Northing (x = 0.8 m) Cross-Section for Imposed Case 1. The center of the Z-9 trench
is located at (x, y) = (0 m, 0 m).
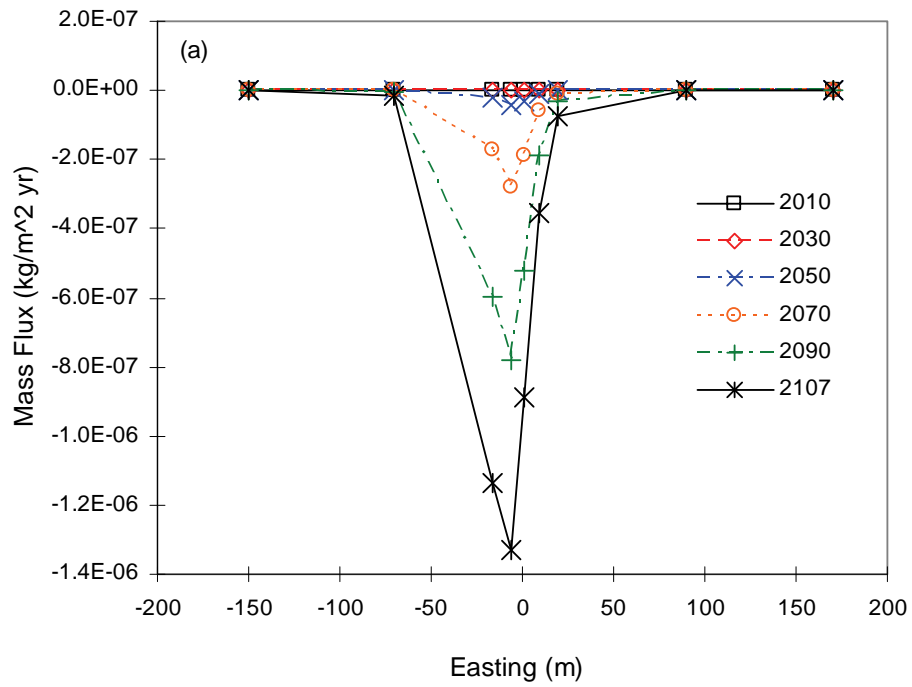
(a)
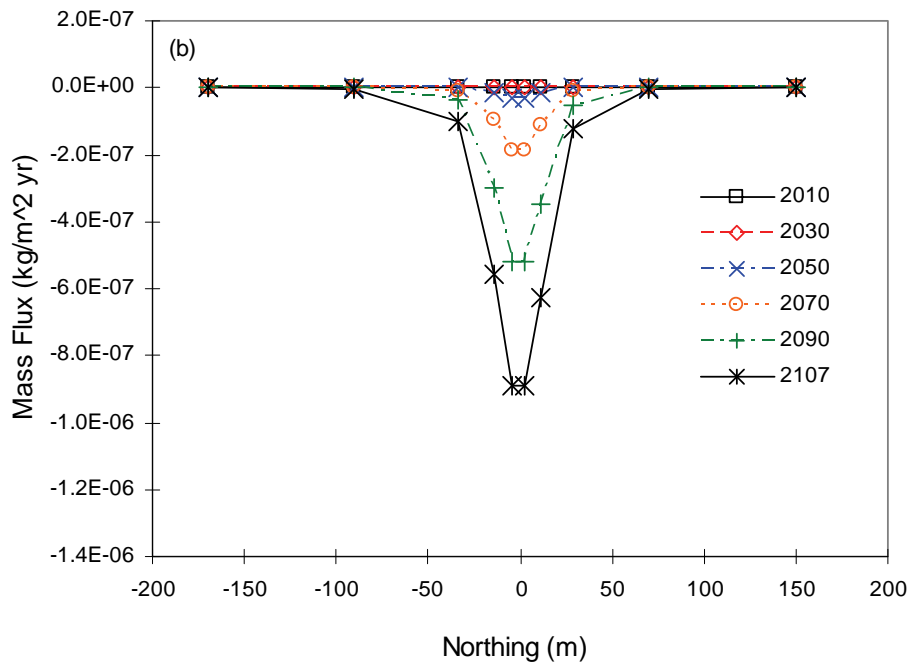
(b)

Figure 5.59.   Aqueous Phase CT Flux Distribution at the Water Table at (a) an Easting (y = -4.6 m) and (b) a Northing (x = 0.8 m) Cross-Section for Imposed Case 2. The center of the Z-9 trench is located at (x, y) = (0 m, 0 m).

5.39
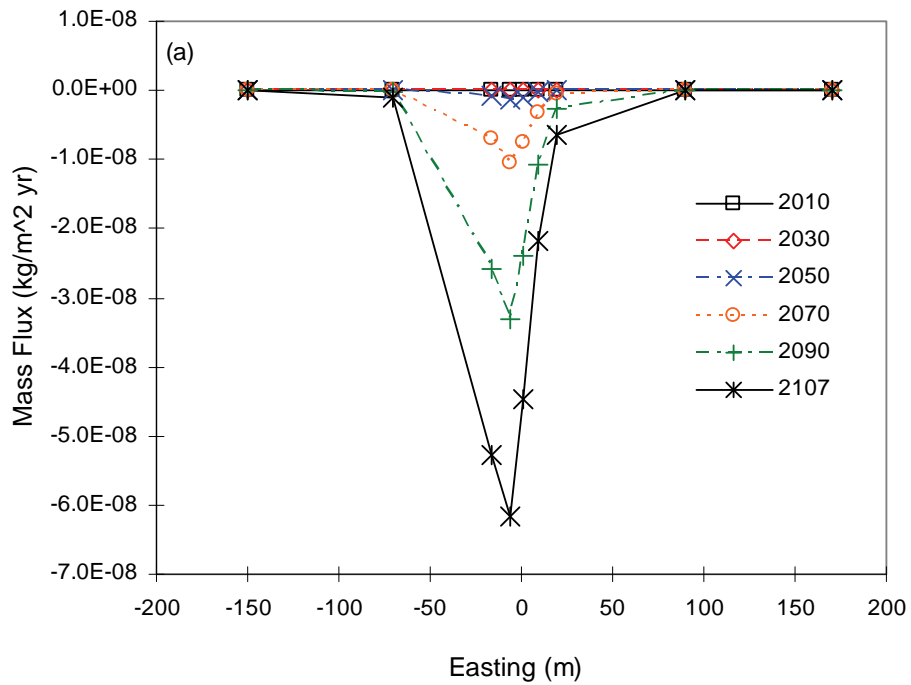
(a)
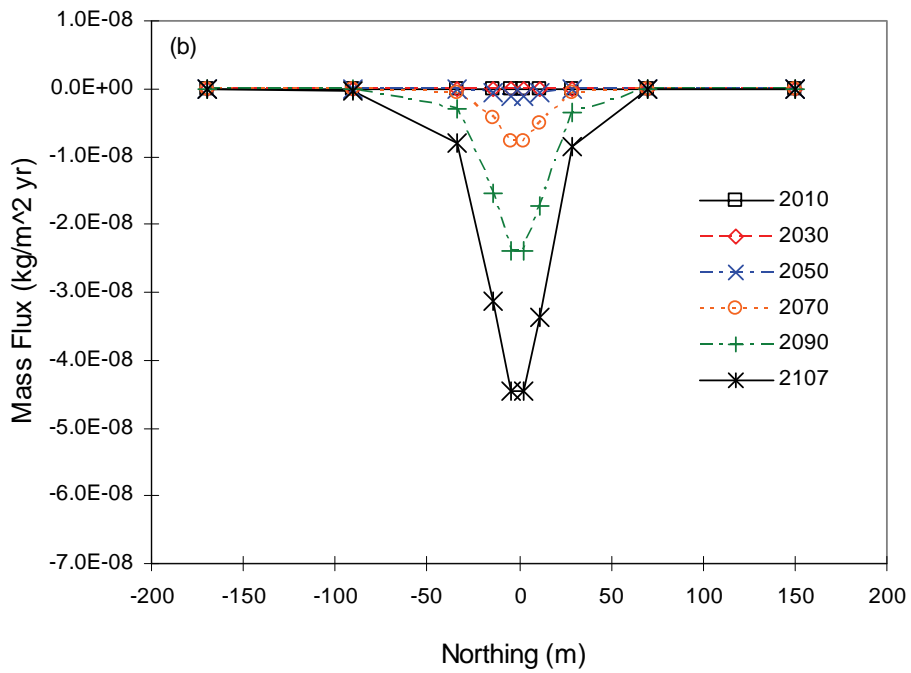
(b)

Figure 5.60. Aqueous Phase CT Flux Distribution at the Water Table at (a) an Easting (y = -4.6 m) and (b) a Northing (x = 0.8 m) Cross-Section for Imposed Case 3. The center of the Z-9 trench is located at (x, y) = (0 m, 0 m).
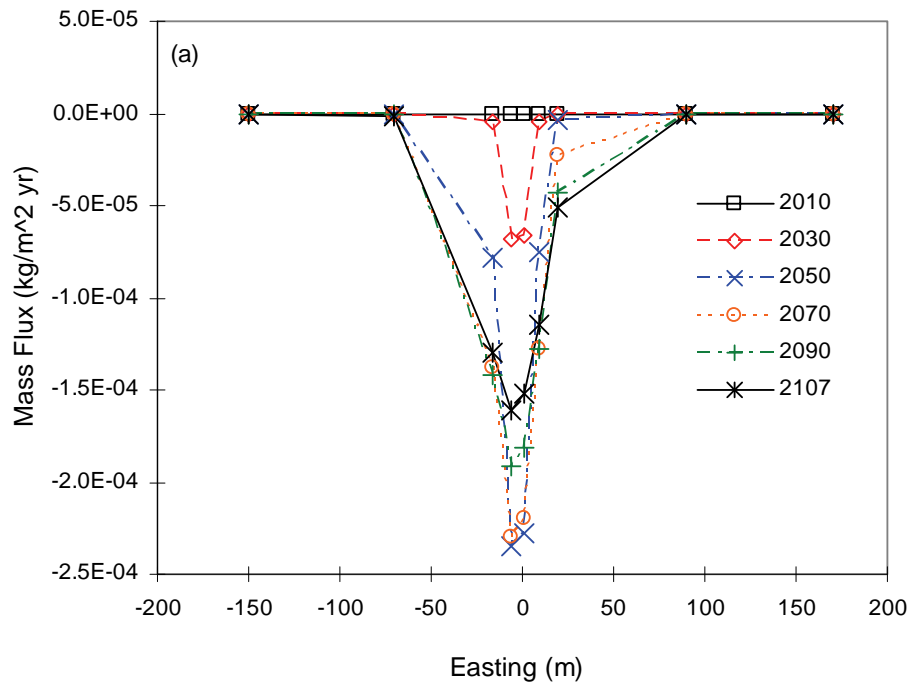
(a)
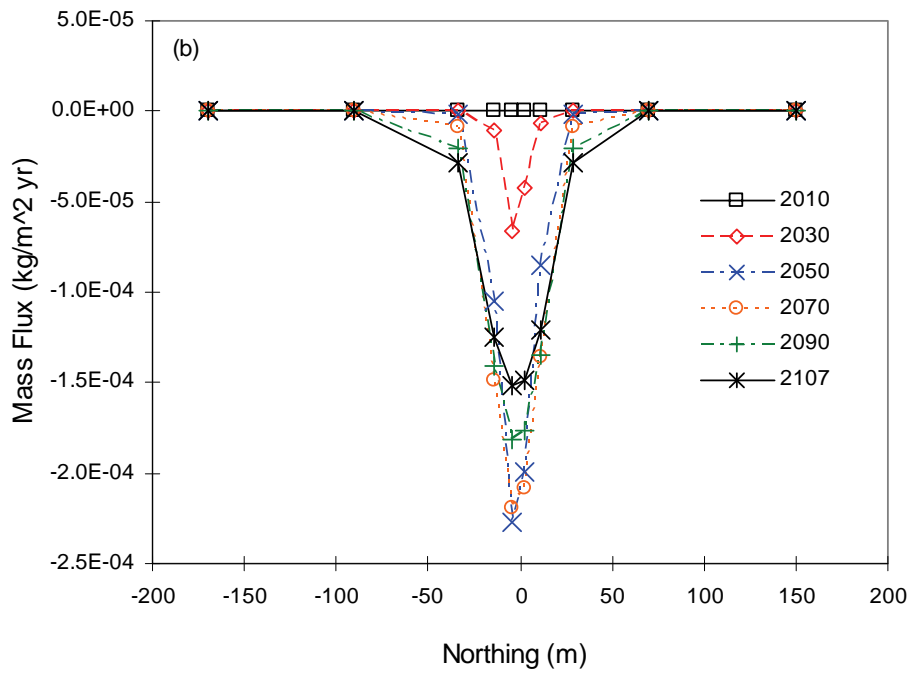
(b)

Figure 5.61.   Aqueous Phase CT Flux Distribution at the Water Table at (a) an Easting (y = -4.6 m) and
(b) a Northing (x = 0.8 m) Cross-Section for Imposed Case 4. The center of the Z-9 trench
is located at (x, y) = (0 m, 0 m).
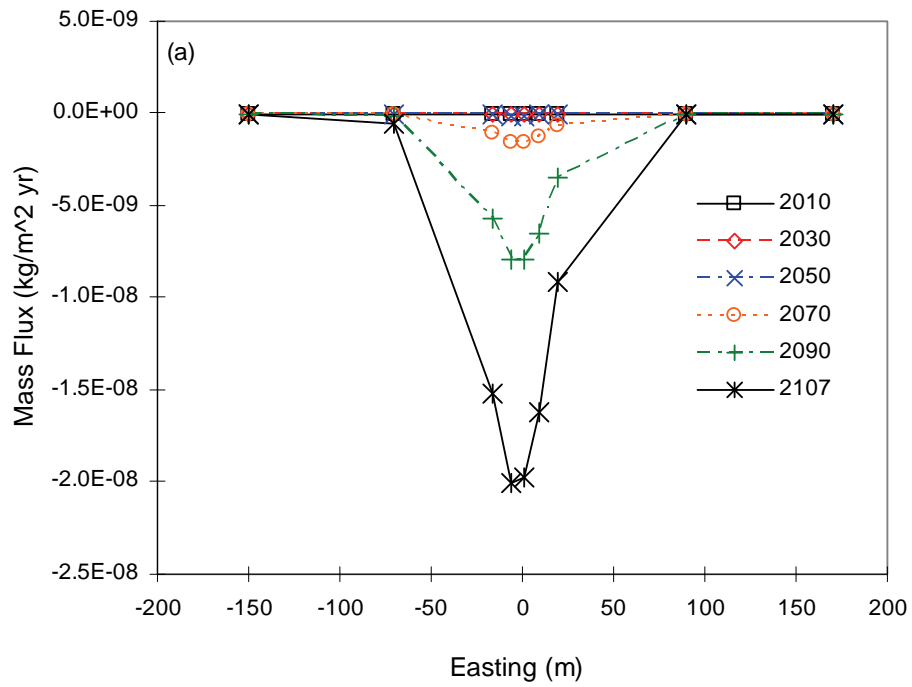
(a)
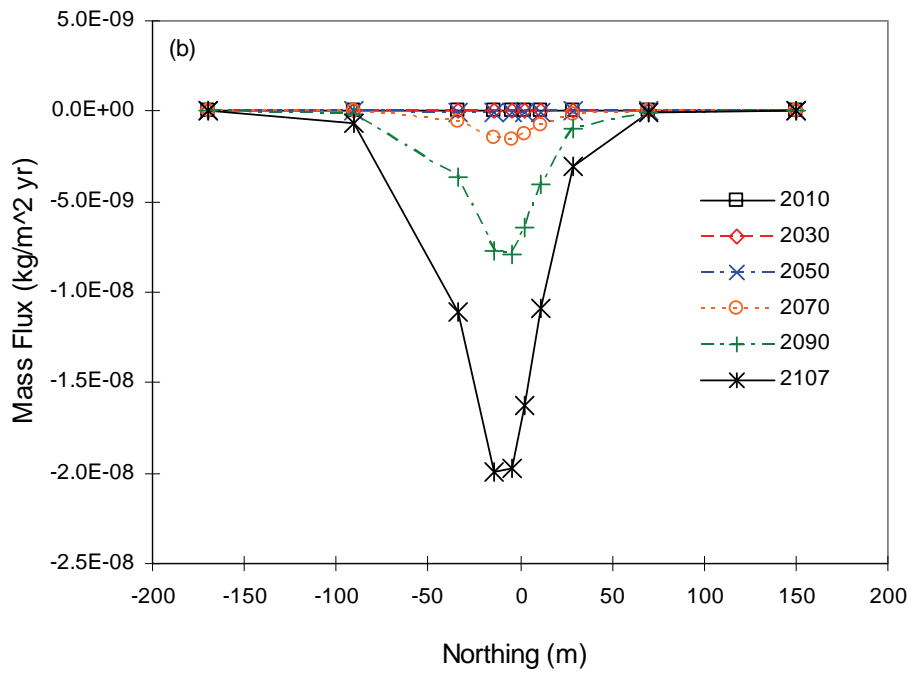
(b)

Figure 5.62.   Aqueous Phase CT Flux Distribution at the Water Table at (a) an Easting (y = -4.6 m) and (b) a Northing (x = 0.8 m) Cross-Section for Imposed Case 5. The center of the Z-9 trench is located at (x, y) = (0 m, 0 m).
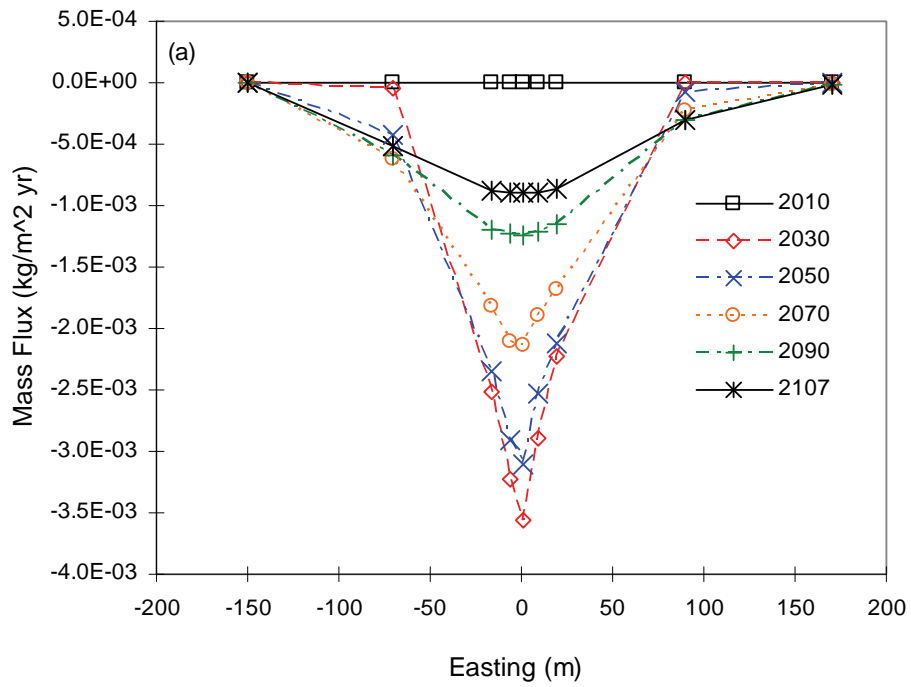
(a)
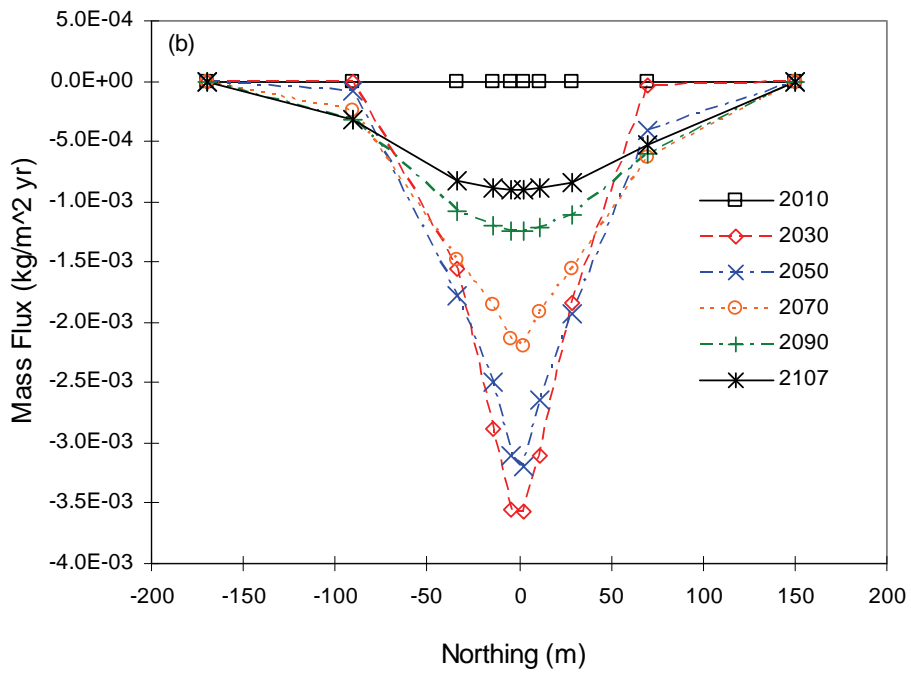
(b)

Figure 5.63. Aqueous Phase CT Flux Distribution at the Water Table at (a) an Easting (y = -4.6 m) and (b) a Northing (x = 0.8 m) Cross-Section for Imposed Case 6. The center of the Z-9 trench is located at (x, y) = (0 m, 0 m).
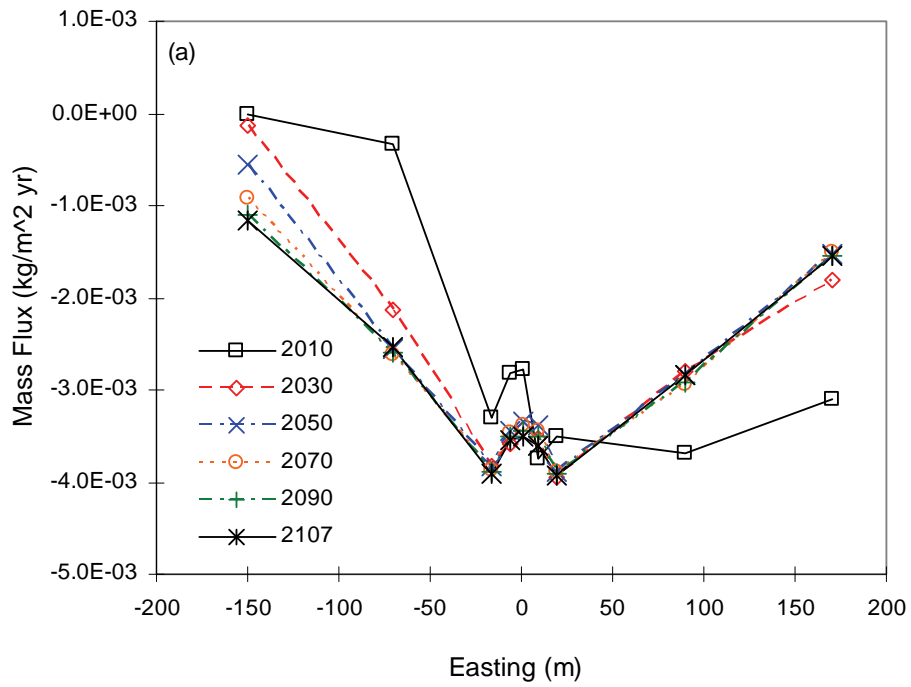
(a)
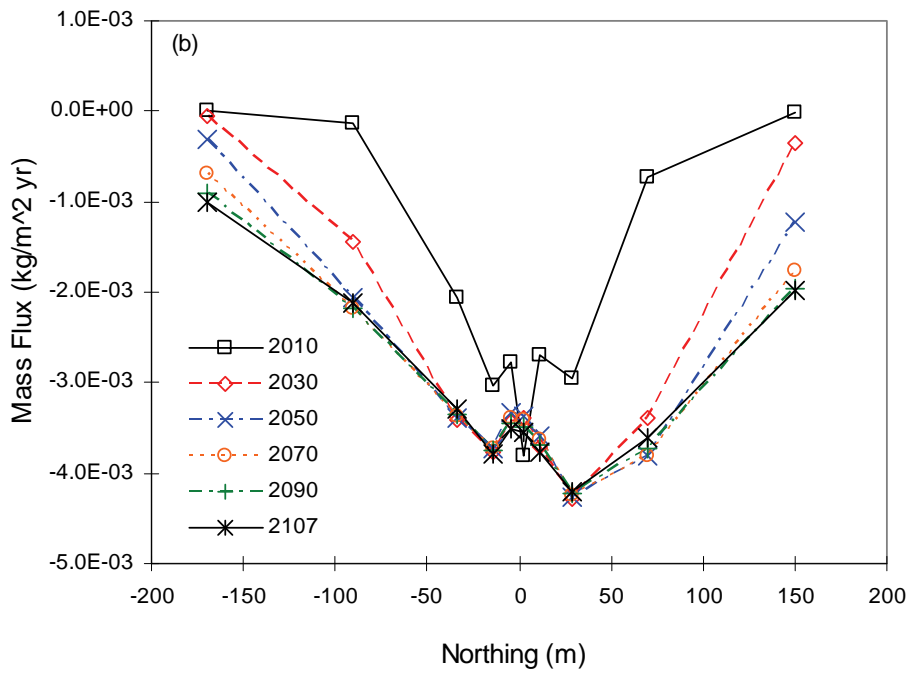
(b)

Figure 5.64.   Aqueous Phase CT Flux Distribution at the Water Table at (a) an Easting (y = -4.6 m) and (b) a Northing (x = 0.8 m) Cross-Section for the Modeled Case. The center of the Z-9 trench is located at (x, y) = (0 m, 0 m).

5.3 Phase CT Mass Partitioning

The CT phase partitioning over time over the whole domain, the vadose zone, the aquifer, the 65-ft Silt Lens, and the Cold Creek Unit have been shown in separate figures for the seven simulations. An overview of the figure numbers has been listed in Table 5.5.

Table 5.5. Overview of CT Partitioning Figures for the Seven Simulations.

	IC-1	IC-2	IC-3	IC-4	IC-5	IC-6	MC
Section	*5.3.1.*	*5.3.2.*	*5.3.3.*	*5.3.4.*	*5.3.5.*	*5.3.6.*	*5.3.7.*
Whole Domain	5.65	5.70	5.75	5.80	5.85	5.90	5.95
Vadose Zone	5.66	5.71	5.76	5.81	5.86	5.91	5.96
Aquifer	5.67	5.72	5.77	5.82	5.87	5.92	5.97
65-ft Silt Lens	5.68	5.73	5.78	5.83	5.88	5.93	5.98
Cold Creek Unit	5.69	5.74	5.79	5.84	5.89	5.94	5.99

The figures for the whole computational domain show that the total mass for each simulation decreased gradually over time. However, the vast majority of the CT mass that was originally present in the domain at 2007 is predicted to be still present in the domain by 2107. As is shown in Table 5.6, most of the mass eventually is sorbed to the porous media. This result is directly related to the imposed K_d factor of 0.2 ml/g. Only the modeled case is predicted to have DNAPL CT present at 2107.

Table 5.6. Total CT Mass at 2007, 2107, and CT Phase Partitioning in 2107

Simulation	Total CT (kg) 2007	Total CT (kg) 2107	Difference (kg)	Sorbed CT (kg) 2107	Gas phase CT (kg) 2107	Aqueous phase CT (kg) 2107	CT DNAPL (kg) 2107
IC-1	607.4	564.6	42.8	453.6	71.8	39.2	-
IC-2	90.0	81.0	9.0	59.4	15.6	6.0	-
IC-3	9.0	8.0	1.0	5.8	1.6	0.6	-
IC-4	22.2	17.3	38.2	11.7	4.1	1.5	-
IC-5	585.2	547.0	4.9	441.2	68.0	37.8	-
IC-6	20,122	17,986	2,136	15,020	1,637	1,330	-
MC	388,676	299,599	89,077	231,576	22,821	19,116	26,086

Since most of the CT mass for all simulations remained in the vadose zone, the CT mass partitioning for this zone strongly resembles the plots depicting the whole domain. The distributions in the aquifer also show that most of the CT mass in groundwater is in sorbed form for all simulations. As discussed already in Section 5.1, total CT mass in the 65-ft silt lens and the Cold Creek Unit decreased rapidly in imposed cases 1 – 5, while holding on the CT in imposed case 6 and the modeled case. For the modeled case, DNAPL CT remained in the Cold Creek Unit throughout 2107, while DNAPL CT is predicted to be present through 2060 for imposed case 6.

5.3.1 Imposed Case 1
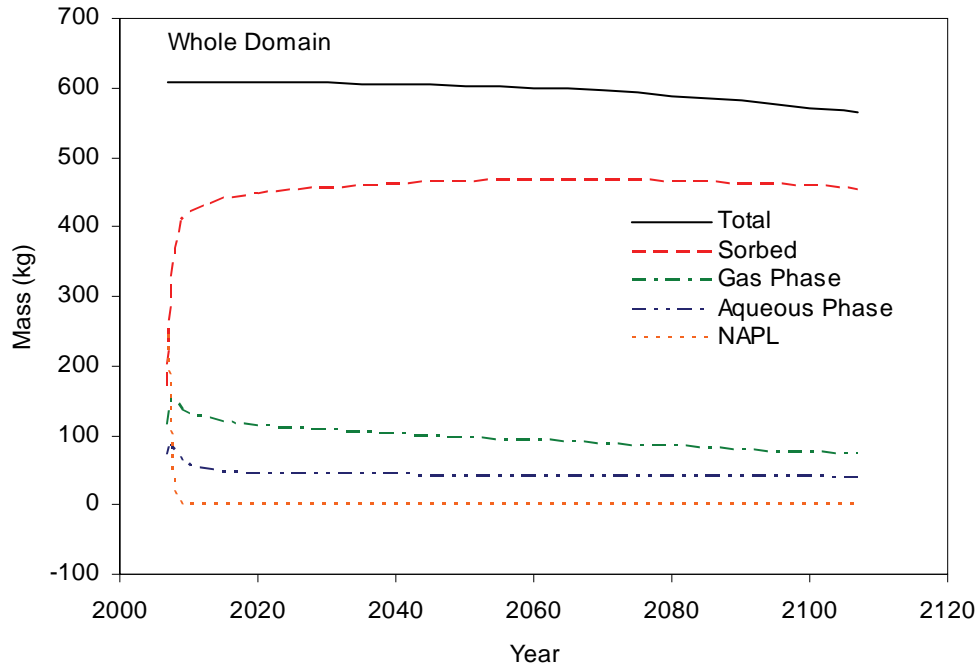
Figure 5.65. CT Mass Partitioning in the Whole Domain for Imposed Case 1
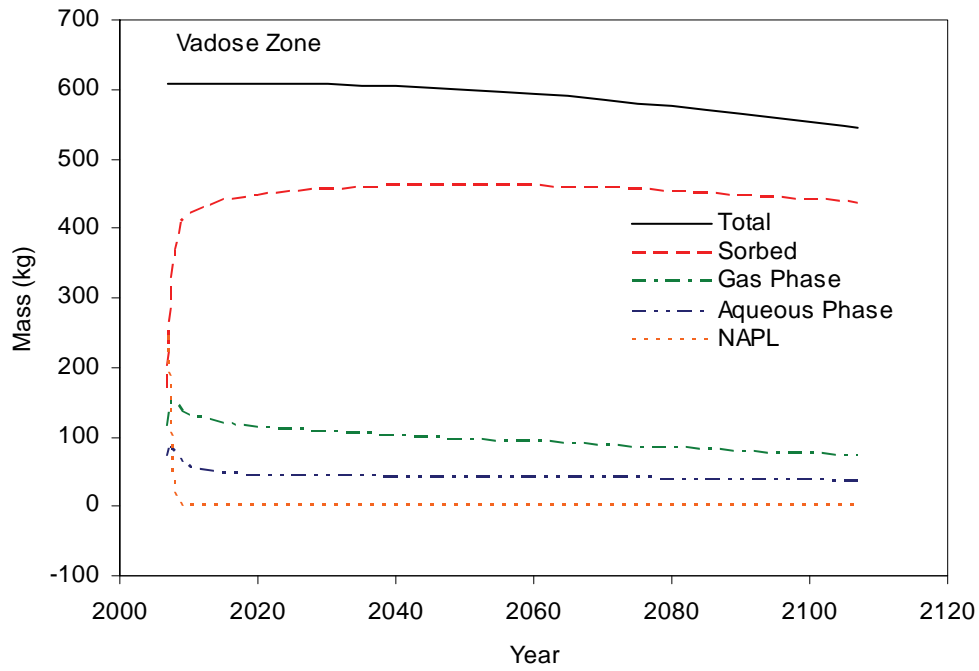
Figure 5.66. CT Mass Partitioning in the Vadose Zone for Imposed Case 1
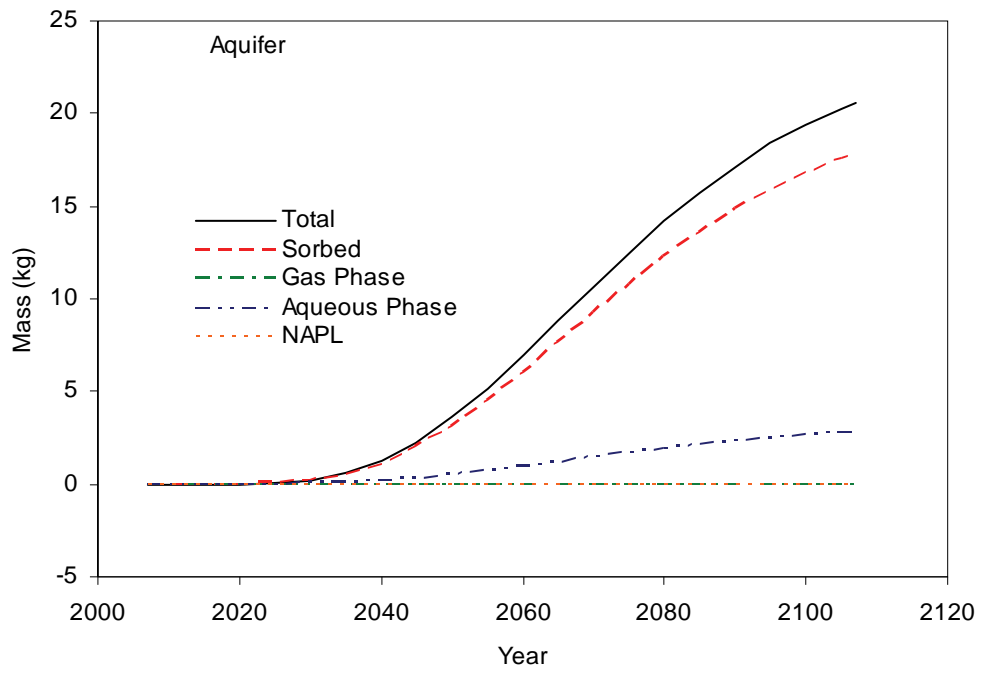
Figure 5.67. CT Mass Partitioning in the Aquifer for Imposed Case 1
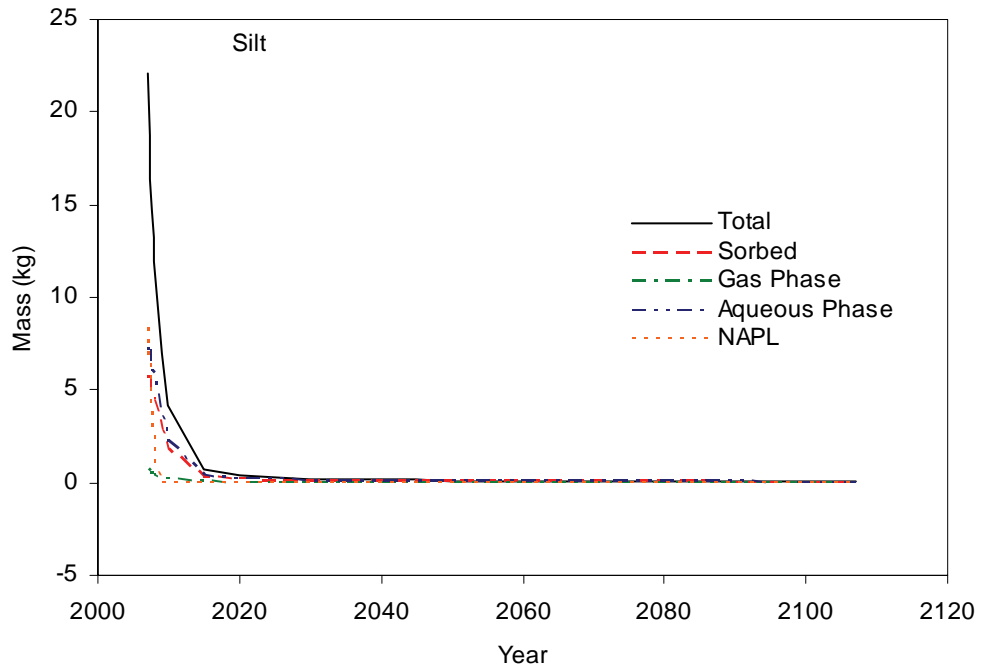
Figure 5.68. CT Mass Partitioning in the 65-ft Silt Lens for Imposed Case 1
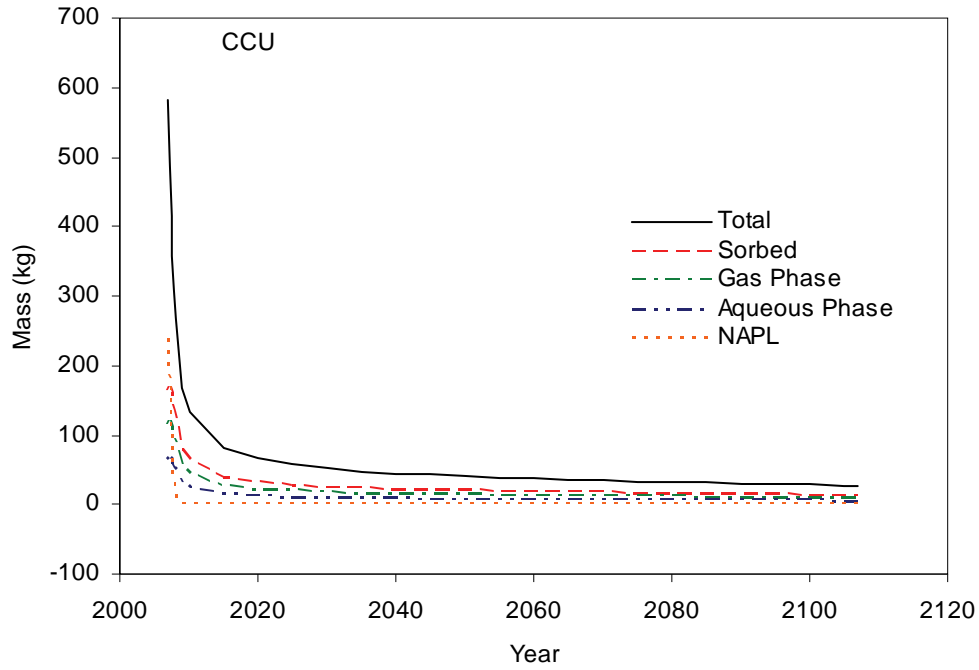
Figure 5.69. CT Mass Partitioning in the Cold Creek Unit for Imposed Case 1

5.3.2   Imposed Case 2
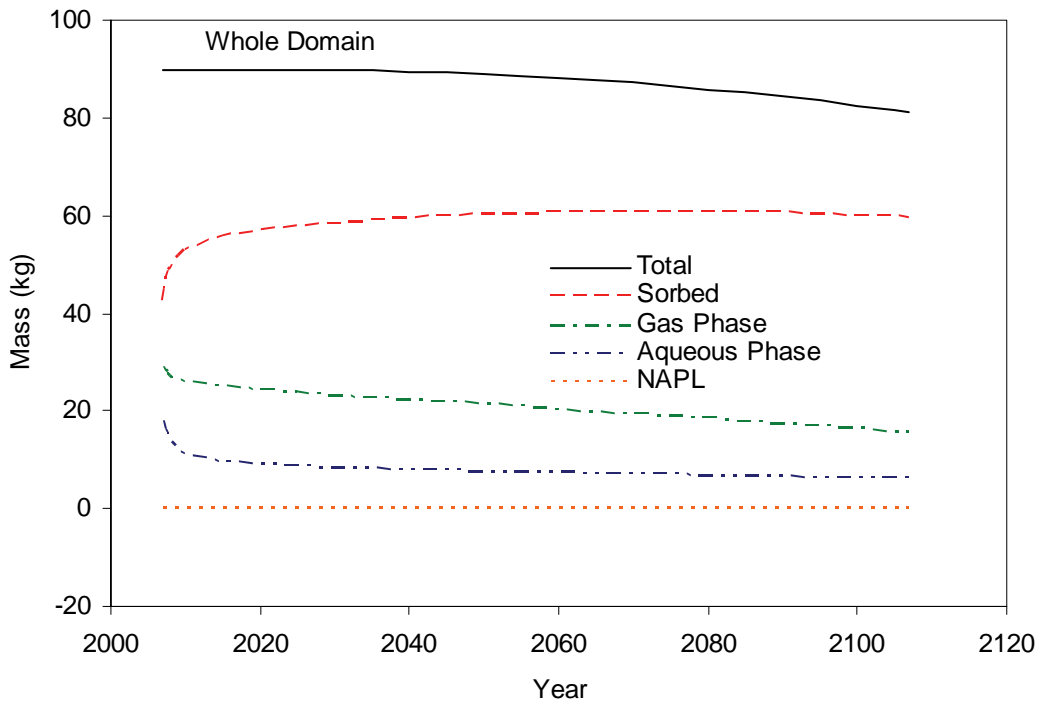
Figure 5.70. CT Mass Partitioning in the Whole Domain for Imposed Case 2
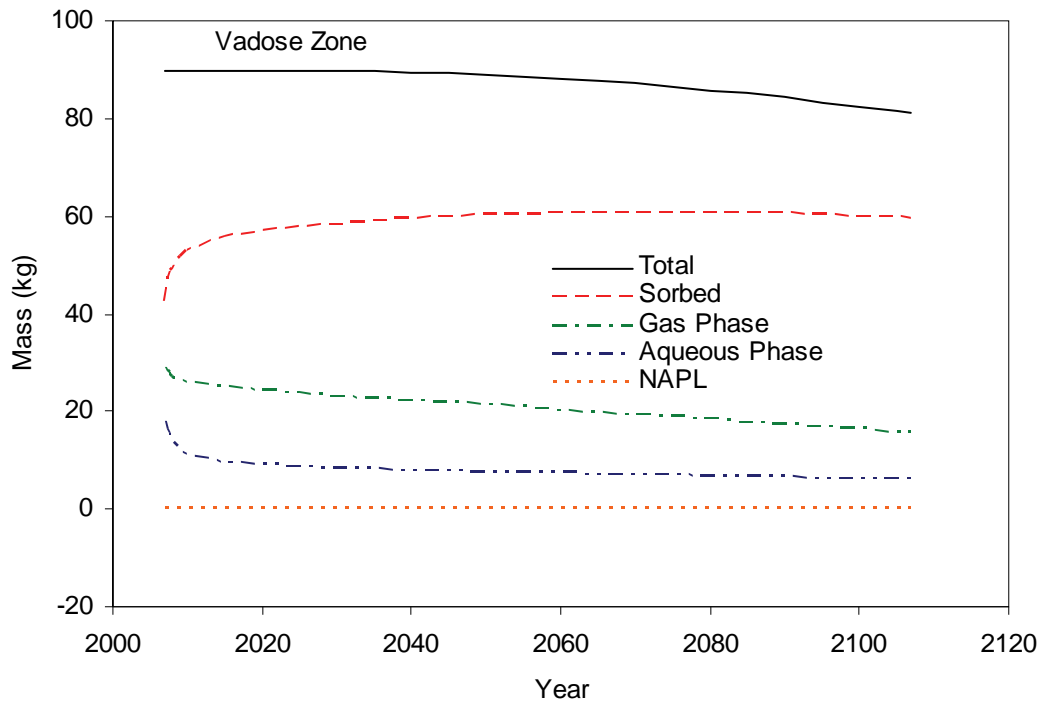
Figure 5.71. CT Mass Partitioning in the Vadose Zone for Imposed Case 2
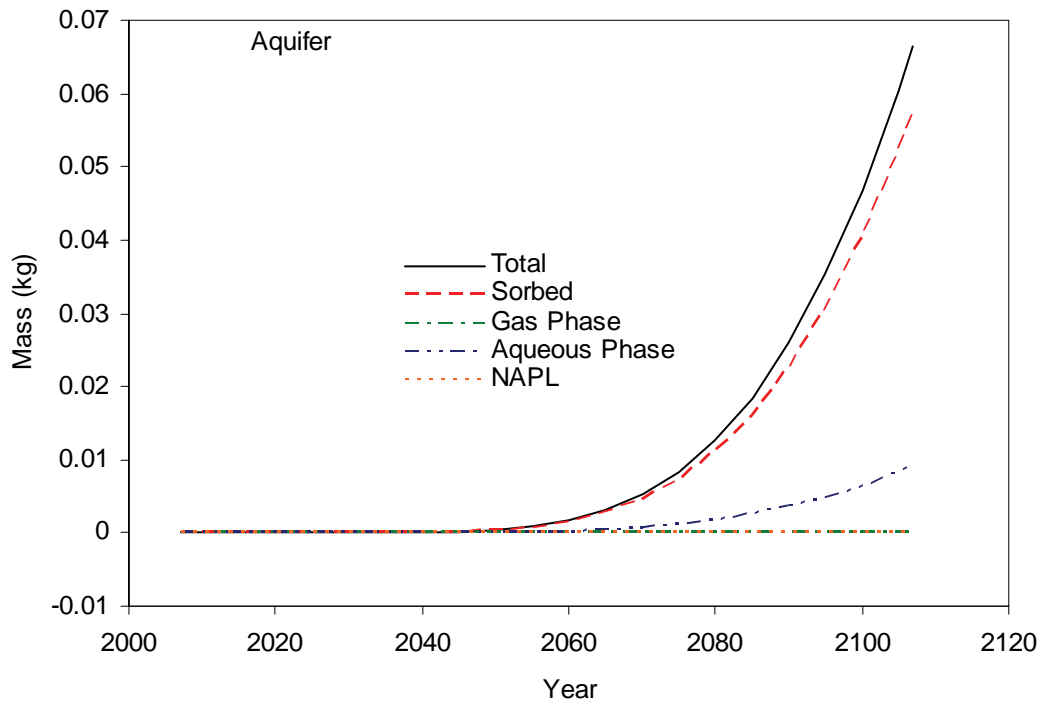
Figure 5.72. CT Mass Partitioning in the Aquifer for Imposed Case 2
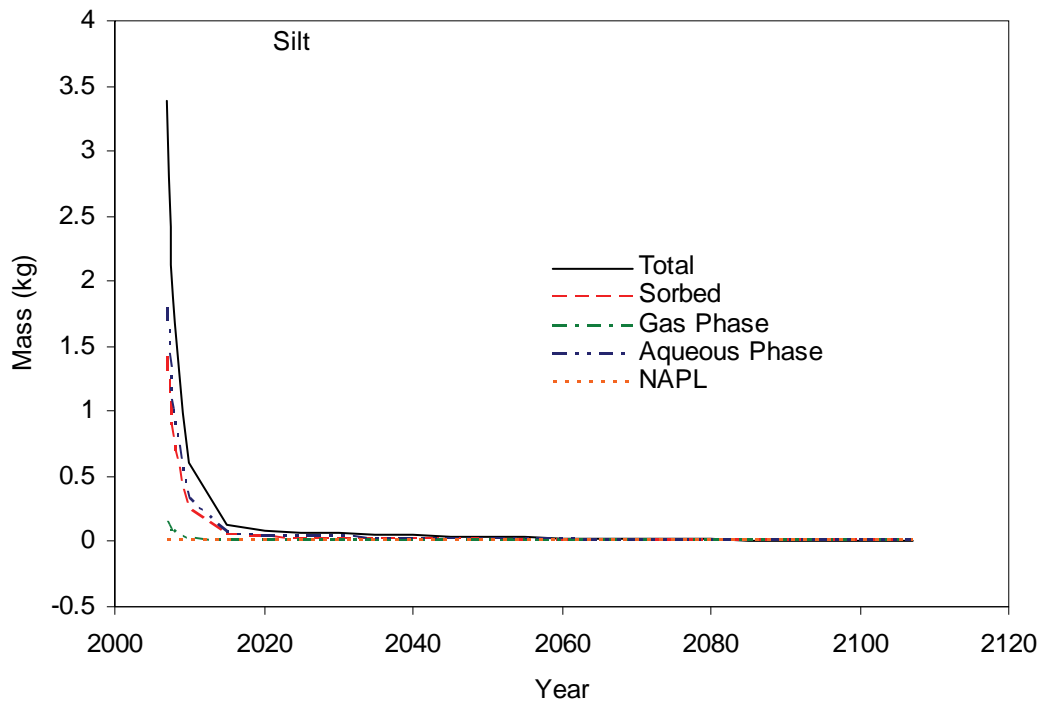
Figure 5.73. CT Mass Partitioning in the 65-ft Silt Lens for Imposed Case 2
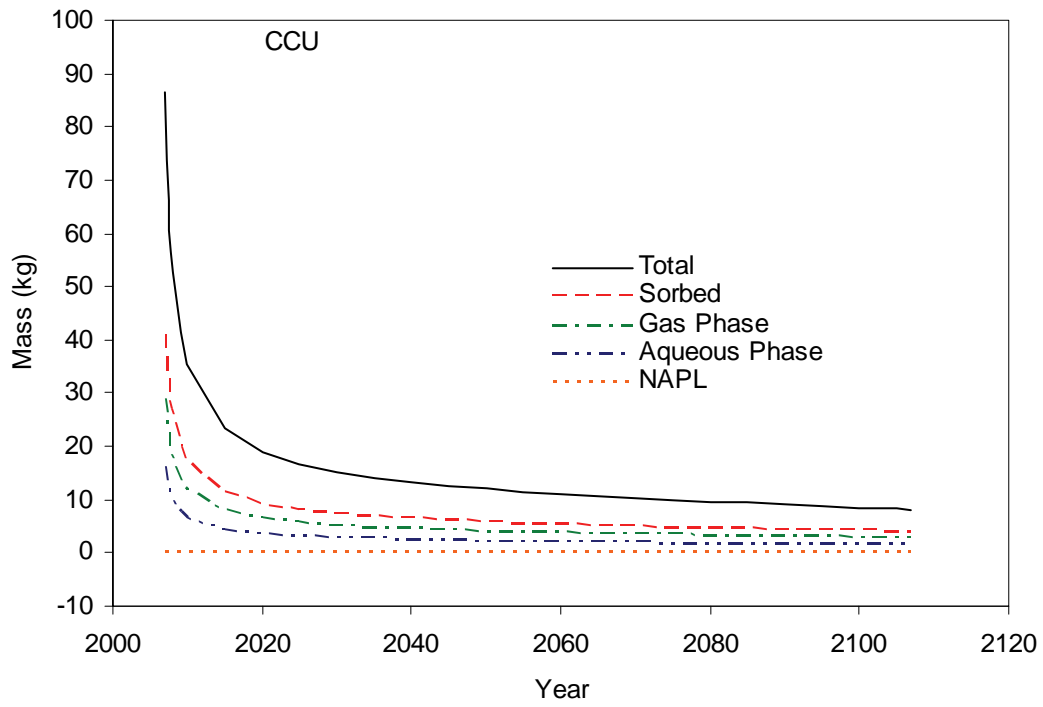
Figure 5.74. CT Mass Partitioning in the Cold Creek Unit for Imposed Case 2

5.3.3 Imposed Case 3
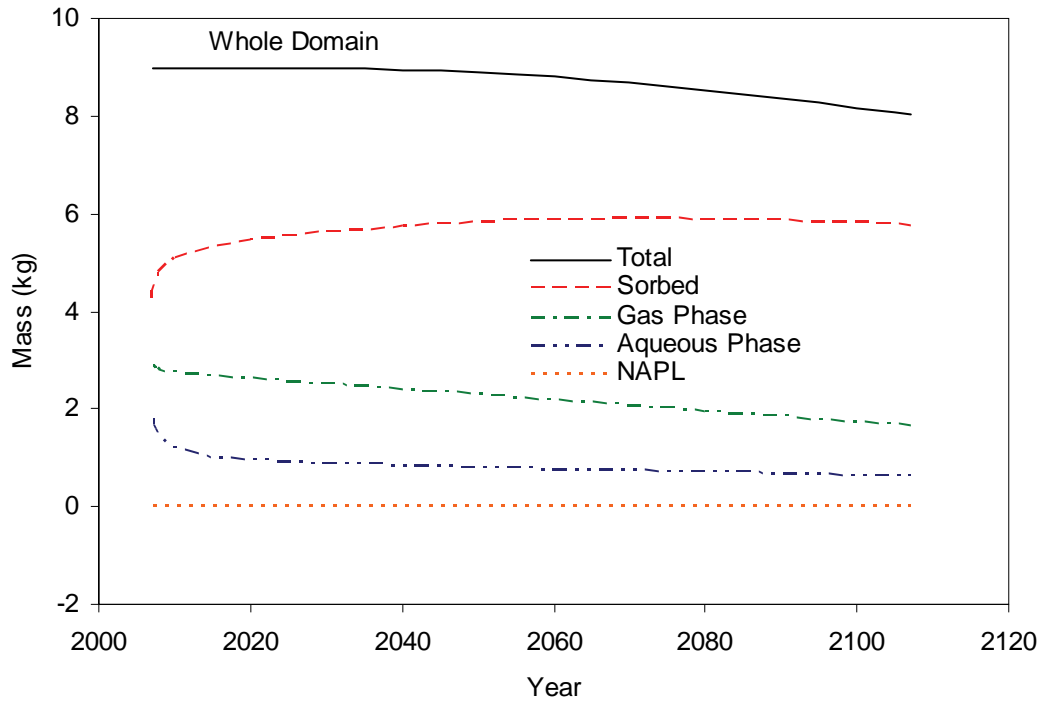
Figure 5.75. CT Mass Partitioning in the Whole Domain for Imposed Case
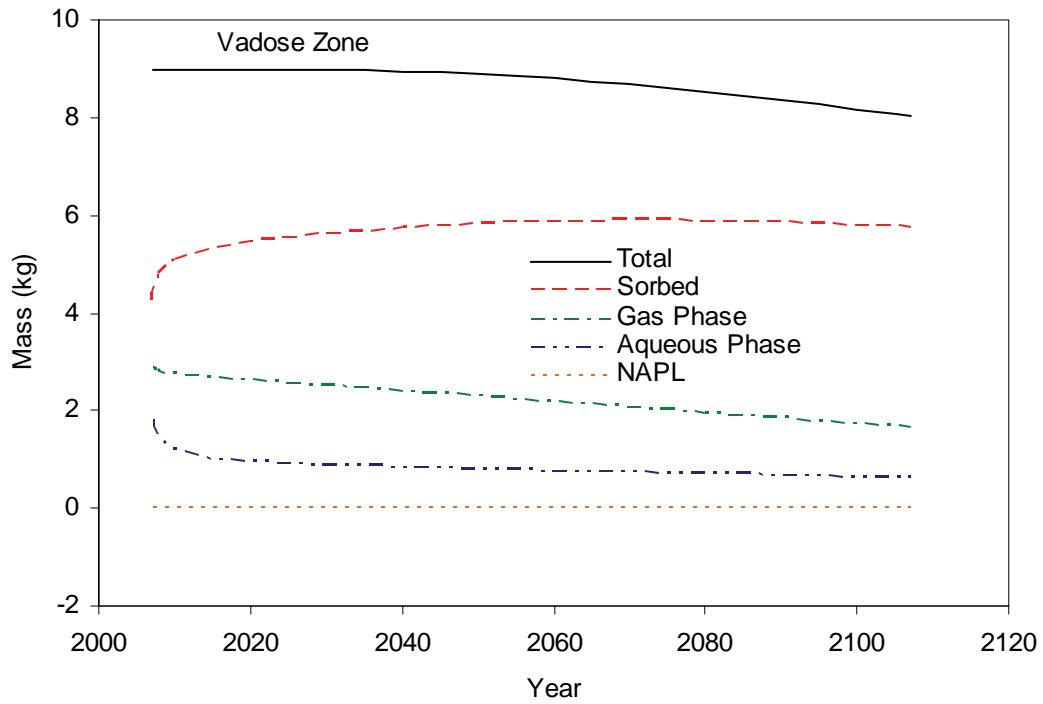
Figure 5.76. CT Mass Partitioning in the Vadose Zone for Imposed Case 3
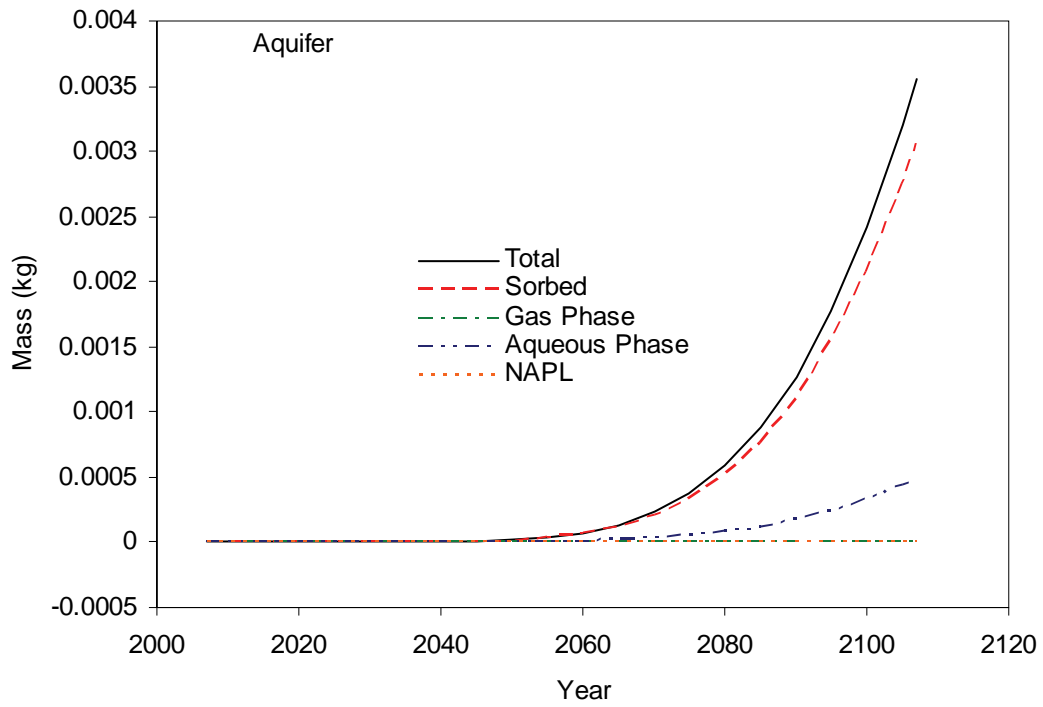
Figure 5.77. CT Mass Partitioning in the Aquifer for the Imposed Case 3
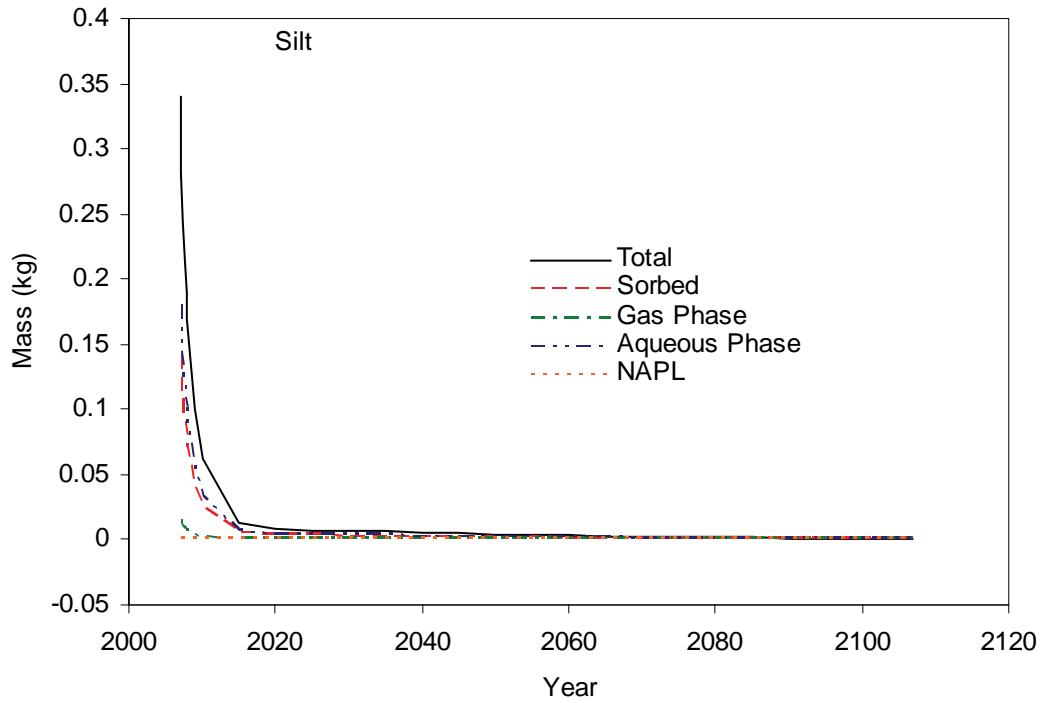
Figure 5.78. CT Mass Partitioning in the 65-ft Silt Lens for Imposed Case 3
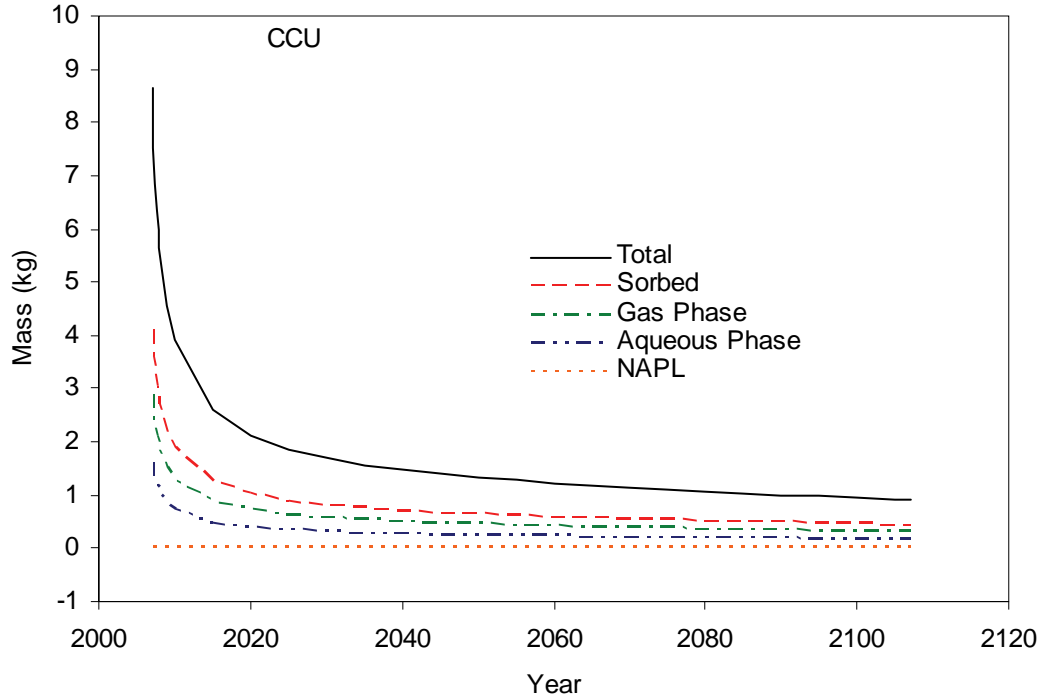
Figure 5.79. CT Mass Partitioning in the Cold Creek Unit for Imposed Case 3

5.3.4 Imposed Case 4
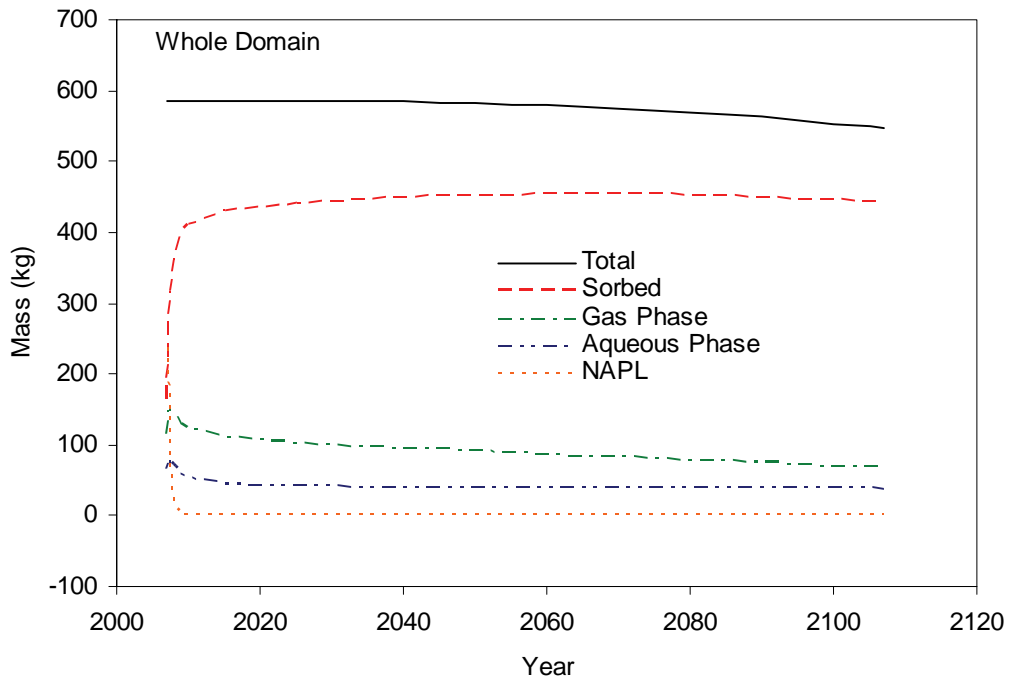
Figure 5.80. CT Mass Partitioning in the Whole Domain for Imposed Case 4
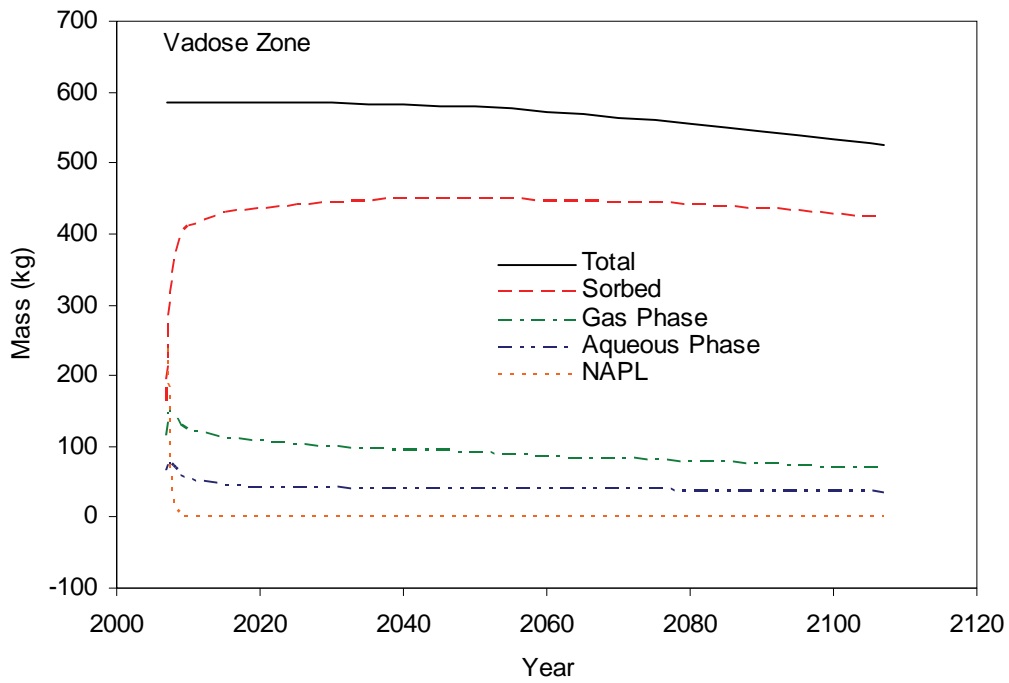
Figure 5.81. CT Mass Partitioning in the Vadose Zone for Imposed Case 4
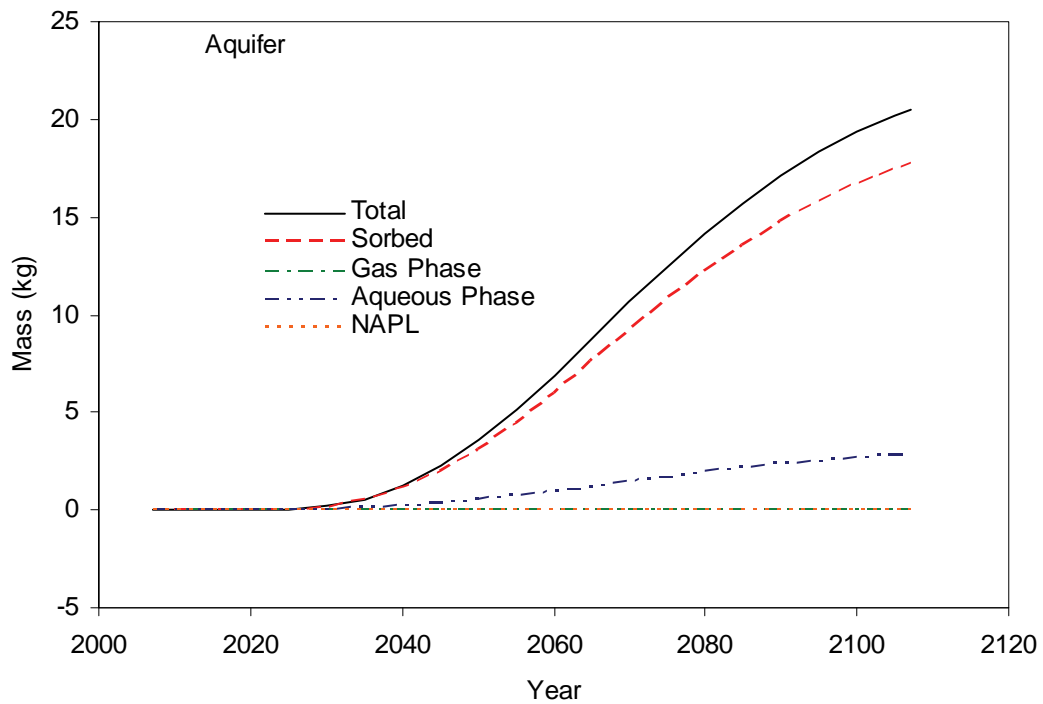
Figure 5.82. CT Mass Partitioning in the Aquifer for Imposed Case 4
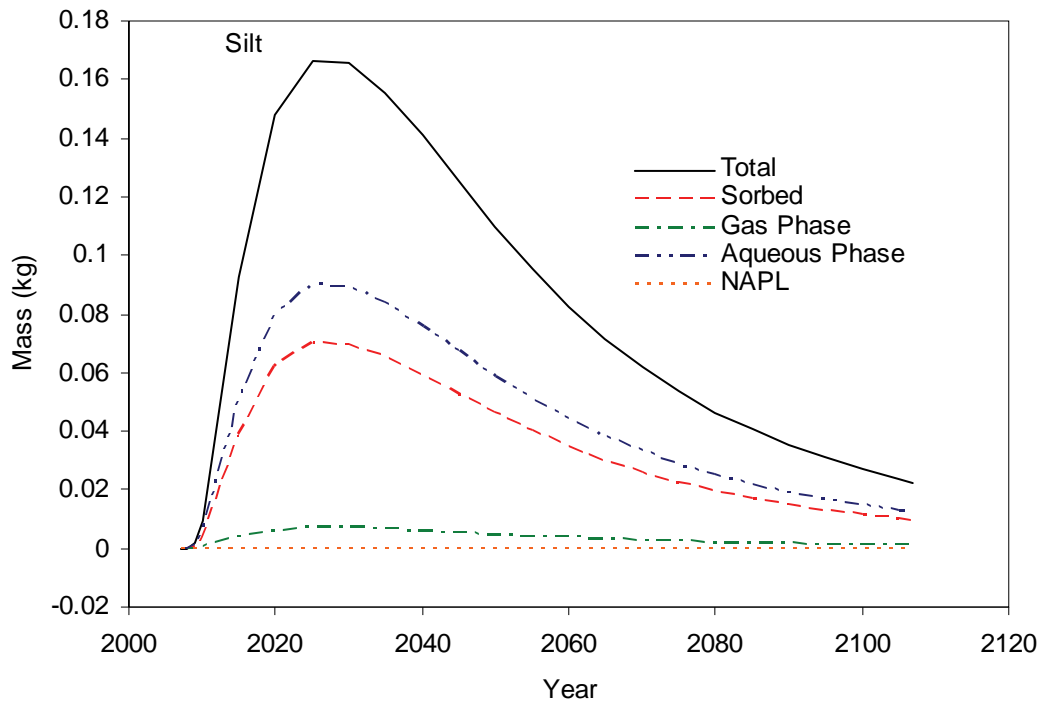
Figure 5.83. CT Mass Partitioning in the 65-ft Silt Lens for Imposed Case 4
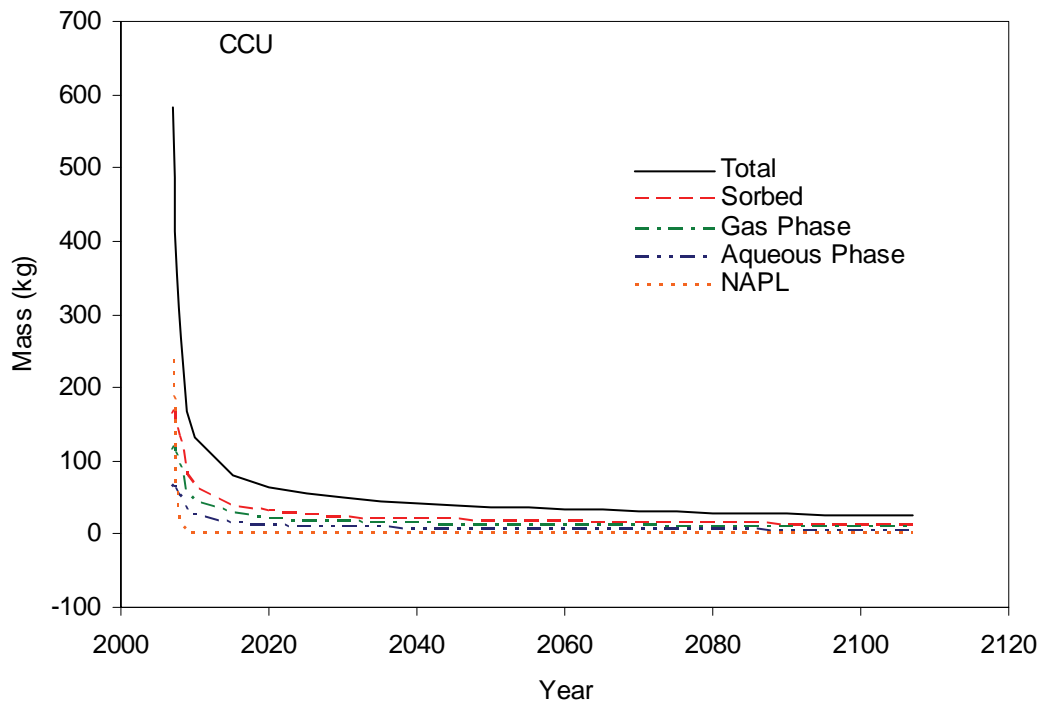
Figure 5.84. CT Mass Partitioning in the Cold Creek Unit for Imposed Case 4

5.3.5 Imposed Case 5
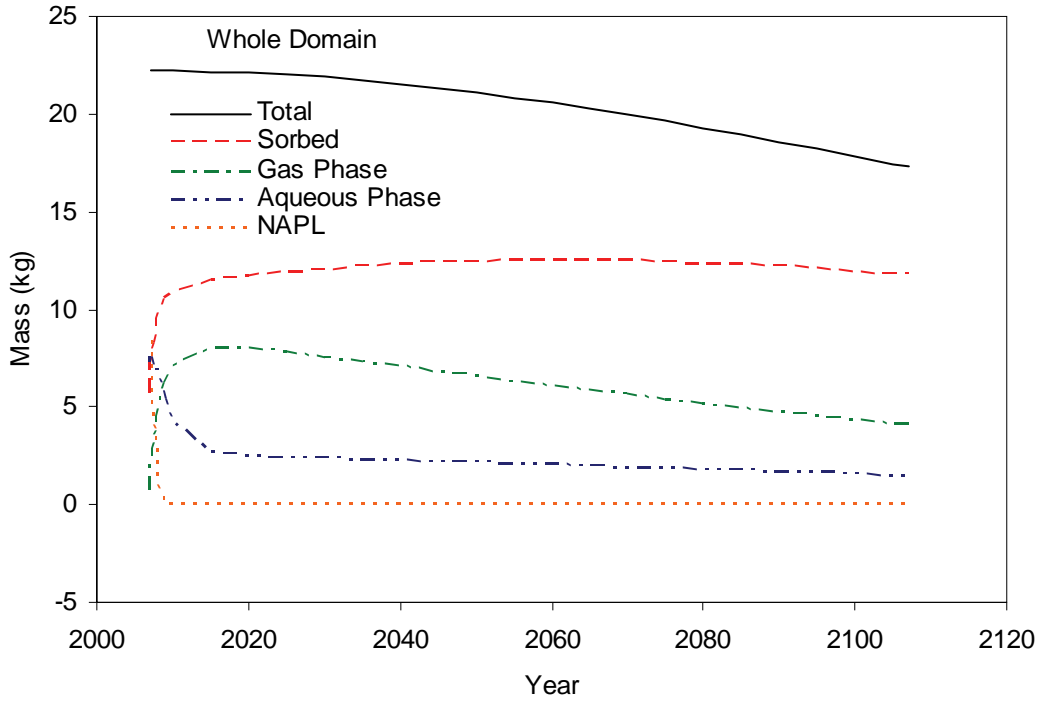
Figure 5.85. CT Mass Partitioning in the Whole Domain for Imposed Case 5
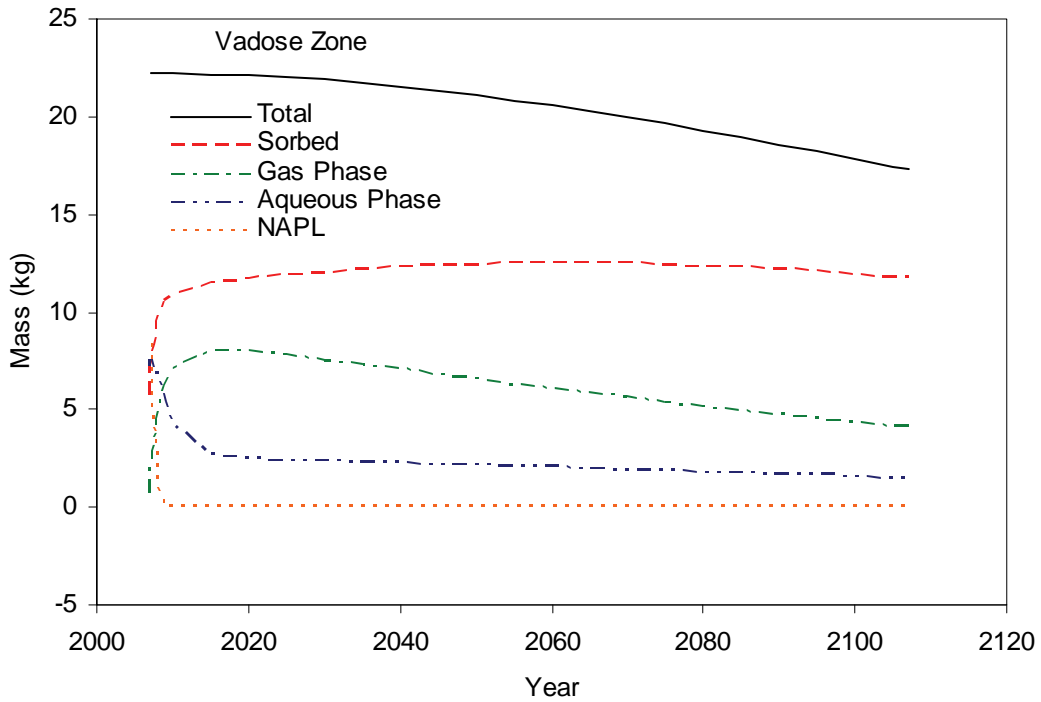
Figure 5.86. CT Mass Partitioning in the Vadose Zone for Imposed Case 5
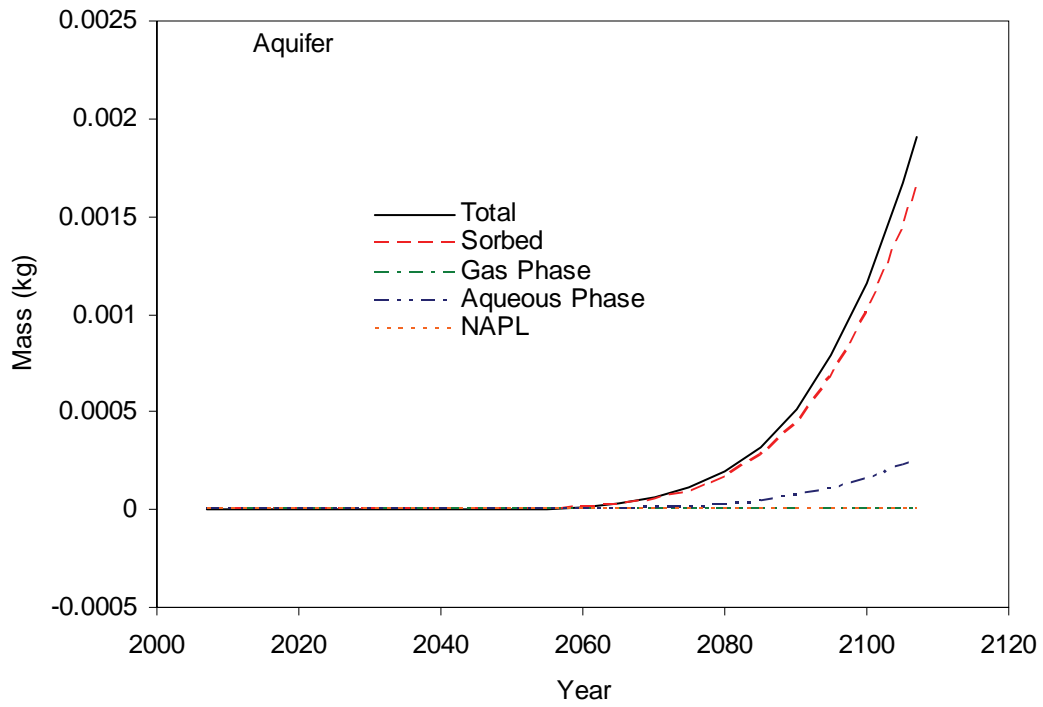
Figure 5.87. CT Mass Partitioning in the Aquifer for Imposed Case 5
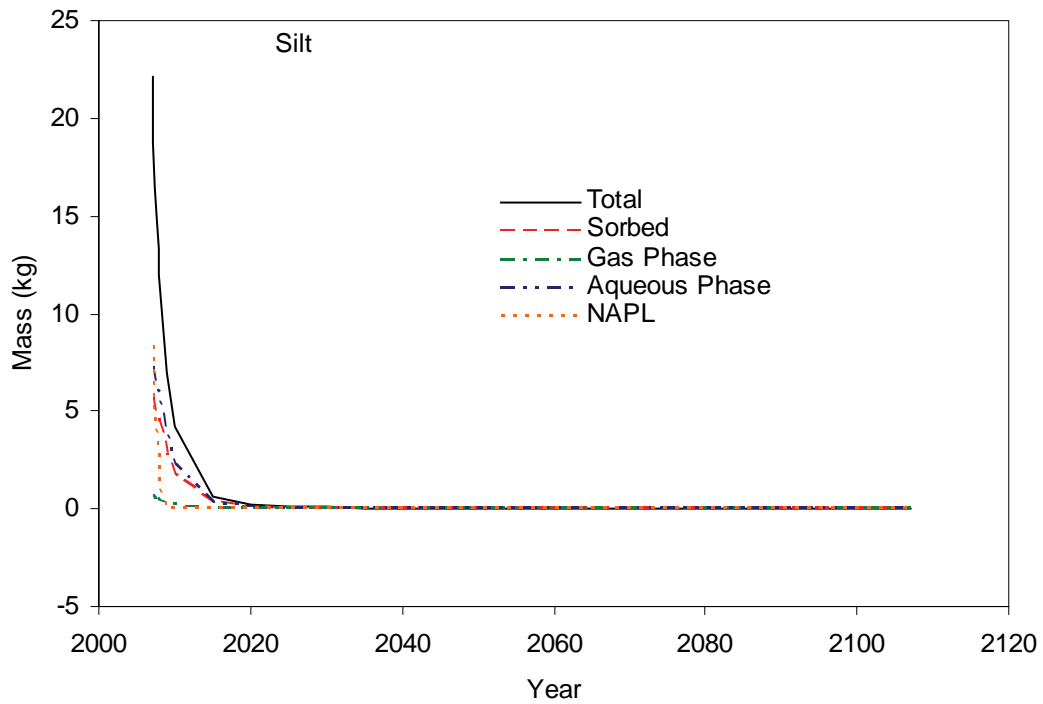
Figure 5.88. CT Mass Partitioning in the 65-ft Silt Lens for Imposed Case 5
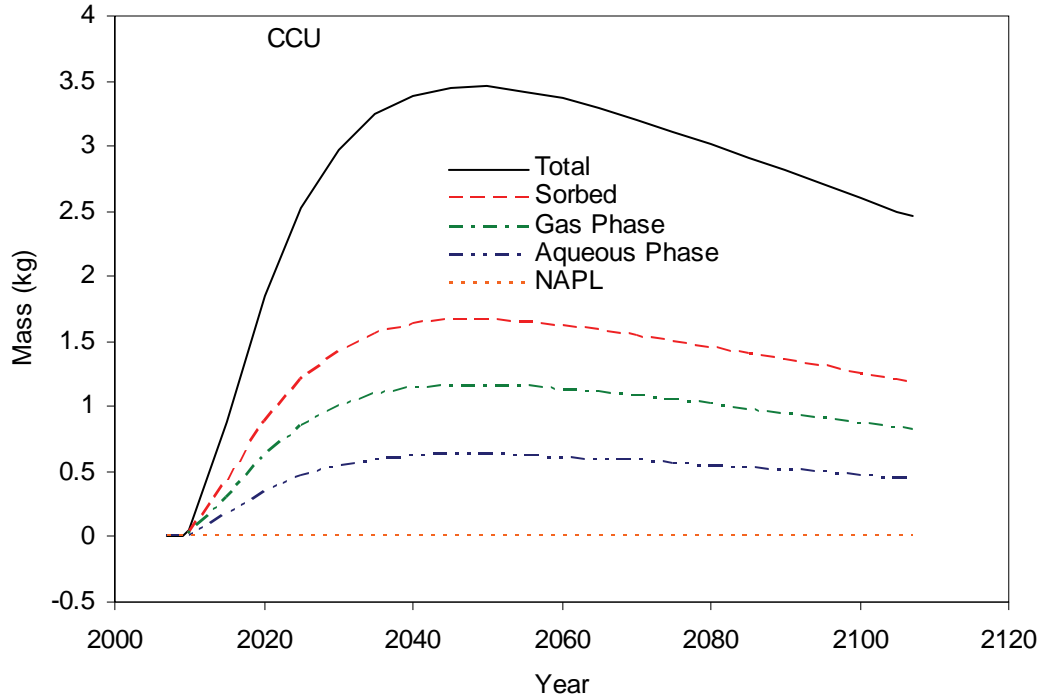
Figure 5.89. CT Mass Partitioning in the Cold Creek Unit for Imposed Case 5

5.3.6 Imposed Case 6
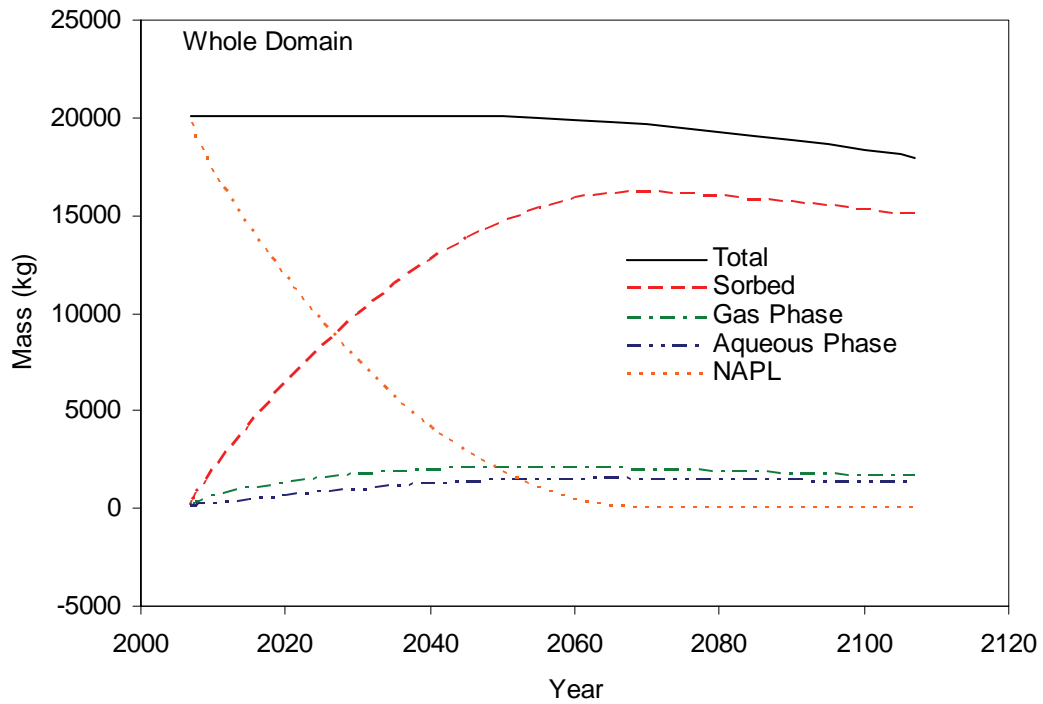
Figure 5.90. CT Mass Partitioning in the Whole Domain for Imposed Case 6
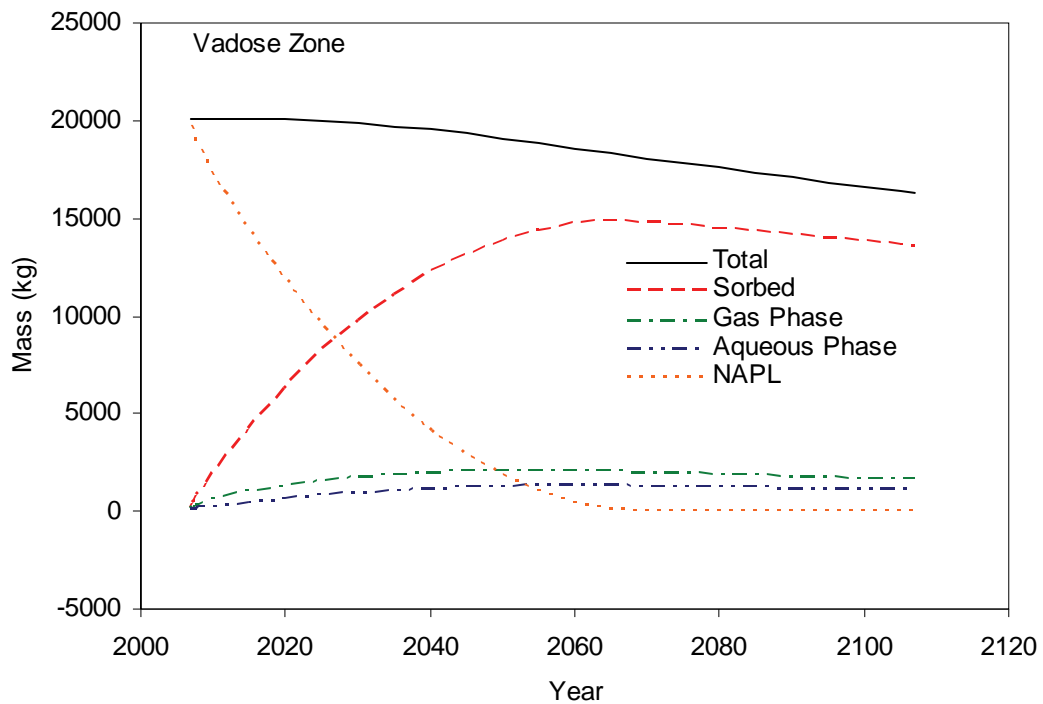
Figure 5.91. CT Mass Partitioning in the Vadose Zone for Imposed Case 6
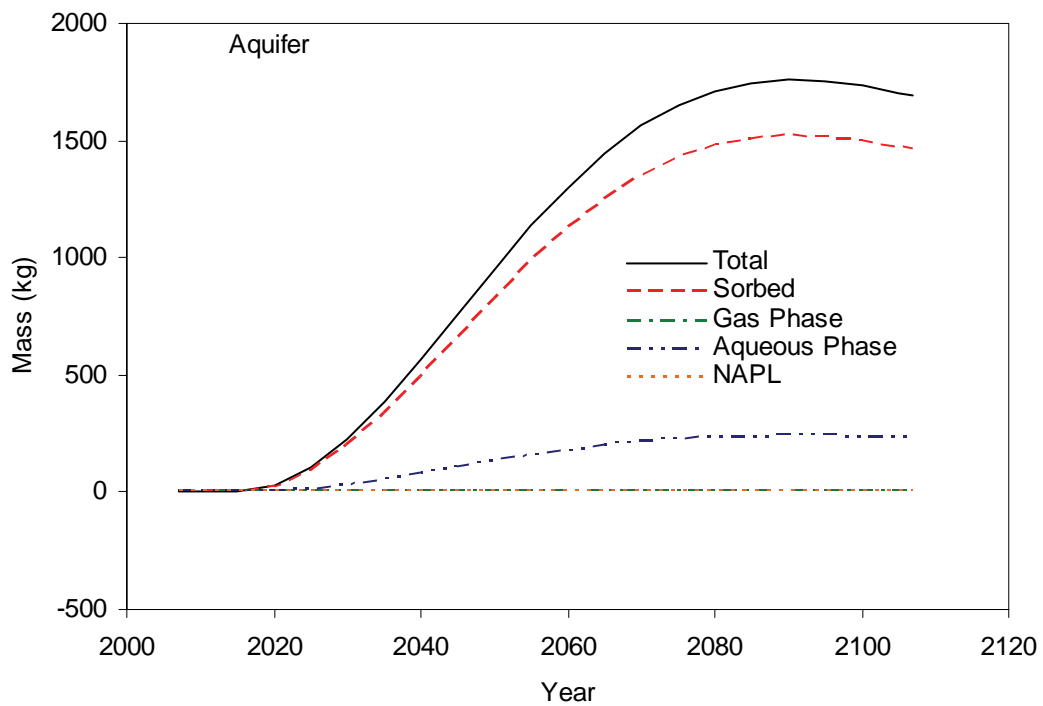
Figure 5.92. CT Mass Partitioning in the Aquifer for Imposed Case 6
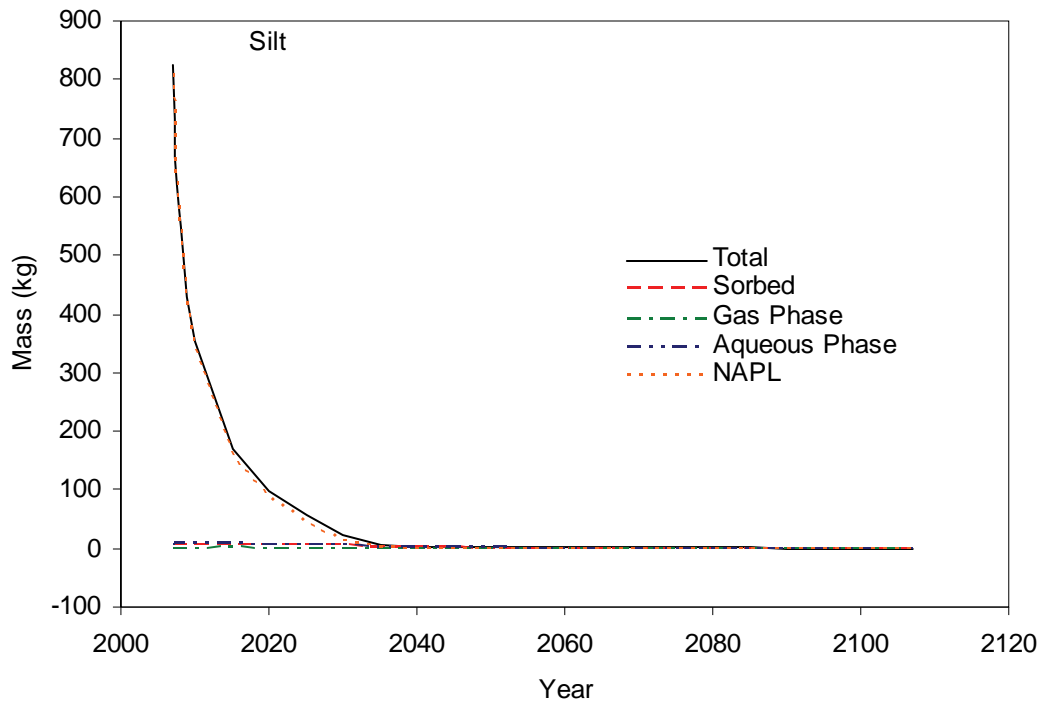
Figure 5.93. CT Mass Partitioning in the 65-ft Silt Lens for Imposed Case 6
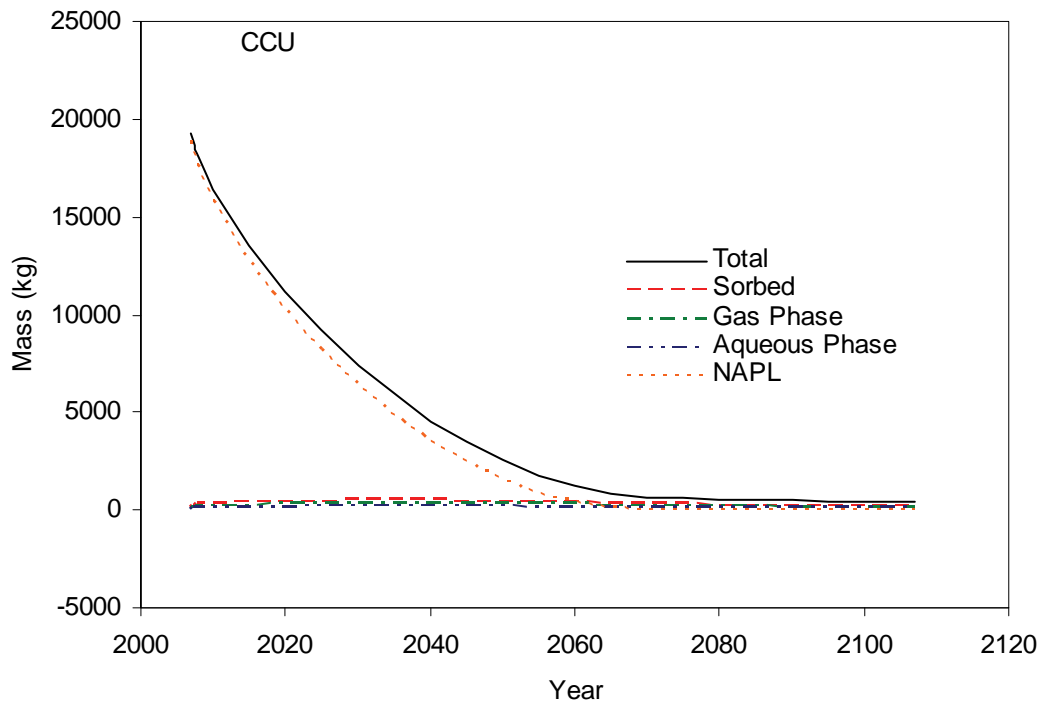
Figure 5.94. CT Mass Partitioning in the Cold Creek Unit for Imposed Case 6

5.3.7   Modeled Case
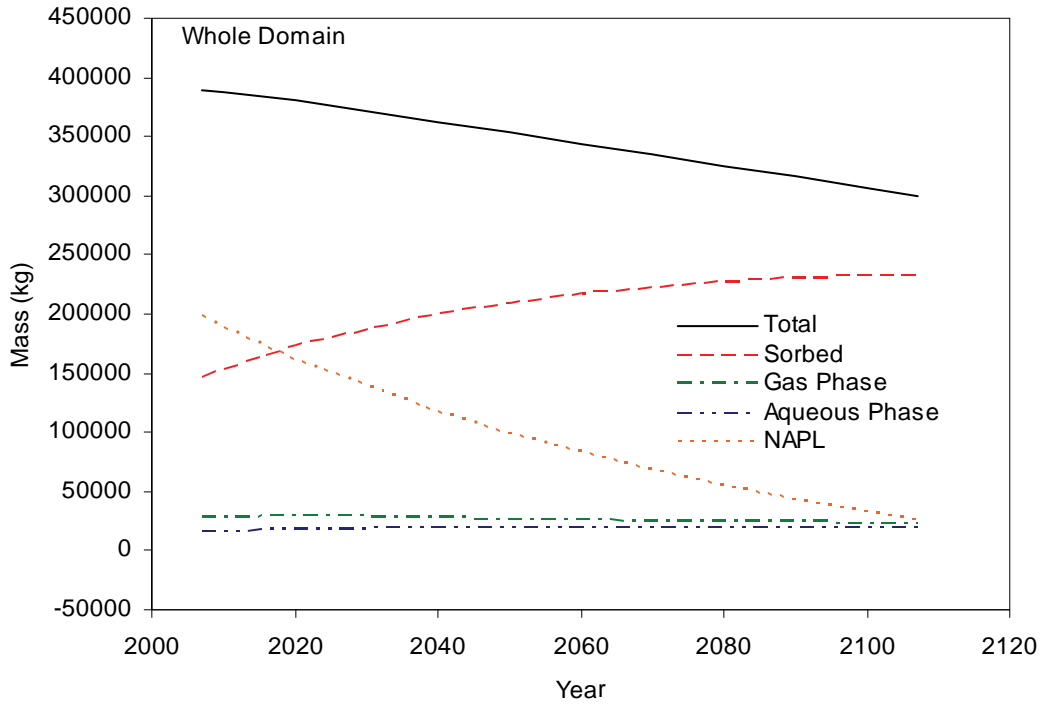
Figure 5.95. CT Mass Partitioning in the Whole Domain for the Modeled Case
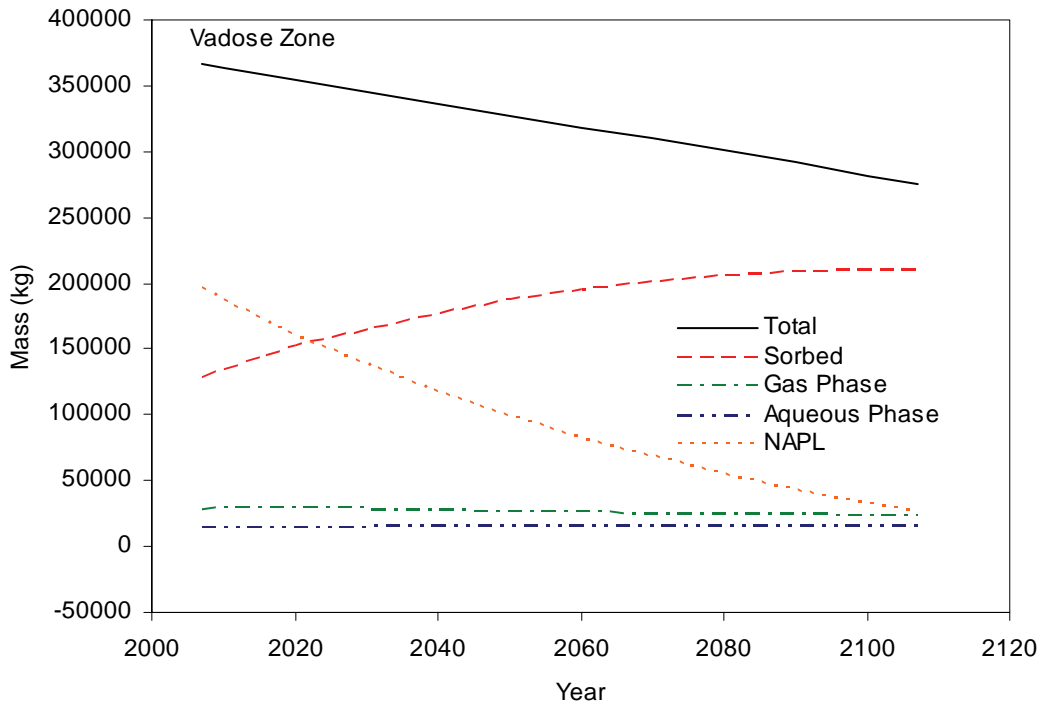
Figure 5.96. CT Mass Partitioning in the Vadose Zone for the Modeled Case
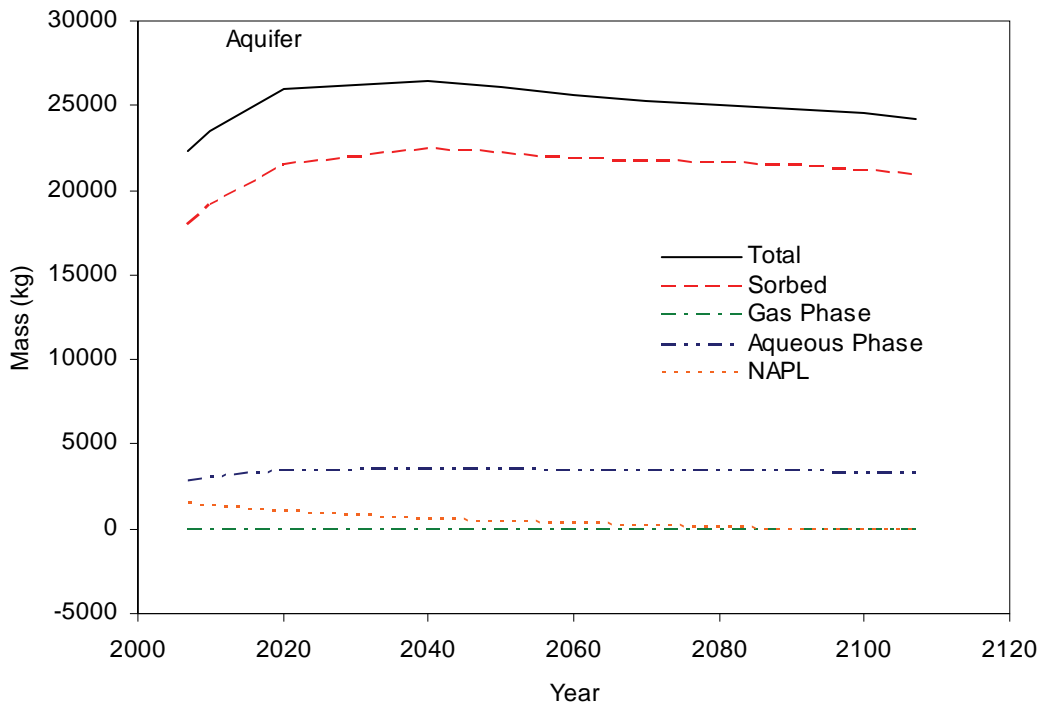
Figure 5.97. CT Mass Partitioning in the Aquifer for the Modeled Case
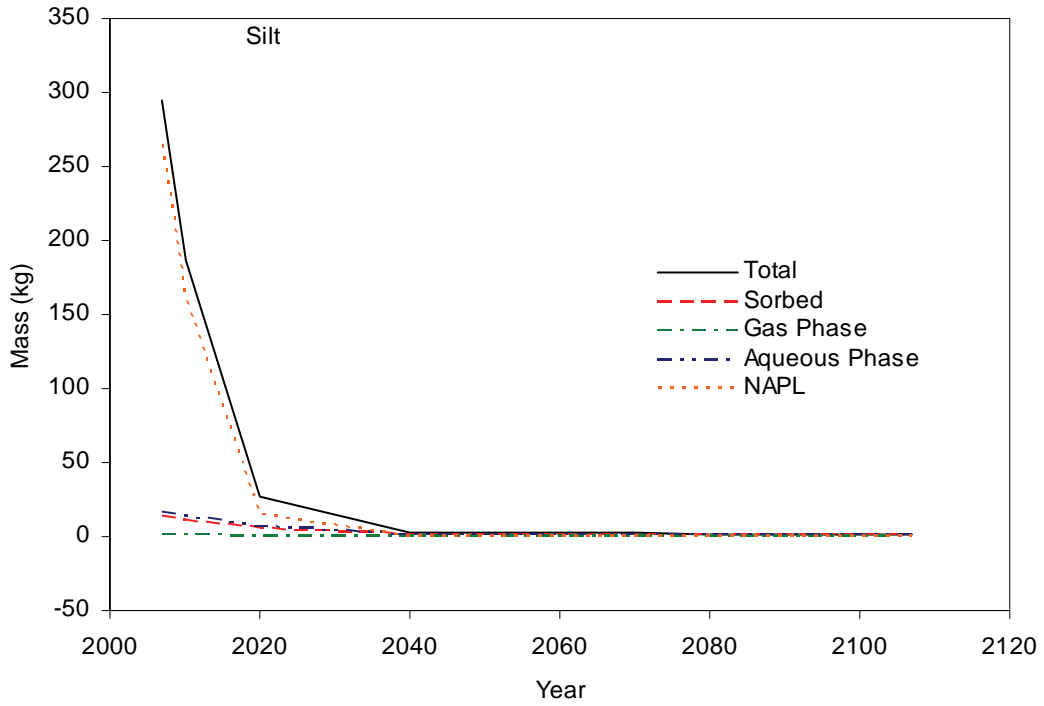
Figure 5.98. CT Mass Partitioning in the 65-ft Silt Lens for the Modeled Case
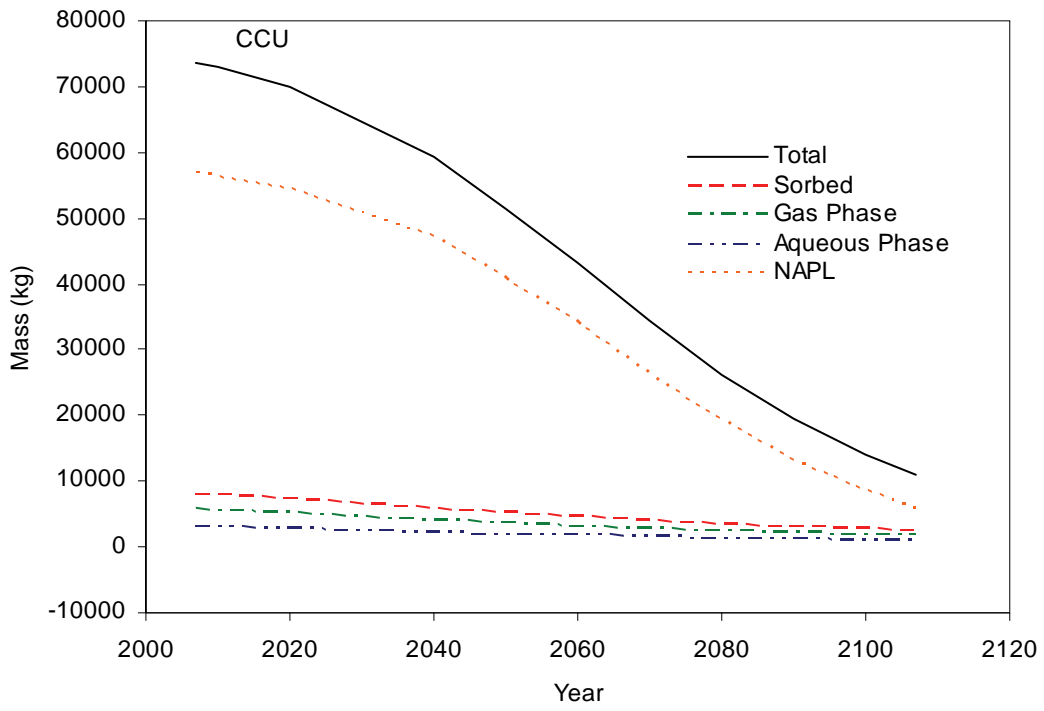
Figure 5.99. CT Mass Partitioning in the Cold Creek Unit for the Modeled Case

6.0   Summary and Conclusions

CT was discharged to waste sites that are included in the 200-PW-1 Operable Unit in the Hanford 200 West Area. Fluor Hanford, Inc. is conducting a CERCLA RI/FS for the 200-PW-1 Operable Unit. As part of this overall effort, PNNL was contracted to develop a large-scale flow and transport model configuration integrating the CT and aqueous phase waste sites and to conduct local-scale modeling below the 216-Z-9 site to predict future CT behavior, through use of numerical flow and transport modeling. This work supports the U.S. DOE's efforts to characterize the nature and distribution of CT in the 200 West Area and subsequently select an appropriate final remedy.

Large-Scale Model Configuration

A large-scale model was configured for a domain size of 1,429 m (west-east) by 1,711 m (south-north). The model considered CT and wastewater discharge from the 216-Z-9, 216-Z-1A, and 216-Z-18 sites, as well as wastewater disposal from the 216-U-10, 216-U-14, 216-Z-1:2, 216-Z-3, 216-Z-7, 216-Z-12, 216-Z-17, 216-Z-18, 216-Z-20, 216-Z-1A, 216-T-19, 2607-WA, 2607-WB, 2607-Z, and 284-WB sites. Simulations were conducted with and without soil vapor extraction from the well system in the vicinity of the three CT disposal sites. A base-case simulation was conducted using hydraulic property values reported in Oostrom et al. (2004; 2006a; 2006b) for local-scale simulations of the individual CT waste sites. Two sensitivity simulations were also performed using reduced permeability values and increased nonwetting-fluid entry pressure values for the Cold Creek Unit. Waste water disposal resulted in increased water saturations in the Cold Creek Unit and a water table increase throughout the computational domain. The increased water saturations in the Cold Creek Unit reduced the downward movement of DNAPL CT and gaseous CT. Compared to the base-case simulation, the simulations conducted with smaller Cold Creek Unit permeability values resulted in reduced DNAPL CT movement across the water table. Compared to previous modeling exercises (Oostrom et al. 2004; 2006a; 2006b), for all three cases SVE (with the assumption of equilibrium volatilization) was very effective despite the larger overall water saturations.

Predicted Future CT Distribution Beneath the 216-Z-9 Site Using Local-Scale Simulations

CT Mass Flow Rates and Cumulative Transport Across the Water Table and Domain Boundaries

The computed aqueous CT mass flow rates across the water table for imposed case 6 and the modeled case, with relatively large DNAPL CT amounts in 2007, are considerably larger than for imposed cases 1 – 5. The maximum CT mass flow rate for imposed case 6 is 45 kg/yr and for the modeled case 469 kg/yr, while the maximum rate for the other five cases is 0.56 kg/yr (imposed case 1). The maximum rates for the imposed cases 2, 3, and 5, are several orders of magnitude smaller than the value for imposed case 1. The reason imposed cases 2 and 3 report smaller mass flow rates is directly related to the smaller imposed total mass compared to imposed case 1. The results for imposed case 4 are similar than from imposed case 1, indicating the limited effect of the emplaced CT in the 65-ft silt lens. The only simulation with DNAPL CT transport across the water table was the modeled case, at a maximum rate of 450 kg/yr (at 2007).

For all the simulations most of the CT mass initially present at 2007 remained in the system through 2107. Fractions, ranging from 10 to approximately 25% of the original mass, in place were transported

out of the domain across the model boundaries through the gas and aqueous phases. Gas CT disappeared mainly through the top and south boundaries. Dissolved aqueous phase CT moved out of the system via groundwater movement through the east boundary. The results for imposed case 4 were again similar to the results of imposed case 1. Aqueous and gas phase CT movement across the domain boundaries were orders of magnitude smaller for imposed cases 2, 3, and 5 than for cases 1 and 4. Mass flow rates and cumulative masses for imposed case 6 are approximately one order of magnitude larger than for imposed case 1. The cumulative transported masses for the modeled case are, in turn, considerably larger than for imposed case 6. Most of the removed mass in the modeled case was transported out of the domain via groundwater movement. The large difference between the two cases is related to the fact that for the modeled case, DNAPL CT penetrated the water table and dissolved over time. For imposed case 6, no DNAPL CT was transported across the water table.

Aqueous Phase CT Fluxes Across the Water Table

Computed aqueous phase mass fluxes across the water demonstrate that for imposed cases 1 through 5, the maximum flux is approximately directly below the disposal site. This result is expected since the imposed CT was in those parts of the 65-ft silt lens and the Cold Creek Unit that are located directly underneath the 216-Z-9 site. The CT mass fluxes for imposed cases 1 and 4, with 350,000 µg/kg CT emplaced in the Cold Creek Unit, are considerably larger than for imposed cases 2, 3, and 5. Although the fluxes for these three cases are smaller, they continue to increase over the duration of the simulation. For imposed cases 1 and 4, the maximum mass fluxes are obtained between 2050 and 2070. For imposed case 6, the computed fluxes are approximately one order of magnitude larger than for imposed cases 1 and 4, with concentration peaks around 2030. The modeled case shows CT mass fluxes with values close to what was observed for imposed case 6. The main differences between the modeled case and imposed case 6 are that the CT mass fluxes are maintained over a much larger area and that the flux values are almost constant between 2030 and 2107.

CT Phase Partitioning

The simulations show that the total CT mass present in the computational domain for each simulation only decreased gradually over time. The vast majority of the CT mass that was originally present in the domain at 2007 is predicted to be still present in the domain by 2107. Most of the CT mass eventually becomes sorbed to the porous media. This result is directly related to the imposed K_d factor of 0.2 mL/g.

Only the modeled case is predicted to have DNAPL CT present at 2107. The total CT mass in the 65-ft silt lens and the Cold Creek Unit decreases rapidly in imposed cases 1 – 5, while for imposed case 6 and the modeled case these zones hold on to the CT mass longer. For the modeled case, DNAPL CT remained in the Cold Creek Unit throughout 2107, while DNAPL CT is predicted to be present through 2060 for imposed case 6.

Recommendations for Future Research and Simulations

The large-scale model can be considered as a base tool for subsequent numerical investigations, such as sensitivity analyses, and remediation simulations. The model configuration also allows for detailed smaller-scale flow and transport modeling in the subsurface of disposal sites of special interest, such as the 216-Z1A, 216-Z-9 and 216-18 sites.

An important next modeling step is to reconcile the current large-scale numerical model needs with the detailed conceptual model described in DOE-RL (2006a). Model boundary and initial conditions, as well as the geological model, need to be update with the findings in this report. The main boundary conditions for consideration are disposal volume, rate, and area, and the extent of DNAPL surface volatilization. Incorporating the state-of-knowledge conceptual model described in DOE-RL (2006a) in the current model may help to improve the simulated CT distributions and SVE extraction results.

The large-scale model predicts extraction of more CT by SVE than has been observed in the field. There are several possible reasons for the discrepancy between observed and simulated results, including uncertainties in flow rates, fluid-media properties, and disposal history (e.g., volumes, rates, and timing). The differences also result from the current model configuration based on equilibrium phase partitioning, meaning simulations do not account for any rate-limited (kinetic) interfacial mass transfer effects. Another reason why modeled SVE removal rates are larger than the observed rates is the assumption that the DNAPL composition remains unaltered over time. In reality, during SVE, CT is removed from the DNAPL, lowering its molar fraction and vapor pressure. The reduced vapor pressure, in turn, leads to decreasing vapor concentration and removal rates. A multicomponent version of the simulator, allowing for kinetic volatilization, is likely needed to improve simulation of SVE.

The local-scale modeling results clearly show the dominance of sorbed CT partitioning. The considerable sorption is directly related to the assumption of a constant K_d of 0.2 mL/g, which was imposed on all porous media. Additional simulations with different K_d values and values that are porous media and moisture-content dependent are needed to obtain a better understanding of the role of sorption for CT transport.

7.0 References

Anderson JD. 1976. *Input and Decayed Values of Radioactive Liquid Wastes Discharged to the Ground in the 200 Areas Through 1975*. ARH-CD-745, Atlantic Richfield Hanford Company Report, Richland, Washington.

Brooks RH and AT Corey. 1964. "Hydraulic Properties of Porous Media." *Hydrology Paper 3*, Civil Engineering Department, Colorado State University, Fort Collins, Colorado.

Burdine NT. 1953. "Relative Permeability Calculations from Pore-Size Distribution Data." *Petr. Trans., Am. Inst. Mining Metall. Eng*. 198:71-77.

Comprehensive Environmental Response, Compensation, and Liability Act. 1980. Public Law 96-510, as amended, 94 Stat. 2767, 42 USC 9601 et seq.

DOE-RL. 2002. *Standardized Stratigraphic Nomenclature for Post-Ringold Formation Sediments Within the Central Pasco Basin*. DOE/RL-2002-39, U.S. Department of Energy, Richland Operations Office, Richland, Washington.

DOE-RL. 2004. *Plutonium/Organic-Rich Process Condensate/Process Waste Group Operable Unit RI/FS Work Plan, Includes: 200-PW-1, 200-PW-3, and 200-PW-6 Operable Units*. DOE/RL-2001-01, Rev. 0 (Reissue), U.S. Department of Energy, Richland Operations Office, Richland, Washington.

DOE-RL. 2006a. *Remedial Investigation Report for the Plutonium/Organic-Rich Process Condensate/Process Waste Group Operable Unit: Includes the 200-PW-1, 200-PW-3, and 200-PW-6 Operable Units*. DOE/RL-2006-51, Draft A, U.S. Department of Energy, Richland Operations Office, Richland, Washington.

DOE-RL. 2006b. *Remedial Investigation Report for the 200-ZP-1 Groundwater Operable Unit*. DOE/RL-2006-24, Rev. 0, U.S. Department of Energy, Richland Operations Office, Richland, Washington.

FHI. 2006. *Performance Evaluation Report for Soil Vapor Extraction Operations at the 200-PW-1 Carbon Tetrachloride Site, Fiscal Year 2005*. WMP-30426, Rev. 0., Fluor Hanford, Inc., Richland, Washington.

Hartman MJ, LF Morasch, and WD Webber. 2006. *Hanford Site Groundwater Monitoring for Fiscal Year 2005*. PNNL-15670, Pacific Northwest National Laboratory, Richland, Washington.

Hofstee C, RC Walker, and JH Dane. 1998. "Infiltration and Redistribution of Perchloroethylene in Partially Saturated, Stratified Porous Media." *J. Contam. Hydrol.* 34:293-313.

Hoitink DJ, KW Burk, JV Ramsdell, Jr., and WJ Shaw. 2005. *Hanford Site Climatological Summary 2004 with Historical Data.* PNNL-15160, Pacific Northwest National Laboratory, Richland, Washington.

Khaleel R and EJ Freeman. 1995. *Variability and Scaling of Hydraulic Properties for 200 Area Soils, Hanford Site*. WHC-EP-0883, Westinghouse Hanford Company, Richland, Washington.

Khaleel R, TE Jones, AJ Knepp, FM Mann, DA Myers, PM Rogers, RJ Serne, and MI Wood. 2001. *Modeling Data Package for S-SX Field Investigation Report (FIR)*. RPP-6296, Rev. 0, CH2MHILL Hanford Group, Inc., Richland, Washington.

Klinkenberg LJ. 1941. "The Permeability of Porous Media to Liquids and Gases." *Drilling and Production Practice*, 200-213, American Petroleum Institute, New York.

Lenhard RJ. 1994. "Scaling Fluid Content-Pressure Relations of Different Fluid Systems in Porous Media." In *Proc. 14th Annual American Geophysical Union Hydrology Days*, HJ Morel-Seytoux (ed.), Hydrology Days Publ., Atherton, California.

Lenhard RJ, M Oostrom, and JH Dane. 2004. "A Constitutive Model for Air-NAPL-Water Flow in the Vadose Zone Accounting for Immobile Non-Occluded (Residual) NAPL in Strongly Water-Wet Porous Media." *J. of Contaminant Hydrology* 73:283-304.

Lenhard RJ, JC Parker, and S Mishra. 1989. "On the Correspondence Between Brooks-Corey and van Genuchten Models." *J. of Irrigation and Drainage Engineering* 115:744-751.

Leverett MC. 1941. "Capillary Behavior in Porous Solids." *Trans. Soc. Pet. Eng. AIME* 142:152-169.

Miller EE and RD Miller. 1956. "Physical Theory for Capillary Flow Phenomena." *J. Appl. Phys.* 27:324-332.

Mualem Y. 1976. "A New Model for Predicting the Hydraulic Conductivity of Unsaturated Porous Media." *Water Resour. Res*. 12:513-522.

Murray CJ, Y Chien, and MJ Truex. 2006. *Geostatistical Analysis of the Inventory of Carbon Tetrachloride in the Unconfined Aquifer in the 200 West Area of the Hanford Site*. Letter Report from C Murray, Y. Chien, Pacific Northwest National Laboratory, to Fluor Hanford, Inc., Richland, Washington.

Oostrom M and RJ Lenhard. 1998. "Comparison of Relative Permeability-Saturation-Pressure Parametric Models for Infiltration and Redistribution of a Light Nonaqueous Phase Liquid in Sandy Porous Media." *Adv. in Water Resour*. 21:145-157.

Oostrom M and RJ Lenhard. 2003. "Carbon Tetrachloride Flow Behavior in Unsaturated Hanford Caliche Material: An Investigation of Residual NAPL." *Vadose Zone J*. 2:25-33.

Oostrom M, C Hofstee, and JH Dane. 1997. "Light Nonaqueous-Phase Liquid Movement in a Variably Saturated Sand." *Soil Science Society of America J*. 61:1547-1554.

Oostrom M, C Hofstee, RC Walker, and JH Dane. 1999. "Movement and Remediation of Trichloro-ethylene in a Saturated, Heterogeneous Porous Medium. 1. Spill Behavior and Initial Dissolution." *J. of Contaminant Hydrol*. 37:159-178.

Oostrom M, C Hofstee, RJ Lenhard, and TW Wietsma. 2003. "Flow Behavior and Residual Saturation Formation of Injected Carbon Tetrachloride in Unsaturated Heterogeneous Porous Media." *J. of Contaminant Hydrology*. 64:93-112.

Oostrom, M, ML Rockhold, PD Thorne, GV Last, and MJ Truex. 2004. *Three-Dimensional Modeling of DNAPL in the Subsurface of the 216-Z-9 Trench and the Hanford Site*. PNNL-14895, Pacific Northwest National Laboratory, Richland, Washington.

Oostrom, M, ML Rockhold, PD Thorne, GV Last, and MJ Truex. 2006a. *Carbon Tetrachloride Flow and Mass Flow Rate in the Subsurface of the 216-Z-9 Trench at the Hanford Site: Heterogeneous Model Development and Soil Vapor Extraction Modeling*. PNNL-15914, Pacific Northwest National Laboratory, Richland, Washington.

Oostrom, M, ML. Rockhold, PD Thorne, GV Last, and MJ Truex. 2006b. *Carbon Tetrachloride Flow and Mass Flow Rate in the Subsurface of the 216-Z-18 Crib and 216-Z-1A Tile Field at the Hanford Site: Multifluid Flow Simulations and Conceptual Model Update*. PNNL-16198, Pacific Northwest National Laboratory, Richland, Washington.

Rohay, VJ. 2002. *Performance Evaluation Report for Soil Vapor Extraction Operations at the Carbon Tetrachloride Site, February 1992 – September 2001*. BHI-00720, Rev. 6, Bechtel Hanford, Inc., Richland, Washington.

Rohay, VJ, KJ Swett, and GV Last. 1994. *Conceptual Model of the Carbon Tetrachloride Contamination in the 200 West Area at the Hanford Site*. WHC-SD-EN-TI-248, Rev. 0, Westinghouse Hanford Company, Richland, Washington.

Schroth MH, JD Istok, JS Selker, M Oostrom, and MD White. 1998. "Multifluid Flow in Bedded Porous Media: Laboratory Experiments and Numerical Simulations." *Adv. in Water Resour.* 22:169-183.

van Genuchten M. 1980. "A Closed-Form Equation for Predicting the Hydraulic Conductivity of Unsaturated Soils." *Soil Sci. Am. J.* 44:892-898.

White MD and M Oostrom. 2006. *STOMP, Subsurface Transport Over Multiple Phases. Version 4.0. User's Guide*. PNNL-15782, Pacific Northwest National Laboratory, Richland, Washington.

White MD, M Oostrom, and RJ Lenhard. 2004. "A Practical Model for Mobile, Residual, and Entrapped NAPL in Porous Media." *Ground Water* 42:734-746.

Appendix A

Tabular Results for 216-Z-9 Fluxes

Appendix A – Tabular Results for 216-Z-9 Fluxes

Table A.1. Vertical Aqueous CT Flux, Gas CT Concentration, and Aqueous CT Concentration at the Nodes Above the Water Table and the Aqueous CT Concentration Below the Water Table at an Easting and a Northing Cross Section in Year 2010 for Imposed Case 1

	Vadose Zone			Aquifer
Easting Distance (m)	**Vertical Aqueous CT Flux, kg/m^2 yr**	**Gas CT Concentration, ppmv**	**Aqueous CT Concentration, mg/L**	**Aqueous CT Concentration, mg/L**
-150.000	0.000E+00	0.000E+00	0.000E+00	0.000E+00
-70.000	0.000E+00	0.000E+00	0.000E+00	0.000E+00
-16.800	0.000E+00	0.000E+00	0.000E+00	0.000E+00
-6.050	0.000E+00	0.000E+00	0.000E+00	0.000E+00
0.758	0.000E+00	0.000E+00	0.000E+00	0.000E+00
9.050	0.000E+00	0.000E+00	0.000E+00	0.000E+00
19.300	0.000E+00	0.000E+00	0.000E+00	0.000E+00
90.000	0.000E+00	0.000E+00	0.000E+00	0.000E+00
170.000	0.000E+00	0.000E+00	0.000E+00	0.000E+00
Northing Distance (m)	**Vertical Aqueous CT Flux, kg/m^2 yr**	**Gas CT Concentration, ppmv**	**Aqueous CT Concentration, mg/L**	**Aqueous CT Concentration, mg/L**
-170.000	0.000E+00	0.000E+00	0.000E+00	0.000E+00
-90.000	0.000E+00	0.000E+00	0.000E+00	0.000E+00
-33.500	0.000E+00	0.000E+00	0.000E+00	0.000E+00
-14.288	0.000E+00	0.000E+00	0.000E+00	0.000E+00
-4.575	0.000E+00	0.000E+00	0.000E+00	0.000E+00
2.745	0.000E+00	0.000E+00	0.000E+00	0.000E+00
10.863	0.000E+00	0.000E+00	0.000E+00	0.000E+00
28.500	0.000E+00	0.000E+00	0.000E+00	0.000E+00
70.000	0.000E+00	0.000E+00	0.000E+00	0.000E+00
150.000	0.000E+00	0.000E+00	0.000E+00	0.000E+00

Table A.2.   Vertical Aqueous CT Flux, Gas CT Concentration, and Aqueous CT Concentration at the Nodes Above the Water Table and the Aqueous CT Concentration Below the Water Table at an Easting and a Northing Cross Section in Year 2030 for Imposed Case 1

	Vadose Zone			Aquifer
Easting Distance (m)	Vertical Aqueous CT Flux, kg/m^2 yr	Gas CT Concentration, ppmv	Aqueous CT Concentration, mg/L	Aqueous CT Concentration, mg/L
-150.000	0.000E+00	0.000E+00	0.000E+00	0.000E+00
-70.000	-2.819E-10	8.152E-03	5.391E-08	6.527E-10
-16.800	-4.628E-06	1.304E+02	8.621E-04	3.038E-06
-6.050	-6.793E-05	1.933E+03	1.278E-02	6.421E-05
0.758	-6.667E-05	1.906E+03	1.260E-02	1.365E-04
9.050	-4.598E-06	1.322E+02	8.742E-04	1.353E-04
19.300	-5.557E-08	1.612E+00	1.066E-05	1.069E-04
90.000	-1.488E-09	4.340E-02	2.870E-07	1.788E-05
170.000	-1.943E-10	5.728E-03	3.788E-08	2.522E-06
Northing Distance (m)	Vertical Aqueous CT Flux, kg/m^2 yr	Gas CT Concentration, ppmv	Aqueous CT Concentration, mg/L	Aqueous CT Concentration, mg/L
-170.000	0.000E+00	0.000E+00	0.000E+00	0.000E+00
-90.000	-4.756E-13	1.380E-05	9.125E-11	9.139E-13
-33.500	-2.702E-08	7.711E-01	5.100E-06	6.128E-08
-14.288	-1.073E-05	3.062E+02	2.025E-03	2.255E-05
-4.575	-6.667E-05	1.906E+03	1.260E-02	1.365E-04
2.745	-4.209E-05	1.205E+03	7.970E-03	7.936E-05
10.863	-6.403E-06	1.836E+02	1.214E-03	1.175E-05
28.500	-2.640E-08	7.587E-01	5.017E-06	5.306E-08
70.000	-1.938E-12	5.543E-05	3.666E-10	3.965E-12
150.000	0.000E+00	0.000E+00	0.000E+00	0.000E+00

Table A.3. Vertical Aqueous CT Flux, Gas CT Concentration, and Aqueous CT Concentration at the Nodes Above the Water Table and the Aqueous CT Concentration Below the Water Table at an Easting and a Northing Cross Section in Year 2050 for Imposed Case 1

	Vadose Zone			Aquifer
Easting Distance (m)	Vertical Aqueous CT Flux, kg/m^2 yr	Gas CT Concentration, ppmv	Aqueous CT Concentration, mg/L	Aqueous CT Concentration, mg/L
-150.000	-3.775E-13	1.155E-05	7.641E-11	0.000E+00
-70.000	-2.682E-08	7.849E-01	5.191E-06	7.672E-08
-16.800	-7.853E-05	2.275E+03	1.504E-02	7.231E-05
-6.050	-2.353E-04	6.896E+03	4.560E-02	4.013E-04
0.758	-2.276E-04	6.700E+03	4.431E-02	6.427E-04
9.050	-7.551E-05	2.235E+03	1.478E-02	8.065E-04
19.300	-3.984E-06	1.188E+02	7.855E-04	7.853E-04
90.000	-7.173E-08	2.103E+00	1.391E-05	3.966E-04
170.000	-2.370E-08	6.981E-01	4.617E-06	1.577E-04
Northing Distance (m)	Vertical Aqueous CT Flux, kg/m^2 yr	Gas CT Concentration, ppmv	Aqueous CT Concentration, mg/L	Aqueous CT Concentration, mg/L
-170.000	-1.001E-14	2.746E-07	1.816E-12	0.000E+00
-90.000	-9.083E-11	2.648E-03	1.751E-08	2.771E-10
-33.500	-1.539E-06	4.492E+01	2.970E-04	4.213E-06
-14.288	-1.056E-04	3.099E+03	2.049E-02	2.805E-04
-4.575	-2.276E-04	6.700E+03	4.431E-02	6.427E-04
2.745	-1.998E-04	5.896E+03	3.899E-02	5.363E-04
10.863	-8.544E-05	2.525E+03	1.670E-02	2.093E-04
28.500	-1.517E-06	4.478E+01	2.962E-04	3.828E-06
70.000	-3.251E-10	9.405E-03	6.220E-08	8.837E-10
150.000	0.000E+00	0.000E+00	0.000E+00	0.000E+00

Table A.4. Vertical Aqueous CT Flux, Gas CT Concentration, and Aqueous CT Concentration at the Nodes Above the Water Table and the Aqueous CT Concentration Below the Water Table at an Easting and a Northing Cross Section in Year 2070 for Imposed Case 1

	Vadose Zone			Aquifer
Easting Distance (m)	Vertical Aqueous CT Flux, kg/m^2 yr	Gas CT Concentration, ppmv	Aqueous CT Concentration, mg/L	Aqueous CT Concentration, mg/L
-150.000	-1.071E-11	3.276E-04	2.166E-09	3.256E-11
-70.000	-2.323E-07	6.820E+00	4.510E-05	7.455E-07
-16.800	-1.385E-04	4.042E+03	2.673E-02	1.853E-04
-6.050	-2.305E-04	6.808E+03	4.503E-02	5.655E-04
0.758	-2.198E-04	6.523E+03	4.314E-02	7.996E-04
9.050	-1.278E-04	3.810E+03	2.520E-02	1.039E-03
19.300	-2.254E-05	6.769E+02	4.477E-03	1.106E-03
90.000	-2.792E-07	8.201E+00	5.423E-05	8.337E-04
170.000	-1.492E-07	4.394E+00	2.906E-05	5.528E-04
Northing Distance (m)	Vertical Aqueous CT Flux, kg/m^2 yr	Gas CT Concentration, ppmv	Aqueous CT Concentration, mg/L	Aqueous CT Concentration, mg/L
-170.000	-1.001E-12	2.744E-05	1.815E-10	2.318E-12
-90.000	-1.508E-09	4.402E-02	2.911E-07	5.328E-09
-33.500	-8.901E-06	2.612E+02	1.727E-03	2.732E-05
-14.288	-1.490E-04	4.404E+03	2.913E-02	4.985E-04
-4.575	-2.198E-04	6.523E+03	4.314E-02	7.996E-04
2.745	-2.085E-04	6.203E+03	4.102E-02	7.341E-04
10.863	-1.366E-04	4.069E+03	2.691E-02	4.333E-04
28.500	-8.954E-06	2.663E+02	1.761E-03	2.591E-05
70.000	-4.761E-09	1.382E-01	9.141E-07	1.518E-08
150.000	-3.626E-13	1.057E-05	6.988E-11	0.000E+00

Table A.5. Vertical Aqueous CT Flux, Gas CT Concentration, and Aqueous CT Concentration at the Nodes Above the Water Table and the Aqueous CT Concentration Below the Water Table at an Easting and a Northing Cross Section in Year 2090 for Imposed Case 1

	Vadose Zone			Aquifer
Easting Distance (m)	**Vertical Aqueous CT Flux, kg/m^2 yr**	**Gas CT Concentration, ppmv**	**Aqueous CT Concentration, mg/L**	**Aqueous CT Concentration, mg/L**
-150.000	-1.014E-10	3.101E-03	2.051E-08	3.357E-10
-70.000	-7.980E-07	2.345E+01	1.551E-04	2.765E-06
-16.800	-1.425E-04	4.167E+03	2.756E-02	2.584E-04
-6.050	-1.921E-04	5.683E+03	3.759E-02	5.952E-04
0.758	-1.816E-04	5.398E+03	3.570E-02	7.887E-04
9.050	-1.276E-04	3.813E+03	2.522E-02	1.012E-03
19.300	-4.331E-05	1.303E+03	8.616E-03	1.123E-03
90.000	-5.041E-07	1.481E+01	9.794E-05	9.700E-04
170.000	-3.378E-07	9.951E+00	6.581E-05	7.873E-04
Northing Distance (m)	**Vertical Aqueous CT Flux, kg/m^2 yr**	**Gas CT Concentration, ppmv**	**Aqueous CT Concentration, mg/L**	**Aqueous CT Concentration, mg/L**
-170.000	-1.886E-11	5.171E-04	3.420E-09	5.499E-11
-90.000	-9.542E-09	2.786E-01	1.842E-06	3.745E-08
-33.500	-2.026E-05	5.951E+02	3.936E-03	6.921E-05
-14.288	-1.413E-04	4.182E+03	2.765E-02	5.652E-04
-4.575	-1.816E-04	5.398E+03	3.570E-02	7.887E-04
2.745	-1.763E-04	5.256E+03	3.476E-02	7.485E-04
10.863	-1.352E-04	4.036E+03	2.669E-02	5.218E-04
28.500	-2.059E-05	6.133E+02	4.056E-03	6.722E-05
70.000	-2.645E-08	7.687E-01	5.083E-06	9.454E-08
150.000	-5.222E-12	1.521E-04	1.006E-09	1.668E-11

Table A.6. Vertical Aqueous CT Flux, Gas CT Concentration, and Aqueous CT Concentration at the Nodes Above the Water Table and the Aqueous CT Concentration Below the Water Table at an Easting and a Northing Cross Section in Year 2107 for Imposed Case 1

	Vadose Zone			Aquifer
Easting Distance (m)	Vertical Aqueous CT Flux, kg/m^2 yr	Gas CT Concentration, ppmv	Aqueous CT Concentration, mg/L	Aqueous CT Concentration, mg/L
-150.000	-4.243E-10	1.298E-02	8.584E-08	1.477E-09
-70.000	-1.571E-06	4.619E+01	3.055E-04	5.734E-06
-16.800	-1.297E-04	3.794E+03	2.509E-02	2.877E-04
-6.050	-1.614E-04	4.779E+03	3.161E-02	5.776E-04
0.758	-1.519E-04	4.518E+03	2.988E-02	7.393E-04
9.050	-1.145E-04	3.420E+03	2.262E-02	9.338E-04
19.300	-5.171E-05	1.556E+03	1.029E-02	1.052E-03
90.000	-6.519E-07	1.915E+01	1.267E-04	9.581E-04
170.000	-4.805E-07	1.415E+01	9.359E-05	8.324E-04
Northing Distance (m)	Vertical Aqueous CT Flux, kg/m^2 yr	Gas CT Concentration, ppmv	Aqueous CT Concentration, mg/L	Aqueous CT Concentration, mg/L
-170.000	-1.188E-10	3.256E-03	2.153E-08	3.737E-10
-90.000	-3.001E-08	8.760E-01	5.794E-06	1.269E-07
-33.500	-2.836E-05	8.335E+02	5.512E-03	1.063E-04
-14.288	-1.250E-04	3.701E+03	2.448E-02	5.638E-04
-4.575	-1.519E-04	4.518E+03	2.988E-02	7.393E-04
2.745	-1.488E-04	4.436E+03	2.934E-02	7.113E-04
10.863	-1.215E-04	3.630E+03	2.400E-02	5.330E-04
28.500	-2.887E-05	8.603E+02	5.689E-03	1.041E-04
70.000	-7.457E-08	2.167E+00	1.433E-05	2.882E-07
150.000	-2.920E-11	8.507E-04	5.626E-09	1.038E-10

Table A.7. Vertical Aqueous CT Flux, Gas CT Concentration, and Aqueous CT Concentration at the Nodes Above the Water Table and the Aqueous CT Concentration Below the Water Table at an Easting and a Northing Cross Section in Year 2010 for Imposed Case 2

	Vadose Zone			Aquifer
Easting Distance (m)	**Vertical Aqueous CT Flux, kg/m^2 yr**	**Gas CT Concentration, ppmv**	**Aqueous CT Concentration, mg/L**	**Aqueous CT Concentration, mg/L**
-150.000	0.000E+00	0.000E+00	0.000E+00	0.000E+00
-70.000	0.000E+00	0.000E+00	0.000E+00	0.000E+00
-16.800	0.000E+00	0.000E+00	0.000E+00	0.000E+00
-6.050	0.000E+00	0.000E+00	0.000E+00	0.000E+00
0.758	0.000E+00	0.000E+00	0.000E+00	0.000E+00
9.050	0.000E+00	0.000E+00	0.000E+00	0.000E+00
19.300	0.000E+00	0.000E+00	0.000E+00	0.000E+00
90.000	0.000E+00	0.000E+00	0.000E+00	0.000E+00
170.000	0.000E+00	0.000E+00	0.000E+00	0.000E+00
Northing Distance (m)	**Vertical Aqueous CT Flux, kg/m^2 yr**	**Gas CT Concentration, ppmv**	**Aqueous CT Concentration, mg/L**	**Aqueous CT Concentration, mg/L**
-170.000	0.000E+00	0.000E+00	0.000E+00	0.000E+00
-90.000	0.000E+00	0.000E+00	0.000E+00	0.000E+00
-33.500	0.000E+00	0.000E+00	0.000E+00	0.000E+00
-14.288	0.000E+00	0.000E+00	0.000E+00	0.000E+00
-4.575	0.000E+00	0.000E+00	0.000E+00	0.000E+00
2.745	0.000E+00	0.000E+00	0.000E+00	0.000E+00
10.863	0.000E+00	0.000E+00	0.000E+00	0.000E+00
28.500	0.000E+00	0.000E+00	0.000E+00	0.000E+00
70.000	0.000E+00	0.000E+00	0.000E+00	0.000E+00
150.000	0.000E+00	0.000E+00	0.000E+00	0.000E+00

Table A.8.   Vertical Aqueous CT Flux, Gas CT Concentration, and Aqueous CT Concentration at the Nodes Above the Water Table and the Aqueous CT Concentration Below the Water Table at an Easting and a Northing Cross Section in Year 2030 for Imposed Case 2

	Vadose Zone			Aquifer
Easting Distance (m)	**Vertical Aqueous CT Flux, kg/m^2 yr**	**Gas CT Concentration, ppmv**	**Aqueous CT Concentration, mg/L**	**Aqueous CT Concentration, mg/L**
-150.000	0.000E+00	0.000E+00	0.000E+00	0.000E+00
-70.000	-7.678E-14	2.220E-06	1.468E-11	0.000E+00
-16.800	-2.184E-10	6.152E-03	4.068E-08	1.639E-10
-6.050	-8.595E-10	2.446E-02	1.617E-07	1.106E-09
0.758	-6.516E-10	1.862E-02	1.232E-07	1.649E-09
9.050	-1.128E-10	3.242E-03	2.144E-08	1.599E-09
19.300	-4.735E-12	1.374E-04	9.087E-10	1.212E-09
90.000	-1.166E-14	3.399E-07	2.248E-12	1.632E-10
170.000	0.000E+00	0.000E+00	0.000E+00	1.982E-11
Northing Distance (m)	**Vertical Aqueous CT Flux, kg/m^2 yr**	**Gas CT Concentration, ppmv**	**Aqueous CT Concentration, mg/L**	**Aqueous CT Concentration, mg/L**
-170.000	0.000E+00	0.000E+00	0.000E+00	0.000E+00
-90.000	0.000E+00	0.000E+00	0.000E+00	0.000E+00
-33.500	-2.712E-12	7.738E-05	5.117E-10	6.952E-12
-14.288	-2.216E-10	6.322E-03	4.181E-08	5.724E-10
-4.575	-6.516E-10	1.862E-02	1.232E-07	1.649E-09
2.745	-5.880E-10	1.683E-02	1.113E-07	1.398E-09
10.863	-2.656E-10	7.618E-03	5.038E-08	5.993E-10
28.500	-6.279E-12	1.804E-04	1.193E-09	1.406E-11
70.000	0.000E+00	0.000E+00	0.000E+00	0.000E+00
150.000	0.000E+00	0.000E+00	0.000E+00	0.000E+00

Table A.9. Vertical Aqueous CT Flux, Gas CT Concentration, and Aqueous CT Concentration at the Nodes Above the Water Table and the Aqueous CT Concentration Below the Water Table at an Easting and a Northing Cross Section in Year 2050 for Imposed Case 2

	Vadose Zone			Aquifer
Easting Distance (m)	**Vertical Aqueous CT Flux, kg/m^2 yr**	**Gas CT Concentration, ppmv**	**Aqueous CT Concentration, mg/L**	**Aqueous CT Concentration, mg/L**
-150.000	0.000E+00	0.000E+00	0.000E+00	0.000E+00
-70.000	-2.763E-11	8.087E-04	5.348E-09	7.446E-11
-16.800	-1.975E-08	5.722E-01	3.784E-06	1.942E-08
-6.050	-4.401E-08	1.290E+00	8.530E-06	7.980E-08
0.758	-3.080E-08	9.067E-01	5.996E-06	1.090E-07
9.050	-7.642E-09	2.262E-01	1.496E-06	1.143E-07
19.300	-6.569E-10	1.958E-02	1.295E-07	9.951E-08
90.000	-3.543E-12	1.039E-04	6.871E-10	2.831E-08
170.000	-8.282E-13	2.440E-05	1.614E-10	7.220E-09
Northing Distance (m)	**Vertical Aqueous CT Flux, kg/m^2 yr**	**Gas CT Concentration, ppmv**	**Aqueous CT Concentration, mg/L**	**Aqueous CT Concentration, mg/L**
-170.000	0.000E+00	0.000E+00	0.000E+00	0.000E+00
-90.000	-9.200E-13	2.682E-05	1.774E-10	2.216E-12
-33.500	-4.955E-10	1.446E-02	9.560E-08	1.722E-09
-14.288	-1.338E-08	3.927E-01	2.597E-06	4.815E-08
-4.575	-3.080E-08	9.067E-01	5.996E-06	1.090E-07
2.745	-2.975E-08	8.777E-01	5.804E-06	1.012E-07
10.863	-1.597E-08	4.720E-01	3.121E-06	5.197E-08
28.500	-9.107E-10	2.688E-02	1.778E-07	2.845E-09
70.000	-1.758E-12	5.087E-05	3.364E-10	4.664E-12
150.000	0.000E+00	0.000E+00	0.000E+00	0.000E+00

Table A.10. Vertical Aqueous CT Flux, Gas CT Concentration, and Aqueous CT Concentration at the Nodes Above the Water Table and the Aqueous CT Concentration Below the Water Table at an Easting and a Northing Cross Section in Year 2070 for Imposed Case 2

	Vadose Zone			Aquifer
Easting Distance (m)	Vertical Aqueous CT Flux, kg/m^2 yr	Gas CT Concentration, ppmv	Aqueous CT Concentration, mg/L	Aqueous CT Concentration, mg/L
-150.000	-1.745E-13	5.338E-06	3.530E-11	0.000E+00
-70.000	-6.434E-10	1.889E-02	1.249E-07	1.974E-09
-16.800	-1.740E-07	5.077E+00	3.358E-05	2.151E-07
-6.050	-2.804E-07	8.283E+00	5.478E-05	6.524E-07
0.758	-1.890E-07	5.607E+00	3.708E-05	8.430E-07
9.050	-5.824E-08	1.737E+00	1.149E-05	9.088E-07
19.300	-7.750E-09	2.327E-01	1.539E-06	8.444E-07
90.000	-6.591E-11	1.936E-03	1.280E-08	3.587E-07
170.000	-2.279E-11	6.713E-04	4.440E-09	1.387E-07
Northing Distance (m)	Vertical Aqueous CT Flux, kg/m^2 yr	Gas CT Concentration, ppmv	Aqueous CT Concentration, mg/L	Aqueous CT Concentration, mg/L
-170.000	-1.970E-13	5.402E-06	3.572E-11	0.000E+00
-90.000	-3.789E-11	1.106E-03	7.314E-09	1.182E-10
-33.500	-7.365E-09	2.161E-01	1.429E-06	3.102E-08
-14.288	-9.669E-08	2.858E+00	1.890E-05	4.350E-07
-4.575	-1.890E-07	5.607E+00	3.708E-05	8.430E-07
2.745	-1.871E-07	5.565E+00	3.680E-05	8.117E-07
10.863	-1.133E-07	3.376E+00	2.233E-05	4.726E-07
28.500	-1.137E-08	3.382E-01	2.237E-06	4.443E-08
70.000	-5.366E-11	1.558E-03	1.030E-08	1.775E-10
150.000	-2.669E-14	7.776E-07	5.143E-12	0.000E+00

Table A.11. Vertical Aqueous CT Flux, Gas CT Concentration, and Aqueous CT Concentration at the Nodes Above the Water Table and the Aqueous CT Concentration Below the Water Table at an Easting and a Northing Cross Section in Year 2090 for Imposed Case 2

	Vadose Zone			Aquifer
Easting Distance (m)	**Vertical Aqueous CT Flux, kg/m^2 yr**	**Gas CT Concentration, ppmv**	**Aqueous CT Concentration, mg/L**	**Aqueous CT Concentration, mg/L**
-150.000	-2.903E-12	8.881E-05	5.873E-10	9.276E-12
-70.000	-4.799E-09	1.410E-01	9.327E-07	1.620E-08
-16.800	-5.955E-07	1.741E+01	1.152E-04	9.139E-07
-6.050	-7.830E-07	2.317E+01	1.532E-04	2.238E-06
0.758	-5.209E-07	1.548E+01	1.024E-04	2.782E-06
9.050	-1.872E-07	5.592E+00	3.699E-05	3.033E-06
19.300	-3.377E-08	1.016E+00	6.717E-06	2.924E-06
90.000	-4.037E-10	1.186E-02	7.844E-08	1.586E-06
170.000	-1.772E-10	5.219E-03	3.451E-08	7.980E-07
Northing Distance (m)	**Vertical Aqueous CT Flux, kg/m^2 yr**	**Gas CT Concentration, ppmv**	**Aqueous CT Concentration, mg/L**	**Aqueous CT Concentration, mg/L**
-170.000	-4.138E-12	1.134E-04	7.501E-10	1.096E-11
-90.000	-4.293E-10	1.253E-02	8.288E-08	1.521E-09
-33.500	-3.877E-08	1.139E+00	7.532E-06	1.901E-07
-14.288	-3.019E-07	8.936E+00	5.910E-05	1.614E-06
-4.575	-5.209E-07	1.548E+01	1.024E-04	2.782E-06
2.745	-5.206E-07	1.551E+01	1.026E-04	2.724E-06
10.863	-3.453E-07	1.031E+01	6.816E-05	1.744E-06
28.500	-5.231E-08	1.558E+00	1.031E-05	2.439E-07
70.000	-4.943E-10	1.436E-02	9.499E-08	1.890E-09
150.000	-6.136E-13	1.788E-05	1.182E-10	1.549E-12

Table A.12. Vertical Aqueous CT Flux, Gas CT Concentration, and Aqueous CT Concentration at the Nodes Above the Water Table and the Aqueous CT Concentration Below the Water Table at an Easting and a Northing Cross Section in Year 2107 for Imposed Case 2

	Vadose Zone			Aquifer
Easting Distance (m)	**Vertical Aqueous CT Flux, kg/m^2 yr**	**Gas CT Concentration, ppmv**	**Aqueous CT Concentration, mg/L**	**Aqueous CT Concentration, mg/L**
-150.000	-1.702E-11	5.205E-04	3.442E-09	5.937E-11
-70.000	-1.597E-08	4.694E-01	3.104E-06	5.761E-08
-16.800	-1.135E-06	3.319E+01	2.195E-04	2.077E-06
-6.050	-1.333E-06	3.945E+01	2.609E-04	4.434E-06
0.758	-8.873E-07	2.638E+01	1.745E-04	5.377E-06
9.050	-3.524E-07	1.053E+01	6.964E-05	5.883E-06
19.300	-7.720E-08	2.322E+00	1.536E-05	5.786E-06
90.000	-1.171E-09	3.440E-02	2.275E-07	3.601E-06
170.000	-5.825E-10	1.716E-02	1.135E-07	2.106E-06
Northing Distance (m)	**Vertical Aqueous CT Flux, kg/m^2 yr**	**Gas CT Concentration, ppmv**	**Aqueous CT Concentration, mg/L**	**Aqueous CT Concentration, mg/L**
-170.000	-2.728E-11	7.478E-04	4.946E-09	8.152E-11
-90.000	-1.876E-09	5.477E-02	3.622E-07	7.312E-09
-33.500	-1.008E-07	2.963E+00	1.959E-05	5.524E-07
-14.288	-5.596E-07	1.657E+01	1.096E-04	3.379E-06
-4.575	-8.873E-07	2.638E+01	1.745E-04	5.377E-06
2.745	-8.891E-07	2.650E+01	1.753E-04	5.301E-06
10.863	-6.261E-07	1.870E+01	1.237E-04	3.615E-06
28.500	-1.244E-07	3.706E+00	2.451E-05	6.587E-07
70.000	-1.904E-09	5.532E-02	3.659E-07	8.098E-09
150.000	-4.142E-12	1.207E-04	7.980E-10	1.403E-11

Table A.13. Vertical Aqueous CT Flux, Gas CT Concentration, and Aqueous CT Concentration at the Nodes Above the Water Table and the Aqueous CT Concentration Below the Water Table at an Easting and a Northing Cross Section in Year 2010 for Imposed Case 3

	Vadose Zone			Aquifer
Easting Distance (m)	**Vertical Aqueous CT Flux, kg/m^2 yr**	**Gas CT Concentration, ppmv**	**Aqueous CT Concentration, mg/L**	**Aqueous CT Concentration, mg/L**
-150.000	0.000E+00	0.000E+00	0.000E+00	0.000E+00
-70.000	0.000E+00	0.000E+00	0.000E+00	0.000E+00
-16.800	0.000E+00	0.000E+00	0.000E+00	0.000E+00
-6.050	0.000E+00	0.000E+00	0.000E+00	0.000E+00
0.758	0.000E+00	0.000E+00	0.000E+00	0.000E+00
9.050	0.000E+00	0.000E+00	0.000E+00	0.000E+00
19.300	0.000E+00	0.000E+00	0.000E+00	0.000E+00
90.000	0.000E+00	0.000E+00	0.000E+00	0.000E+00
170.000	0.000E+00	0.000E+00	0.000E+00	0.000E+00
Northing Distance (m)	**Vertical Aqueous CT Flux, kg/m^2 yr**	**Gas CT Concentration, ppmv**	**Aqueous CT Concentration, mg/L**	**Aqueous CT Concentration, mg/L**
-170.000	0.000E+00	0.000E+00	0.000E+00	0.000E+00
-90.000	0.000E+00	0.000E+00	0.000E+00	0.000E+00
-33.500	0.000E+00	0.000E+00	0.000E+00	0.000E+00
-14.288	0.000E+00	0.000E+00	0.000E+00	0.000E+00
-4.575	0.000E+00	0.000E+00	0.000E+00	0.000E+00
2.745	0.000E+00	0.000E+00	0.000E+00	0.000E+00
10.863	0.000E+00	0.000E+00	0.000E+00	0.000E+00
28.500	0.000E+00	0.000E+00	0.000E+00	0.000E+00
70.000	0.000E+00	0.000E+00	0.000E+00	0.000E+00
150.000	0.000E+00	0.000E+00	0.000E+00	0.000E+00

Table A.14. Vertical Aqueous CT Flux, Gas CT Concentration, and Aqueous CT Concentration at the Nodes Above the Water Table and the Aqueous CT Concentration Below the Water Table at an Easting and a Northing Cross Section in Year 2030 for Imposed Case 3

	Vadose Zone			Aquifer
Easting Distance (m)	**Vertical Aqueous CT Flux, kg/m^2 yr**	**Gas CT Concentration, ppmv**	**Aqueous CT Concentration, mg/L**	**Aqueous CT Concentration, mg/L**
-150.000	0.000E+00	0.000E+00	0.000E+00	0.000E+00
-70.000	0.000E+00	0.000E+00	0.000E+00	0.000E+00
-16.800	-7.038E-12	1.982E-04	1.311E-09	5.227E-12
-6.050	-2.389E-11	6.799E-04	4.496E-09	3.202E-11
0.758	-1.889E-11	5.399E-04	3.570E-09	4.705E-11
9.050	-4.661E-12	1.340E-04	8.862E-10	4.729E-11
19.300	-3.587E-13	1.041E-05	6.884E-11	3.643E-11
90.000	0.000E+00	0.000E+00	0.000E+00	4.499E-12
170.000	0.000E+00	0.000E+00	0.000E+00	0.000E+00
Northing Distance (m)	**Vertical Aqueous CT Flux, kg/m^2 yr**	**Gas CT Concentration, ppmv**	**Aqueous CT Concentration, mg/L**	**Aqueous CT Concentration, mg/L**
-170.000	0.000E+00	0.000E+00	0.000E+00	0.000E+00
-90.000	0.000E+00	0.000E+00	0.000E+00	0.000E+00
-33.500	-1.417E-13	4.042E-06	2.673E-11	0.000E+00
-14.288	-7.370E-12	2.103E-04	1.391E-09	1.843E-11
-4.575	-1.889E-11	5.399E-04	3.570E-09	4.705E-11
2.745	-1.777E-11	5.087E-04	3.364E-09	4.214E-11
10.863	-9.293E-12	2.665E-04	1.763E-09	2.087E-11
28.500	-3.134E-13	9.006E-06	5.956E-11	0.000E+00
70.000	0.000E+00	0.000E+00	0.000E+00	0.000E+00
150.000	0.000E+00	0.000E+00	0.000E+00	0.000E+00

Table A.15. Vertical Aqueous CT Flux, Gas CT Concentration, and Aqueous CT Concentration at the Nodes Above the Water Table and the Aqueous CT Concentration Below the Water Table at an Easting and a Northing Cross Section in Year 2050 for Imposed Case 3

	Vadose Zone			Aquifer
Easting Distance (m)	Vertical Aqueous CT Flux, kg/m^2 yr	Gas CT Concentration, ppmv	Aqueous CT Concentration, mg/L	Aqueous CT Concentration, mg/L
-150.000	0.000E+00	0.000E+00	0.000E+00	0.000E+00
-70.000	-1.410E-12	4.126E-05	2.729E-10	3.611E-12
-16.800	-7.119E-10	2.062E-02	1.364E-07	7.341E-10
-6.050	-1.436E-09	4.209E-02	2.784E-07	2.722E-09
0.758	-1.072E-09	3.156E-02	2.087E-07	3.690E-09
9.050	-3.598E-10	1.065E-02	7.042E-08	3.985E-09
19.300	-5.067E-11	1.511E-03	9.990E-09	3.532E-09
90.000	-1.208E-13	3.543E-06	2.343E-11	9.840E-10
170.000	-2.053E-14	6.048E-07	4.000E-12	2.451E-10
Northing Distance (m)	Vertical Aqueous CT Flux, kg/m^2 yr	Gas CT Concentration, ppmv	Aqueous CT Concentration, mg/L	Aqueous CT Concentration, mg/L
-170.000	0.000E+00	0.000E+00	0.000E+00	0.000E+00
-90.000	-8.861E-14	2.583E-06	1.708E-11	0.000E+00
-33.500	-3.140E-11	9.161E-04	6.058E-09	1.006E-10
-14.288	-5.325E-10	1.562E-02	1.033E-07	1.836E-09
-4.575	-1.072E-09	3.156E-02	2.087E-07	3.690E-09
2.745	-1.056E-09	3.117E-02	2.061E-07	3.526E-09
10.863	-6.414E-10	1.896E-02	1.254E-07	2.050E-09
28.500	-5.117E-11	1.510E-03	9.988E-09	1.542E-10
70.000	-1.455E-13	4.209E-06	2.784E-11	0.000E+00
150.000	0.000E+00	0.000E+00	0.000E+00	0.000E+00

Table A.16. Vertical Aqueous CT Flux, Gas CT Concentration, and Aqueous CT Concentration at the Nodes Above the Water Table and the Aqueous CT Concentration Below the Water Table at an Easting and a Northing Cross Section in Year 2070 for Imposed Case 3

	Vadose Zone			Aquifer
Easting Distance (m)	Vertical Aqueous CT Flux, kg/m^2 yr	Gas CT Concentration, ppmv	Aqueous CT Concentration, mg/L	Aqueous CT Concentration, mg/L
-150.000	-8.200E-15	2.509E-07	1.659E-12	0.000E+00
-70.000	-3.509E-11	1.030E-03	6.813E-09	1.078E-10
-16.800	-6.881E-09	2.008E-01	1.328E-06	9.017E-09
-6.050	-1.048E-08	3.096E-01	2.047E-06	2.531E-08
0.758	-7.639E-09	2.267E-01	1.499E-06	3.265E-08
9.050	-3.069E-09	9.152E-02	6.052E-07	3.613E-08
19.300	-6.100E-10	1.832E-02	1.211E-07	3.419E-08
90.000	-2.625E-12	7.709E-05	5.099E-10	1.420E-08
170.000	-8.482E-13	2.498E-05	1.652E-10	5.336E-09
Northing Distance (m)	Vertical Aqueous CT Flux, kg/m^2 yr	Gas CT Concentration, ppmv	Aqueous CT Concentration, mg/L	Aqueous CT Concentration, mg/L
-170.000	-1.392E-14	3.817E-07	2.524E-12	0.000E+00
-90.000	-3.947E-12	1.152E-04	7.619E-10	1.140E-11
-33.500	-5.192E-10	1.523E-02	1.007E-07	1.996E-09
-14.288	-4.431E-09	1.310E-01	8.661E-07	1.881E-08
-4.575	-7.639E-09	2.267E-01	1.499E-06	3.265E-08
2.745	-7.629E-09	2.269E-01	1.501E-06	3.193E-08
10.863	-5.113E-09	1.523E-01	1.007E-06	2.061E-08
28.500	-6.936E-10	2.063E-02	1.364E-07	2.586E-09
70.000	-4.695E-12	1.363E-04	9.015E-10	1.456E-11
150.000	0.000E+00	0.000E+00	0.000E+00	0.000E+00

Table A.17. Vertical Aqueous CT Flux, Gas CT Concentration, and Aqueous CT Concentration at the Nodes Above the Water Table and the Aqueous CT Concentration Below the Water Table at an Easting and a Northing Cross Section in Year 2090 for Imposed Case 3

	Vadose Zone			Aquifer
Easting Distance (m)	Vertical Aqueous CT Flux, kg/m^2 yr	Gas CT Concentration, ppmv	Aqueous CT Concentration, mg/L	Aqueous CT Concentration, mg/L
-150.000	-2.225E-13	6.806E-06	4.501E-11	0.000E+00
-70.000	-2.761E-10	8.114E-03	5.366E-08	9.383E-10
-16.800	-2.573E-08	7.522E-01	4.975E-06	4.207E-08
-6.050	-3.306E-08	9.782E-01	6.469E-06	9.723E-08
0.758	-2.392E-08	7.109E-01	4.701E-06	1.210E-07
9.050	-1.084E-08	3.239E-01	2.142E-06	1.351E-07
19.300	-2.719E-09	8.179E-02	5.409E-07	1.326E-07
90.000	-1.831E-11	5.379E-04	3.557E-09	7.053E-08
170.000	-7.350E-12	2.165E-04	1.432E-09	3.438E-08
Northing Distance (m)	Vertical Aqueous CT Flux, kg/m^2 yr	Gas CT Concentration, ppmv	Aqueous CT Concentration, mg/L	Aqueous CT Concentration, mg/L
-170.000	-4.434E-13	1.215E-05	8.038E-11	7.104E-13
-90.000	-4.544E-11	1.327E-03	8.774E-09	1.540E-10
-33.500	-2.933E-09	8.616E-02	5.698E-07	1.306E-08
-14.288	-1.554E-08	4.601E-01	3.043E-06	7.757E-08
-4.575	-2.392E-08	7.109E-01	4.701E-06	1.210E-07
2.745	-2.393E-08	7.132E-01	4.717E-06	1.194E-07
10.863	-1.723E-08	5.143E-01	3.401E-06	8.316E-08
28.500	-3.399E-09	1.013E-01	6.696E-07	1.501E-08
70.000	-4.453E-11	1.294E-03	8.557E-09	1.623E-10
150.000	-5.880E-14	1.713E-06	1.133E-11	0.000E+00

Table A.18. Vertical Aqueous CT Flux, Gas CT Concentration, and Aqueous CT Concentration at the Nodes Above the Water Table and the Aqueous CT Concentration Below the Water Table at an Easting and a Northing Cross Section in Year 2107 for Imposed Case 3

	Vadose Zone			Aquifer
Easting Distance (m)	**Vertical Aqueous CT Flux, kg/m^2 yr**	**Gas CT Concentration, ppmv**	**Aqueous CT Concentration, mg/L**	**Aqueous CT Concentration, mg/L**
-150.000	-1.346E-12	4.117E-05	2.723E-10	4.408E-12
-70.000	-9.551E-10	2.807E-02	1.857E-07	3.478E-09
-16.800	-5.269E-08	1.541E+00	1.019E-05	1.027E-07
-6.050	-6.170E-08	1.826E+00	1.208E-05	2.098E-07
0.758	-4.464E-08	1.327E+00	8.779E-06	2.551E-07
9.050	-2.182E-08	6.519E-01	4.312E-06	2.851E-07
19.300	-6.339E-09	1.907E-01	1.261E-06	2.852E-07
90.000	-5.887E-11	1.730E-03	1.144E-08	1.749E-07
170.000	-2.618E-11	7.710E-04	5.099E-09	9.905E-08
Northing Distance (m)	**Vertical Aqueous CT Flux, kg/m^2 yr**	**Gas CT Concentration, ppmv**	**Aqueous CT Concentration, mg/L**	**Aqueous CT Concentration, mg/L**
-170.000	-2.974E-12	8.151E-05	5.391E-10	8.333E-12
-90.000	-2.002E-10	5.844E-03	3.865E-08	7.487E-10
-33.500	-7.957E-09	2.338E-01	1.546E-06	3.953E-08
-14.288	-3.128E-08	9.261E-01	6.125E-06	1.754E-07
-4.575	-4.464E-08	1.327E+00	8.779E-06	2.551E-07
2.745	-4.460E-08	1.330E+00	8.794E-06	2.524E-07
10.863	-3.363E-08	1.004E+00	6.641E-06	1.846E-07
28.500	-8.439E-09	2.515E-01	1.663E-06	4.218E-08
70.000	-1.745E-10	5.070E-03	3.353E-08	7.064E-10
150.000	-4.377E-13	1.275E-05	8.434E-11	8.382E-13

Table A.19. Vertical Aqueous CT Flux, Gas CT Concentration, and Aqueous CT Concentration at the Nodes Above the Water Table and the Aqueous CT Concentration Below the Water Table at an Easting and a Northing Cross Section in Year 2010 for Imposed Case 4

	Vadose Zone			Aquifer
Easting Distance (m)	**Vertical Aqueous CT Flux, kg/m^2 yr**	**Gas CT Concentration, ppmv**	**Aqueous CT Concentration, mg/L**	**Aqueous CT Concentration, mg/L**
-150.000	0.000E+00	0.000E+00	0.000E+00	0.000E+00
-70.000	0.000E+00	0.000E+00	0.000E+00	0.000E+00
-16.800	0.000E+00	0.000E+00	0.000E+00	0.000E+00
-6.050	0.000E+00	0.000E+00	0.000E+00	0.000E+00
0.758	0.000E+00	0.000E+00	0.000E+00	0.000E+00
9.050	0.000E+00	0.000E+00	0.000E+00	0.000E+00
19.300	0.000E+00	0.000E+00	0.000E+00	0.000E+00
90.000	0.000E+00	0.000E+00	0.000E+00	0.000E+00
170.000	0.000E+00	0.000E+00	0.000E+00	0.000E+00
Northing Distance (m)	**Vertical Aqueous CT Flux, kg/m^2 yr**	**Gas CT Concentration, ppmv**	**Aqueous CT Concentration, mg/L**	**Aqueous CT Concentration, mg/L**
-170.000	0.000E+00	0.000E+00	0.000E+00	0.000E+00
-90.000	0.000E+00	0.000E+00	0.000E+00	0.000E+00
-33.500	0.000E+00	0.000E+00	0.000E+00	0.000E+00
-14.288	0.000E+00	0.000E+00	0.000E+00	0.000E+00
-4.575	0.000E+00	0.000E+00	0.000E+00	0.000E+00
2.745	0.000E+00	0.000E+00	0.000E+00	0.000E+00
10.863	0.000E+00	0.000E+00	0.000E+00	0.000E+00
28.500	0.000E+00	0.000E+00	0.000E+00	0.000E+00
70.000	0.000E+00	0.000E+00	0.000E+00	0.000E+00
150.000	0.000E+00	0.000E+00	0.000E+00	0.000E+00

Table A.20. Vertical Aqueous CT Flux, Gas CT Concentration, and Aqueous CT Concentration at the Nodes Above the Water Table and the Aqueous CT Concentration Below the Water Table at an Easting and a Northing Cross Section in Year 2030 for Imposed Case 4

	Vadose Zone			Aquifer
Easting Distance (m)	**Vertical Aqueous CT Flux, kg/m^2 yr**	**Gas CT Concentration, ppmv**	**Aqueous CT Concentration, mg/L**	**Aqueous CT Concentration, mg/L**
-150.000	0.000E+00	0.000E+00	0.000E+00	0.000E+00
-70.000	-2.807E-10	8.117E-03	5.368E-08	6.500E-10
-16.800	-4.616E-06	1.300E+02	8.598E-04	3.029E-06
-6.050	-6.782E-05	1.930E+03	1.276E-02	6.410E-05
0.758	-6.658E-05	1.903E+03	1.259E-02	1.363E-04
9.050	-4.587E-06	1.319E+02	8.722E-04	1.351E-04
19.300	-5.539E-08	1.607E+00	1.063E-05	1.067E-04
90.000	-1.486E-09	4.334E-02	2.866E-07	1.786E-05
170.000	-1.941E-10	5.719E-03	3.782E-08	2.518E-06
Northing Distance (m)	**Vertical Aqueous CT Flux, kg/m^2 yr**	**Gas CT Concentration, ppmv**	**Aqueous CT Concentration, mg/L**	**Aqueous CT Concentration, mg/L**
-170.000	0.000E+00	0.000E+00	0.000E+00	0.000E+00
-90.000	-4.729E-13	1.372E-05	9.072E-11	9.086E-13
-33.500	-2.694E-08	7.686E-01	5.083E-06	6.108E-08
-14.288	-1.071E-05	3.056E+02	2.021E-03	2.250E-05
-4.575	-6.658E-05	1.903E+03	1.259E-02	1.363E-04
2.745	-4.201E-05	1.203E+03	7.955E-03	7.920E-05
10.863	-6.384E-06	1.831E+02	1.211E-03	1.171E-05
28.500	-2.628E-08	7.553E-01	4.995E-06	5.282E-08
70.000	-1.926E-12	5.507E-05	3.642E-10	3.939E-12
150.000	0.000E+00	0.000E+00	0.000E+00	0.000E+00

Table A.21. Vertical Aqueous CT Flux, Gas CT Concentration, and Aqueous CT Concentration at the Nodes Above the Water Table and the Aqueous CT Concentration Below the Water Table at an Easting and a Northing Cross Section in Year 2050 for Imposed Case 4

	Vadose Zone			Aquifer
Easting Distance (m)	**Vertical Aqueous CT Flux, kg/m^2 yr**	**Gas CT Concentration, ppmv**	**Aqueous CT Concentration, mg/L**	**Aqueous CT Concentration, mg/L**
-150.000	-3.747E-13	1.147E-05	7.583E-11	0.000E+00
-70.000	-2.666E-08	7.802E-01	5.160E-06	7.626E-08
-16.800	-7.830E-05	2.268E+03	1.500E-02	7.206E-05
-6.050	-2.350E-04	6.887E+03	4.554E-02	4.005E-04
0.758	-2.273E-04	6.692E+03	4.425E-02	6.416E-04
9.050	-7.533E-05	2.230E+03	1.474E-02	8.051E-04
19.300	-3.964E-06	1.182E+02	7.815E-04	7.840E-04
90.000	-7.161E-08	2.100E+00	1.389E-05	3.960E-04
170.000	-2.366E-08	6.969E-01	4.609E-06	1.574E-04
Northing Distance (m)	**Vertical Aqueous CT Flux, kg/m^2 yr**	**Gas CT Concentration, ppmv**	**Aqueous CT Concentration, mg/L**	**Aqueous CT Concentration, mg/L**
-170.000	-8.711E-15	2.389E-07	1.580E-12	0.000E+00
-90.000	-8.992E-11	2.621E-03	1.734E-08	2.744E-10
-33.500	-1.532E-06	4.470E+01	2.956E-04	4.192E-06
-14.288	-1.054E-04	3.093E+03	2.045E-02	2.799E-04
-4.575	-2.273E-04	6.692E+03	4.425E-02	6.416E-04
2.745	-1.995E-04	5.887E+03	3.893E-02	5.352E-04
10.863	-8.518E-05	2.517E+03	1.665E-02	2.085E-04
28.500	-1.507E-06	4.449E+01	2.942E-04	3.802E-06
70.000	-3.221E-10	9.318E-03	6.162E-08	8.754E-10
150.000	0.000E+00	0.000E+00	0.000E+00	0.000E+00

Table A.22. Vertical Aqueous CT Flux, Gas CT Concentration, and Aqueous CT Concentration at the Nodes Above the Water Table and the Aqueous CT Concentration Below the Water Table at an Easting and a Northing Cross Section in Year 2070 for Imposed Case 4

	Vadose Zone			Aquifer
Easting Distance (m)	**Vertical Aqueous CT Flux, kg/m^2 yr**	**Gas CT Concentration, ppmv**	**Aqueous CT Concentration, mg/L**	**Aqueous CT Concentration, mg/L**
-150.000	-1.060E-11	3.244E-04	2.145E-09	3.225E-11
-70.000	-2.305E-07	6.769E+00	4.477E-05	7.401E-07
-16.800	-1.381E-04	4.031E+03	2.666E-02	1.846E-04
-6.050	-2.302E-04	6.799E+03	4.496E-02	5.642E-04
0.758	-2.196E-04	6.515E+03	4.309E-02	7.980E-04
9.050	-1.275E-04	3.802E+03	2.514E-02	1.037E-03
19.300	-2.242E-05	6.733E+02	4.453E-03	1.104E-03
90.000	-2.787E-07	8.186E+00	5.413E-05	8.321E-04
170.000	-1.489E-07	4.386E+00	2.900E-05	5.518E-04
Northing Distance (m)	**Vertical Aqueous CT Flux, kg/m^2 yr**	**Gas CT Concentration, ppmv**	**Aqueous CT Concentration, mg/L**	**Aqueous CT Concentration, mg/L**
-170.000	-8.686E-13	2.381E-05	1.575E-10	2.003E-12
-90.000	-1.484E-09	4.331E-02	2.864E-07	5.248E-09
-33.500	-8.850E-06	2.597E+02	1.717E-03	2.716E-05
-14.288	-1.488E-04	4.397E+03	2.908E-02	4.972E-04
-4.575	-2.196E-04	6.515E+03	4.309E-02	7.980E-04
2.745	-2.082E-04	6.194E+03	4.096E-02	7.324E-04
10.863	-1.362E-04	4.058E+03	2.684E-02	4.318E-04
28.500	-8.884E-06	2.642E+02	1.747E-03	2.570E-05
70.000	-4.705E-09	1.366E-01	9.034E-07	1.500E-08
150.000	-3.568E-13	1.040E-05	6.875E-11	0.000E+00

Table A.23. Vertical Aqueous CT Flux, Gas CT Concentration, and Aqueous CT Concentration at the Nodes Above the Water Table and the Aqueous CT Concentration Below the Water Table at an Easting and a Northing Cross Section in Year 2090 for Imposed Case 4

	Vadose Zone			Aquifer
Easting Distance (m)	Vertical Aqueous CT Flux, kg/m^2 yr	Gas CT Concentration, ppmv	Aqueous CT Concentration, mg/L	Aqueous CT Concentration, mg/L
-150.000	-1.002E-10	3.064E-03	2.026E-08	3.317E-10
-70.000	-7.912E-07	2.325E+01	1.538E-04	2.742E-06
-16.800	-1.421E-04	4.156E+03	2.748E-02	2.573E-04
-6.050	-1.917E-04	5.674E+03	3.752E-02	5.935E-04
0.758	-1.813E-04	5.390E+03	3.565E-02	7.867E-04
9.050	-1.274E-04	3.805E+03	2.516E-02	1.010E-03
19.300	-4.310E-05	1.296E+03	8.573E-03	1.120E-03
90.000	-5.030E-07	1.478E+01	9.773E-05	9.677E-04
170.000	-3.372E-07	9.931E+00	6.568E-05	7.855E-04
Northing Distance (m)	Vertical Aqueous CT Flux, kg/m^2 yr	Gas CT Concentration, ppmv	Aqueous CT Concentration, mg/L	Aqueous CT Concentration, mg/L
-170.000	-1.640E-11	4.496E-04	2.974E-09	4.859E-11
-90.000	-9.319E-09	2.721E-01	1.799E-06	3.666E-08
-33.500	-2.014E-05	5.916E+02	3.912E-03	6.876E-05
-14.288	-1.410E-04	4.174E+03	2.760E-02	5.635E-04
-4.575	-1.813E-04	5.390E+03	3.565E-02	7.867E-04
2.745	-1.760E-04	5.246E+03	3.469E-02	7.464E-04
10.863	-1.348E-04	4.025E+03	2.662E-02	5.198E-04
28.500	-2.042E-05	6.084E+02	4.024E-03	6.665E-05
70.000	-2.609E-08	7.581E-01	5.014E-06	9.325E-08
150.000	-5.116E-12	1.491E-04	9.858E-10	1.634E-11

Table A.24. Vertical Aqueous CT Flux, Gas CT Concentration, and Aqueous CT Concentration at the Nodes Above the Water Table and the Aqueous CT Concentration Below the Water Table at an Easting and a Northing Cross Section in Year 2107 for Imposed Case 4

	Vadose Zone			Aquifer
Easting Distance (m)	Vertical Aqueous CT Flux, kg/m^2 yr	Gas CT Concentration, ppmv	Aqueous CT Concentration, mg/L	Aqueous CT Concentration, mg/L
-150.000	-4.186E-10	1.280E-02	8.467E-08	1.457E-09
-70.000	-1.557E-06	4.577E+01	3.027E-04	5.682E-06
-16.800	-1.293E-04	3.783E+03	2.502E-02	2.863E-04
-6.050	-1.611E-04	4.770E+03	3.154E-02	5.756E-04
0.758	-1.516E-04	4.509E+03	2.982E-02	7.371E-04
9.050	-1.142E-04	3.412E+03	2.257E-02	9.312E-04
19.300	-5.147E-05	1.549E+03	1.024E-02	1.049E-03
90.000	-6.504E-07	1.911E+01	1.264E-04	9.555E-04
170.000	-4.794E-07	1.412E+01	9.338E-05	8.303E-04
Northing Distance (m)	Vertical Aqueous CT Flux, kg/m^2 yr	Gas CT Concentration, ppmv	Aqueous CT Concentration, mg/L	Aqueous CT Concentration, mg/L
-170.000	-1.037E-10	2.842E-03	1.880E-08	3.312E-10
-90.000	-2.913E-08	8.505E-01	5.625E-06	1.236E-07
-33.500	-2.820E-05	8.286E+02	5.480E-03	1.056E-04
-14.288	-1.247E-04	3.693E+03	2.442E-02	5.619E-04
-4.575	-1.516E-04	4.509E+03	2.982E-02	7.371E-04
2.745	-1.485E-04	4.427E+03	2.928E-02	7.089E-04
10.863	-1.212E-04	3.619E+03	2.394E-02	5.308E-04
28.500	-2.864E-05	8.534E+02	5.644E-03	1.032E-04
70.000	-7.345E-08	2.135E+00	1.412E-05	2.839E-07
150.000	-2.852E-11	8.309E-04	5.495E-09	1.015E-10

Table A.25. Vertical Aqueous CT Flux, Gas CT Concentration, and Aqueous CT Concentration at the Nodes Above the Water Table and the Aqueous CT Concentration Below the Water Table at an Easting and a Northing Cross Section in Year 2010 for Imposed Case 5

	Vadose Zone			Aquifer
Easting Distance (m)	**Vertical Aqueous CT Flux, kg/m^2 yr**	**Gas CT Concentration, ppmv**	**Aqueous CT Concentration, mg/L**	**Aqueous CT Concentration, mg/L**
-150.000	0.000E+00	0.000E+00	0.000E+00	0.000E+00
-70.000	0.000E+00	0.000E+00	0.000E+00	0.000E+00
-16.800	0.000E+00	0.000E+00	0.000E+00	0.000E+00
-6.050	0.000E+00	0.000E+00	0.000E+00	0.000E+00
0.758	0.000E+00	0.000E+00	0.000E+00	0.000E+00
9.050	0.000E+00	0.000E+00	0.000E+00	0.000E+00
19.300	0.000E+00	0.000E+00	0.000E+00	0.000E+00
90.000	0.000E+00	0.000E+00	0.000E+00	0.000E+00
170.000	0.000E+00	0.000E+00	0.000E+00	0.000E+00
Northing Distance (m)	**Vertical Aqueous CT Flux, kg/m^2 yr**	**Gas CT Concentration, ppmv**	**Aqueous CT Concentration, mg/L**	**Aqueous CT Concentration, mg/L**
-170.000	0.000E+00	0.000E+00	0.000E+00	0.000E+00
-90.000	0.000E+00	0.000E+00	0.000E+00	0.000E+00
-33.500	0.000E+00	0.000E+00	0.000E+00	0.000E+00
-14.288	0.000E+00	0.000E+00	0.000E+00	0.000E+00
-4.575	0.000E+00	0.000E+00	0.000E+00	0.000E+00
2.745	0.000E+00	0.000E+00	0.000E+00	0.000E+00
10.863	0.000E+00	0.000E+00	0.000E+00	0.000E+00
28.500	0.000E+00	0.000E+00	0.000E+00	0.000E+00
70.000	0.000E+00	0.000E+00	0.000E+00	0.000E+00
150.000	0.000E+00	0.000E+00	0.000E+00	0.000E+00

Table A.26. Vertical Aqueous CT Flux, Gas CT Concentration, and Aqueous CT Concentration at the Nodes Above the Water Table and the Aqueous CT Concentration Below the Water Table at an Easting and a Northing Cross Section in Year 2030 for Imposed Case 5

	Vadose Zone			Aquifer
Easting Distance (m)	Vertical Aqueous CT Flux, kg/m^2 yr	Gas CT Concentration, ppmv	Aqueous CT Concentration, mg/L	Aqueous CT Concentration, mg/L
-150.000	0.000E+00	0.000E+00	0.000E+00	0.000E+00
-70.000	0.000E+00	0.000E+00	0.000E+00	0.000E+00
-16.800	-2.879E-13	8.109E-06	5.363E-11	0.000E+00
-6.050	-5.543E-13	1.577E-05	1.043E-10	7.326E-13
0.758	-5.622E-13	1.607E-05	1.063E-10	9.808E-13
9.050	-4.290E-13	1.233E-05	8.157E-11	1.103E-12
19.300	-1.868E-13	5.421E-06	3.585E-11	9.353E-13
90.000	0.000E+00	0.000E+00	0.000E+00	0.000E+00
170.000	0.000E+00	0.000E+00	0.000E+00	0.000E+00
Northing Distance (m)	Vertical Aqueous CT Flux, kg/m^2 yr	Gas CT Concentration, ppmv	Aqueous CT Concentration, mg/L	Aqueous CT Concentration, mg/L
-170.000	0.000E+00	0.000E+00	0.000E+00	0.000E+00
-90.000	0.000E+00	0.000E+00	0.000E+00	0.000E+00
-33.500	-5.354E-14	1.528E-06	1.010E-11	0.000E+00
-14.288	-4.365E-13	1.246E-05	8.237E-11	7.614E-13
-4.575	-5.622E-13	1.607E-05	1.063E-10	9.808E-13
2.745	-3.911E-13	1.120E-05	7.404E-11	0.000E+00
10.863	-1.563E-13	4.484E-06	2.965E-11	0.000E+00
28.500	-8.077E-15	2.321E-07	1.535E-12	0.000E+00
70.000	0.000E+00	0.000E+00	0.000E+00	0.000E+00
150.000	0.000E+00	0.000E+00	0.000E+00	0.000E+00

Table A.27. Vertical Aqueous CT Flux, Gas CT Concentration, and Aqueous CT Concentration at the Nodes Above the Water Table and the Aqueous CT Concentration Below the Water Table at an Easting and a Northing Cross Section in Year 2050 for Imposed Case 5

	Vadose Zone			Aquifer
Easting Distance (m)	Vertical Aqueous CT Flux, kg/m^2 yr	Gas CT Concentration, ppmv	Aqueous CT Concentration, mg/L	Aqueous CT Concentration, mg/L
-150.000	0.000E+00	0.000E+00	0.000E+00	0.000E+00
-70.000	-4.622E-13	1.353E-05	8.945E-11	7.732E-13
-16.800	-6.563E-11	1.901E-03	1.257E-08	8.521E-11
-6.050	-1.060E-10	3.105E-03	2.054E-08	2.266E-10
0.758	-1.082E-10	3.184E-03	2.106E-08	3.087E-10
9.050	-8.730E-11	2.583E-03	1.709E-08	3.930E-10
19.300	-4.127E-11	1.230E-03	8.137E-09	4.121E-10
90.000	-2.222E-14	6.515E-07	4.309E-12	1.145E-10
170.000	0.000E+00	0.000E+00	0.000E+00	2.481E-11
Northing Distance (m)	Vertical Aqueous CT Flux, kg/m^2 yr	Gas CT Concentration, ppmv	Aqueous CT Concentration, mg/L	Aqueous CT Concentration, mg/L
-170.000	0.000E+00	0.000E+00	0.000E+00	0.000E+00
-90.000	-2.768E-13	8.070E-06	5.337E-11	0.000E+00
-33.500	-2.294E-11	6.693E-04	4.426E-09	6.228E-11
-14.288	-9.428E-11	2.766E-03	1.829E-08	2.681E-10
-4.575	-1.082E-10	3.184E-03	2.106E-08	3.087E-10
2.745	-8.136E-11	2.400E-03	1.588E-08	2.296E-10
10.863	-4.107E-11	1.214E-03	8.026E-09	1.119E-10
28.500	-4.583E-12	1.353E-04	8.946E-10	1.182E-11
70.000	-2.254E-14	6.521E-07	4.312E-12	0.000E+00
150.000	0.000E+00	0.000E+00	0.000E+00	0.000E+00

Table A.28. Vertical Aqueous CT Flux, Gas CT Concentration, and Aqueous CT Concentration at the Nodes Above the Water Table and the Aqueous CT Concentration Below the Water Table at an Easting and a Northing Cross Section in Year 2070 for Imposed Case 5

	Vadose Zone			Aquifer
Easting Distance (m)	Vertical Aqueous CT Flux, kg/m^2 yr	Gas CT Concentration, ppmv	Aqueous CT Concentration, mg/L	Aqueous CT Concentration, mg/L
-150.000	-9.230E-15	2.823E-07	1.867E-12	0.000E+00
-70.000	-1.466E-11	4.305E-04	2.847E-09	4.581E-11
-16.800	-1.057E-09	3.085E-02	2.040E-07	1.721E-09
-6.050	-1.550E-09	4.578E-02	3.028E-07	3.966E-09
0.758	-1.571E-09	4.662E-02	3.083E-07	5.268E-09
9.050	-1.290E-09	3.847E-02	2.544E-07	6.732E-09
19.300	-6.495E-10	1.950E-02	1.290E-07	7.320E-09
90.000	-1.239E-12	3.637E-05	2.406E-10	3.127E-09
170.000	-1.417E-13	4.175E-06	2.761E-11	1.042E-09
Northing Distance (m)	Vertical Aqueous CT Flux, kg/m^2 yr	Gas CT Concentration, ppmv	Aqueous CT Concentration, mg/L	Aqueous CT Concentration, mg/L
-170.000	-1.258E-13	3.448E-06	2.280E-11	0.000E+00
-90.000	-1.265E-11	3.691E-04	2.441E-09	3.449E-11
-33.500	-5.275E-10	1.548E-02	1.024E-07	1.670E-09
-14.288	-1.468E-09	4.340E-02	2.870E-07	4.887E-09
-4.575	-1.571E-09	4.662E-02	3.083E-07	5.268E-09
2.745	-1.236E-09	3.675E-02	2.431E-07	4.106E-09
10.863	-7.129E-10	2.124E-02	1.405E-07	2.303E-09
28.500	-1.200E-10	3.568E-03	2.359E-08	3.701E-10
70.000	-1.523E-12	4.421E-05	2.924E-10	3.997E-12
150.000	0.000E+00	0.000E+00	0.000E+00	0.000E+00

Table A.29. Vertical Aqueous CT Flux, Gas CT Concentration, and Aqueous CT Concentration at the Nodes Above the Water Table and the Aqueous CT Concentration Below the Water Table at an Easting and a Northing Cross Section in Year 2090 for Imposed Case 5

	Vadose Zone			Aquifer
Easting Distance (m)	**Vertical Aqueous CT Flux, kg/m^2 yr**	**Gas CT Concentration, ppmv**	**Aqueous CT Concentration, mg/L**	**Aqueous CT Concentration, mg/L**
-150.000	-2.568E-13	7.854E-06	5.194E-11	0.000E+00
-70.000	-1.348E-10	3.962E-03	2.620E-08	4.710E-10
-16.800	-5.751E-09	1.682E-01	1.112E-06	1.135E-08
-6.050	-7.914E-09	2.342E-01	1.549E-06	2.343E-08
0.758	-7.916E-09	2.353E-01	1.556E-06	3.036E-08
9.050	-6.518E-09	1.947E-01	1.288E-06	3.848E-08
19.300	-3.485E-09	1.048E-01	6.932E-07	4.257E-08
90.000	-1.406E-11	4.129E-04	2.731E-09	2.410E-08
170.000	-1.992E-12	5.867E-05	3.880E-10	1.061E-08
Northing Distance (m)	**Vertical Aqueous CT Flux, kg/m^2 yr**	**Gas CT Concentration, ppmv**	**Aqueous CT Concentration, mg/L**	**Aqueous CT Concentration, mg/L**
-170.000	-2.461E-12	6.745E-05	4.461E-10	5.745E-12
-90.000	-1.484E-10	4.334E-03	2.866E-08	4.613E-10
-33.500	-3.643E-09	1.070E-01	7.079E-07	1.310E-08
-14.288	-7.755E-09	2.296E-01	1.518E-06	2.943E-08
-4.575	-7.916E-09	2.353E-01	1.556E-06	3.036E-08
2.745	-6.412E-09	1.911E-01	1.264E-06	2.442E-08
10.863	-4.058E-09	1.211E-01	8.011E-07	1.507E-08
28.500	-9.220E-10	2.747E-02	1.816E-07	3.245E-09
70.000	-2.012E-11	5.847E-04	3.867E-09	6.373E-11
150.000	-3.638E-14	1.060E-06	7.010E-12	0.000E+00

Table A.30. Vertical Aqueous CT Flux, Gas CT Concentration, and Aqueous CT Concentration at the Nodes Above the Water Table and the Aqueous CT Concentration Below the Water Table at an Easting and a Northing Cross Section in Year 2107 for Imposed Case 5

	Vadose Zone			Aquifer
Easting Distance (m)	**Vertical Aqueous CT Flux, kg/m^2 yr**	**Gas CT Concentration, ppmv**	**Aqueous CT Concentration, mg/L**	**Aqueous CT Concentration, mg/L**
-150.000	-1.566E-12	4.789E-05	3.167E-10	5.266E-12
-70.000	-5.131E-10	1.508E-02	9.975E-08	1.934E-09
-16.800	-1.516E-08	4.434E-01	2.932E-06	3.453E-08
-6.050	-2.002E-08	5.927E-01	3.920E-06	6.612E-08
0.758	-1.976E-08	5.875E-01	3.885E-06	8.400E-08
9.050	-1.625E-08	4.856E-01	3.211E-06	1.053E-07
19.300	-9.113E-09	2.742E-01	1.813E-06	1.173E-07
90.000	-6.111E-11	1.795E-03	1.187E-08	7.854E-08
170.000	-9.475E-12	2.791E-04	1.846E-09	4.087E-08
Northing Distance (m)	**Vertical Aqueous CT Flux, kg/m^2 yr**	**Gas CT Concentration, ppmv**	**Aqueous CT Concentration, mg/L**	**Aqueous CT Concentration, mg/L**
-170.000	-1.526E-11	4.183E-04	2.766E-09	4.119E-11
-90.000	-6.530E-10	1.907E-02	1.261E-07	2.221E-09
-33.500	-1.106E-08	3.251E-01	2.150E-06	4.386E-08
-14.288	-1.992E-08	5.899E-01	3.901E-06	8.362E-08
-4.575	-1.976E-08	5.875E-01	3.885E-06	8.400E-08
2.745	-1.630E-08	4.860E-01	3.214E-06	6.893E-08
10.863	-1.094E-08	3.268E-01	2.161E-06	4.517E-08
28.500	-3.030E-09	9.031E-02	5.972E-07	1.179E-08
70.000	-9.648E-11	2.804E-03	1.854E-08	3.343E-10
150.000	-3.460E-13	1.008E-05	6.666E-11	0.000E+00

Table A.31.   Vertical Aqueous CT Flux, Gas CT Concentration, and Aqueous CT Concentration at the Nodes Above the Water Table and the Aqueous CT Concentration Below the Water Table at an Easting and a Northing Cross Section in Year 2010 for Imposed Case 6

	Vadose Zone			Aquifer
Easting Distance (m)	Vertical Aqueous CT Flux, kg/m^2 yr	Gas CT Concentration, ppmv	Aqueous CT Concentration, mg/L	Aqueous CT Concentration, mg/L
-150.000	0.000E+00	0.000E+00	0.000E+00	0.000E+00
-70.000	0.000E+00	0.000E+00	0.000E+00	0.000E+00
-16.800	-4.808E-15	1.242E-07	8.213E-13	0.000E+00
-6.050	-5.717E-13	1.484E-05	9.814E-11	0.000E+00
0.758	-4.934E-13	1.286E-05	8.502E-11	0.000E+00
9.050	-1.247E-14	3.273E-07	2.165E-12	0.000E+00
19.300	0.000E+00	0.000E+00	0.000E+00	0.000E+00
90.000	0.000E+00	0.000E+00	0.000E+00	0.000E+00
170.000	0.000E+00	0.000E+00	0.000E+00	0.000E+00
Northing Distance (m)	Vertical Aqueous CT Flux, kg/m^2 yr	Gas CT Concentration, ppmv	Aqueous CT Concentration, mg/L	Aqueous CT Concentration, mg/L
-170.000	0.000E+00	0.000E+00	0.000E+00	0.000E+00
-90.000	0.000E+00	0.000E+00	0.000E+00	0.000E+00
-33.500	0.000E+00	0.000E+00	0.000E+00	0.000E+00
-14.288	-7.784E-14	2.033E-06	1.344E-11	0.000E+00
-4.575	-4.934E-13	1.286E-05	8.502E-11	0.000E+00
2.745	-8.471E-14	2.209E-06	1.461E-11	0.000E+00
10.863	-2.216E-14	5.801E-07	3.837E-12	0.000E+00
28.500	0.000E+00	0.000E+00	0.000E+00	0.000E+00
70.000	0.000E+00	0.000E+00	0.000E+00	0.000E+00
150.000	0.000E+00	0.000E+00	0.000E+00	0.000E+00

Table A.32. Vertical Aqueous CT Flux, Gas CT Concentration, and Aqueous CT Concentration at the Nodes Above the Water Table and the Aqueous CT Concentration Below the Water Table at an Easting and a Northing Cross Section in Year 2030 for Imposed Case 6

	Vadose Zone			Aquifer
Easting Distance (m)	Vertical Aqueous CT Flux, kg/m^2 yr	Gas CT Concentration, ppmv	Aqueous CT Concentration, mg/L	Aqueous CT Concentration, mg/L
-150.000	-2.885E-11	8.841E-04	5.847E-09	6.964E-11
-70.000	-4.598E-05	1.330E+03	8.794E-03	1.119E-04
-16.800	-2.513E-03	7.077E+04	4.678E-01	6.777E-03
-6.050	-3.234E-03	9.208E+04	6.086E-01	1.207E-02
0.758	-3.558E-03	1.018E+05	6.730E-01	1.545E-02
9.050	-2.891E-03	8.322E+04	5.501E-01	1.987E-02
19.300	-2.221E-03	6.452E+04	4.265E-01	2.335E-02
90.000	-2.708E-06	7.898E+01	5.223E-04	1.162E-02
170.000	-2.548E-07	7.509E+00	4.966E-05	2.752E-03
Northing Distance (m)	Vertical Aqueous CT Flux, kg/m^2 yr	Gas CT Concentration, ppmv	Aqueous CT Concentration, mg/L	Aqueous CT Concentration, mg/L
-170.000	-8.732E-13	2.398E-05	1.586E-10	1.334E-12
-90.000	-1.959E-06	5.681E+01	3.757E-04	3.669E-06
-33.500	-1.563E-03	4.460E+04	2.949E-01	5.328E-03
-14.288	-2.888E-03	8.247E+04	5.452E-01	1.286E-02
-4.575	-3.558E-03	1.018E+05	6.730E-01	1.545E-02
2.745	-3.568E-03	1.023E+05	6.760E-01	1.527E-02
10.863	-3.100E-03	8.900E+04	5.883E-01	1.361E-02
28.500	-1.846E-03	5.307E+04	3.509E-01	6.721E-03
70.000	-3.389E-05	9.691E+02	6.409E-03	6.796E-05
150.000	-2.084E-11	6.084E-04	4.024E-09	3.632E-11

Table A.33. Vertical Aqueous CT Flux, Gas CT Concentration, and Aqueous CT Concentration at the Nodes Above the Water Table and the Aqueous CT Concentration Below the Water Table at an Easting and a Northing Cross Section in Year 2050 for Imposed Case 6

	Vadose Zone			Aquifer
Easting Distance (m)	Vertical Aqueous CT Flux, kg/m^2 yr	Gas CT Concentration, ppmv	Aqueous CT Concentration, mg/L	Aqueous CT Concentration, mg/L
-150.000	-9.605E-09	2.939E-01	1.944E-06	2.777E-08
-70.000	-4.168E-04	1.219E+04	8.063E-02	1.499E-03
-16.800	-2.342E-03	6.786E+04	4.486E-01	1.248E-02
-6.050	-2.912E-03	8.539E+04	5.644E-01	1.757E-02
0.758	-3.112E-03	9.172E+04	6.063E-01	2.088E-02
9.050	-2.529E-03	7.492E+04	4.953E-01	2.503E-02
19.300	-2.125E-03	6.341E+04	4.192E-01	2.875E-02
90.000	-7.346E-05	2.154E+03	1.425E-02	3.193E-02
170.000	-4.863E-06	1.433E+02	9.474E-04	2.109E-02
Northing Distance (m)	Vertical Aqueous CT Flux, kg/m^2 yr	Gas CT Concentration, ppmv	Aqueous CT Concentration, mg/L	Aqueous CT Concentration, mg/L
-170.000	-6.124E-10	1.680E-02	1.111E-07	1.292E-09
-90.000	-8.160E-05	2.379E+03	1.573E-02	2.389E-04
-33.500	-1.783E-03	5.204E+04	3.441E-01	1.177E-02
-14.288	-2.489E-03	7.309E+04	4.831E-01	1.819E-02
-4.575	-3.112E-03	9.172E+04	6.063E-01	2.088E-02
2.745	-3.194E-03	9.435E+04	6.237E-01	2.104E-02
10.863	-2.637E-03	7.799E+04	5.155E-01	1.913E-02
28.500	-1.923E-03	5.679E+04	3.754E-01	1.339E-02
70.000	-4.144E-04	1.199E+04	7.928E-02	1.508E-03
150.000	-1.090E-08	3.176E-01	2.100E-06	2.524E-08

Table A.34. Vertical Aqueous CT Flux, Gas CT Concentration, and Aqueous CT Concentration at the Nodes Above the Water Table and the Aqueous CT Concentration Below the Water Table at an Easting and a Northing Cross Section in Year 2070 for Imposed Case 6

	Vadose Zone			Aquifer
Easting Distance (m)	Vertical Aqueous CT Flux, kg/m^2 yr	Gas CT Concentration, ppmv	Aqueous CT Concentration, mg/L	Aqueous CT Concentration, mg/L
-150.000	-1.882E-07	5.757E+00	3.808E-05	5.960E-07
-70.000	-6.219E-04	1.826E+04	1.207E-01	2.902E-03
-16.800	-1.819E-03	5.311E+04	3.511E-01	1.299E-02
-6.050	-2.100E-03	6.208E+04	4.104E-01	1.682E-02
0.758	-2.144E-03	6.366E+04	4.208E-01	1.919E-02
9.050	-1.891E-03	5.643E+04	3.731E-01	2.237E-02
19.300	-1.679E-03	5.045E+04	3.335E-01	2.553E-02
90.000	-2.228E-04	6.543E+03	4.327E-02	3.444E-02
170.000	-1.255E-05	3.696E+02	2.445E-03	2.967E-02
Northing Distance (m)	Vertical Aqueous CT Flux, kg/m^2 yr	Gas CT Concentration, ppmv	Aqueous CT Concentration, mg/L	Aqueous CT Concentration, mg/L
-170.000	-1.788E-08	4.901E-01	3.241E-06	4.396E-08
-90.000	-2.407E-04	7.026E+03	4.646E-02	9.911E-04
-33.500	-1.476E-03	4.332E+04	2.864E-01	1.299E-02
-14.288	-1.855E-03	5.485E+04	3.626E-01	1.744E-02
-4.575	-2.144E-03	6.366E+04	4.208E-01	1.919E-02
2.745	-2.197E-03	6.542E+04	4.325E-01	1.942E-02
10.863	-1.918E-03	5.719E+04	3.781E-01	1.812E-02
28.500	-1.558E-03	4.635E+04	3.065E-01	1.432E-02
70.000	-6.265E-04	1.819E+04	1.203E-01	3.401E-03
150.000	-2.365E-07	6.890E+00	4.557E-05	6.476E-07

Table A.35. Vertical Aqueous CT Flux, Gas CT Concentration, and Aqueous CT Concentration at the Nodes Above the Water Table and the Aqueous CT Concentration Below the Water Table at an Easting and a Northing Cross Section in Year 2090 for Imposed Case 6

	Vadose Zone			Aquifer
Easting Distance (m)	**Vertical Aqueous CT Flux, kg/m^2 yr**	**Gas CT Concentration, ppmv**	**Aqueous CT Concentration, mg/L**	**Aqueous CT Concentration, mg/L**
-150.000	-1.144E-06	3.498E+01	2.313E-04	3.879E-06
-70.000	-5.965E-04	1.753E+04	1.159E-01	3.374E-03
-16.800	-1.191E-03	3.485E+04	2.304E-01	1.098E-02
-6.050	-1.232E-03	3.648E+04	2.412E-01	1.329E-02
0.758	-1.240E-03	3.687E+04	2.438E-01	1.461E-02
9.050	-1.216E-03	3.634E+04	2.403E-01	1.656E-02
19.300	-1.157E-03	3.480E+04	2.301E-01	1.868E-02
90.000	-3.034E-04	8.913E+03	5.894E-02	2.823E-02
170.000	-1.830E-05	5.390E+02	3.565E-03	2.759E-02
Northing Distance (m)	**Vertical Aqueous CT Flux, kg/m^2 yr**	**Gas CT Concentration, ppmv**	**Aqueous CT Concentration, mg/L**	**Aqueous CT Concentration, mg/L**
-170.000	-1.533E-07	4.203E+00	2.779E-05	4.271E-07
-90.000	-3.203E-04	9.352E+03	6.185E-02	1.729E-03
-33.500	-1.078E-03	3.168E+04	2.095E-01	1.145E-02
-14.288	-1.206E-03	3.570E+04	2.361E-01	1.397E-02
-4.575	-1.240E-03	3.687E+04	2.438E-01	1.461E-02
2.745	-1.244E-03	3.708E+04	2.452E-01	1.469E-02
10.863	-1.213E-03	3.624E+04	2.396E-01	1.432E-02
28.500	-1.114E-03	3.320E+04	2.195E-01	1.236E-02
70.000	-6.010E-04	1.747E+04	1.155E-01	4.276E-03
150.000	-1.502E-06	4.375E+01	2.894E-04	4.705E-06

Table A.36. Vertical Aqueous CT Flux, Gas CT Concentration, and Aqueous CT Concentration at the Nodes Above the Water Table and the Aqueous CT Concentration Below the Water Table at an Easting and a Northing Cross Section in Year 2107 for Imposed Case 6

	Vadose Zone			Aquifer
Easting Distance (m)	**Vertical Aqueous CT Flux, kg/m^2 yr**	**Gas CT Concentration, ppmv**	**Aqueous CT Concentration, mg/L**	**Aqueous CT Concentration, mg/L**
-150.000	-3.140E-06	9.605E+01	6.352E-04	1.120E-05
-70.000	-5.221E-04	1.535E+04	1.015E-01	3.333E-03
-16.800	-8.792E-04	2.572E+04	1.701E-01	9.232E-03
-6.050	-8.911E-04	2.638E+04	1.745E-01	1.089E-02
0.758	-8.962E-04	2.666E+04	1.763E-01	1.183E-02
9.050	-8.935E-04	2.671E+04	1.766E-01	1.321E-02
19.300	-8.657E-04	2.605E+04	1.723E-01	1.474E-02
90.000	-3.084E-04	9.061E+03	5.992E-02	2.250E-02
170.000	-2.068E-05	6.092E+02	4.029E-03	2.278E-02
Northing Distance (m)	**Vertical Aqueous CT Flux, kg/m^2 yr**	**Gas CT Concentration, ppmv**	**Aqueous CT Concentration, mg/L**	**Aqueous CT Concentration, mg/L**
-170.000	-5.542E-07	1.519E+01	1.005E-04	1.696E-06
-90.000	-3.248E-04	9.484E+03	6.272E-02	2.102E-03
-33.500	-8.270E-04	2.431E+04	1.607E-01	9.787E-03
-14.288	-8.887E-04	2.632E+04	1.741E-01	1.145E-02
-4.575	-8.962E-04	2.666E+04	1.763E-01	1.183E-02
2.745	-8.966E-04	2.674E+04	1.768E-01	1.188E-02
10.863	-8.909E-04	2.661E+04	1.760E-01	1.169E-02
28.500	-8.480E-04	2.528E+04	1.671E-01	1.046E-02
70.000	-5.273E-04	1.533E+04	1.013E-01	4.395E-03
150.000	-4.226E-06	1.231E+02	8.142E-04	1.468E-05

Table A.37. Vertical Aqueous CT Flux, Gas CT Concentration, and Aqueous CT Concentration at the Nodes Above the Water Table and the Aqueous CT Concentration Below the Water Table at an Easting and a Northing Cross Section in Year 2010 for Modeled Case 1

	Vadose Zone			Aquifer
Easting Distance (m)	Vertical Aqueous CT Flux, kg/m^2 yr	Gas CT Concentration, ppmv	Aqueous CT Concentration, mg/L	Aqueous CT Concentration, mg/L
-150.000	-2.680E-06	7.065E+01	4.673E-04	6.666E-06
-70.000	-3.348E-04	8.136E+03	5.381E-02	9.637E-04
-16.800	-3.302E-03	7.687E+04	5.081E-01	7.855E-03
-6.050	-2.809E-03	6.830E+04	4.515E-01	1.148E-02
0.758	-2.772E-03	6.886E+04	4.552E-01	1.315E-02
9.050	-3.747E-03	9.256E+04	6.118E-01	1.675E-02
19.300	-3.498E-03	8.029E+04	5.307E-01	1.995E-02
90.000	-3.684E-03	8.127E+04	5.372E-01	2.211E-01
170.000	-3.097E-03	6.839E+04	4.521E-01	4.718E-01
Northing Distance (m)	Vertical Aqueous CT Flux, kg/m^2 yr	Gas CT Concentration, ppmv	Aqueous CT Concentration, mg/L	Aqueous CT Concentration, mg/L
-170.000	-5.506E-07	1.328E+01	8.783E-05	1.273E-06
-90.000	-1.286E-04	3.201E+03	2.117E-02	4.384E-04
-33.500	-2.052E-03	4.800E+04	3.173E-01	6.643E-03
-14.288	-3.035E-03	7.170E+04	4.740E-01	1.208E-02
-4.575	-2.772E-03	6.886E+04	4.552E-01	1.315E-02
2.745	-3.802E-03	9.590E+04	6.339E-01	1.432E-02
10.863	-2.702E-03	6.400E+04	4.231E-01	1.292E-02
28.500	-2.956E-03	6.242E+04	4.127E-01	9.522E-03
70.000	-7.238E-04	1.425E+04	9.422E-02	1.492E-03
150.000	-6.103E-06	1.216E+02	8.044E-04	1.415E-05

Table A.38. Vertical Aqueous CT Flux, Gas CT Concentration, and Aqueous CT Concentration at the Nodes Above the Water Table and the Aqueous CT Concentration Below the Water Table at an Easting and a Northing Cross Section in Year 2030 for Modeled Case 1

	Vadose Zone			Aquifer
Easting Distance (m)	**Vertical Aqueous CT Flux, kg/m^2 yr**	**Gas CT Concentration, ppmv**	**Aqueous CT Concentration, mg/L**	**Aqueous CT Concentration, mg/L**
-150.000	-1.315E-04	4.008E+03	2.650E-02	4.667E-04
-70.000	-2.141E-03	6.100E+04	4.033E-01	1.367E-02
-16.800	-3.833E-03	1.051E+05	6.950E-01	3.354E-02
-6.050	-3.587E-03	1.068E+05	7.062E-01	3.952E-02
0.758	-3.434E-03	1.068E+05	7.062E-01	6.249E-02
9.050	-3.525E-03	1.068E+05	7.062E-01	8.322E-02
19.300	-3.950E-03	1.058E+05	6.992E-01	7.717E-02
90.000	-2.803E-03	6.763E+04	4.471E-01	7.810E-02
170.000	-1.815E-03	4.393E+04	2.904E-01	1.075E-01
Northing Distance (m)	**Vertical Aqueous CT Flux, kg/m^2 yr**	**Gas CT Concentration, ppmv**	**Aqueous CT Concentration, mg/L**	**Aqueous CT Concentration, mg/L**
-170.000	-4.869E-05	1.333E+03	8.817E-03	1.786E-04
-90.000	-1.450E-03	4.197E+04	2.775E-01	8.567E-03
-33.500	-3.415E-03	9.527E+04	6.297E-01	3.326E-02
-14.288	-3.762E-03	1.054E+05	6.966E-01	4.013E-02
-4.575	-3.434E-03	1.068E+05	7.062E-01	6.249E-02
2.745	-3.399E-03	1.069E+05	7.062E-01	1.861E-01
10.863	-3.713E-03	1.068E+05	7.062E-01	4.513E-02
28.500	-4.286E-03	1.017E+05	6.723E-01	3.872E-02
70.000	-3.388E-03	7.064E+04	4.670E-01	2.019E-02
150.000	-3.543E-04	7.198E+03	4.760E-02	1.116E-03

Table A.39. Vertical Aqueous CT Flux, Gas CT Concentration, and Aqueous CT Concentration at the Nodes Above the Water Table and the Aqueous CT Concentration Below the Water Table at an Easting and a Northing Cross Section in Year 2050 for Modeled Case 1

	Vadose Zone			Aquifer
Easting Distance (m)	**Vertical Aqueous CT Flux, kg/m^2 yr**	**Gas CT Concentration, ppmv**	**Aqueous CT Concentration, mg/L**	**Aqueous CT Concentration, mg/L**
-150.000	-5.482E-04	1.674E+04	1.107E-01	2.682E-03
-70.000	-2.562E-03	7.392E+04	4.886E-01	2.462E-02
-16.800	-3.824E-03	1.057E+05	6.983E-01	4.656E-02
-6.050	-3.448E-03	1.069E+05	7.062E-01	1.033E-01
0.758	-3.339E-03	1.069E+05	7.062E-01	2.553E-01
9.050	-3.394E-03	1.068E+05	7.062E-01	4.202E-01
19.300	-3.887E-03	1.061E+05	7.015E-01	4.062E-01
90.000	-2.845E-03	6.912E+04	4.569E-01	2.418E-01
170.000	-1.518E-03	3.691E+04	2.440E-01	1.456E-01
Northing Distance (m)	**Vertical Aqueous CT Flux, kg/m^2 yr**	**Gas CT Concentration, ppmv**	**Aqueous CT Concentration, mg/L**	**Aqueous CT Concentration, mg/L**
-170.000	-3.153E-04	8.643E+03	5.716E-02	1.628E-03
-90.000	-2.054E-03	5.991E+04	3.961E-01	2.106E-02
-33.500	-3.395E-03	9.649E+04	6.378E-01	4.774E-02
-14.288	-3.722E-03	1.060E+05	7.004E-01	5.387E-02
-4.575	-3.339E-03	1.069E+05	7.062E-01	2.553E-01
2.745	-3.366E-03	1.069E+05	7.062E-01	4.157E-01
10.863	-3.584E-03	1.069E+05	7.062E-01	1.658E-01
28.500	-4.257E-03	1.019E+05	6.738E-01	5.361E-02
70.000	-3.805E-03	7.951E+04	5.256E-01	3.641E-02
150.000	-1.227E-03	2.476E+04	1.637E-01	6.209E-03

Table A.40. Vertical Aqueous CT Flux, Gas CT Concentration, and Aqueous CT Concentration at the Nodes Above the Water Table and the Aqueous CT Concentration Below the Water Table at an Easting and a Northing Cross Section in Year 2070 for Modeled Case 1

	Vadose Zone			Aquifer
Easting Distance (m)	Vertical Aqueous CT Flux, kg/m^2 yr	Gas CT Concentration, ppmv	Aqueous CT Concentration, mg/L	Aqueous CT Concentration, mg/L
-150.000	-9.132E-04	2.790E+04	1.845E-01	5.725E-03
-70.000	-2.623E-03	7.591E+04	5.018E-01	3.092E-02
-16.800	-3.860E-03	1.059E+05	7.000E-01	5.335E-02
-6.050	-3.457E-03	1.069E+05	7.062E-01	1.533E-01
0.758	-3.381E-03	1.069E+05	7.062E-01	2.999E-01
9.050	-3.434E-03	1.068E+05	7.062E-01	4.696E-01
19.300	-3.894E-03	1.062E+05	7.020E-01	4.840E-01
90.000	-2.942E-03	7.164E+04	4.736E-01	3.975E-01
170.000	-1.502E-03	3.656E+04	2.417E-01	2.991E-01
Northing Distance (m)	Vertical Aqueous CT Flux, kg/m^2 yr	Gas CT Concentration, ppmv	Aqueous CT Concentration, mg/L	Aqueous CT Concentration, mg/L
-170.000	-6.795E-04	1.863E+04	1.232E-01	4.992E-03
-90.000	-2.188E-03	6.393E+04	4.227E-01	3.001E-02
-33.500	-3.371E-03	9.611E+04	6.353E-01	5.519E-02
-14.288	-3.720E-03	1.063E+05	7.026E-01	6.107E-02
-4.575	-3.381E-03	1.069E+05	7.062E-01	2.999E-01
2.745	-3.420E-03	1.069E+05	7.062E-01	4.146E-01
10.863	-3.625E-03	1.069E+05	7.062E-01	2.205E-01
28.500	-4.254E-03	1.019E+05	6.734E-01	6.114E-02
70.000	-3.810E-03	7.973E+04	5.271E-01	4.546E-02
150.000	-1.756E-03	3.543E+04	2.343E-01	1.307E-02

Table A.41. Vertical Aqueous CT Flux, Gas CT Concentration, and Aqueous CT Concentration at the Nodes Above the Water Table and the Aqueous CT Concentration Below the Water Table at an Easting and a Northing Cross Section in Year 2090 for Modeled Case 1

	Vadose Zone			Aquifer
Easting Distance (m)	Vertical Aqueous CT Flux, kg/m^2 yr	Gas CT Concentration, ppmv	Aqueous CT Concentration, mg/L	Aqueous CT Concentration, mg/L
-150.000	-1.096E-03	3.350E+04	2.215E-01	8.160E-03
-70.000	-2.596E-03	7.520E+04	4.971E-01	3.423E-02
-16.800	-3.892E-03	1.059E+05	6.997E-01	5.681E-02
-6.050	-3.505E-03	1.069E+05	7.062E-01	1.608E-01
0.758	-3.449E-03	1.069E+05	7.062E-01	2.821E-01
9.050	-3.515E-03	1.068E+05	7.062E-01	4.191E-01
19.300	-3.911E-03	1.059E+05	7.000E-01	4.403E-01
90.000	-2.927E-03	7.132E+04	4.715E-01	4.046E-01
170.000	-1.546E-03	3.765E+04	2.489E-01	3.533E-01
Northing Distance (m)	Vertical Aqueous CT Flux, kg/m^2 yr	Gas CT Concentration, ppmv	Aqueous CT Concentration, mg/L	Aqueous CT Concentration, mg/L
-170.000	-9.163E-04	2.512E+04	1.661E-01	8.981E-03
-90.000	-2.182E-03	6.381E+04	4.218E-01	3.522E-02
-33.500	-3.342E-03	9.533E+04	6.301E-01	5.887E-02
-14.288	-3.755E-03	1.068E+05	7.062E-01	6.483E-02
-4.575	-3.449E-03	1.069E+05	7.062E-01	2.821E-01
2.745	-3.492E-03	1.069E+05	7.062E-01	3.655E-01
10.863	-3.696E-03	1.069E+05	7.062E-01	2.118E-01
28.500	-4.233E-03	1.012E+05	6.691E-01	6.476E-02
70.000	-3.728E-03	7.808E+04	5.161E-01	4.994E-02
150.000	-1.951E-03	3.935E+04	2.602E-01	1.866E-02

Table A.42. Vertical Aqueous CT Flux, Gas CT Concentration, and Aqueous CT Concentration at the Nodes Above the Water Table and the Aqueous CT Concentration Below the Water Table at an Easting and a Northing Cross Section in Year 2107 for Modeled Case 1

	Vadose Zone			Aquifer
Easting Distance (m)	Vertical Aqueous CT Flux, kg/m^2 yr	Gas CT Concentration, ppmv	Aqueous CT Concentration, mg/L	Aqueous CT Concentration, mg/L
-150.000	-1.155E-03	3.530E+04	2.334E-01	9.463E-03
-70.000	-2.536E-03	7.349E+04	4.858E-01	3.538E-02
-16.800	-3.910E-03	1.056E+05	6.983E-01	5.791E-02
-6.050	-3.555E-03	1.069E+05	7.062E-01	1.508E-01
0.758	-3.512E-03	1.069E+05	7.062E-01	2.498E-01
9.050	-3.598E-03	1.068E+05	7.062E-01	3.555E-01
19.300	-3.923E-03	1.055E+05	6.975E-01	3.746E-01
90.000	-2.839E-03	6.920E+04	4.574E-01	3.649E-01
170.000	-1.546E-03	3.765E+04	2.489E-01	3.386E-01
Northing Distance (m)	Vertical Aqueous CT Flux, kg/m^2 yr	Gas CT Concentration, ppmv	Aqueous CT Concentration, mg/L	Aqueous CT Concentration, mg/L
-170.000	-1.012E-03	2.776E+04	1.836E-01	1.191E-02
-90.000	-2.127E-03	6.221E+04	4.113E-01	3.750E-02
-33.500	-3.298E-03	9.410E+04	6.220E-01	5.998E-02
-14.288	-3.794E-03	1.068E+05	7.062E-01	6.610E-02
-4.575	-3.512E-03	1.069E+05	7.062E-01	2.498E-01
2.745	-3.557E-03	1.069E+05	7.062E-01	3.160E-01
10.863	-3.765E-03	1.068E+05	7.062E-01	1.855E-01
28.500	-4.196E-03	1.003E+05	6.630E-01	6.571E-02
70.000	-3.613E-03	7.572E+04	5.005E-01	5.138E-02
150.000	-1.975E-03	3.984E+04	2.634E-01	2.183E-02

Appendix B

Quality Assurance

Appendix B

Quality Assurance

DOE Order 414.1C is the underlying quality requirement that guided efforts reported herein. The requirements of DOE Order 414.1C and related 10 CFR 830, Subpart A, are integrated into the elements of the PNNL Standards Based Management System (SBMS). Work associated with this report was conducted to comply with the applicable requirements in SBMS. Specifically, software quality assurance was implemented according to the "Safety Software Subject Area" in SBMS. This section documents software-associated quality assurance and is consistent with the quality assurance plan identified for the 200-PW-1/3/6 Operable Units (VET-1350-PQAP, Rev. 0 [Vista Engineering 2006]).

Tables B.1 and B.2 describe the software, its category, and how it was used for the results presented in this report.

Table B.1. Acquired Commercial Design and Analysis Software

Software	Version	Category	Requisition / Supplier	Purpose
Microsoft Excel®[1]	Excel 2003 11.8146.8132 SP2	Commercial Design and Analysis	PNNL MSP	Data plotting / analysis / calculations
Perl	Perl v5.8.5	Commercial Design and Analysis	PNNL license in RHEL	Batch processing / data formatting
Linux commands/packages – grep, sed, sort, awk	Part of RHEL release	Commercial Design and Analysis	PNNL license in RHEL	Batch processing / data formatting
Intel Fortran Compiler	Version 9.1 2006	Commercial Design and Analysis	Intel	Fortran compiler
Tecplot	Tecplot 10.0-6-014	Commercial Design and Analysis	Tecplot – Linux license	Data plotting, contouring, and visualization

---

[1] Microsoft Excel is a registered trademark of Microsoft Corporation, Redmond, Washington.

Software	Version	Category	Requisition / Supplier	Purpose
EarthVision by Dynamic Graphics, Inc.	7.0.1	Commercial Design and Analysis	Dynamic Graphics, Inc. Originally procured around 1991. Updated to version 7 in 2002. Company website: www.dgi.com	Hydrogeologic interpretation and GIS. Three-dimensional surfaces and visualization
Portland Group Fortran Compiler	Version 5.0	Commercial Design and Analysis	Portland Group International, individual workstation license	Fortran compiler
GIS = Geographic Information System MSP = Managed Software Program RHEL = Redhat Enterprise Linux				

Table B.2. Custom Software

PNNL Custom Software	Platform / Version	Category	Configuration Management
STOMP-WOA (MODE 5)	Linux version – official safety software release 043007	Custom Development	STOMP Configuration Management Plan
STOMP-WOA-Sc (MODE 5)	Parallel Version for MPP2	Custom Development	STOMP Configuration Management Plan
outputTo.pl	Linux	Custom Development	(Part of STOMP)
plotTo.pl	Linux	Custom Development	(Part of STOMP)
splib	Linux	Acquired	(Part of STOMP)
Model Input Build	Linux- FORTRAN and Perl programs	Custom Development	Version identification and/or date in filename. Document changes in program-header comment block. Older versions saved in archive folder. Maintain software log with program names, brief description, and latest versions.
Data Formatting	Linux- FORTRAN and Perl programs	Custom Development	(Same as above)
Model Result Processing	Tecplot Macros	Custom Development	(Same as above)
Model Result Processing	Linux- FORTRAN and Perl programs	Custom Development	(Same as above)
Input Files / Scenarios / Characterization Data	Linux		Maintained a simulation log with location, date, purpose of runs

In addition to the configuration management described in Tables B.1 and B.2, data files were subjected to configuration management. The managed data are divided into three types:

Electronic Data Transfer Packages (EDTPs). Produced by data providers in the form of electronic files that convey the data in a data package to the modeling team.

STOMP input files. Produced by the modeling team. Source data provided in the EDTPs are used to develop STOMP input files.

Simulation results and post-processed data. Produced by the modeling team.

The following data management procedures were followed:

- For any data type, a data change request (DCR) form was initiated.

- For each EDTP file, a data configuration information (DCI) file in text format was prepared. The name of the DCI file is comprised of the full name of the data file, plus archival date and "_DCI.txt." The DCI files contain the following information:

    – Name and date of file preparer

    – Original and archived file names

    – Name of data provider and/or data source

    – DCR number

    – Notes: any other information of value.

- The EDTPs were verified and the verification is documented in a verification log or in the DCR

- The model (STOMP) input files were prepared using the verified EDTP data. The verification was documented in 1) a verification log; 2) in the DCRs, or 3) by including the verifier's name in the model input file as comment lines.

- Once finalized, the EDTPs and the input files were archived by including the date and DCR number in the name of each data file or the folder that contains a group of files. The archival information was documented in the DCRs.

- Simulation results and post-processed data were archived using a folder structure consistent with the section numbering used in the report. An application log was filled to document the simulation scenarios.

Verification and validation of the STOMP code and associated custom software is documented as part of the STOMP code management and as shown in Table B.2. Verification for data manipulation software (e.g., Excel, Tecplot) was conducted using a Computational Computer Program Package Form (Rev. 0). The form documents the software and verification that is performed and identifies the reviewer. Completed forms are filed with the final versions of the computer files as part of project documentation.

References

DOE Order 414.1C. 2005. "Quality Assurance." U.S. Department of Energy, Washington, D.C.

10 CFR 830 Subpart A. 2002. "Quality Assurance Requirements." U.S. Department of Energy, Washington, D.C.

Vista Engineering Technologies. 2006. 200 PW1 Feasibility Study. VET-1350-Rev. 0, Vista Engineering Technologies, Richland, Washington.

No. of
Copies

No. of
Copies

OFFSITE

    Wes Bratton
    Ken Moser
    Vista Engineering
    8203 West Quinault Avenue
    Kennewick, WA 99336

    R.S. Dinicola
    U.S. Geological Survey
    Washington Water Science Center
    1210 Pacific Ave., Suite 600
    Tacoma, WA 98402

ONSITE

3 **DOE Richland Operations Office**

J. G. Morse	A6-38
K. M. Thompson	A6-38
A. C. Tortoso	A6-38

6 **Fluor Hanford, Inc.**

M. E. Byrnes	E6-44
C. Sutton	E6-44
D. S. Miller	E6-44
S. W. Petersen	E6-44
V. J. Rohay	E6-44
A. F. Shattuck	E6-44

U.S. Environmental Protection Agency

D. A. Faulk	B1-46

Washington State Department of Ecology

D. Goswami	H0-57

8 **Pacific Northwest National Laboratory**

A.R. Felmy	K8-96
M. D. Freshley	K9-33
G. V. Last	K6-81
M. Oostrom	K9-33
M. L. Rockhold	K9-36
P. D. Thorne	K9-33
M. J. Truex	K6-96
Hanford Technical Library	P8-55